Activation of Small Molecules by Solid-Supported Frustrated Lewis Pairs

by

Junyi Xing

This thesis is submitted in partial fulfilment of the requirement for the degree of

Doctor of Philosophy at the University of Oxford

Lady Margaret Hall

Oxford

March 2017

The work described in this thesis was carried out in the Chemistry Research Laboratory, Mansfield Road, Oxford between October 2012 and July 2016 under the supervision of Professor Dermot O'Hare. All the work is my own unless stated to the contrary, and has not been previously submitted for any degree at this or any other university.

Junyi Xing

Lady Margaret Hall

March 2017

Abstract

Activation of Small Molecule by Solid-Supported Frustrated Lewis Pairs

Junyi Xing
Lady Margaret Hall

D.Phil Thesis
Hilary Term 2017

The aims of this thesis have been to develop heterogeneous frustrated Lewis pairs for the catalytic activation of small molecules. Frustrated Lewis pairs capable of H_2 activation and CO_2 hydrogenation based on electron-deficient tri-arylboranes and sterically encumbered phosphines have been immobilised on silica. The reactivity of these heterogeneous systems with small molecules has been tested and compared with a variety of soluble siloxane and silsesquioxane molecular models. The use of layered double hydroxides as a potential support for the immobilisation of FLPs has also been explored.

Chapter One introduces the methanol economy and provides a background to recent advances in CO_2 capture and hydrogenation. The development of frustrated Lewis pairs, their reactivity with small molecules, together with theoretical studies on the mechanism of H_2 cleavage and CO_2 fixation by FLPs are summarised. Recent developments on heterogeneous frustrated Lewis pairs is discussed, in addition to a brief account of surface organometallic chemistry grafting procedures on silica and layered double hydroxide (LDH) supports.

Chapter Two reports H_2 heterolytic cleavage by $[B(C_6Cl_5)(C_6F_5)_2/P^tBu_3]$ FLP and the H_2 reduction of CO_2 to give the methoxyborate $[(C_6Cl_5)(C_6F_5)_2BOCH_3][HP^tBu_3]$. These results are compared with formato- and methoxyborate derivatives prepared independently *via* reaction of formic acid and MeOH with $[B(C_6Cl_5)(C_6F_5)_2/P^tBu_3]$. The products are characterised by FTIR and NMR spectroscopy, $[(C_6Cl_5)(C_6F_5)_2BOCHO][HP^tBu_3]$ is characterised by single crystal X-ray structure analysis.

Chapter Three details the synthesis of a group of siloxane and silsesquioxane bound Lewis acids $[(^tBuO)_3SiOB(C_6F_5)_2]$, $[(^tBuO)_3SiOB(Fxyl)_2]$ (Fxyl = 3,5-bis-trifluoromethylphenyl), $[T_8(OB(C_6F_5)_2)_2]$ ($T_8 = (C_4H_9)_8Si_8O_{12}$), $[T_8(OB(Fxyl)_2)_2]$, and preparation of the corresponding FLPs with Lewis bases P^tBu_3 and $PMes_3$ as soluble molecular models for silica-immobilised FLPs. Their ability to activate H_2 is investigated. The side-product $((^tBuO)_3Si)_2OBC_6F_5$ is characterised by single crystal X-ray structure analysis.

Chapter Four describes the preparation of heterogeneous Lewis acids by immobilisation of $-B(C_6F_5)_2$ and $-B(Fxyl)_2$ on the surface of thermally pretreated silica, and the subsequent formation of the corresponding solid-supported FLPs (*s*-FLPs) by addition of P^tBu_3 to the Lewis acids. s-FLPs are shown to activate H_2, D_2 and CD_3OD. The products are characterised by FTIR and solid state NMR (SSNMR) spectroscopy.

Chapter Five investigates the immobilisation of $B(C_6F_5)_2$ on a thermally pretreated aqueous miscible organic layered double hydroxide (AMO-LDH) support, and formation of LDH-FLP by addition of a Lewis base, P^tBu_3. The $B(C_6F_5)_2$ modified LDH-FLP is shown to react with H_2 and D_2 and the products are characterised by SSNMR and FTIR spectroscopy.

Chapter Six provides experimental procedures, characterisation techniques and data for those compounds described in the preceding chapters.

Acknowledgements

Firstly, I would like to express my sincere gratitude to Professor Dermot O'Hare, for granting me this valuable opportunity of coming to Oxford to conduct research in his group. I am grateful for the guidance, patience and continuous support he provided throughout my DPhil project. I am also very much thankful for his support of my various grant applications (LMH Warr-goodman Scholarship, LMH academic development fund, RSC travel bursary), which provided the funds necessary for me to be able to travel and present my research at domestic and international conferences (Main Group Discussion Group, Pacifichem 2015 in Hawaii and 250th ACS National Meeting in Boston).

I reserve my special thanks for JC, who kindly agreed to be my lab mentor and has been watching over my project since the start (I know I was a bit of a pain in the butt, but thanks for not giving up on me!). He taught me the skills of handling air and moisture sensitive compounds, the dark magic of recrystallisation, enforcing lab safety by being tidy (unlike our vibrant Duncan) and dressing appropriately (definitely no "short suits"), how to be efficient in the labs by making detailed daily and weekly schedules, and even how to write my very first scientific paper.

I owe huge a thank you to Dr Nick Rees who has been running my enormous pile of SSNMR samples, wandering tirelessly up and down the building, sweating away in the glovebox showing me how to pack and unpack the rotors. I must also thank Zoë, Tom and Sam for running my low-quality crystals and solving the distorted structures; Sandy for the BET samples; Chunping for TEM and SEM; Team solid-state (Chunping, Kate, Miaosen, Clara) for the insightful comments and stimulating discussions about silica and LDHs.

I am greatly indebted to all those who have put works aside to proof-read my thesis (Chris, Duncan, JC, Zoe, Sandy and Chunping). This wouldn't have been a more communicable piece of work without their critiques and suggestions.

I must also thank all O'Hare members past and present for making these past four years so enjoyable: Coops (my fume-hood neighbour) for teaching me the "Coops" style of organometallic chemistry, and the "authentic" way of making potassium mirrors; Mark Chadwick for teaching me how to safely dispose a late-night failed "uranium Grignard experiment", and maintaining the O'Hare clubbing and drinking traditions (PT and Gin/Rum); Safety Sam for showing me how to use the FTIR machine, the solvent stills, sharing her knowledge of FLP chemistry, and most importantly making delicious dinners and cakes; Tom Arnold for inviting me to wine tastings twice every week, stretching my alcohol tolerance enormously, and teaching me the skills of blind tasting; Dr always-Wright for his Friday football sessions, expertise in fire suppression, and skilful addition of water to pyrophoric compounds; vibrant Duncan for the ambiguous reverse hand quotation gesture, stimulating discussions about FLP chemistry, and the good collection of dirty glassware at the back of his fume-hood; good Golf and bad Phoom for demonstrating how to have a great work/life balance; Haohong for setting an example of a bad work/life balance; two-pint Henry for showing his expert dancing skills at college balls and night clubs; Yue for the food pantry, group cinema & dinner events and enforcing afternoon teas. I will miss all of you dearly when I leave Oxford.

Last but not the least, I would like to thank all my family members and friends who have been encouraging me, supporting me both spiritually and emotionally during my DPhil and throughout my life.

Abbreviations

1	$B(C_6Cl_5)(C_6F_5)_2$
η_Q	asymmetry parameter
$\Delta\delta_{m,p}$	δp-$C_6F_5 - \delta m$-C_6F_5
AMO-LDH	Aqueous miscible organic layered double hydroxide
^{t}Bu	*tert*-Butyl
CP	Cross polarisation
C_Q	Quadrupolar coupling constant
DP	Direct polarisation
EXAFS	Extended X-ray absorption fine structure
XANES	X-ray absoprtion near edge structure
FLP	Frustrated Lewis Pair
FTIR	Fourier-Transform Infrared
Fxyl	3,5-bis-trifluoromethylphenyl
HahnEcho	Erwin Hahn spin echo
HPDEC	High power decoupled
LA	Lewis Acid
LB	Lewis Base

LDH-BCF	$Mg_3Al\text{-}CO_3/B(C_6F_5)_2$
LDH-FLP	$Mg_3Al\text{-}CO_3/[B(C_6F_5)_2/P^tBu_3]$
Me	Methyl
Mes	Mesityl
$Mg_3Al\text{-}CO_3$	$[Mg_6Al_2(OH)_{16}]CO_3{\cdot}4H_2O$
POSS	Polyhedral oligomeric silsesquioxanes
***s*-BCF**	$[\equiv SiOB(C_6F_5)_2]$
***s*-BFxyl**	$[\equiv SiOB(Fxyl)_2]$
***s*-FLP1**	$[\equiv SiOB(C_6F_5)_2/P^tBu_3]$
***s*-FLP2**	$[\equiv SiOB(Fxyl)_2/P^tBu_3]$
SSNMR	Solid-state nuclear magnetic resonance
$SiO_{2\text{-}500}$	Silica thermally treated at 500 °C under vacuum for 6 hours
o-Tolyl	*ortho*-Tolyl
p-Tolyl	*para*-Tolyl
T_8	$(C_4H_9)_8Si_8O_{12}$
MAS	Magic angle spinning

Table of Contents

CHAPTER ONE

Introduction

1.1 Overview

This thesis discusses the investigation of small molecule activation using metal-free frustrated Lewis pairs (FLPs), and the immobilisation of active FLPs on silica, and a layered double hydroxide (LDH), thus developing heterogeneous FLP catalysts potentially suitable for industrial applications. The capability to heterolytically split H_2, and the possibility to hydrogenate CO_2 and other small molecules using these FLPs will be described in the following chapters. The focus of this chapter is to summarise the requirement for renewable fuels, alternative methods and researches conducted into CO_2 reduction, FLP mediated small molecule activation, and recent development of solid-state FLP catalysts.

1.2 Fossil Fuel Depletion, CO_2 Emission and Global Warming

Ever since the industrial revolution, oil, coal and gas has been the main resources for the world energy supply. Currently, the global energy market which is worth around 1.5 trillion dollars is still dominated by fossil fuels.[1] According to the World Energy Outlook 2007, energy derived from fossil fuels will remain the major source, and is still expected to meet 84% of world energy demand in 2030. However, with the current consumption rate, these precious resources will diminish in the next 40-100 years under current estimates.[2] Despite the increased public attention and outrage after the recent Deepwater Horizon explosion incident, revealing the dangers involved in the hunt for fossil fuels, the energy

consumption and environmental burdens per capita continue to rise, especially in developing countries.[3]

The majority of the world's energy production relies on the combustion of fossil fuels, leading to the release of CO_2 into the atmosphere. In addition, fossil fuel power plants are responsible for nearly 40% of the total of emissions of carbon dioxide while exhaust gases from petrol engines accounts for about 13%.[4] Current estimation shows that CO_2 production by humans is almost double the amount that can be transformed *via* natural photosynthesis. This net increase in CO_2 emissions arguably contributes towards the increase in global temperature and climate change due to the generally recognised "greenhouse effect", thus has been regarded as a serious environmental hazard. Hence, the increasing concerns over environmental impacts have prompted the development of efficient CO_2 capture/storage and utilisation systems.[4–12]

In principle, strategies for tackling CO_2 emissions can be divided into three main categories: limiting the amount of CO_2 produced, efficient capture and storage of CO_2, and direct transformation of CO_2 into useful chemicals.[10–15] The first strategy requires strict regulations on reducing emissions, and switching from fossil fuel to renewable technologies such as biomass, nuclear, wind, hydro and solar power.[10,15–19] Effective capture and storage of CO_2 is a relatively well-established area, including the use of conventional scrubber agents such as monoethanolamine (MEA) and potassium carbonate, membrane separation technologies, and porous materials (e.g. molecular sieves and functionalised metal organic frameworks (MOF).[4–7,14,20,21]

CO_2 is the most economical and abundant carbon source, therefore it would be highly desirable to utilise CO_2 as C_1 building block for organic syntheses.[22] Utilisation of CO_2 through direct chemical transformation into useful materials not only contributes towards the mitigation of current environmental issues, but also provides opportunities for

the exploration of new concepts and industrial advancements.[23] However, CO_2 has not been used extensively as a carbon source in current laboratories, and only a limited few industrial processes utilise CO_2. This is primarily due to the thermodynamic stability of the CO_2 molecule (ΔG_f° = –396 kJ mol^{-1}), thus high energy substances with the aid of a catalyst under forcing reaction conditions are typically required for the transformation of CO_2 into other chemicals. Hydrogenation of CO_2 produces two class of compounds: Class A (chemicals, such as salicylic acid, polycarbonates, urea), and Class B (fuels, such as methane).[9,11,12,24] Methanol can be placed in the middle as it is both an industrial raw material and a suitable and proven fuel for current internal combustion engines (ICE).

1.3 The Methanol Economy

The depletion of fossil fuel reserves and ever increasing transportation vehicle density compelled scientists to search for alternative sources of the transportation fuels. It is particularly desirable if those fuels can be employed successfully in current engines with little or no modifications.[25,26]

Although H_2 can be generated from electrolysis of H_2O and used directly as a clean and renewable fuel, the storage and transportation of H_2 is highly inconvenient because of its extremely low boiling point (−253 °C) and highly explosive nature, making it less desirable as a fuel. However, methanol as a hydrogenation product of CO_2, is a proven fuel suitable for current internal combustion engine (ICE) due to its excellent combustion characteristics. Although it contains only about half the energy density of gasoline, it has a higher octane number of 108.[27,28] Since methanol is a room temperature liquid and has a high octane number, methanol has been used in race cars since the 1960s. Gasoline-powered cars can be modified to run on methanol at a very modest cost, therefore wide commercial use of methanol in ICE vehicles would therefore not represent any difficulties.

Table 1.1 Energy density by volume and octane number of various fuels.[27,28]

	Energy density by volume (MJ L^{-1})	**Octane number**
$H_{2(l)}$	10.1	>130
CH_3OH	15.6	108
Petroleum	34.2	86-93

Owing to the serious limitations to using hydrogen as fuel, Nobel Laureate George Olah proposed the "methanol economy" as a more feasible alternative. In this way, hydrogen can be stored by converting CO_2 to methanol. Since H_2 can be generated renewably by photoelectrolysis, combining with an efficient CO_2 reduction processes a neutral carbon cycle can be derived (Scheme 1.1).[26,29]

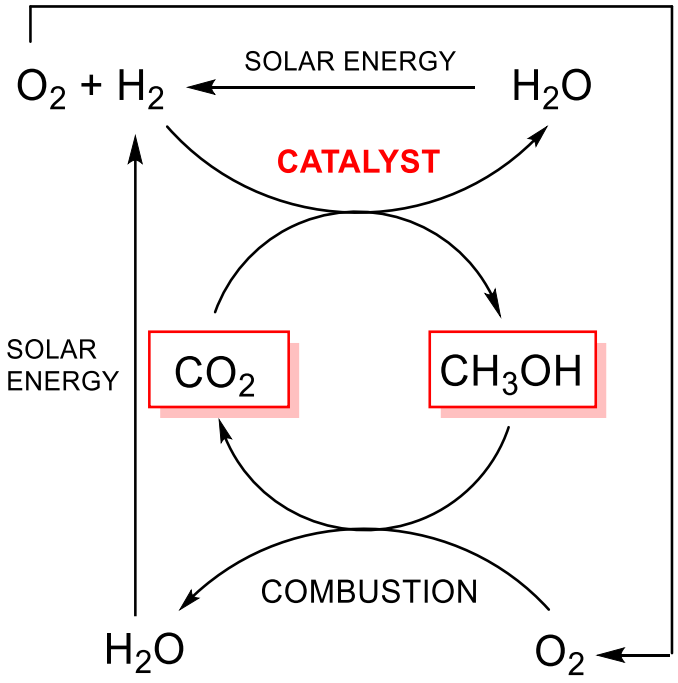

Scheme 1.1 Proposed methanol fuel cycle.[26,29]

1.4 Hydrogenation of CO_2 to Methanol

Catalytic hydrogenation of CO_2 to CO, methanol and other hydrocarbons *via* the reverse water gas shift (RWGS) reaction (Scheme 1.2, Eq 1) is thermodynamically favourable due to the concomitant production of H_2O, and has been regarded as the most promising process for chemical reduction of CO_2. Such process has been achieved using both homogeneous and heterogeneous catalysts.[10,13,22,30,31] The latter has been widely investigated and generally preferred due to their high stability, easy handling and product separation, facile catalyst recycling, and low running cost for large-scale production processes. However, only very few research papers have described the homogeneous catalysis of such reactions.

(1) $CO_2\ (aq) + H_2(aq) \longrightarrow CO\ (aq) + H_2O(l)$

$\Delta G° = 11\ kJ\ mol^{-1}; \Delta H° = 11\ kJ\ mol^{-1}; \Delta S° = -0.8\ kJ\ mol^{-1} K^{-1}$

(2) $CO_2\ (aq) + 3H_2(aq) \longrightarrow CH_3OH\ (aq) + H_2O(l)$

$\Delta G° = -79\ kJ\ mol^{-1}; \Delta H° = -106\ kJ\ mol^{-1}; \Delta S° = -88\ kJ\ mol^{-1} K^{-1}$

(3) $CO_2\ (aq) + 4H_2(aq) \longrightarrow CH_4\ (aq) + 2H_2O(l)$

$\Delta G° = -193\ kJ\ mol^{-1}; \Delta H° = -230\ kJ\ mol^{-1}; \Delta S° = -125\ kJ\ mol^{-1} K^{-1}$

Scheme 1.2 Thermodynamics of CO_2 hydrogenation.[32]

Although many metal-based catalysts have been studied for the heterogeneous hydrogenation of CO_2, the majority of the catalysts contain Cu as the main active component, together with different modifiers (Zn, Zr, Cr, Ni, Ga, Si, B, Cr, Ce, V, Ti

etc.).[33–35] Notably, ZnO can improve dispersion and stabilisation of Cu,[36,37] and the vacant lattice oxygen sites consisting of an electron pair has shown to improve the activity and selectivity of the Cu/ZnO catalyst for methanol production.[38] Moreover, SiO_2, Al_2O_3 and ZrO_2 have been considered as excellent stabiliser/promoter/support for methanol synthesis catalysts.[34,35,39,40] Whilst supporting Cu/ZnO on ZrO_2 and/or Al_2O_3 exhibit improved catalyst activity for methanol production than conventional Cu/ZnO due to the enhanced Cu dispersion on the surface,[35,41,42] addition of small amount of silica especially hydrophobic SiO_2 greatly improves the long-term stability of the catalyst allowing stable methanol production at temperature up to 270 °C .[35,43,44]

Noble metals are excellent candidates for H_2 activation, which have been used to improve the catalytic performance of Cu/ZnO. Melián-Cabrera *et al*. reported that using Pd to modify Cu/ZnO or Cu/Zn/Al_2O_3 leads to a highly reduced catalyst surface, which facilitates the hydrogenation process, and increases methanol yield.[45] In addition, supported Pd catalysts (on Ga_2O_3, ZnO, CeO_2) also demonstrated considerable activity and selectivity for methanol production from CO_2/H_2.[46,47] Liang *et al*. reported the development of Pd-ZnO immobilised on multi-walled carbon nanotubes, which exhibited excellent CO_2 hydrogenation to methanol performance.[48]

The use of noble metals for hydrogenation of CO_2 to methanol also extends to homogeneous catalysis. Ruthenium, rhodium, and palladium compounds have shown excellent CO_2 hydrogenation properties.[30] Watanabe and co-workers reported that $Ru_3(CO)_{12}$ in the presence of KI effectively catalyses RWGS reaction to give CO, which further reacts to give methanol and methane.[49,50] Although Rh and Pd complexes have been reported to catalyse formic acid production from CO_2, these complexes do not produce methanol.[32,51,52] In general, homogeneous noble-metal catalysts suffer some critical

drawbacks, including the expensive raw materials, sensitivity to air and moisture, side-product formation and low activity.

In recent years, metal-free catalyst for the hydrogenation of CO_2 to methanol have attracted considerable amount of attention. Ying *et al*. reported the first organo-catalytic reduction of CO_2 methanol by *N*-heterocyclic carbine (NHC) using hydrosilane as a source of hydrogen. Remarkably, the reaction proceeded under ambient conditions, and has demonstrated superior efficiency compared to metal catalysts in CO_2 hydrosilyation reactions.[53] In 2009, Ashley *et al*. demonstrated that CO_2 can be converted to methanol under H_2 by a metal-free species known as a "Frustrated Lewis Pair".[54]

1.5 Frustrated Lewis Pair

The concept of a Lewis acid and a Lewis base was first introduced by Lewis in 1923.[55] An electronically deficient substance that can accept a lone pair of electrons from another molecule is categorised as a Lewis acid, whereas any species that donates a lone pair of electrons to a Lewis acid (LA) is therefore classified as a Lewis base (LB). In general, a Lewis acid reacts with a Lewis base, resulting in the formation of a stable Lewis adduct as the product. However, if the steric bulk around the donor and acceptor atoms is sufficiently large, dative bond formation can be significantly hindered or even prevented, thus preserving the Lewis acidic and basic centres (Figure 1.1). One example was reported as early as 1942, by Brown and co-workers, when no reaction was observed between bulky Lewis base lutidine ($C_5H_3Me_2N$) and Lewis acid trimethylborane (BMe_3).[56] By comparing the molecular structure with other pyridine-borane adducts, it was suggested that this unexpected observation was due to steric repulsion of the methyl groups in the lutidine and trimethylborane. Although several examples of such unusual bulky Lewis acid and base pairs with non-classical behaviour have been discovered in the subsequent years, very little

research has been done on the chemical reactivity of these non-self-quenching systems in the past.[3] The term "Frustrated Lewis Pair" (FLP) was later coined by Stephan to describe such non-classical behaviour between bulky Lewis acids and bases (Figure 1.1).[57]

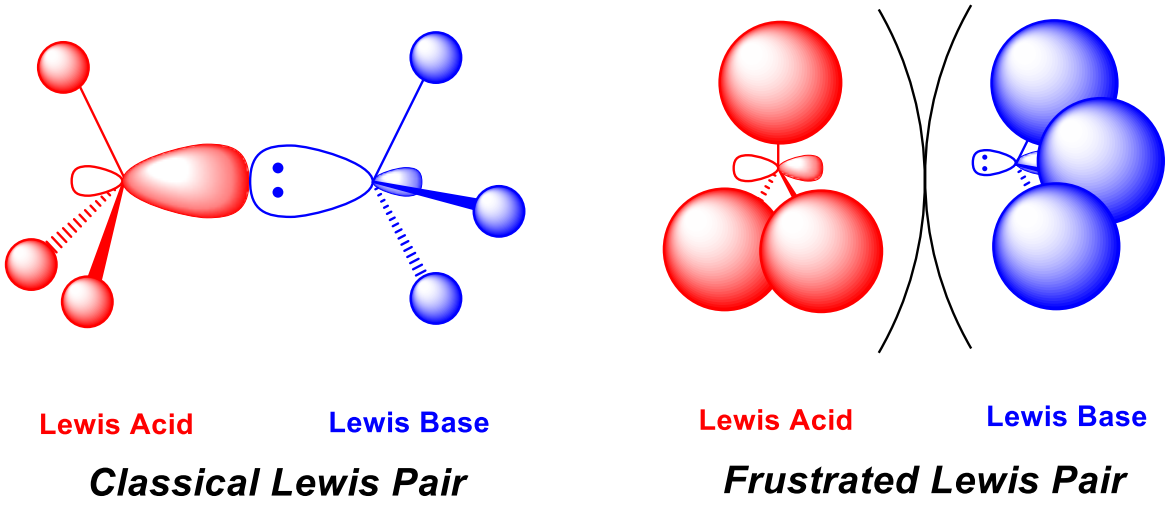

Figure 1.1 A classical Lewis adduct and a "Frustrated Lewis Pair"

1.5.1 Heterolytic H_2 Cleavage by Frustrated Lewis Pairs

While investigating the reactivity of such "frustrated" systems, Stephan and co-workers discovered a unique phosphino-borate system $(C_6H_2Me_3)_2PC_6F_4B(C_6F_5)_2$ which is capable of reversible H_2 activation (Scheme 1.3).[58] This important finding has countered the long-existed dogma that only transition metals are capable of performing such activation. Shortly after their initial discovery, Stephan and co-workers further demonstrated that by replacing the esoteric phosphino-borate systems with simpler combinations of sterically demanding PR_3 (R = ^{t}Bu , $C_6H_2Me_3$) and $B(C_6F_5)_3$ in 1:1 ratio led to the formation of unquenched systems that are also capable of heterolytic cleavage of H_2 to generate the corresponding $[R_3PH][HB(C_6F_5)_3]$.[59] However, in contrast to $(C_6H_2Me_3)_2PC_6F_4B(C_6F_5)_2$, $[R_3PH][HB(C_6F_5)_3]$ salts do not release H_2 even with heating to

above 100 °C. The Erker group extended such activation of H_2 by including intramolecular alkyl-bridged phosphine/borane Lewis pairs, which have demonstrated rapid H_2 cleavage properties. Interestingly, the species $(C_6H_2Me_3)_2PC_2H_4B(C_6F_5)_2$ have been found to exist in an equilibrium between four-membered Lewis adduct ring complex and open chain FLP.[60] These early works have prompted rapid expansion of the scope of Lewis acids and bases that generates FLPs by many research groups. Systematic studies have probed electrophilic Lewis acids (derived from group 13-15) in combination with Lewis basic nucleophiles (derived from group 14-16) in both intermolecular and intramolecular systems, demonstrating exceptional capacities to activate H_2.[61,62]

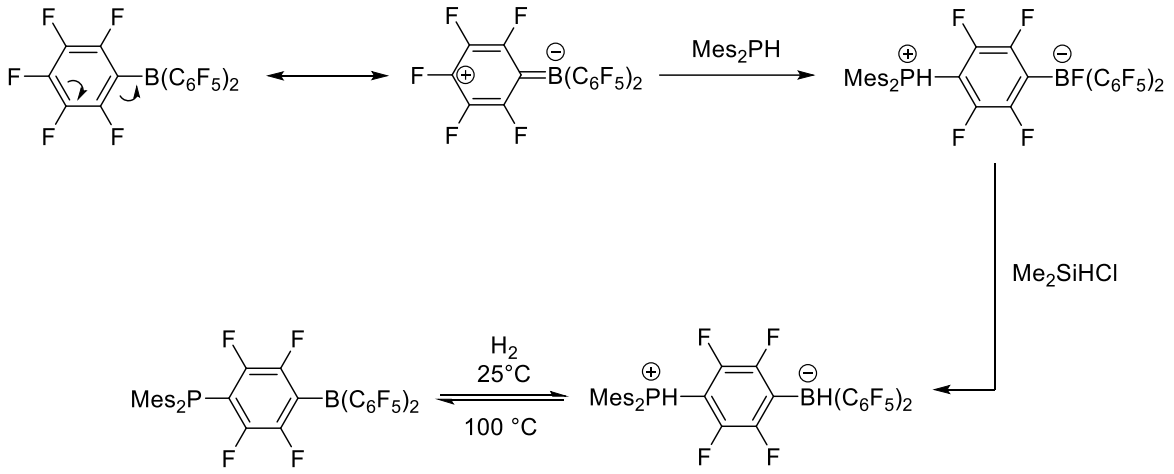

Scheme 1.3 First example of reversible H_2 activation by metal-free species.

It is now generally accepted that the electrostatic field that exists in the cavity of the frustrated Lewis pair plays a major role in the polarisation of the H−H σ bond in H_2, and enforcement of heterolytic cleavage (Figure 1.2). Computational theoretical analysis of H_2 cleavage by FLP by Grimme *et al*. revealed that sterically frustrated Lewis acid and base generate an "encounter complex", in which the steric hindrance precludes dative bond formation, but is stabilised by van der Waal's interactions.[63] The encounter complex then

reacts with H_2 in a bimolecular fashion to generate a high energy preparation state (prepared Lewis pair), and once H_2 enters the FLP interior, the H_2 heterolysis proceeds in an essentially barrierless way. Further analysis of the transition-state (prepared Lewis pair) showed that the entrance process involves bending of one of the aromatic ring in order to open up the FLP cavity. Subsequently, the H_2 molecule migrates into this cavity forming a non-linear encounter complex with a B-H-H angle of approximately 140°,[63] as opposed to the linear model initially proposed by Pápai.[64]

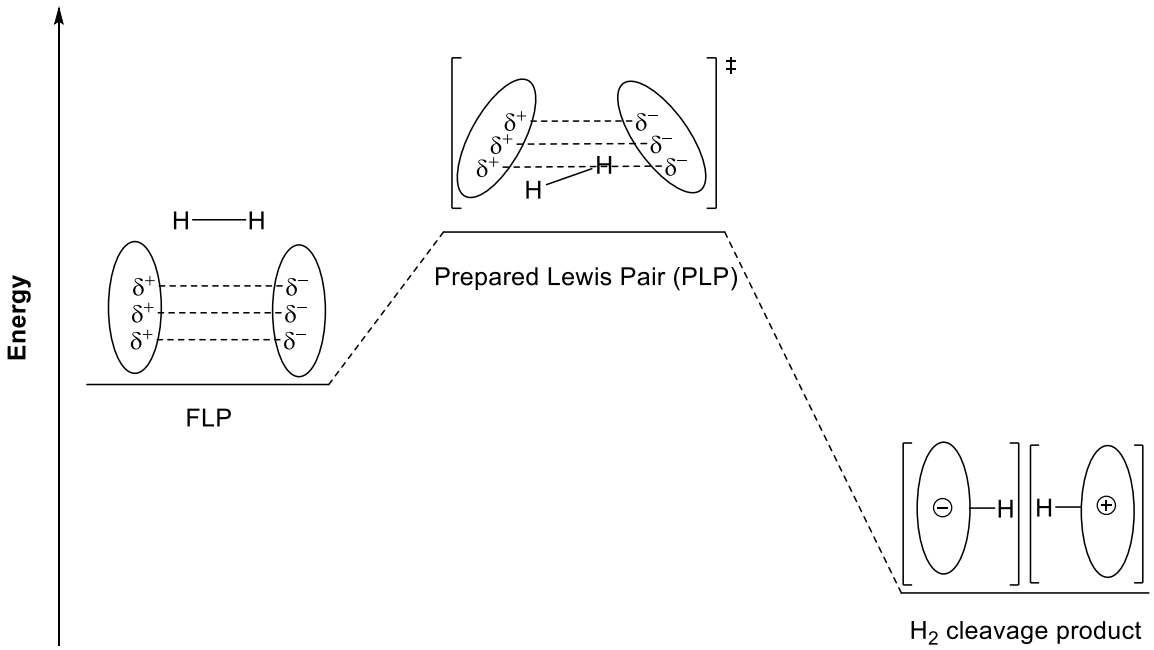

Figure 1.2 Simplified model for FLP mediated H_2 heterolytic cleavage showing a non-linear encounter complex as the transition state.[63]

1.5.2 FLP mediated Catalytic Hydrogenation

Hydrogenation lies at the heart of many important industrial chemical transformations, ranging from upgrading of crude oil to synthesis of pharmaceutical, agricultural and fine chemicals.[65] The majority of hydrogenation catalysts currently employed by industries are metal based homogeneous or heterogeneous catalysts,[66,67]

however, non-biological metal-free systems that reversibly activate H_2 are rare. The main issue with using transition metal based catalysts despite their high activity, is the possible contamination of the final product with trace metals. For some industries, especially in fine chemicals and pharmaceuticals, presence of even trace amounts of toxic metals cannot be tolerated. Therefore, replacement of transition metal catalysts with metal-free main group catalysts without sacrificing the catalytic properties is of high interest.[68]

Stephan and co-workers demonstrated that the $(C_6H_2Me_3)_2PC_6F_4B(C_6F_5)_2$ and $B(C_6F_5)_3$ system can be applied to metal-free hydrogenation catalysis,[58] and showed the capability of reducing imines (Scheme 1.4a), nitriles and aziridines with molecular hydrogen to produce primary and secondary amines in high yields under relatively mild conditions.[69–71] This hydrogenation strategy was subsequently extended to include the reduction of enamines[60] and silyl enol ethers[72] using related $(C_6H_2Me_3)_2PC_2H_4B(C_6F_5)_2$ and $C_{10}H_6(PPh_2)_2/B(C_6F_5)_3$ FLP catalysts respectively (Scheme 1.4b and Scheme 1.4c). These initial works have prompted substantial efforts into the development of alternative metal-free FLP systems that are capable of reducing a wider range of substrates.[61,62,73–80]

Hydrogenation of carbonyl derivatives are of high interest. However, due to the high oxophilicity of boron and generation of the highly stable B−O bond in the reduction intermediates, application of FLPs in catalytic hydrogenation of carbonyls was deemed unlikely. Indeed, Longobardi and co-workers reported that initial attempts to hydrogenate ketones and aldehydes in toluene has resulted in the formation of stable boronic esters.[81] Recently, Stephan and Ashley have simultaneously found that conducing hydrogenation of ketone and aldehydes to their corresponding alcohols by $B(C_6F_5)_3$ in ethereal-solvents had enabled catalytic turnovers with conversions >99% under mild reaction conditions (Scheme 1.4c).[82,83] The mechanism for the hydrogenation was suggested to occur *via* initial hydrogen cleavage by ether/$B(C_6F_5)_3$ followed by carbonyl activation by hydrogen

bonding of the protonated ether, then hydride delivery from $B(C_6F_5)_3$ and regeneration of ether/$B(C_6F_5)_3$. Interestingly, a combination of molecular sieve and $B(C_6F_5)_3$ in toluene also enabled catalytic hydrogenation or even reductive deoxygenation of ketones and aldehydes.[84] In the effort to broaden the substrate scope, the Stephan group has applied FLP hydrogenation to *N*-heterocycles, including substituted quinnoline, phenanthrolin, acridine and several indole derivatives.[85] Soós *et al*. achieved catalytic reduction of *N*-heterocycles using sterically encumbered borane $B(C_6F_5)_2(C_6H_2Me_3)$ with yields generally exceeding 80% (Scheme 1.4e).[86]

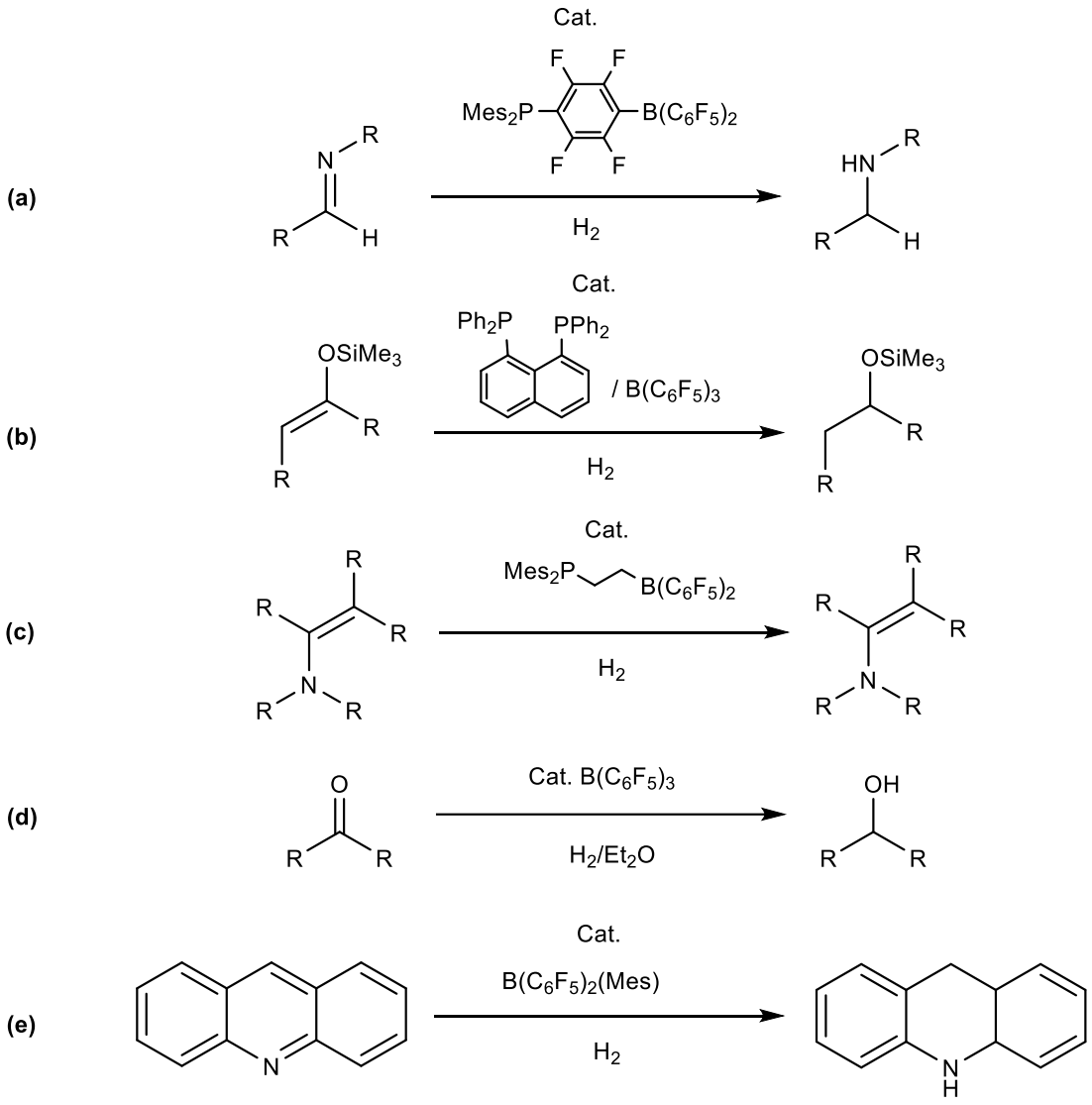

Scheme 1.4 Examples of FLP catalysed hydrogenation of polar substrates.[58,60,72,82,83,86]

Seeking to further broaden the substrate scope for FLP hydrogenations, the Paradies group worked jointly with Stephan and Grimme *et al*. to study FLP hydrogenation of olefins (Figure 1.5a).[87] The investigation was initiated by employing a weakly basic phosphine $(C_6F_5)Ph_2P$ in combination with $B(C_6F_5)_3$ to generate an FLP, which showed no signs of reaction when exposed to H_2 at 25 °C. However, when the mixture was cooled, reversible H_2 activation was observed in the temperature range between −60 and −80 °C. More importantly, this process generates a highly acidic conjugate acid ($[HP(C_6F_5)Ph_2]^+$ cation) that is capable of protonating olefinic double bonds, generating an electrophilic carbocation capable to accept a hydride from the borohydride anion ($[(C_6F_5)_3BH]^-$) to afford the corresponding reduced hydrocarbon and regeneration of the FLP catalyst. The Stephan group subsequently demonstrated that combination of Et_2O with BCF can also effect catalytic hydrogenation of olefins.[88] Building on these initial findings, Paradies *et al*. realised that in contrast to the previous olefin reductions, the mechanism to which electron deficient nitro-olefins are reduced follows a reversed order of proton and hydride delivery (Figure 1.5b).[89–91] In related fashion, Alcarazo and co-workers demonstrated catalytic reduction of allenic esters using a combination of $B(C_6F_5)_3$ and either (1,4)-diazabicyclo[2.2.2]octane (DABCO) or 2,6-lutidine (Figure 1.5c).[92] Subsequently, Paradies *et al*. showed catalytic hydrogenation/hydrosilylation of enones using a [2,2]paracyclophane derived bisphophine/$B(C_6F_5)_3$ FLP.[93] Moreover, Soós *et al*. also demonstrated catalytic reduction of carvone to the corresponding ketone using $B(C_6F_5)_3$/DABCO FLP.[94] Remarkably, Repo *et al*. further extended the scope of substrate, effecting selective catalytic reduction of nonfunctionalised alkynes to give *cis*-alkenes using intramolecular $C_6H_4(NMe_2)B(C_6F_5)_2$ (Figure 1.5d).[95] Mechanistic studies revealed that the active species responsible for the alkyne reduction was $C_6H_4(NMe_2)BH(C_6F_5)$ (product derived from protonation of the parent FLP liberating C_6F_5H).

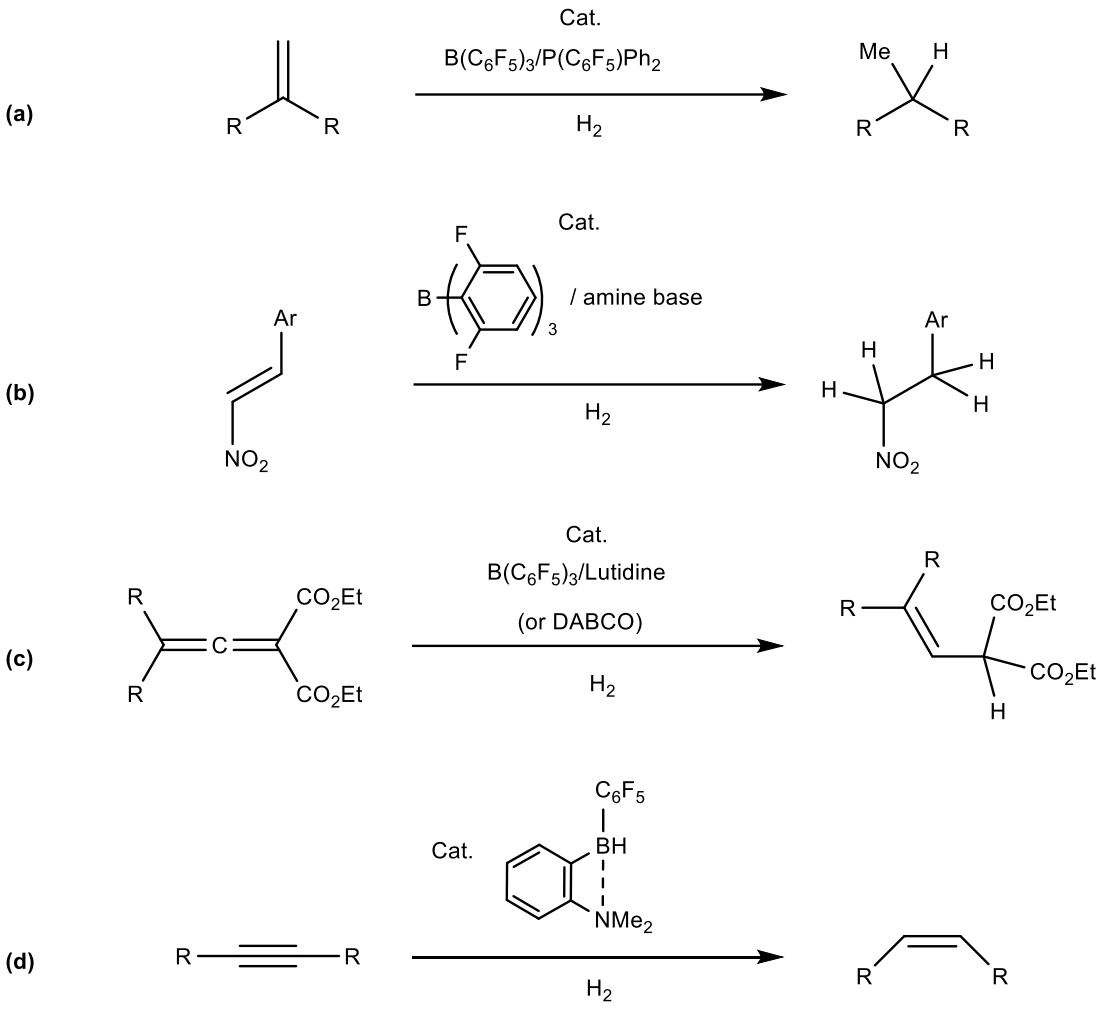

Scheme 1.5 Examples of FLP catalysed hydrogenation of olefins.[87,90,92,95]

1.5.3 Broadening the Scope of FLP for H_2 Activation

Modifications of FLP catalysts for asymmetric reduction began in 2010, with the development of a chiral B/P FLP catalyst from the Klankermayer group, which is capable of asymmetrically hydrogenating imines with 83% enantioselectivity (Scheme 1.6a).[96] Recently, Liu and Du developed a highly active and simpler chiral bisborane catalyst (*in situ* derived from binaphthyl chiral dienes) with an improved selectivity for imine reduction (89% ee) (Scheme 1.6b).[97] Repo and co-workers further extended the use of chiral binaphthyl diene ligands by developing highly active aminoborane catalysts, which have exhibited exceptional asymmetric hydrogenation of imines and enamines with

selectivities up to 99% ee (Scheme 1.6c).[98] In related reports, Du *et al*. extended the substrate scope to include silyl enol ethers,[99] pyridines,[100] and a range of 2,3-disubstituted quinoxalines,[101] to give the corresponding chiral alcohol, *cis*-piperidines, and tetrahydroquinoxalines, with selectivities up to 96% ee. Most recently, Du *et al*. achieved highly enantioselective hydrosilylation of 1,2-dicarbonyl compounds using chiral bisborane combined with PCy_3 (Cy = cyclohexyl), to give the corresponding chiral α-hydroxy aldehydes and ketones with selectivities up to 99% ee.

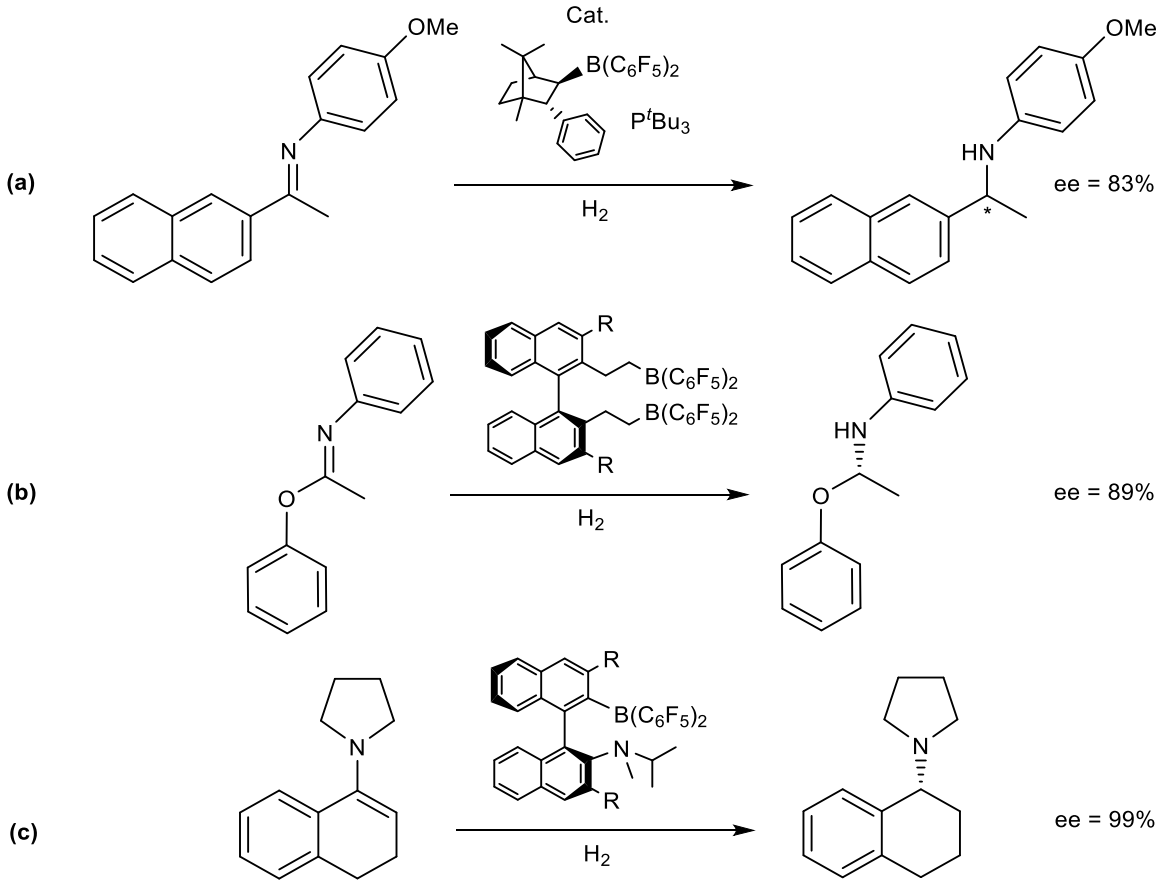

Scheme 1.6 Example reaction of asymmetric hydrogenations by chiral FLP catalysts

Ashley *et al*. synthesised a family of electron deficient boranes $B(C_6Cl_5)_n(C_6F_5)_{3-n}$ (where n = 1-3) derived from the parent Lewis acid $B(C_6F_5)_3$ (Figure 1.3).[102] Such stereoelectronic modification of $B(C_6F_5)_3$ showed that although electrophilicity increases

with increased number of C_6Cl_5 groups, the Lewis acidity decreases due to the steric hinderance. In 2014, Ashely and co-workers demonstrated that $B(C_6Cl_5)(C_6F_5)_2$ and $B(C_6Cl_5)_2(C_6F_5)$ bind reversibly to THF (whereas $B(C_6F_5)_3$ ring opens THF) at room temperature, and showed that these combinations effectively catalyse imine hydrogenations. However, no reactivity was observed with extremely hindered fully substituted $B(C_6Cl_5)_3$.[103] In an alternative approach, Herrington and co-workers synthesised $B(C_6H_3(m\text{-}CF_3)_2)_3$.[104] In contrast to $B(C_6F_5)_3$, 2p-2p orbital interaction between F and aromatic-C is absent in $B(C_6H_3(m\text{-}CF_3)_2)_3$, which lowers π-basicity and hence susceptibility to B−C bond cleavage. $B(C_6H_3(m\text{-}CF_3)_2)_3$ exhibited similar Lewis acidity to $B(C_6F_5)_3$ according to Child's method, and demonstrated H_2 activation when combined with 2,6-tetramethylpiperidine (TMP). Interestingly, a bridging hydride (B−H−B) was observed in the crystal structure of the H_2 activation product, and remarkably this reaction can even be performed in Et_2O. In further efforts to extend the functional group tolerance, the Soós group introduced the concept of "size exclusion", and prompted the notion that steric congestion around the Lewis acid centre would prevent reactions with donor molecules such as H_2O, but allows reaction with H_2, thus developing moisture tolerant FLP catalysts for effective reduction of carbonyls under mild conditions.[77]

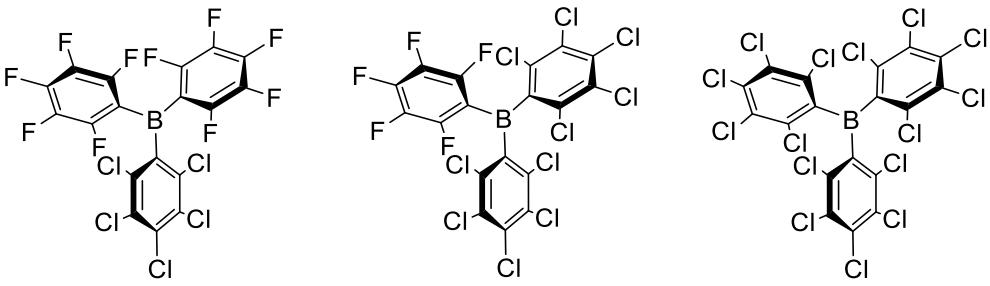

Figure 1.3 Electrophilic boranes developed by Ashley *et al*.[102]

The scope of FLP catalysts have extended beyond electrophilic boranes. The Stephan group demonstrated that an *N*-heterocyclic carbene-stabilised borenium salt $[(IiPr)BC_8H_{14}][B(C_6F_5)_4]$ (IiPr = 1,3-di-iso-propylimidazol-2-ylidene) accessed *via* hydride abstraction from the NHC-borane adduct can also be used to catalyse hydrogenation of imines and enamines (Figure 1.4a).[105,106] Subsequently, Crudden *et al*. developed mesoionic *N*-heterocyclic carbene-stabilised borenium catalysts, which have shown superior catalytic properties for imine and *N*-heterocycle reductions than the conventional NHC-borenium catalysts (Figure 1.4b).[107] The Ingleson group developed a bifunctional acridine-bound borenium cation that is capable to act as a Lewis acid either at the boron centre or at the C9 position of the acridine, depending on reaction conditions, which cleaved H_2 in the presence of a Lewis base (Figure 1.4c).[108] More recently, Clark and Ingleson effected H_2 activation using air and moisture stable carbon Lewis acid *N*-methylacridinium salt combined with 2,6-lutidine (Figure 1.4d).[109]

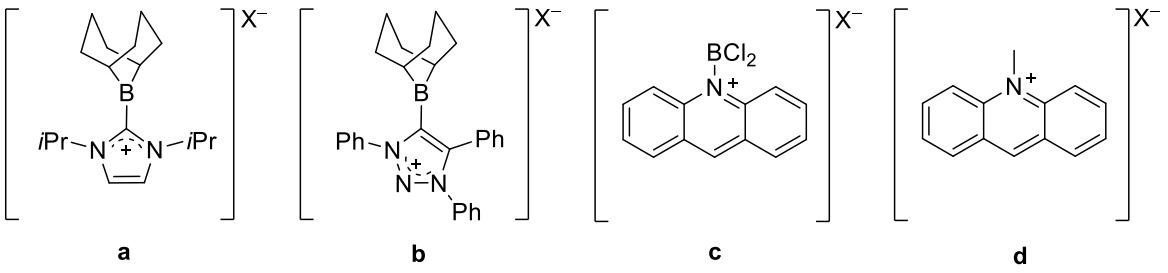

Figure 1.4 Examples of borenium and aridinium Lewis acids.

Silicon-based FLPs were first reported by the Müller group, demonstrating that combination of $[(C_6Me_5)_3Si]^+/[B(C_6F_5)_4]^-$ and $PMes_3$ acted as an FLP, capable of H_2 activation to give corresponding silane and phosphonium borate.[110,111] In a related study, Müller and co-workers developed silylene/silylium FLP capable of H_2 activation at ambient temperature and pressure (Scheme 1.7a).[112] Subsequently, Ashley *et al*. showed

that silylium-phosphine adduct activates H_2 at elevated temperature, presumably *via* thermal dissociation in solution to generate solvated silylium ion and free phosphine.[113]

Phosphenium cations are known to exhibit Lewis acidity. Although they are not widely used in FLP chemistry.[114] The Stephan group recently reported a triphosphabenzene derivative, which exhibited heterolytic cleavage of H_2 (Scheme 1.7b).[115] The proposed mechanism for the H_2 activation involve the resonance structure of the triphosphabenzene in which the positive charge on the phosphorus at 1−position and the negative charge on the carbon at 4−position act as an intramolecular FLP to cleave the H_2 molecule. Building on this notion of phosphorus as a Lewis acid, Caputo and Stephan synthesised highly electrophilic organofluorophosphonium cations as potential Lewis acids for FLP catalysis.[116] In contrast to electrophilic boranes where the Lewis acidity arises from a vacant *p*-orbital, phosphonium cations derives their Lewis acidity from a low lying σ* acceptor orbital orientated opposite the electron withdrawing substituents.[117] Utilising these this Lewis acidity, Stephan *et al*. have shown that electrophilic phosphonium cations are more Lewis acidic than conventional boron-based Lewis acids, and are effective catalyst for hydrodefluorination of fluoroalkanes,[116] dehydrocoupling of silanes with carboxylic acids, olefins, thiols and alcohols,[118] hydrosilylation of olefins, alkynes,[119] and C-F alkylation catalysis.[120–122] Furthermore, combination of $[FP(C_6F_5)_3][B(C_6F_5)_4]$ with sterically encumbered aryl-substituted amines have shown reversible H_2 activation, and catalytic hydrogenation of olefins.[123]

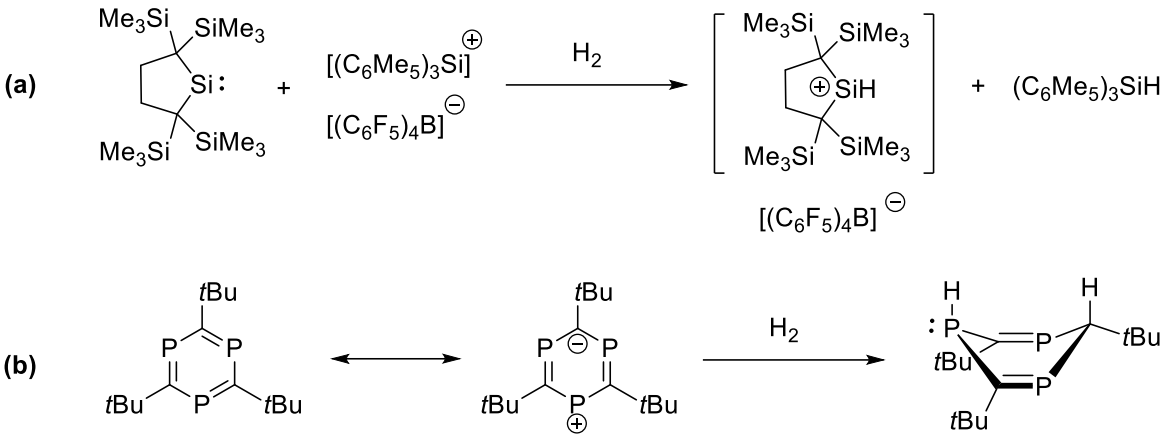

Scheme 1.7 Examples of H_2 activation by FLPs using silicon- and phosphorus-based Lewis acids.

1.5.4 Small Molecule Activation by FLPs

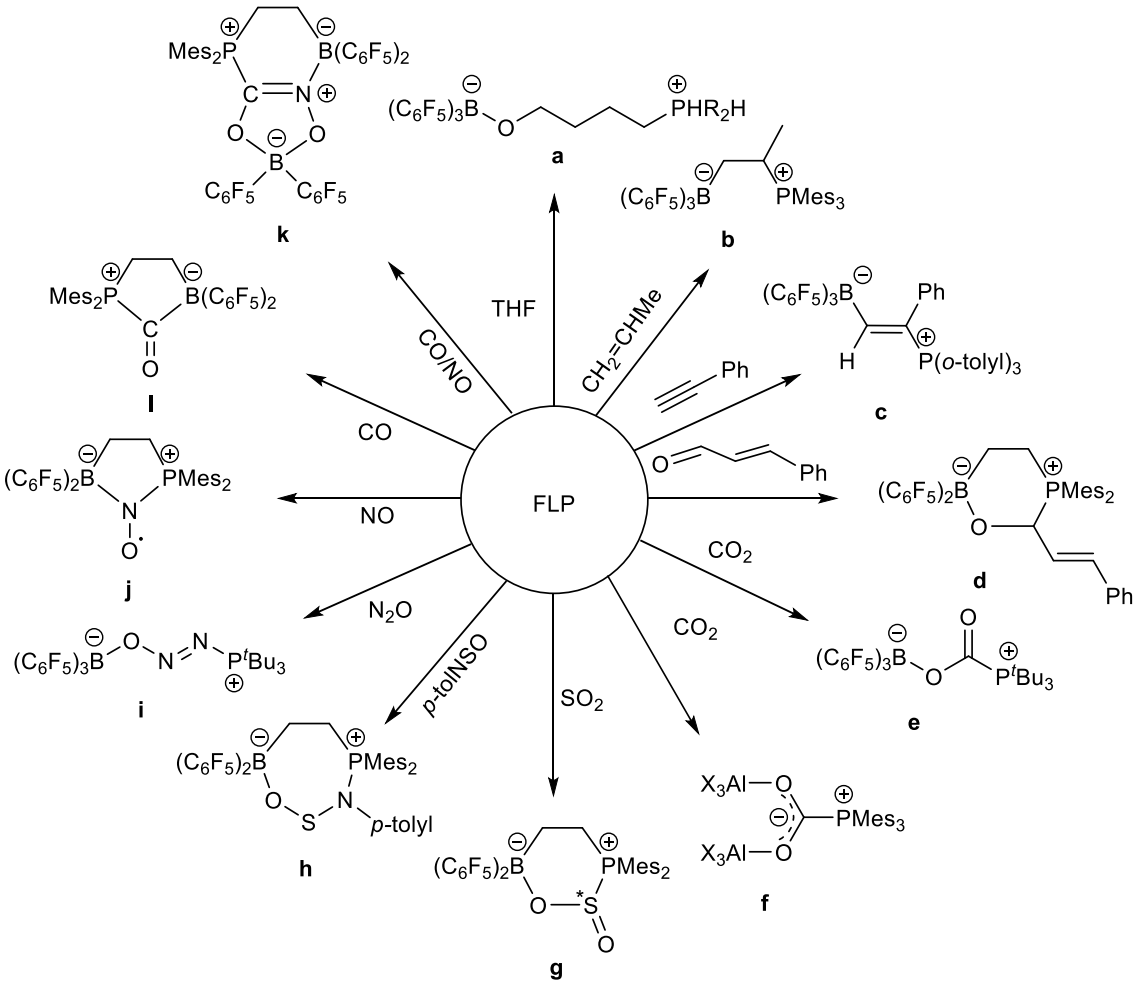

Figure 1.5 Examples of FLP reactions with small molecules

Activation of small molecules by FLPs extends well beyond heterolytic cleavage of H_2. One of the earliest example of FLP reaction with small molecule was the ring opening of THF using a combination of $B(C_6F_5)_3$ and HPR_2 (R = Mes, ^{t}Bu) to afford zwitterionic species $[R_2PH(CH_2)_4OB(C_6F_5)_3]$ (Figure 1.5a).[124] Subsequently, Stephan *et al*. showed that frustrated Lewis pairs react with alkenes *via* 1,2-addition reactions. For example, exposure of a solution of a solution containing $B(C_6F_5)_3$ and $PMes_3$ to $MeCH{=}CH_2$ led to the formation of zwitterionic species $[Mes_3PCH(CH_3)CH_2B(C_6F_5)_3]$ (Figure 1.5b).[57] X-ray data confirmed that the boron centre adds to the less hindered carbon atom.

FLPs have also been found to react with alkynes in a similar fashion. Dureen and Stephan reported that FLPs generated from a combination of $B(C_6F_5)_3$ or $(PhMe)Al(C_6F_5)_3$ and P(*o*-tolyl)$_3$ reacts with terminal alkyne PhC≡CH, to give the corresponding zwitterionic 1,2-addition products in a general formula of [*E*-(*o*-tolyl)$_3$P(Ph)C=C(H)E$(C_6F_5)_3$], (E = B, Al), where the Lewis acids added to the less substituted end of the alkyne (Figure 1.5c).[125] In marked contrast, when $B(C_6F_5)$ or $(PhMe)Al(C_6F_5)_3$ combined with P^{t}Bu$_3$, reaction with the same alkyne produced C−H activation products [Ph−≡−E$(C_6F_5)_3$][HP^{t}Bu$_3$], (E = B, Al). The Stephan group also probed the reactivity of FLPs with conjugated dienes, and found that the addition reactions are predominately 1,4-addition (Scheme 1.8a).[126] Thus in the reaction of $B(C_6F_5)_3$/P^{t}Bu$_3$ with butadiene, 2,3-dimethylbutadinene, 2,3-diphenylbutadiene, and 1,3-cyclohexadiene, corresponding 1,4-addition products were isolated in moderate yields (50-60%). In related chemistry, Erker and co-workers, showed that intramolecular FLP $Mes_2P(C_2H_4)B(C_6F_5)_2$ reacts with norbornene, yielding exclusively *exo*-addition product (Scheme 1.8b).[127] In the same report, Erker *et al*. also demonstrated 1,2-addition reactions of $Mes_2P(C_2H_4)B(C_6F_5)_2$ to a range carbonyl compounds. Remarkably, intramolecular FLP $Mes_2P(C_2H_4)B(C_6F_5)_2$

reacted with bifunctional *trans*-cinnamic aldehyde selectively at the C=O moiety instead of at the C=C double bond position (Figure 1.5d).

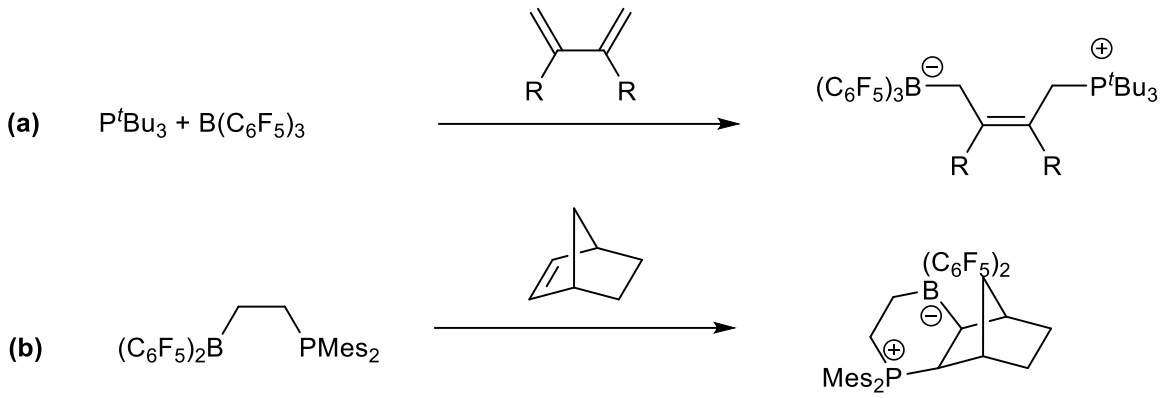

Scheme 1.8 Addition reactions of FLPs with conjugated diene and norbornene.

Building on these initial findings, Stephan *et al*. and Erker *et al*. attempted activation of CO_2 in a collaborative study, and discovered that CO_2 reacted with inter- and intramolecular FLPs in a straight forward fashion.[128] For example, $B(C_6F_5)_3/P^tBu_3$ added across one of the C=O double bonds of CO_2 in bromobenzene at room temperature, with the formation of B−O and P−C bonds, to generate a zwitterionic boronic ester $(C_6F_5)_3BOC(O)P^tBu_3$ with an isolated yield of 89% (Figure 1.5e). Interestingly, heating to above 70 °C resulted in the liberation of CO_2 and concurrent generation of the starting FLP, indicating that the process is reversible. In contrast, reaction of intramolecular FLP $Mes_2P(C_2H_4)B(C_6F_5)_2$ with CO_2 resulted in the formation of a six-membered cyclic boronic ester in 79% yield. While the cyclic CO_2 adduct is reasonably stable in the solid form, it was found to rapidly lose the bound CO_2 at temperatures above 20 °C when dissolved in CH_2Cl_2 or toluene, to return to the starting intramolecular FLP $Mes_2P(C_2H_4)B(C_6F_5)_2$.[128] Lammertsma and co-workers synthesised germinal phosphine-borane species $^tBu_2PCH_2BPh_2$ and demonstrated effective CO_2 capture.[129] Tamm and co-workers also

showed that intramolecular B/N FLP $(C_3H(^tBu)_2N_2)B(C_6F_5)_2$ binds CO_2 to give $(C_3H(^tBu)_2N_2)B(C_6F_5)_2(CO_2)$ adduct in strongly exothermic reaction.[130]

Recently, the thermodynamics of CO_2 capture by FLPs was studied by the group of Kumacheva using microfluidic method,[131,132] passing CO_2 through a microfluidic channel containing a solution of $B(C_6F_5)_2Cl$ and P^tBu_3. The gas bubbles were observed to shrink as the bubble flows through the channel, which results from CO_2 reaction with the FLP in the solution. These data enable the determination of the fundamental thermodynamics of the gas/liquid reaction of CO_2 and FLP. More recently, an elegant computational study by Pu and Privalov on the formation of $(C_6F_5)_3BOC(O)P^tBu_3$ complex revealed that the mechanism for CO_2 capture by $B(C_6F_5)_3/P^tBu_3$ follows a two-step reaction process as opposed to the concerted reaction-path paradigm.[133] The first step involves a nucleophilic attack at the C-atom by P^tBu_3 to generate a $\{^tBu_3P\cdots CO_2\}$ intermediate complex, which results in bending of the O=C=O angle and P−C bond formation, followed by B−O bond formation as the second step (Figure 1.6).

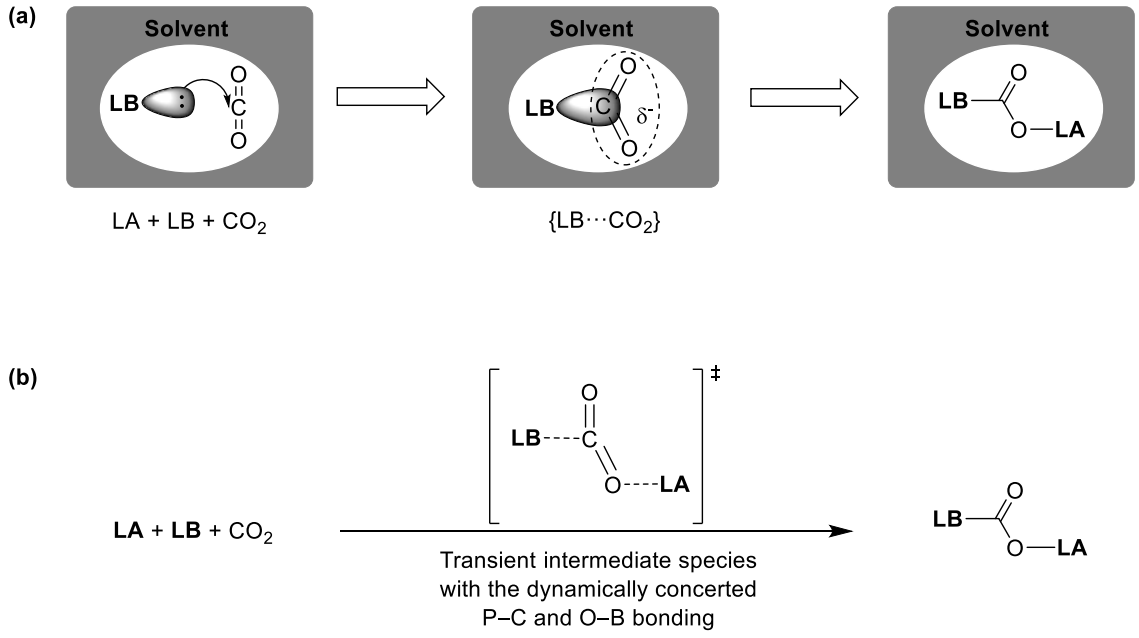

Figure 1.6 Mechanism of CO_2 capture by an FLP: (a) the recently discovered two-step reaction process and (b) the known one-step reaction process.

It is also possible for both oxygen atoms in CO_2 to participate in binding to Lewis acidic centres. Using Al-based Lewis acid, Ménard and Stephan showed that 2:1 mixture of $AlX_3/PMes_3$ reacts with CO_2 to form $Mes_3P(CO_2)(AlX_3)_2$ (X = Cl, Br) (Figure 1.5f), where the phosphine is bound to the C-atom while AlX_3 units are bonded to each of the O-atoms.[134] Stephan and co-workers also probed the reactivity of bisboranes and phosphines with CO_2.[135] A combination of $Me_2C{=}C(BX)_2$ and P^tBu_3 reacted with CO_2 to give heterocyclic species $Me_2C{=}C(BX)_2O_2CP^tBu_3$ (X = Cl, C_6F_5) which both oxygen atoms of CO_2 are boron bound.

Building on the notion of CO_2 activation by frustrated Lewis pairs, Ashley *et al*. demonstrated the stoichiometric hydrogenation of CO_2 by metal-free frustrated Lewis pairs.[54] The $B(C_6F_5)_3$/TMP system successfully reduced CO_2 to yield a methoxyborate species $[(C_6F_5)_3BOCH_3][H{-}TMP]$ after 6 days at 160 °C (Scheme 1.9). NMR spectroscopic analyses of the reaction mixture revealed the presence of small quantities of formatoborate species $[(C_6F_5)_3BOC(O)H][H{-}TMP]$ as a reaction intermediate. Attempted isolation of methanol from the reaction mixture *via* vacuum distillation at 160 °C allowed small quantities of methanol to be extracted (17-25%) at the sacrifice of the FLP.

In 2011, Tran *et al*. also attempted CO_2 hydrogenation using a $B(C_6F_5)_3$/lutidine system, which resulted in the formation of formatoborate species $[(C_6F_5)_3BOC(O)H][H{-}Lut]$.[136] However, the attempt to further reduce the formatoborate species to the methoxyborate species was unsuccessful. In an alternative approach, Piers and co-workers used Et_3SiH as an hydride source to convert CO_2 to CH_4 using $B(C_6F_5)_3$/TMP system.[137] Stephan also showed successful reduction of CO_2 to methanol using $PMes_3/AlX_3$ in the presence of ammoniaborane as an alternative hydrogen source for the reduction process.[134] In a related study, Stephan *et al*. reported the hydroboration of CO_2 to methoxyborane using a intramolecular FLP derived from the reaction of

N,N'-diphosphanyl-imidazol-2-ylidene and 9-BBN (9-borabicyclo[3.3.1]nonane).[138] Subsequently, Wang and Stephan reported that phosphine can also be used to catalyse the reduction of CO_2 to methoxyborate using 9-BBN as the reducing reagent.[139] Remarkably, Dobrovetsky and Stephan achieved catalytic CO_2 reduction to CO mediated by *in situ* generated *bis*-phosphaylide and $ZnBr_2$, with excess phosphine.[140] Fontaine *et al*. reported one of the most efficient system for the catalytic hydroboration of CO_2 to date, using ambiphilic intramolecular FLP 1-Bcat-2-PPh_2-C_6H_4 (Cat = catechol) in the presence of a range of hydroboranes (HBR_2 = HBCat, HBPin (pinacolborane), 9-BBN, $BH_3{\cdot}SMe_2$ and $BH_3{\cdot}THF$) to generate methoxyborate species CH_3BR_2 or $(CH_3OBO)_3$ with turn over frequency over 900 h^{-1} at 70 °C.[141,142] Subsequently, the same group demonstrated stoichiometric hydrogenation of CO_2 to give a mixture of formato- and methoxyborate species using intramolecular B/N FLP 1-$BMes_2$-2-NMe_2-C_6H_4 under mild reaction conditions compared to the $B(C_6F_5)_3$/TMP system reported by Ashley *et al*.

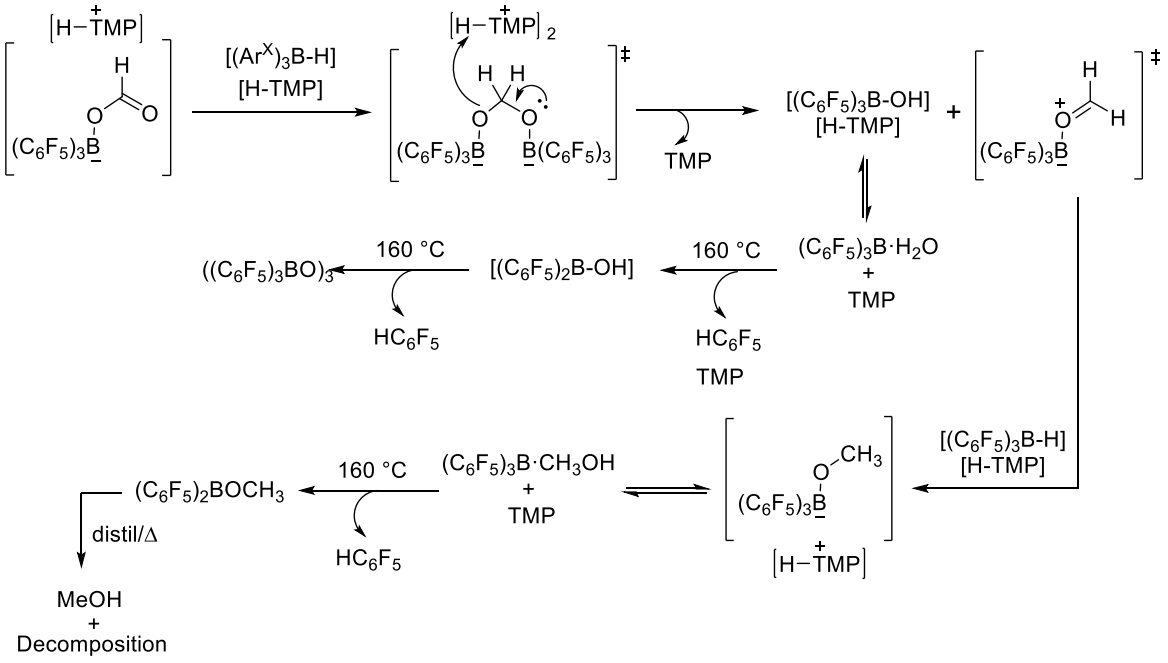

Scheme 1.9 Proposed mechanism for the conversion of $[(C_6F_5)_3BOC(O)H][TMPH]$ to $[(C_6F_5)_3BOCH_3][H\text{-}TMP]$ and the formation of $[(C_6F_5)_3BOH]^-$ as a side product.[54]

In addition to CO_2, other small molecules, such as SO_2, N_2O, NO and CO can also be captured by frustrated Lewis pairs. Reaction of FLPs with SO_2 affords inter- and intramolecular adducts such as $(C_6F_5)_3BOS(O)P^tBu_3$ (Scheme 1.10a) and $Mes_2P(CH_2)_2B(C_6F_5)_2(SO_2)$ (Figure 1.5g) in a fashion analogous to CO_2.[143] While the connectivity is similar to that of the CO_2 adducts, these species exhibit a pseudo-pyramidal geometry due to the lone pairs on the S-atom, and thus giving rise to a centre of chirality. In a collaborative report, Stephan *et al*. and Erker *et al*. reported a series of SO_2 adducts derived from chiral intramolecular FLPs, which have been obtained as a mixture of diastereomers resulting from the chirality at the S-atom (Scheme 1.10). The analogous reaction of *N*-sulfinylamine compounds with P/B FLPs leads to the formation of a 1,3-addition product, with P−N and O−B bond formation.[144] The intramolecular FLP adduct $Mes_2P(CH_2)_2B(C_6F_5)_2(RNSO)$ exhibits an unusual seven-membered heterocycle (Figure 1.5h). Theses RNSO adducts have been found to acts as a source of SO, reacts with phosphines to afford phosphine oxide and phosphine sulphide, with concurrent formation of the five-membered cyclic $Mes_2P(CH_2)_2P(C_6F_5)_2(NR)$ adduct.

In a similar fashion to CO_2 capture, the Stephan group employed intermolecular FLPs $B(C_6F_5)_3/P^tBu_3$ and $Al(C_6F_5)_3/P^tBu_3$ to capture N_2O, affording linear adducts of $^tBu_3P(N_2O)B(C_6F_5)_3$[145] (Figure 1.5i) and $^tBu_3P(N_2O)Al(C_6F_5)_3$,[146] in which the P-atom bound to the terminal N, and boron or aluminium to O. $^tBu_3P(N_2O)B(C_6F_5)_3$ was found to be stable at room temperature, but releases N_2 at temperatures above 135 °C or on protonolysis. In contrast, further reaction of the $^tBu_3P(N_2O)Al(C_6F_5)_3$ species with a second equivalent of $Al(C_6F_5)_3$ leads to evolution of N_2 and formation of a transient "frustrated radical pair" comprised of phosphoniumyl radical cation $[^tBu_3P^{\bullet}]^+$ and Al_2-oxy radical anion $[(\mu\text{-}O^{\bullet})(Al(C_6F_5)_3)_2]^-$. Interestingly, such radical pair was shown to effect alkyl and aryl C−H bond activation.[146] Remarkably, the Aldridge group recently developed a unique

intramolecular FLP $\{(C_6H_4)_2(O)CMe_2\}(PMes_2)(B(C_6F_5)_2)$ with finely tuned binding and activation thermodynamics through tailored FLP design, achieving close to room temperature reversible N_2O capture and H_2 activation.[147]

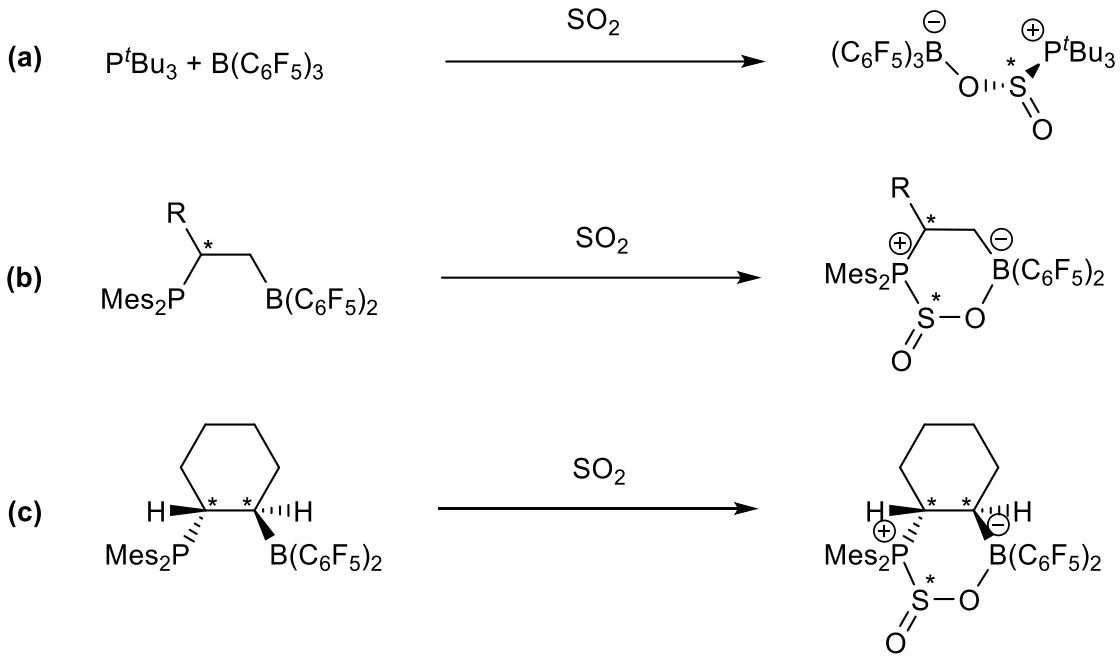

Scheme 1.10 Example reactions of SO_2 capture by FLPs.

Erker *et al*. reported that ethylene-bridged P/B FLP $Mes_2P(CH_2)_2B(C_6F_5)_2$ reacts with NO rapidly and cleanly to form a five-membered heterocyclic FLP-NO persistent radical $Mes_2P(CH_2)_2B(C_6F_5)_2(NO^{\bullet})$ (Figure 1.5j, Scheme 1.11a).[148] Such species is a highly reactive oxygen-centred radical, reacting with a variety of substrates by H-abstraction. This reactivity has been shown to extend to other intramolecular P/B FLPs systems, and the detailed kinetic and mechanistic studies of these species have also been reported.[149,150] In contrast, reaction of intermolecular FLP $B(C_6F_5)_3/P^tBu_3$ with NO results in the formation of the known $^tBu_3P(N_2O)B(C_6F_5)_3$ adduct, presumably generated *via* disproportionation of NO to give N_2O and phosphine oxide upon reaction of NO with phosphine (Scheme 1.11b).[148]

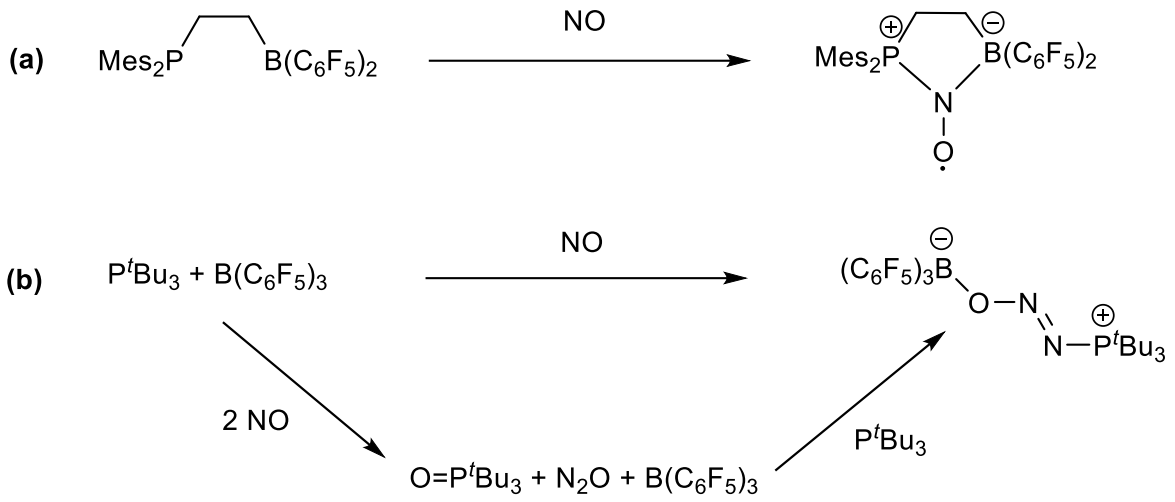

Scheme 1.11 Contrast reactivity of inter- and intra- molecular FLPs with NO.[148]

Cooperative B/P addition to CO have also been demonstrated by the Erker group using vicinal intramolecular $Mes_2P(CH_2)_2B(C_6F_5)_2$ and norbornene-bound P/B FLPs to generate the corresponding bridged carbonyl adducts (Figure 1.5k).[151,152] In both cases, the CO acts as a σ-donor and a π-acceptor similar to the interaction with a transition metal, however, the acceptor and donor sites lie on the B- and P-atoms instead. Stoichiometric reduction of CO could also be achieved using inter- and intramolecular FLPs in the presence of $HB(C_6F_5)_2$[153] or H_2[154] to afford the corresponding formyl-borane complexes. Combining the strategies for CO and NO capture, Erker and co-workers very recently described a CO-NO coupling reaction using $Mes_2P(CH_2)_2B(C_6F_5)_2$ and $HB(C_6F_5)_2$, resulting in the formation of a C=N double bond *via* a radical pathway (Figure 1.5l).[155]

1.6 Surface Chemistry and Heterogeneous FLP

The field of catalysis can be divided into two main categories: homogeneous and heterogeneous. The former is mainly linked to molecular organometallic chemistry,

whereas the latter involves surface and solid-state chemistry.[156] Currently, almost 90% of the chemical industries employ heterogeneous catalysts due to some of their well-documented advantages over their homogeneous analogues, including reduced reactor fouling and facile catalyst separation.[157] Although FLPs have demonstrated extensive solution phase catalytic hydrogenation activity, for the successful implementation of this technology in large-scale hydrogenation applications, development of heterogeneous FLP catalysts will be required.

Recently, heterogeneous FLP catalysts have emerged from the group of Guo and Wang. The team showed that although clean gold surface is inactive to H_2, the gold surface could serve as a Lewis acid when combined with imines/nitriles, to effect hydrogen activation and subsequently hydrogenation of CN multiple bonds.[158] Because these Lewis bases do not bind to the surface Lewis acids, this system act as an FLP to activate H_2, representing the first biphasic FLP catalyst. Ozin and colleagues have studied the photocatalytic conversion of CO_2 to CO *via* gas-phase reverse water gas shift reaction using a nanostructured indium oxide with a general formula of $[In_2O_{3-x}(OH)_y]$.[159] Such photo-catalysed transformation has been detected to occur at the surface defect sites where an O-vacant site is adjacent to a hydroxylated site [InOH···In].[160] Spectroscopic, kinetic and DFT data support the mechanism in which the Lewis basic InOH and Lewis acidic indium synergistically activates H_2, prompting the reduction CO_2 to CO and H_2O. More recent elegant computational work by Ozin *et al*. revealed the mechanism for the photocatalytic reduction CO_2 to CO by indium oxide. The calculated experiment suggests a structural change of the FLP at 180 °C, showing an increased distance between the LA and LB by 0.04 Å and decreased activation energy barrier associated with gaseous H_2 splitting over the FLP sites. However, by-product water was found to block surface active sites, preventing sustained catalytic activity.

Very recently, the group of Dai developed conjugated nanoporous polymers (CNP) embedded with Lewis basic pyridine sites.[161] These nanoporous materials have been designed with encumbered microenvironment capable of forming an FLP within the polymeric structure when impregnated with $B(C_6F_5)_3$. Impressively, these heterogeneous FLP systems have demonstrated effective activation of H_2 and subsequent hydrogenation of ketones. Attempted recycling of the catalyst was found to have a significant drop in catalyst activity, as a result of dissolution and removal of the Lewis acid. However, the activity can be restored by addition of $B(C_6F_5)_3$, even after four recycles.

In an alternative approach, Taoufik and co-workers developed silica-supported frustrated Lewis pairs, demonstrating *Z*-selective reduction of alkynes to cis-alkenes in the presence of H_2 (40 bar) with conversion rate as high as 99.6% and selectivity >86%.[162] The supported system was prepared by immobilising a functionalised tri-aryl phosphine on an alumina-treated silica support, with subsequent addition of either $B(C_6F_5)_3$ or $HB(C_6F_5)_2$. The latter combination was found most active, and the authors suggested that the mechanism for the reduction follows alkyne activation *via* hydroboration, followed by H_2 splitting and protonation.

1.7 Catalyst Supports

Most commonly used supports for surface catalysis are inorganic supports, with silica being the most popular choice due to its inert chemical properties and high abundancy. Common procedure for the preparation of silica supported catalysts[163] involves the reaction of the pre-catalysts with partial dehydroxylated/modified silica.[157,162,164–167] The grafting process usually occurs at the surface hydroxyl sites, through hydrolysis, alcoholysis and hydrogenolysis reactions, leading to chemically bound supported catalysts.[156,157,168]

Silicas used in supported catalysis are normally thermally treated prior to use in order to remove any physically adsorbed water (dehydration), and excess silanol groups (dehydroxylation). The purpose of the treatment is to prevent water and close by hydroxyl groups from participating in further side reactions with the supported catalyst. The surface of amorphous silica contains four types of Si environments (Figure 1.7): i) siloxane groups (≡SiOSi≡), (***Q***^{4}); (ii) isolated silanols (≡SiOH), (***Q***^{3}); (iii) geminal silanediols (=Si(OH)$_2$), (***Q***^{2}); (iv) vicinal silanols (hydrogen-bonded neighbouring ≡SiOH or =Si(OH)$_2$). The ***Q***^{n} terminology is usually used in NMR spectroscopy to define the number of O atoms bonded to a central Si atom.

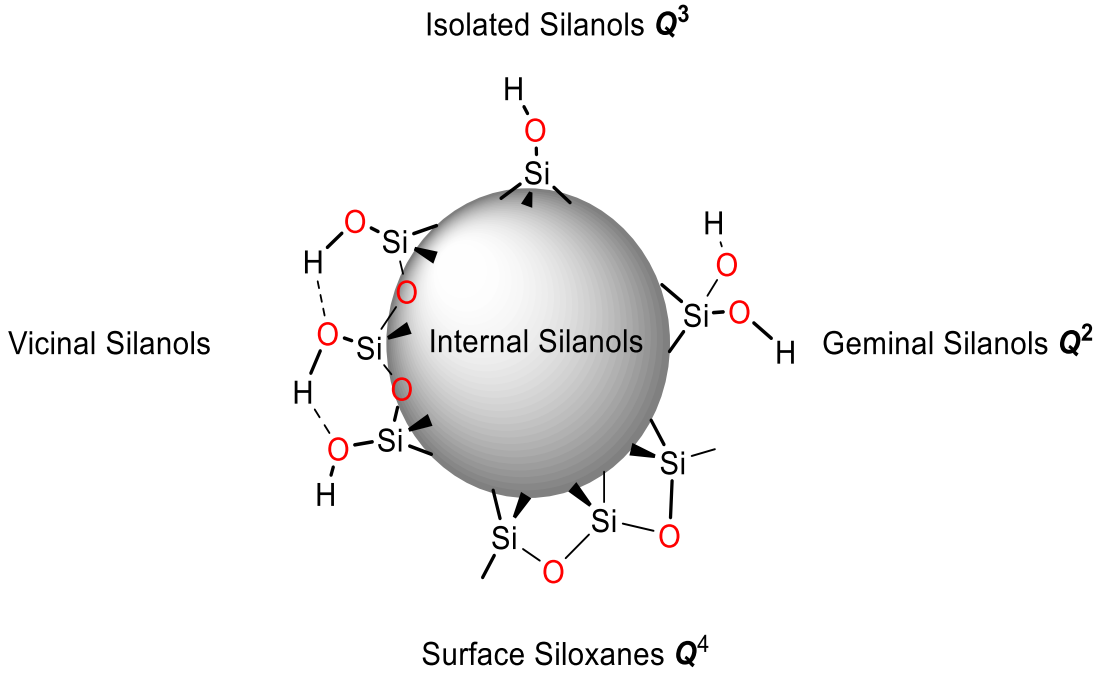

Figure 1.7 Types of silanol groups and siloxane bridges on silica surface.

Depending on the temperature which the silica sample was heated, the composition of the different silanol sites will change (Table 1.2). For single-site olefin polymerisation catalysts, often silica supports are pre-treated at temperatures above 700 °C to remove unwanted geminal and vicinal hydroxyl pairs, in order to achieve a well-defined surface

supported species.[163] The Zhuravlev model predicts the concentration of surface accessible OH groups (α_{OH}) per unit area as a function of temperature. Although different synthetic methods can result in silicas with different specific surface area and porosity, reports show that the α_{OH} at a given temperature remain similar for all samples tested.[169] Therefore this method was incorporated in this study in conjunction with BET analysis to determine the α_{OH} for the silica used.

Table 1.2 Surface concentration of different types of OH groups as a function of temperature.[169]

Temperature (°C)	Total OH (OH nm^{-2})	Isolated OH (OH nm^{-2})	Geminal OH (OH nm^{-2})	Vicinal OH (OH nm^{-2})
180-200	4.60	1.20	0.6	2.80
300	3.55	1.65	0.50	1.40
400	2.35	2.05	0.30	0
500	1.80	1.55	0.25	0
600	1.50	1.30	0.20	0
700	1.15	0.90	0.25	0
900	0.40	0.40	0	0

Many other supports have also been used as catalyst supports, including alumina, $MgCl_2$, Zeolites and mineral clays such as hydrotalcite.[157,170–173] Recently, a family of hydrotalcite-like clay material named layered double hydroxides (LDHs) have attracted considerable amount of attention as catalyst supports for surface catalysis (Figure 1.8).[174,175]

LDHs consist of positively charged mixed metal hydroxide host layers (divalent metal cations such as Mg^{2+}, Fe^{2+}, Cu^{2+}, and trivalent metals cations such as Al^{3+}, Cr^{3+}, Mn^{3+}) and exchangeable inorganic or organic charge-compensating anionic guests in between the layers, with an general expression of $[M^{2+}_{1-x}M^{3+}_{x}(OH)_2]^{x+}(A^{n-})_{x/n}\cdot mH_2O$, where commonly M denotes metal cations and A^{n-} denotes anions.[176–178] The value of x is equal to the molar ratio $M^{2+}/(M^{2+} + M^{3+})$ and is generally in the range of 0.2−0.33.

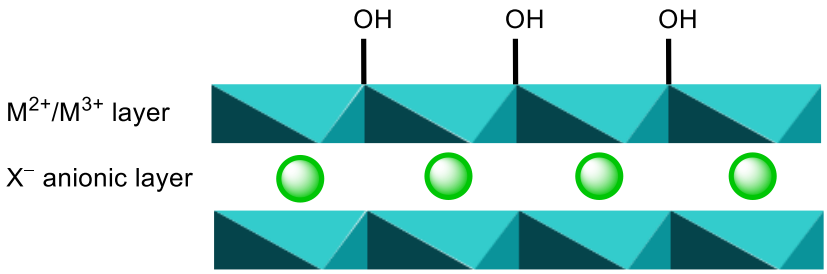

Figure 1.8 Illustration of a layered double hydroxide showing surface hydroxyl groups, positively charged metal layers and interlayer anions.

The OH groups in the LDH orientated toward the interlayer region may participate in the hydrogen bonding to intercalated water molecules and interactions with other anionic hosts. The strength of interlayer attraction is relatively low, affording LDHs with excellent interlayer expansion character, allowing intercalation of a wider selection of guests.[179–182] Complete exfoliation of the layers can also be achieved to give positively charged two-dimensional nanosheets, which can be used as nanocomposites for polymers or serve as building blocks for making new nanomaterials.[183,184] The wide tunability of a broad selection of metal cations (M^{2+}/M^{3+}), and interchangeable interlayer charge balancing anions results in highly diverse host/guest assemblies and nano-architectures. This compositional flexibility gives LDHs versatile physical and chemical properties, which captured much attention in the application of LDHs both as catalysts/precursors or as supports in the field of catalysis, biomedicine, electrochemistry and environmental technologies.[174,175,178,185–188] Owing to their high content of hydroxyl groups (almost half of their total mass) and uniform distribution of M^{2+}/M^{3+} cations without clusters of like cations (well-defined crystalline morphology), these materials make potentially great templates for the formation of nano-catalysts/supported catalysts with well-defined specific surface morphology.[177] Moreover, LDHs have also been proven to be effective supports for the immobilisation of anionic catalysts in the interlayer region.[189] The uniform distribution

of positive charges on the LDH layers provides uniform distribution and stability of intercalated anionic catalysts through electrostatic host-guest interactions.

LDHs currently can be produced at an industrial scale using well-established synthetic protocols. However, the LDHs produced *via* these conventional methods are often highly aggregated due to their high charge density and hydrophilicity. As a result, the low surface areas of the isolated LDHs make the application as a catalyst support less preferred compared to silica. Recently, the O'Hare group reported the synthesis of a new family of hydrocarbon dispersible, hydrophobic LDHs using an Aqueous Miscible Organic Solvent Treatment (AMOST) method.[190] The AMO-LDHs (with a chemical composition expressed as $[M^{2+}_{1-x}M^{3+}_{x}(OH)_2]^{x+}(A^{n-})_{x/n}\cdot mH_2O\cdot$c(AMO-solvent)) exhibit surface areas and pore volumes nearly two orders of magnitude higher than conventional LDHs. These improved properties make LDHs an excellent choice as alternative catalyst support.

1.8 Aim of Research

The aim of the thesis is to build on the initial work developed within the O'Hare group on FLP mediated hydrogenation of CO_2 to methanol, using FLPs containing C_6Cl_5-substitued triarylboranes combined with phosphines. Hydrogen activation and CO_2 reduction behaviour will be investigated. Furthermore, the thesis will attempt to develop proof-of-concept solid-supported FLP catalysts using silica and LDH as supports. New solid-phase FLPs will be fully characterised using modern solid-state techniques and investigated for H_2 activation performance.

1.9 References

1 J. Goldemberg, *Energy Policy*, 2006, **34**, 2185–2190.
2 S. Shafiee and E. Topal, *Energy Policy*, 2009, **37**, 181–189.
3 A. R. Brandt, A. Millard-Ball, M. Ganser and S. M. Gorelick, *Environ. Sci. Technol.*,

2013, **47**, 8031–8041.
4 R. Carapellucci and A. Milazzo, *Proc. Inst. Mech. Eng., Part A*, 2003, **217**, 505–517.
5 E. A. Roth, S. Agarwal and R. K. Gupta, *Energy Fuels*, 2013, **27**, 4129–4136.
6 A. Torrisi, R. G. Bell and C. Mellot-Draznieks, *Cryst. Growth Des.*, 2010, **10**, 2839–2841.
7 K. Smith, G. Xiao, K. Mumford, J. Gouw, I. Indrawan, N. Thanumurthy, D. Quyn, R. Cuthbertson, A. Rayer, N. Nicholas, A. Lee, G. da Silva, S. Kentish, T. Harkin, A. Qader, C. Anderson, B. Hooper and G. Stevens, *Energy Fuels*, 2014, **28**, 299–306.
8 M. Aresta, A. Dibenedetto and A. Angelini, *Chem. Rev.*, 2014, **114**, 1709–1742.
9 O. Ola, M. Mercedes Maroto-Valer and S. Mackintosh, *Energy Procedia*, 2013, **37**, 6704–6709.
10 W. Wang, S. Wang, X. Ma and J. Gong, *Chem. Soc. Rev.*, 2011, **40**, 3703–3727.
11 M. Mikkelsen, M. Jørgensen and F. C. Krebs, *Energy Environ. Sci.*, 2010, **3**, 43–81.
12 X. Xiaoding and J. a Moulijn, *Energy Fuels*, 1996, **10**, 305–325.
13 P. G. Jessop, F. Joó and C.-C. Tai, *Coord. Chem. Rev.*, 2004, **248**, 2425–2442.
14 H. Yang, Z. Xu, M. Fan, R. Gupta, R. B. Slimane, A. E. Bland and I. Wright, *J. Environ. Sci.*, 2008, **20**, 14–27.
15 D. Mohan, C. U. Pittman, and P. H. Steele, *Energy Fuels*, 2006, **20**, 848–889.
16 M. Z. Jacobson and M. A. Delucchi, *Energy Policy*, 2011, **39**, 1154–1169.
17 M. Besson, P. Gallezot and C. Pinel, *Chem. Rev.*, 2014, **114**, 1827–1870.
18 S. Czernik and A. V. Bridgwater, *Energy Fuels*, 2004, **18**, 590–598.
19 P. Mäki-Arvela, I. L. Simakova, T. Salmi and D. Y. Murzin, *Chem. Rev.*, 2014, **114**, 1909–1971.
20 Y. Jiang, O. Blacque, T. Fox and H. Berke, *J. Am. Chem. Soc.*, 2013, **135**, 7751–7760.
21 S. Seo, L. D. Simoni, M. Ma, M. A. DeSilva, Y. Huang, M. a Stadtherr and J. F. Brennecke, *Energy Fuels*, 2014, **28**, 5968–5977.
22 C. Song, *Catal. Today*, 2006, **115**, 2–32.
23 G. Centi and S. Perathoner, in *Studies in Surface Science and Catalysis*, Elsevier, Seoul, Korea, 2004.
24 T. Sakakura, J.-C. Choi and H. Yasuda, *Chem. Rev.*, 2007, **107**, 2365–2387.
25 B. L. Salvi, K. A. Subramanian and N. L. Panwar, *Renewable Sustainable Energy Rev.*, 2013, **25**, 404–419.
26 G. A. Olah, A. Goeppert and G. K. S. Prakash, *J. Org. Chem.*, 2009, **74**, 487–498.
27 W.-Q. Han and C.-D. Yao, *Fuel*, 2015, **150**, 29–40.
28 V. R. Surisetty, A. K. Dalai and J. Kozinski, *Appl. Catal., A*, 2011, **404**, 1–11.
29 G. A. Olah, A. Goeppert and G. K. S. Prakash, *Beyond Oil and Gas: The Methanol Economy*, Wiley-VCH Verlag GmbH & Co. KGaA, Weinheim, Germany, 2009.
30 I. Omae, *Catal. Today*, 2006, **115**, 33–52.
31 J. Ma, N. Sun, X. Zhang, N. Zhao, F. Xiao, W. Wei and Y. Sun, *Catal. Today*, 2009, **148**, 221–231.
32 P. G. Jessop, T. Ikariya and R. Noyori, *Chem. Rev.*, 1995, **95**, 259–272.
33 B. J. Liaw and Y. Z. Chen, *Appl. Catal., A*, 2001, **206**, 245–256.

34 M. Saito and K. Murata, *Catal. Surv. Asia*, 2004, **8**, 285–294.

35 F. Arena, K. Barbera, G. Italiano, G. Bonura, L. Spadaro and F. Frusteri, *J. Catal.*, 2007, **249**, 185–194.

36 J. Yoshihara and C. T. Campbell, *J. Catal.*, 1996, **161**, 776–782.

37 C. V. Ovesen, B. S. Clausen, J. Schiøtz, P. Stoltze, H. Topsøe and J. K. Nørskov, *J. Catal.*, 1997, **168**, 133–142.

38 S. Fujita, S. Moribe, Y. Kanamori, M. Kakudate and N. Takezawa, *Appl. Catal., A*, 2001, **207**, 121–128.

39 J. Toyir, P. R. de la Piscina, J. L. G. Fierro and N. Homs, *Appl. Catal., B*, 2001, **29**, 207–215.

40 J. Liu, J. Shi, D. He, Q. Zhang, X. Wu, Y. Liang and Q. Zhu, *Appl. Catal., A*, 2001, **218**, 113–119.

41 F. Arena, G. Italiano, K. Barbera, G. Bonura, L. Spadaro and F. Frusteri, *Catal. Today*, 2009, **143**, 80–85.

42 F. Arena, G. Italiano, K. Barbera, S. Bordiga, G. Bonura, L. Spadaro and F. Frusteri, *Appl. Catal., A*, 2008, **350**, 16–23.

43 Y. Ma, Q. Sun, D. Wu, W.-H. Fan, Y.-L. Zhang and J.-F. Deng, *Appl. Catal., A*, 1998, **171**, 45–55.

44 D. Jingfa, S. Qi, Z. Yulong, C. Songying and W. Dong, *Appl. Catal., A*, 1996, **139**, 75–85.

45 I. Fierro, J. L. G., López Granados, M. & Melián-Cabrera, *J. Catal.*, 2002, **210**, 285–294.

46 L. Fan and K. Fujimoto, *J. Catal.*, 1994, **150**, 217–220.

47 S. E. Collins, M. A. Baltanás, J. L. Garcia Fierro and A. L. Bonivardi, *J. Catal.*, 2002, **211**, 252–264.

48 X.-L. Liang, X. Dong, G.-D. Lin and H.-B. Zhang, *Appl. Catal., B*, 2009, **88**, 315–322.

49 K. Tominaga, Y. Sasaki, M. Kawai, T. Watanabe and M. Saito, *J. Chem. Soc. Chem. Commun.*, 1993, 629–631.

50 K. Tominaga, Y. Sasaki, T. Watanabe and M. Saito, *Bull. Chem. Soc. Jpn.*, 1995, **68**, 2837–2842.

51 R. Fornika, H. Görls, B. Seemann and W. Leitner, *J. Chem. Soc. Chem. Commun.*, 1995, 1479–1481.

52 B. Denise and R. P. A. Sneeden, *J. Organomet. Chem.*, 1981, **221**, 111–116.

53 S. N. Riduan, Y. Zhang and J. Y. Ying, *Angew. Chem., Int. Ed.*, 2009, **48**, 3322–3325.

54 A. E. Ashley, A. L. Thompson and D. O'Hare, *Angew. Chem., Int. Ed.*, 2009, **48**, 9839–9843.

55 G. N. Lewis, *Valence and the Structure of Atoms and Molecules*, Chemical Catalogue Company, New York, 1923.

56 H. C. Brown, H. I. Schlesinger and S. Z. Cardon, *J. Am. Chem. Soc.*, 1942, **64**, 325–329.

57 J. S. J. McCahill, G. C. Welch and D. W. Stephan, *Angew. Chem., Int. Ed.*, 2007, **46**, 4968–4971.

58 G. C. Welch, R. R. S. Juan, J. D. Masuda and D. W. Stephan, *Science*, 2006, **314**, 1124–1126.

59 G. C. Welch and D. W. Stephan, *J. Am. Chem. Soc.*, 2007, **129**, 1880–1881.

60 P. Spies, S. Schwendemann, S. Lange, G. Kehr, R. Fröhlich and G. Erker, *Angew. Chem., Int. Ed.*, 2008, **47**, 7543–7546.

61 D. W. Stephan and G. Erker, *Angew. Chem., Int. Ed.*, 2015, **54**, 6400–6441.

62 D. W. Stephan and G. Erker, *Angew. Chem., Int. Ed.*, 2010, **49**, 46–76.

63 S. Grimme, H. Kruse, L. Goerigk and G. Erker, *Angew. Chem., Int. Ed.*, 2010, **49**, 1402–1405.

64 T. A. Rokob, A. Hamza, A. Stirling, T. Soós and I. Pápai, *Angew. Chem., Int. Ed.*, 2008, **47**, 2435–2438.

65 J. G. de Vries and C. J. Elsevier, *The Handbook of Homogeneous Hydrogenation*, Wiley-VCH Verlag GmbH, Weinheim, Germany, 2006.

66 D. M. Heinekey, A. Lledós and J. M. Lluch, *Chem. Soc. Rev.*, 2004, **33**, 175–182.

67 G. S. McGrady and G. Guilera, *Chem. Soc. Rev.*, 2003, **32**, 383–392.

68 P. P. Power, *Nature*, 2010, **463**, 171–177.

69 P. A. Chase, G. C. Welch, T. Jurca and D. W. Stephan, *Angew. Chem., Int. Ed.*, 2007, **46**, 8050–8053.

70 P. A. Chase and D. W. Stephan, *Angew. Chem., Int. Ed.*, 2008, **47**, 7433–7437.

71 P. A. Chase, T. Jurca and D. W. Stephan, *Chem. Commun.*, 2008, **2**, 1701–1703.

72 H. Wang, R. Fröhlich, G. Kehr and G. Erker, *Chem. Commun.*, 2008, **92**, 5966–5968.

73 D. W. Stephan, *Org. Biomol. Chem.*, 2008, **6**, 1535–1539.

74 D. W. Stephan, *Acc. Chem. Res.*, 2015, **48**, 306–316.

75 D. W. Stephan, *Org. Biomol. Chem.*, 2012, **10**, 5740–5746.

76 D. W. Stephan, *J. Am. Chem. Soc.*, 2015, **137**, 10018–10032.

77 Á. Gyömöre, M. Bakos, T. Földes, I. Pápai, A. Domján and T. Soós, *ACS Catal.*, 2015, **5**, 5366–5372.

78 G. Ghattas, D. Chen, F. Pan and J. Klankermayer, *Dalton Trans.*, 2012, **41**, 9026–9028.

79 J. S. Reddy, B.-H. Xu, T. Mahdi, R. Fröhlich, G. Kehr, D. W. Stephan and G. Erker, *Organometallics*, 2012, **31**, 5638–5649.

80 D. W. Stephan, S. Greenberg, T. W. Graham, P. Chase, J. J. Hastie, S. J. Geier, J. M. Farrell, C. C. Brown, Z. M. Heiden, G. C. Welch and M. Ullrich, *Inorg. Chem.*, 2011, **50**, 12338–12348.

81 L. E. Longobardi, C. Tang and D. W. Stephan, *Dalton Trans.*, 2014, **43**, 15723–15726.

82 T. Mahdi and D. W. Stephan, *J. Am. Chem. Soc.*, 2014, **136**, 15809–15812.

83 D. J. Scott, M. J. Fuchter and A. E. Ashley, *J. Am. Chem. Soc.*, 2014, **136**, 15813–15816.

84 T. Mahdi and D. W. Stephan, *Angew. Chem., Int. Ed.*, 2015, **54**, 8511–8514.

85 S. J. Geier, P. A. Chase and D. W. Stephan, *Chem. Commun.*, 2010, **46**, 4884–4886.

86 G. Erős, K. Nagy, H. Mehdi, I. Pápai, P. Nagy, P. Király, G. Tárkányi and T. Soós, *Chem. - Eur. J.*, 2012, **18**, 574–585.

87 L. Greb, P. Oña-Burgos, B. Schirmer, S. Grimme, D. W. Stephan and J. Paradies, *Angew. Chem., Int. Ed.*, 2012, **51**, 10164–10168.
88 L. J. Hounjet, C. Bannwarth, C. N. Garon, C. B. Caputo, S. Grimme and D. W. Stephan, *Angew. Chem., Int. Ed.*, 2013, **52**, 7492–7495.
89 J. Paradies, *Synlett*, 2013, **24**, 777–780.
90 L. Greb, C.-G. Daniliuc, K. Bergander and J. Paradies, *Angew. Chem., Int. Ed.*, 2013, **52**, 5876–5879.
91 J. Paradies, *Angew. Chem., Int. Ed.*, 2014, **53**, 3552–3557.
92 B. Inés, D. Palomas, S. Holle, S. Steinberg, J. A. Nicasio and M. Alcarazo, *Angew. Chem., Int. Ed.*, 2012, **51**, 12367–12369.
93 L. Greb, P. Oña-Burgos, A. Kubas, F. C. Falk, F. Breher, K. Fink and J. Paradies, *Dalton Trans.*, 2012, **41**, 9056–9060.
94 G. Erős, H. Mehdi, I. Pápai, T. A. Rokob, P. Király, G. Tárkányi and T. Soós, *Angew. Chem., Int. Ed.*, 2010, **49**, 6559–6563.
95 K. Chernichenko, Á. Madarász, I. Pápai, M. Nieger, M. Leskelä and T. Repo, *Nat. Chem.*, 2013, **5**, 718–723.
96 D. Chen, Y. Wang and J. Klankermayer, *Angew. Chem., Int. Ed.*, 2010, **49**, 9475–9478.
97 Y. Liu and H. Du, *J. Am. Chem. Soc.*, 2013, **135**, 6810–6813.
98 M. Lindqvist, K. Borre, K. Axenov, B. Kótai, M. Nieger, M. Leskelä, I. Pápai and T. Repo, *J. Am. Chem. Soc.*, 2015, **137**, 4038–4041.
99 S. Wei and H. Du, *J. Am. Chem. Soc.*, 2014, **136**, 12261–12264.
100 Y. Liu and H. Du, *J. Am. Chem. Soc.*, 2013, **135**, 12968–12971.
101 Z. Zhang and H. Du, *Angew. Chem., Int. Ed.*, 2015, **54**, 623–626.
102 A. E. Ashley, T. J. Herrington, G. G. Wildgoose, H. Zaher, A. L. Thompson, N. H. Rees, T. Krämer and D. O'Hare, *J. Am. Chem. Soc.*, 2011, **133**, 14727–14740.
103 D. J. Scott, M. J. Fuchter and A. E. Ashley, *Angew. Chem., Int. Ed.*, 2014, **53**, 10218–10222.
104 T. J. Herrington, A. J. W. Thom, A. J. P. White and A. E. Ashley, *Dalton Trans.*, 2012, **41**, 9019–9022.
105 J. M. Farrell, J. A. Hatnean and D. W. Stephan, *J. Am. Chem. Soc.*, 2012, **134**, 15728–15731.
106 J. M. Farrell, R. T. Posaratnanathan and D. W. Stephan, *Chem. Sci.*, 2015, **6**, 2010–2015.
107 P. Eisenberger, B. P. Bestvater, E. C. Keske and C. M. Crudden, *Angew. Chem., Int. Ed.*, 2015, **54**, 2467–2471.
108 E. R. Clark and M. J. Ingleson, *Organometallics*, 2013, **32**, 6712–6717.
109 E. R. Clark and M. J. Ingleson, *Angew. Chem., Int. Ed.*, 2014, **53**, 11306–11309.
110 A. Schäfer, M. Reißmann, A. Schäfer, W. Saak, D. Haase and T. Müller, *Angew. Chem., Int. Ed.*, 2011, **50**, 12636–12638.
111 A. Schäfer, M. Reißmann, S. Jung, A. Schäfer, W. Saak, E. Brendler and T. Müller, *Organometallics*, 2013, **32**, 4713–4722.
112 A. Schäfer, M. Reißmann, A. Schäfer, M. Schmidtmann and T. Müller, *Chem. - Eur. J.*, 2014, **20**, 9381–9386.

113 T. J. Herrington, B. J. Ward, L. R. Doyle, J. McDermott, A. J. P. White, P. A. Hunt and A. E. Ashley, *Chem. Commun.*, 2014, **50**, 12753–12756.
114 N. Burford and P. J. Ragogna, *Dalton Trans.*, 2002, 4307–4315.
115 L. E. Longobardi, C. A. Russell, M. Green, N. S. Townsend, K. Wang, A. J. Holmes, S. B. Duckett, J. E. McGrady and D. W. Stephan, *J. Am. Chem. Soc.*, 2014, **136**, 13453–13457.
116 C. B. Caputo, L. J. Hounjet, R. Dobrovetsky and D. W. Stephan, *Science*, 2013, **341**, 1374–1377.
117 K. C. Kumara Swamy and N. Satish Kumar, *Acc. Chem. Res.*, 2006, **39**, 324–333.
118 M. Perez, C. B. Caputo, R. Dobrovetsky and D. W. Stephan, *Proc. Natl. Acad. Sci.*, 2014, **111**, 10917–10921.
119 M. Pérez, L. J. Hounjet, C. B. Caputo, R. Dobrovetsky and D. W. Stephan, *J. Am. Chem. Soc.*, 2013, **135**, 18308–18310.
120 J. Zhu, M. Pérez, C. B. Caputo and D. W. Stephan, *Angew. Chem., Int. Ed.*, 2016, **55**, 1417–1421.
121 J. M. Bayne and D. W. Stephan, *Chem. Soc. Rev.*, 2016, **45**, 765–774.
122 J. Zhu, M. Pérez and D. W. Stephan, *Angew. Chem., Int. Ed.*, 2016, **55**, 8448–8451.
123 T. vom Stein, M. Peréz, R. Dobrovetsky, D. Winkelhaus, C. B. Caputo and D. W. Stephan, *Angew. Chem., Int. Ed.*, 2015, **54**, 10178–10182.
124 G. C. Welch, J. D. Masuda and D. W. Stephan, *Inorg. Chem.*, 2006, **45**, 478–480.
125 M. A. Dureen and D. W. Stephan, *J. Am. Chem. Soc.*, 2009, **131**, 8396–8397.
126 M. Ullrich, K. S.-H. Seto, A. J. Lough and D. W. Stephan, *Chem. Commun.*, 2009, **6**, 2335–2337.
127 C. M. Mömming, S. Frömel, G. Kehr, R. Fröhlich, S. Grimme and G. Erker, *J. Am. Chem. Soc.*, 2009, **131**, 12280–12289.
128 C. M. Mömming, E. Otten, G. Kehr, R. Fröhlich, S. Grimme, D. W. Stephan and G. Erker, *Angew. Chem., Int. Ed.*, 2009, **48**, 6643–6646.
129 F. Bertini, V. Lyaskovskyy, B. J. J. Timmer, F. J. J. de Kanter, M. Lutz, A. W. Ehlers, J. C. Slootweg and K. Lammertsma, *J. Am. Chem. Soc.*, 2012, **134**, 201–204.
130 E. Theuergarten, J. Schlösser, D. Schlüns, M. Freytag, C. G. Daniliuc, P. G. Jones and M. Tamm, *Dalton Trans.*, 2012, **41**, 9101–9110.
131 W. Li, K. Liu, R. Simms, J. Greener, D. Jagadeesan, S. Pinto, A. Günther and E. Kumacheva, *J. Am. Chem. Soc.*, 2012, **134**, 3127–3132.
132 D. Voicu, M. Abolhasani, R. Choueiri, G. Lestari, C. Seiler, G. Menard, J. Greener, A. Guenther, D. W. Stephan and E. Kumacheva, *J. Am. Chem. Soc.*, 2014, **136**, 3875–3880.
133 M. Pu and T. Privalov, *Chem. - Eur. J.*, 2015, **21**, 17708–17720.
134 G. Ménard and D. W. Stephan, *J. Am. Chem. Soc.*, 2010, **132**, 1796–1797.
135 X. Zhao and D. W. Stephan, *Chem. Commun.*, 2011, **47**, 1833–1835.
136 S. D. Tran, T. A. Tronic, W. Kaminsky, D. Michael Heinekey and J. M. Mayer, *Inorg. Chim. Acta*, 2011, **369**, 126–132.
137 A. Berkefeld, W. E. Piers and M. Parvez, *J. Am. Chem. Soc.*, 2010, **132**, 10660–10661.
138 T. Wang and D. W. Stephan, *Chem. - Eur. J.*, 2014, **20**, 3036–3039.

139 T. Wang and D. W. Stephan, *Chem. Commun.*, 2014, **50**, 7007–7010.
140 R. Dobrovetsky and D. W. Stephan, *Angew. Chem., Int. Ed.*, 2013, **52**, 2516–2519.
141 M.-A. Courtemanche, M.-A. Légaré, L. Maron and F.-G. Fontaine, *J. Am. Chem. Soc.*, 2013, **135**, 9326–9329.
142 M. A. Courtemanche, M. A. Légaré, L. Maron and F. G. Fontaine, *J. Am. Chem. Soc.*, 2014, **136**, 10708–10717.
143 M. Sajid, A. Klose, B. Birkmann, L. Liang, B. Schirmer, T. Wiegand, H. Eckert, A. J. Lough, R. Fröhlich, C. G. Daniliuc, S. Grimme, D. W. Stephan, G. Kehr and G. Erker, *Chem. Sci.*, 2013, **4**, 213–219.
144 L. E. Longobardi, V. Wolter and D. W. Stephan, *Angew. Chem., Int. Ed.*, 2015, **54**, 809–812.
145 E. Otten, R. C. Neu and D. W. Stephan, *J. Am. Chem. Soc.*, 2009, **131**, 9918–9919.
146 G. Ménard, J. A. Hatnean, H. J. Cowley, A. J. Lough, J. M. Rawson and D. W. Stephan, *J. Am. Chem. Soc.*, 2013, **135**, 6446–6449.
147 Z. Mo, E. L. Kolychev, A. Rit, J. Campos, H. Niu and S. Aldridge, *J. Am. Chem. Soc.*, 2015, **137**, 12227–12230.
148 A. J. P. Cardenas, B. J. Culotta, T. H. Warren, S. Grimme, A. Stute, R. Fröhlich, G. Kehr and G. Erker, *Angew. Chem., Int. Ed.*, 2011, **50**, 7567–7571.
149 R. Liedtke, F. Scheidt, J. Ren, B. Schirmer, A. J. P. Cardenas, C. G. Daniliuc, J. Eckert, T. H. Warren, S. Grimme, G. Kehr and G. Erker, *J. Am. Chem. Soc.*, 2014, **136**, 9014–9027.
150 J. C. M. Pereira, M. Sajid, G. Kehr, A. M. Wright, B. Schirmer, Z.-W. Qu, S. Grimme, G. Erker and P. C. Ford, *J. Am. Chem. Soc.*, 2014, **136**, 513–519.
151 M. Sajid, G. Kehr, T. Wiegand, H. Eckert, C. Schwickert, R. Pöttgen, A. J. P. Cardenas, T. H. Warren, R. Fröhlich, C. G. Daniliuc and G. Erker, *J. Am. Chem. Soc.*, 2013, **135**, 8882–8895.
152 D. W. Stephan and G. Erker, *Chem. Sci.*, 2014, **5**, 2625–2641.
153 M. Sajid, L.-M. Elmer, C. Rosorius, C. G. Daniliuc, S. Grimme, G. Kehr and G. Erker, *Angew. Chem., Int. Ed.*, 2013, **52**, 2243–2246.
154 R. Dobrovetsky and D. W. Stephan, *J. Am. Chem. Soc.*, 2013, **135**, 4974–4977.
155 K.-Y. Ye, G. Kehr, C. G. Daniliuc, L. Liu, S. Grimme and G. Erker, *Angew. Chem., Int. Ed.*, 2016, **55**, 9216–9219.
156 C. Copéret, M. Chabanas, R. Petroff Saint-Arroman and J.-M. Basset, *Angew. Chem., Int. Ed.*, 2003, **42**, 156–181.
157 J. R. Severn, J. C. Chadwick, R. Duchateau and N. Friederichs, *Chem. Rev.*, 2005, **105**, 4073–4147.
158 G. Lu, P. Zhang, D. Sun, L. Wang, K. Zhou, Z.-X. Wang and G.-C. Guo, *Chem. Sci.*, 2014, **5**, 1082–1090.
159 K. K. Ghuman, L. B. Hoch, P. Szymanski, J. Y. Y. Loh, N. P. Kherani, M. A. El-Sayed, G. A. Ozin and C. V. Singh, *J. Am. Chem. Soc.*, 2016, **138**, 1206–1214.
160 K. K. Ghuman, L. B. Hoch, T. E. Wood, C. Mims, C. V. Singh and G. A. Ozin, *ACS Catal.*, 2016, **6**, 5764–5770.
161 C. Tian, X. Zhu, C. W. Abney, Z. Tian, D. Jiang, K. S. Han, S. M. Mahurin, N. M. Washton and S. Dai, *Chem. Commun.*, 2016, **52**, 11919–11922.

162 K. C. Szeto, W. Sahyoun, N. Merle, J. L. Castelbou, N. Popoff, F. Lefebvre, J. Raynaud, C. Godard, C. Claver, L. Delevoye, R. M. Gauvin and M. Taoufik, *Catal. Sci. Technol.*, 2016, **6**, 882–889.

163 G. G. Hlatky, *Chem. Rev.*, 2000, **100**, 1347–1376.

164 D. W. Sauter, N. Popoff, M. A. Bashir, K. C. Szeto, R. M. Gauvin, L. Delevoye, M. Taoufik and C. Boisson, *Chem. Commun.*, 2016, **52**, 4776–4779.

165 G. L. Rice and S. L. Scott, *Langmuir*, 1997, **13**, 1545–1551.

166 S. Charoenchaidet, S. Chavadej and E. Gulari, *J. Mol. Catal. A: Chem.*, 2002, **185**, 167–177.

167 D. Gajan and C. Copéret, *New J. Chem.*, 2011, **35**, 2403–2408.

168 S. M. George, *Chem. Rev.*, 1995, **95**, 475–476.

169 L. T. Zhuravlev, *Colloids Surf., A*, 2000, **173**, 1–38.

170 T. Miyadera and K. Yoshida, *Chem. Lett.*, 1993, **22**, 1483–1486.

171 R. Burch and P. J. Millington, *Catal. Today*, 1996, **29**, 37–42.

172 T. R. Baldwin and R. Burch, *Appl. Catal.*, 1990, **66**, 337–358.

173 J. Tian, S. Wang, Y. Feng, J. Li and S. Collins, *J. Mol. Catal. A: Chem.*, 1999, **144**, 137–150.

174 S. He, Z. An, M. Wei, D. G. Evans and X. Duan, *Chem. Commun.*, 2013, **49**, 5912–5920.

175 G. Fan, F. Li, D. G. Evans and X. Duan, *Chem. Soc. Rev.*, 2014, **43**, 7040–7066.

176 F. Cavani, F. Trifirò and A. Vaccari, *Catal. Today*, 1991, **11**, 173–301.

177 P. J. Sideris, U. G. Nielsen, Z. Gan and C. P. Grey, *Science*, 2008, **321**, 113–117.

178 Q. Wang and D. O'Hare, *Chem. Rev.*, 2012, **112**, 4124–4155.

179 A. I. Khan, A. Ragavan, B. Fong, C. Markland, M. O'Brien, T. G. Dunbar, G. R. Williams and D. O'Hare, *Ind. Eng. Chem. Res.*, 2009, **48**, 10196–10205.

180 G. R. Williams and D. O'Hare, *Chem. Mater.*, 2005, **17**, 2632–2640.

181 G. R. Williams, T. G. Dunbar, A. J. Beer, A. M. Fogg and D. O'Hare, *J. Mater. Chem.*, 2006, **16**, 1231–1237.

182 A. M. Fogg, A. L. Rohl, G. M. Parkinson and D. O'Hare, *Chem. Mater.*, 1999, **11**, 1194–1200.

183 Q. Wu, A. Olafsen, Ø. B. Vistad, J. Roots and P. Norby, *J. Mater. Chem.*, 2005, **15**, 4695–4700.

184 J.-H. Choy, *J. Phys. Chem. Solids*, 2004, **65**, 373–383.

185 K.-H. Goh, T.-T. Lim and Z. Dong, *Water Res.*, 2008, **42**, 1343–1368.

186 J.-T. Feng, Y.-J. Lin, D. G. Evans, X. Duan and D.-Q. Li, *J. Catal.*, 2009, **266**, 351–358.

187 B. M. Choudary, S. Madhi, N. S. Chowdari, M. L. Kantam and B. Sreedhar, *J. Am. Chem. Soc.*, 2002, **124**, 14127–14136.

188 H. Liu and E. Min, *Green Chem.*, 2006, **8**, 657–662.

189 P. Liu, H. Wang, Z. Feng, P. Ying and C. Li, *J. Catal.*, 2008, **256**, 345–348.

190 C. Chen, M. Yang, Q. Wang, J.-C. Buffet and D. O'Hare, *J. Mater. Chem. A*, 2014, **2**, 15102–15110.

CHAPTER TWO

FLP Mediated H_2 Cleavage and CO_2 Reduction

2.1 Introduction

In light of concerns for climate change and decline of fossil-fuel reserves, direct chemical transformation of carbon dioxide (CO_2) to useful chemical feedstocks has been an ongoing target for many research groups.[1,2] Current effective methods for catalytic CO_2 reduction to generate useful chemicals such as CO, formic acid, formaldehyde, methanol and methane require heterogeneous reverse water gas shift catalysts (Cu/ZnO, Cu-Zn/Al_2O_3, Cu-Ni/γ-Al_2O_3, Ni/CeO) and expensive supported noble metal catalysts such as (Pt, Rh, Ru) often under high temperature condition (>600 °C).[3–5] Reducing system requirements and lowering the cost of catalysts would be desirable.

FLP mediated heterolytic fission of H−H bond[6–36] has prompted substantial efforts into the development of metal-free FLP-catalysts for the hydrogenations of various unsaturated organic substrates.[20,30,32,37–52] As introduced in Chapter One, Ashley *et al*. demonstrated the first example of metal-free CO_2 conversion to methanol under a mild condition (1 bar H_2, 160 °C) using a $B(C_6F_5)_3$ (BCF) and tetramethylpiperidine (TMP) FLP, allowing methanol to be isolated at a moderate yield (17−25%).[53] The proposed mechanism for hydrogenation of CO_2 occurs *via* three major steps; H_2 activation, CO_2 insertion, and partial deoxygenation (Scheme 2.1). However, this system is not catalytic due to decomposition of the methoxyborate intermediate species following a protonlysis mechanism proposed by Ashley (Scheme 2.2). This decomposition pathway was facilitated by aromatic ring activation, through mesomeric electron donation to the aryl ring by fluorine atoms with strong 2*p*-2*p* overlap. As a result, regeneration of the FLP was

inhibited by the protonation of the *ipso*-C of the C_6F_5 ring. Following a similar strategy, Tran *et al.* also demonstrated the reaction of CO_2 with a $B(C_6F_5)_3$/Lutidine FLP proceeded to give the corresponding formatoborate species $[HC(O)OB(C_6F_5)_3^-][LutH^+]$, however, this system was not able to reduce the C=O further to generate a methoxyborate species.[54]

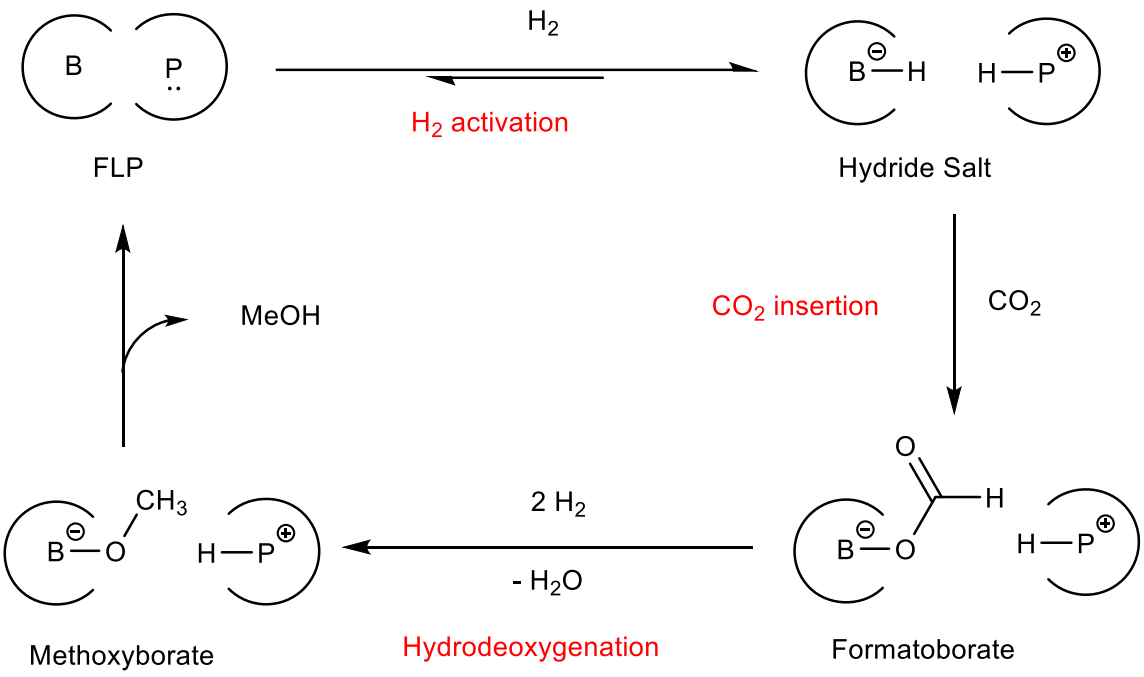

Scheme 2.1 Proposed reaction cycle for FLP mediated CO_2 hydrogenation showing a two-step reduction of CO_2.

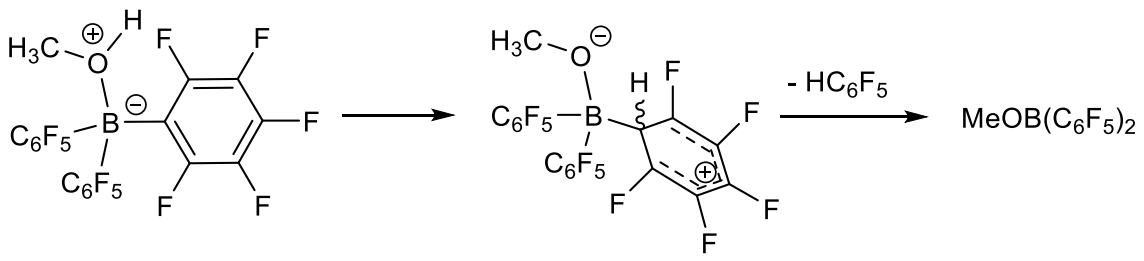

Scheme 2.2 Proposed mechanism for the competing protonation in the methoxyborate species.[53]

In the attempt to develop more reactive FLPs that are less susceptible to decomposition via protonation of the C_6F_5 group, Ashley *et al.* introduced a family of

analogous Lewis acids $B(C_6Cl_5)_n(C_6F_5)_{3-n}$ (where n = 1−3) of the parent molecule BCF.[55] Electrochemical measurement of the series revealed that C_6Cl_5 groups are more electron withdrawing than C_6F_5, with a *ca*. +200 mV shift observed in the reduction potential per C_6F_5 group replaced. Although Cl is less electronegative the F, the overall result of the inductive withdrawing effect is stronger due to weaker 3p-2p aromatic π-orbital overlap, making C_6Cl_5 groups more tolerant of protonolysis. Such stereoelectronic modification of BCF has also shown an increased reactivity of the resulting FLPs with H_2.[11] This has prompted substantial efforts into the development of alternative metal-free FLP-catalysts for the hydrogenations of various unsaturated substrates.[56,23,57–60,37,52,44,61]

Previous investigations have mostly been focusing on using amines as the Lewis base, whereas phosphines have not been studied extensively. A major advantage of using phosphines in FLP reactions is the convenient monitoring of the reactions by ^{31}P NMR spectroscopy. Moreover, the greater Lewis basicity of hindered phosphines compared to amines should also lead to formation of more reactive FLPs.[27,34] Three phosphine bases with different pK_a values have been selected and their potential to form new FLPs will be investigated in this chapter (Figure 2.1). P^{t}Bu$_3$ being the strongest phosphine base among the three,[62,63] has been used extensively in FLP chemistry for H_2 activation.[11,23,34] Despite the synthesis of FLPs based on P(*o*-tolyl)$_3$ and $B(C_6F_5)_3$ by Erker *et al*., to the best of our knowledge employing FLP systems containing tolylphosphine bases in dihydrogen cleavage reactions has not been explored.[64,65] In this chapter, the ability of $B(C_6Cl_5)(C_6F_5)_2$ to form FLPs with phosphine bases will be explored, and their reactivity towards H_2 and CO_2 will be investigated.

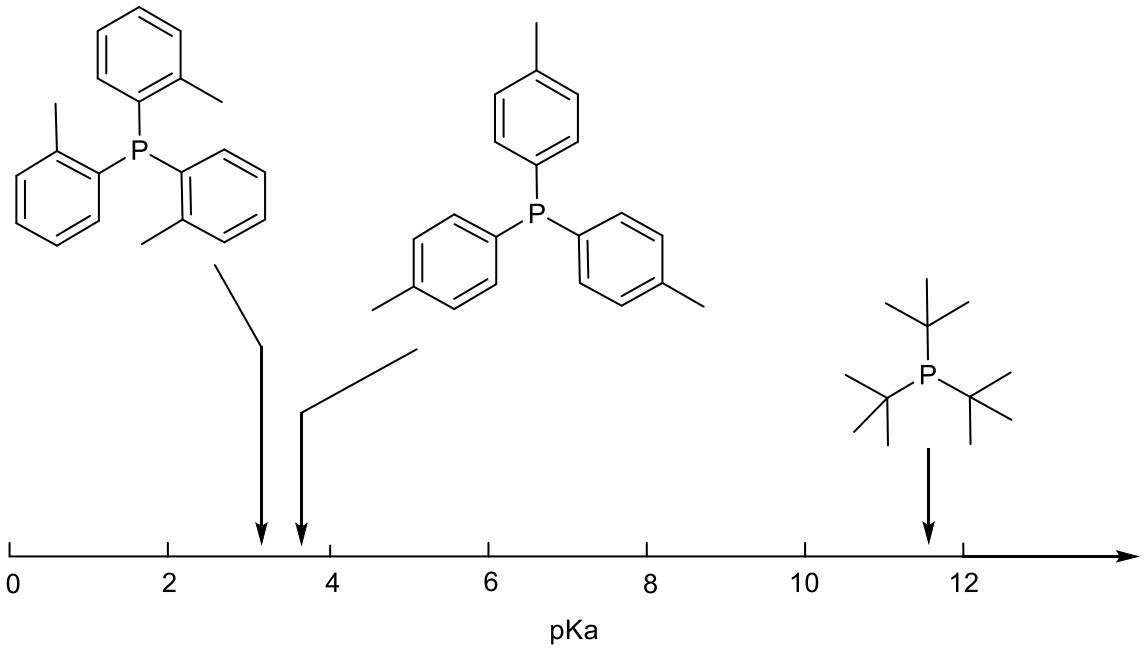

Figure 2.1 pK_a values of Phosphines used in this chapter.[62,63]

2.2 Preparation of Frustrated Lewis Pairs

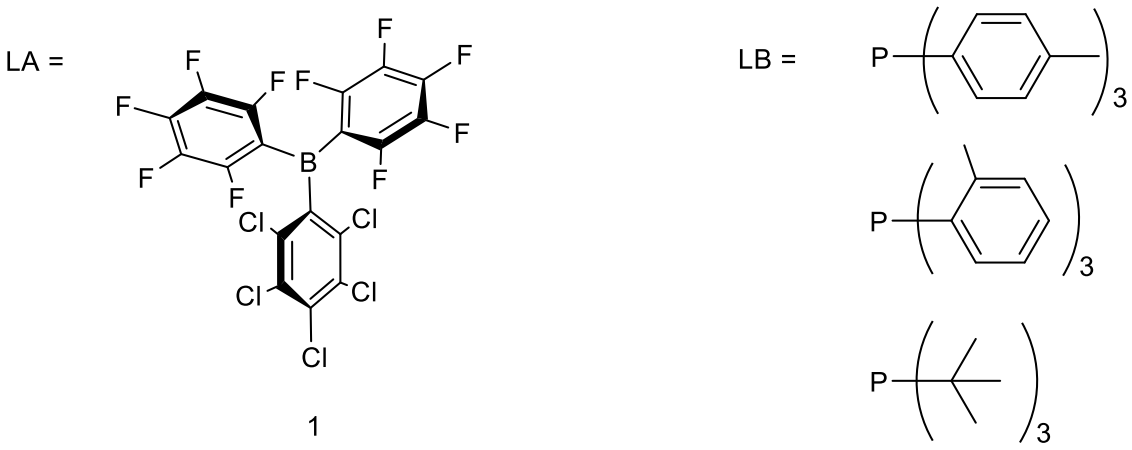

Figure 2.2 Scope of the Lewis pairs investigated for FLP behaviour.

The Lewis acid $B(C_6Cl_5)(C_6F_5)_2$ (**1**) was combined with a stoichiometric amount of PR_3 (R = ^{t}Bu, *o*-tolyl, *p*-tolyl) in benzene-d_6 (Figure 2.2), and the reactions were monitored using ^{11}B and ^{31}P NMR spectroscopy to determine FLP or Lewis adduct formation. All phosphines apart from P(*p*-tolyl)$_3$ were able to form FLPs with **1** as confirmed by the

unchanged chemical shifts of ^{11}B and ^{31}P nuclei before and after combination in solution (Table 2.1).

Table 2.1 Summary of ^{11}B and ^{31}P NMR spectroscopic data for the reactions of $B(C_6Cl_5)(C_6F_5)_2$ with P^tBu_3, P(*o*-tolyl)$_3$ and P(*p*-tolyl)$_3$

	$\delta^{11}B$		**$\delta^{31}P\{^1H\}$**		**$\Delta\delta^{11}B$**	**$\Delta\delta^{31}P\{^1H\}$**	**Conclusion**
	before	after	before	after			
[**1**/P(*p*-tolyl)$_3$]	58.8	−8.4	−7.9	17.9	67.2	25.0	Adduct
[**1**/P(*o*-tolyl)$_3$]	58.8	58.8	−29.7	−29.7	0.0	0.0	FLP
[**1**/P^tBu_3]	58.8	58.8	62.0	62.0	0.0	0.0	FLP

*Chemical shifts are quoted in ppm.

From these preliminary NMR data, it was concluded that reaction of P(*o*-tolyl)$_3$ with **1** resulted in FLP formation, whereas reaction of P(*p*-tolyl) with **1** resulted in adduct formation. This can be rationalised in terms of the difference in their Tolman cone angles (θ/deg).[66] P(*o*-tolyl)$_3$ has a θ of 194°, which is even larger than the θ of P^tBu_3 (182°), thus formation of FLP is expected. However, the θ value for P(*p*-tolyl)$_3$ is only 145° (essentially the same as for the non-substituted PPh_3), which cannot protect the P core from participating in adduct formation.

Upon the formation of [**1**−P(*p*-tolyl)$_3$] Lewis adduct, the resonance observed in the ^{11}B NMR spectrum sharpens drastically and shifts from 58.8 ppm to −8.4 ppm. This is consistent with the quenching of the Lewis acidity and formation of a four-coordinate boron species,[67] where there is reduction of both the quadrupolar coupling constant (C_Q) and asymmetry parameter (η_Q) of the ^{11}B nucleus. Furthermore, the formation of an adduct was also suggested by deshielding of the phosphorus environment (a shift of 25 ppm from free phosphine resonance) in the ^{31}P NMR spectrum.

2.3 Heterolytic H_2 Cleavage by Frustrated Lewis Pairs

2.3.1 Reaction of [1/P^{t}Bu$_3$] with H_2

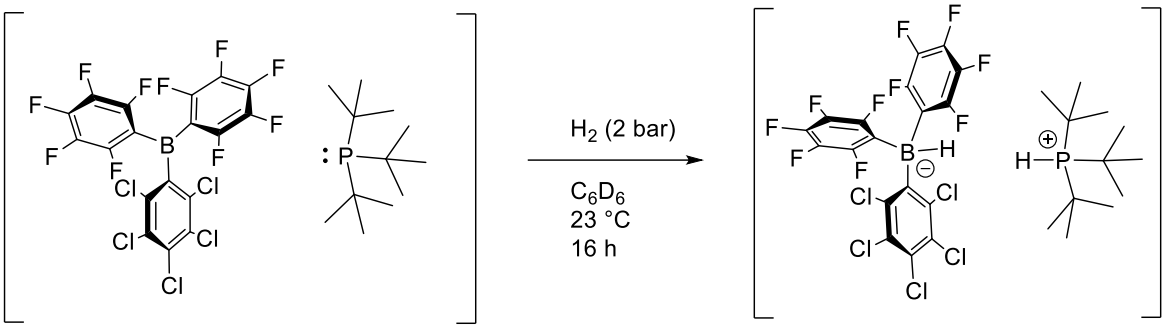

Equation 2.1 Reaction of **1**/P^{t}Bu$_3$ with H_2.

A benzene solution of equimolar **1** and P^{t}Bu$_3$ was exposed to with H_2 (2 bar) (Equation 2.1). After 16 hours of stirring at room temperature, the solvent was evaporated under reduced pressure, to yield [**1**−H][H−P^{t}Bu$_3$] as an off-white solid (85%).

FTIR spectrum of [**1**−H][H−P^{t}Bu$_3$] exhibits a characteristic B−H absorption at 2387 cm^{-1} which is consistent with the literature reported values (Figure 2.3).[53]

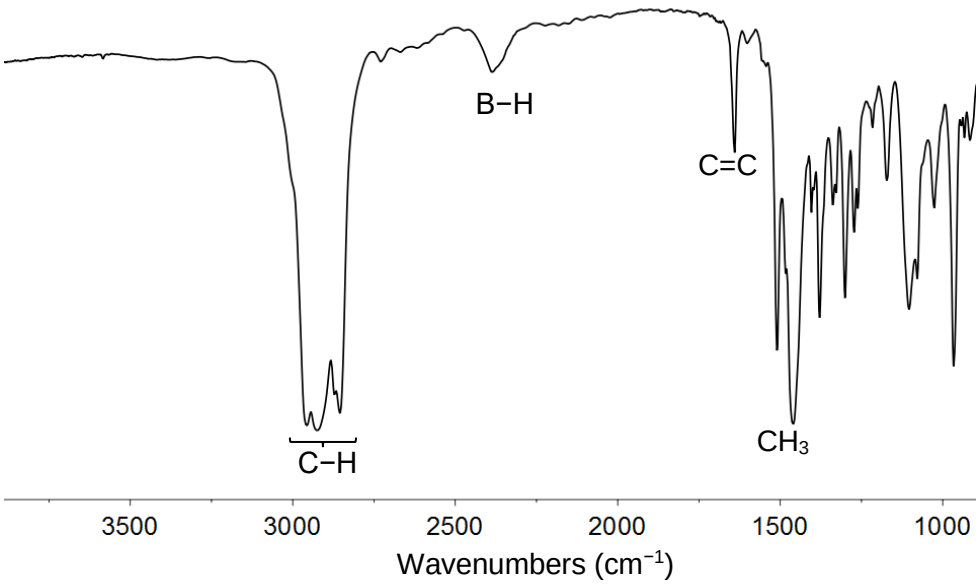

Figure 2.3 FTIR spectrum of [**1**−H][H−P^{t}Bu$_3$] displaying characteristic B−H absorption.

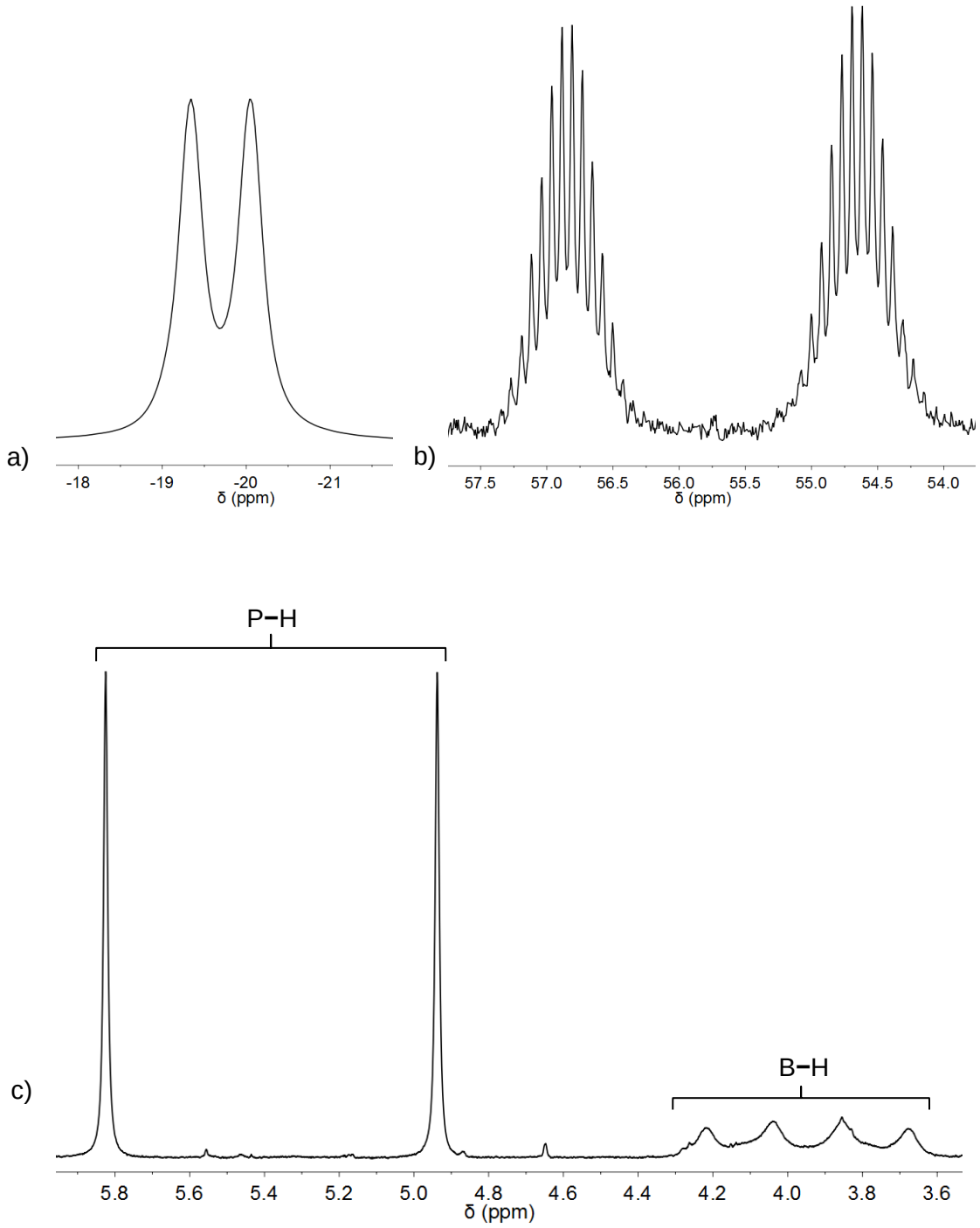

Figure 2.4 a) ^{11}B, b) ^{31}P and c) ^{1}H NMR spectrum of [**1**−H][H−P^{t}Bu$_3$] in CD_3CN.

The ^{11}B NMR spectrum of [**1**−H][H−P^{t}Bu$_3$] exhibits a sharp doublet at −19.7 ppm ($^1J_{BH}$ = 90 Hz), suggesting B−H spin-coupling (Figure 2.4a). The ^{31}P NMR spectrum also shows a doublet of multiplet at 55.7 ppm, ($^1J_{PH}$ = 445 Hz and $^3J_{PH}$ = 16 Hz) corresponding

to a phosphonium species (Figure 2.4b). The ^{1}H NMR spectrum shows a doublet at 5.4 ppm ($^1J_{HP}$ = 445 Hz) and a quadrupolar quartet (1:1:1:1) at 3.94 ppm ($^1J_{HB}$ = 90 Hz) (Figure 2.4c). These results are consistent with the formation of [**1**−H][H−P^{t}Bu$_3$], a H_2 cleavage product of [**1**/P^{t}Bu$_3$], and are in good agreement with the literature reported values of [(C$_6$F$_5$)$_3$B−H][H−P^{t}Bu$_3$].[34]

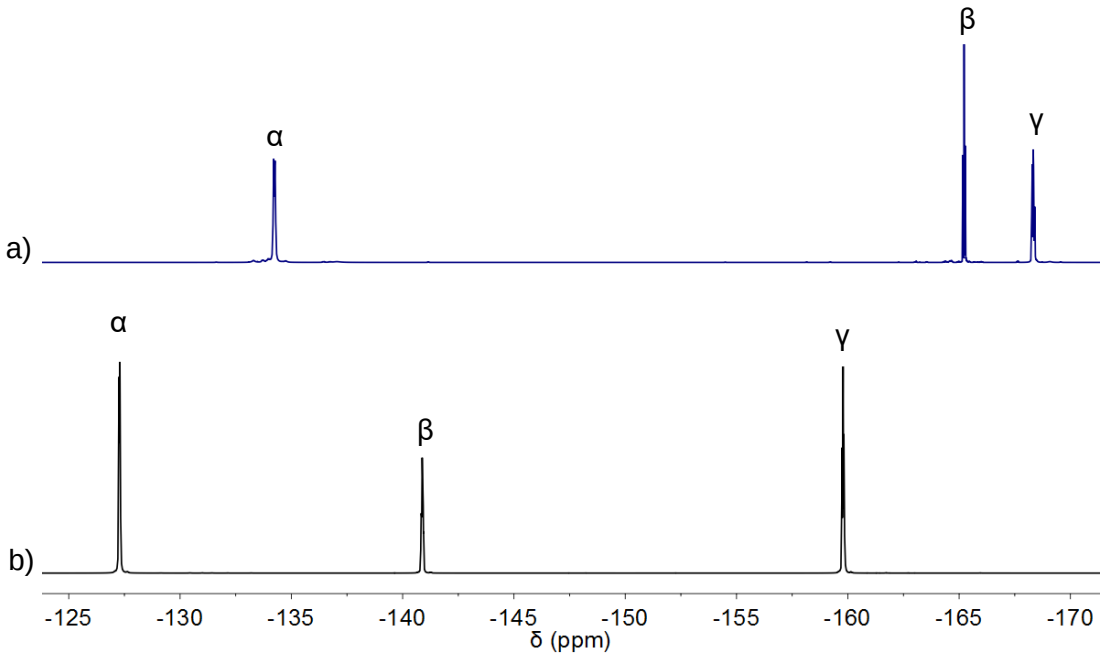

Figure 2.5 ^{19}F NMR spectra of a) **1**/P^{t}Bu$_3$ and b) [**1**−H][H−P^{t}Bu$_3$] showing (α) *ortho*-, (β) *para*- and (γ) *meta*-C$_6F_5$ in CD$_3$CN.

The value of $\Delta\delta_{m,p}$ ($\Delta\delta_{m,p} = \delta p$-C$_6F_5 - \delta m$-C$_6F_5$) for the C$_6F_5$ moiety in the ^{19}F NMR spectrum provides a useful indication of the boron coordination number.[68] A large $\Delta\delta_{m,p}$ value (between 10−25 ppm) suggests a three coordinate boron, whereas a small $\Delta\delta_{m,p}$ value (>7 ppm) indicates a four coordinate boron. In this study, the ^{19}F NMR spectrum of unreacted [**1**/P^{t}Bu$_3$] displays resonances at −127.3 ppm (*ortho*-C$_6F_5$), −140.9 ppm (*para*-C$_6F_5$) and −159.8 ppm (*meta*-C$_6F_5$) with a $\Delta\delta_{m,p}$ value of 18.9, which is consistent

with tri-coordination at the boron centre (Figure 2.5a). Upon reaction with H_2, the resonances for *ortho*-, *para*- and *meta*-C_6F_5 has shifted to −134.4, −165.2 and −168.4 ppm, with a corresponding $\Delta\delta_{m,p}$ value of 3.2 ppm (Figure 2.5b). This value is consistent with a four-coordinate boron, further supporting the formation of [**1**−H][H−P^{t}Bu$_3$] species (Table 2.2).[34]

Table 2.2 ^{19}F NMR spectroscopic data for [**1**/P^{t}Bu$_3$] in C_6D_6 and the H_2 cleavage product [**1**−H] [H−P^{t}Bu$_3$] in CD_3CN

	δ^{19}F			
	ortho-F	*para*-F	*meta*-F	$\Delta\delta_{m,p}$
[**1**/P^{t}Bu$_3$]	−127.3	−140.9	−159.8	18.9
[**1**−H] [H−P^{t}Bu$_3$]	−134.4	−165.2	−168.4	3.2

*Chemical shifts are quoted in ppm.

2.3.2 Reaction of [1/P(*o*-tolyl)$_3$] with H_2

A NMR tube containing a benzene solution of [**1**][P(*o*-tolyl)$_3$] was charged with H_2 (2 bar), however no reaction was observed after 16 hours at 23 °C and 48 hours at 110 °C (unchanged NMR spectra), therefore it was concluded that **1**/P(*o*-tolyl)$_3$ does not react activate H_2. It is postulated that the cone angle of P(*o*-tolyl)$_3$ is too large, and the increased spatial separation between the Lewis acid and Lewis base has reduced the electrostatic field strength (H_2 cleavage mechanism introduced in Chapter One), preventing heterolytic fission of H_2. Nonetheless, the NMR spectra before and after prolonged heating of **1**/P(*o*-tolyl)$_3$ under H_2 showed no thermal decomposition products, indicating that this FLP system has a relatively high thermal stability.

2.4 FLP Mediated CO_2 Hydrogenation

Although FLP mediated hydrogenation of CO_2 can be monitored using ^{1}H, ^{11}B, $^{13}C\{H\}$, ^{19}F and ^{31}P NMR, the NMR spectra often contain a mixtures of products. The intermediate species (formatoborate and methoxyborate complexes) can be independently synthesised through reactions of the FLP with formic acid (**Route A1**) or methanol (**Route A2**) respectively, providing the necessary spectroscopy data for the anticipated reaction intermediates (Scheme 2.3).

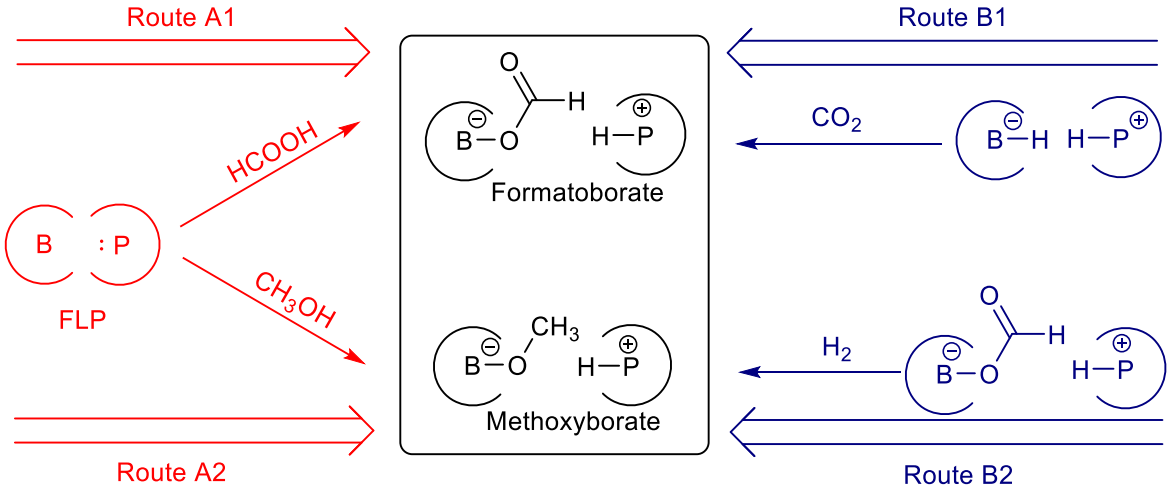

Scheme 2.3 Synthetic routes to the formatoborate and methoxyborate species.

2.4.1 Synthesis of [1−OC(O)H][H−P^{t}Bu$_3$] *via* Route A1

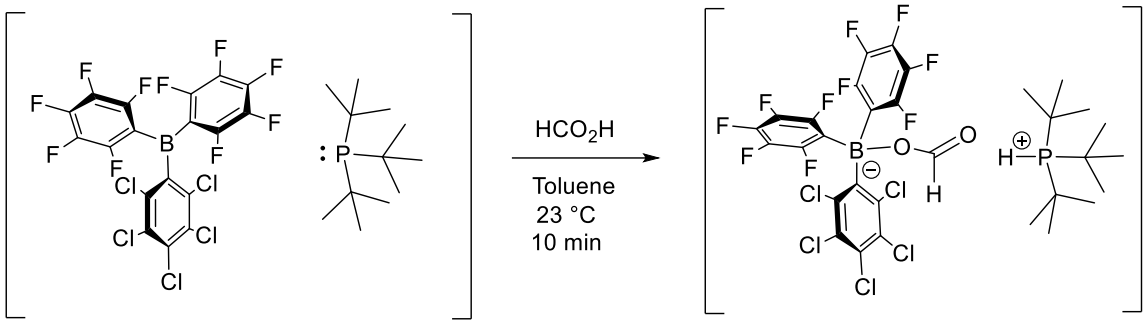

Equation 2.2 Synthesis of [**1**−OC(O)H][H−P^{t}Bu$_3$] through reaction of [**1**/P^{t}Bu$_3$] with formic acid.

[**1**−OC(O)H][H−P(*t*Bu)$_3$] was independently synthesised by reaction of [**1**/P^{t}Bu$_3$] FLP with formic acid in toluene (route A1, Equation 2.2). Precipitation was observed immediately after the addition of formic acid to the FLP mixture, and the reaction was complete within 10 minutes. Isolation of the colourless precipitate yielded analytically pure [**1**−OC(O)H][H−P(*t*Bu)$_3$] in >95% yield.

The ^{13}C {^{1}H} NMR spectrum displays a resonance at 164.5 ppm corresponding to a highly deshielded C-environment, and is assigned to −O**C**(O)H species (Figure 2.6a). A singlet at 30 ppm and a doublet at 37.7 ppm are characteristics of *t*-Bu C-atoms. The ^{1}H NMR spectrum shows a singlet at 8.05 ppm, and is assigned to the −O**C**(O)**H** proton (Figure 2.6b). A large broad doublet at 5.4 ppm ($^1J_{HP}$ = 420 Hz) with relative intensity of 1H and a doublet at 1.6 ppm ($^3J_{HP}$ = 16 Hz) with relative intensity of 27H in the ^{1}H NMR spectrum are characteristics of a [H−P^{t}Bu$_3$]$^+$ species.

The ^{31}P NMR spectrum shows a broad doublet at 55.7 ppm ($^1J_{PH}$ = 420 Hz), which is characteristic of a protonated phosphonium species (Figure 2.67a). The ^{11}B NMR spectrum exhibits a sharp singlet at −1.75 ppm and is assigned to the formatoborate species [**1**−OC(O)H] (Figure 2.7b). The ^{19}F NMR spectrum (Figure 2.7c) is almost identical to that of the borohydride salt [**1**−H][H−P^{t}Bu$_3$] (Table 2.2), and indicates that the boron is

tetra-coordinated. These NMR results are consistent with the literature reported values for $[(C_6F_5)_3B{-}OC(O)H][H{-}TMP]$.[53]

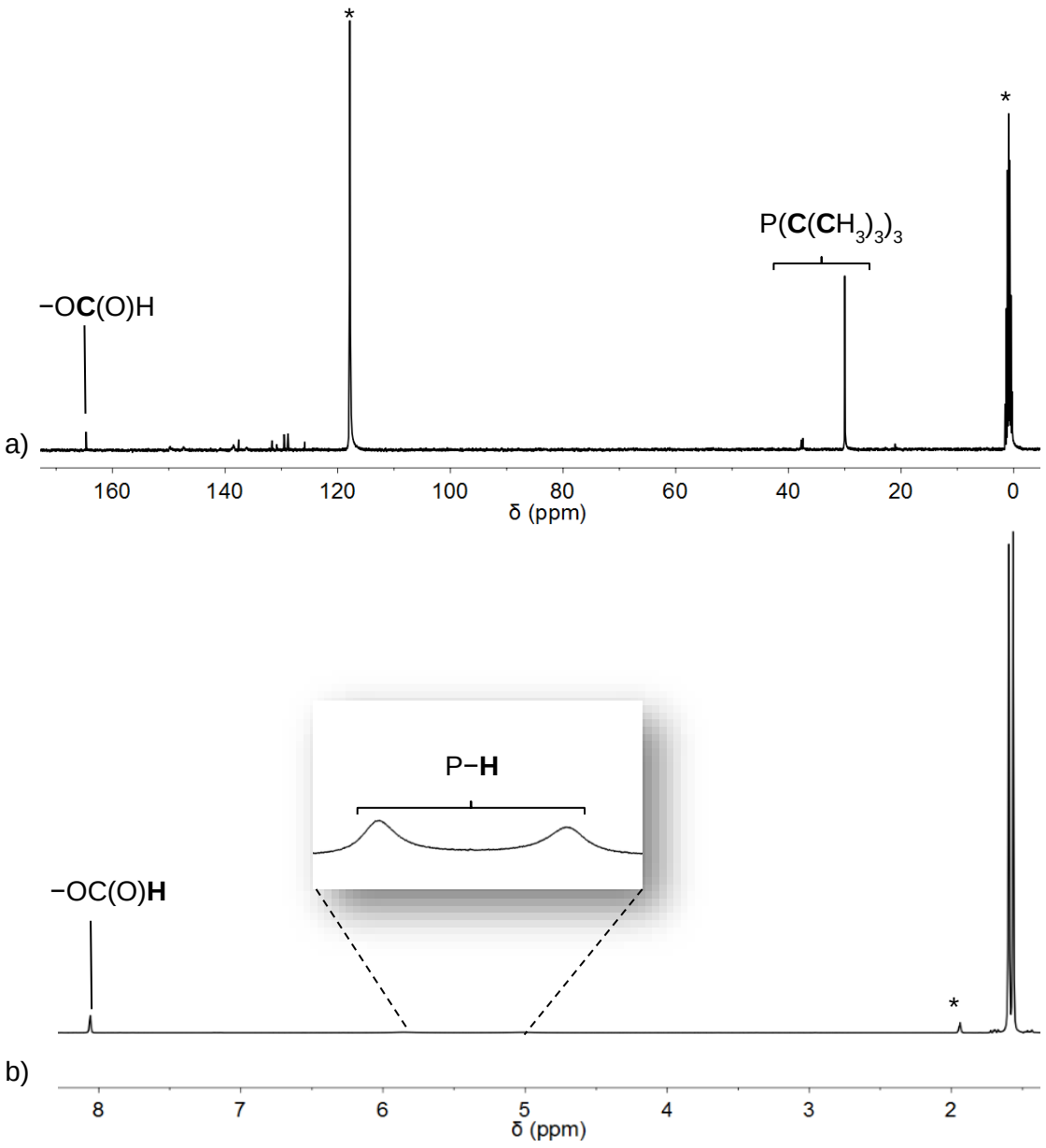

Figure 2.6 a) ^{13}C $\{^1H\}$ and b) ^1H NMR spectrum of [**1**−OC(O)H][H−P(*t*Bu)$_3$] displaying characteristic formate resonances. *residual protio solvent signal.

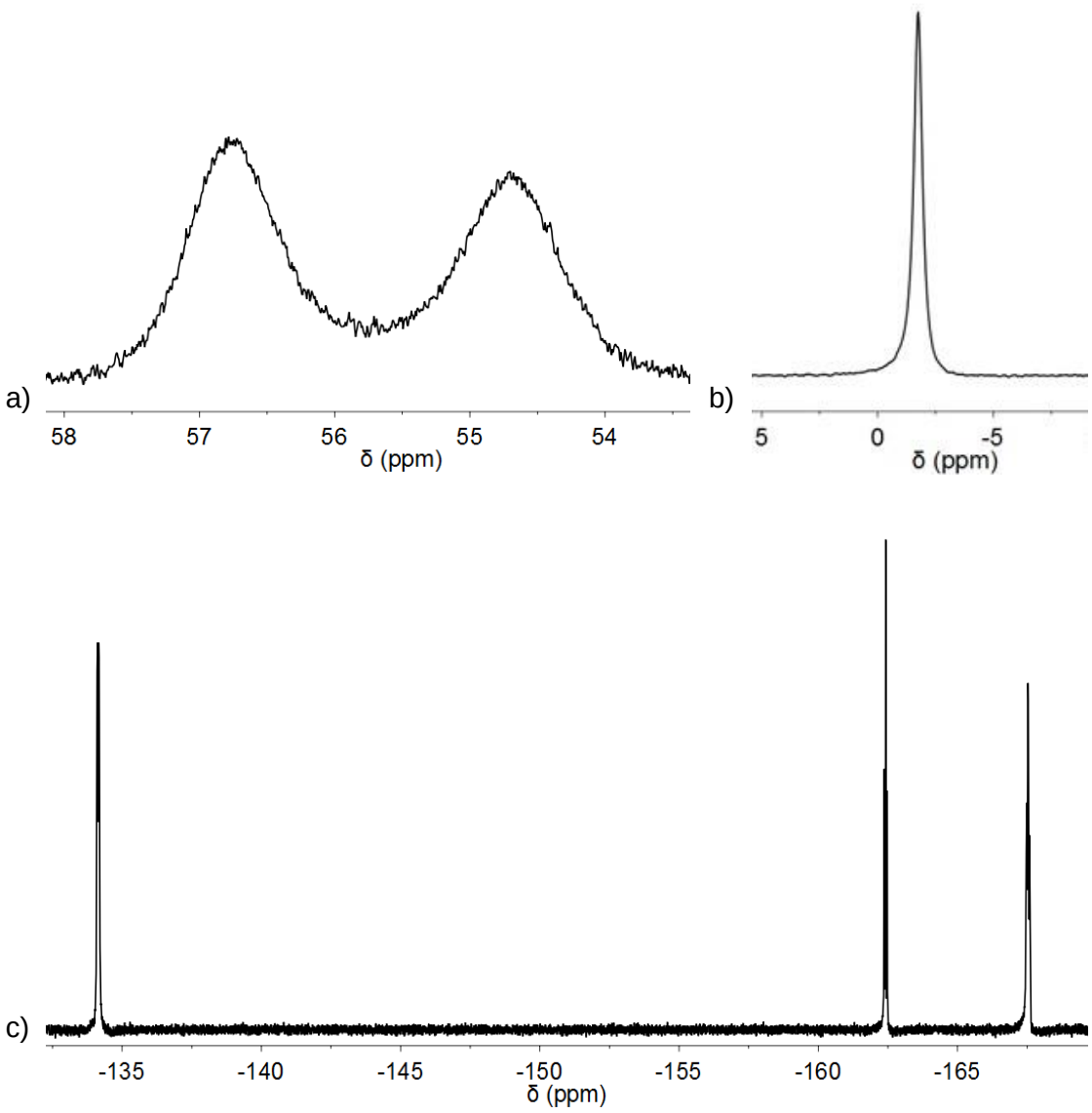

Figure 2.7 a) ^{31}P, b) ^{11}B, and c) ^{19}F NMR spectrum of [**1**−OC(O)H][H−P^{t}Bu$_3$] in CD_3CN.

2.4.2 Solid-state Structure of [1−OC(O)H][H−P^{t}Bu$_3$]

Single crystals suitable for an X-Ray diffraction were grown from a saturated toluene solution at −35 °C. The molecular structure of [**1**−OC(O)H][H−P^{t}Bu$_3$] (Figure 2.8) showed a four-coordinate boron centre in a pseudo-tetrahedral geometry, as seen from the C−B−C and C−B−O angles (Table 2.3). The solid-state molecular structure is consistent with the solution-phase NMR data for [**1**−OC(O)H][H−P^{t}Bu$_3$].

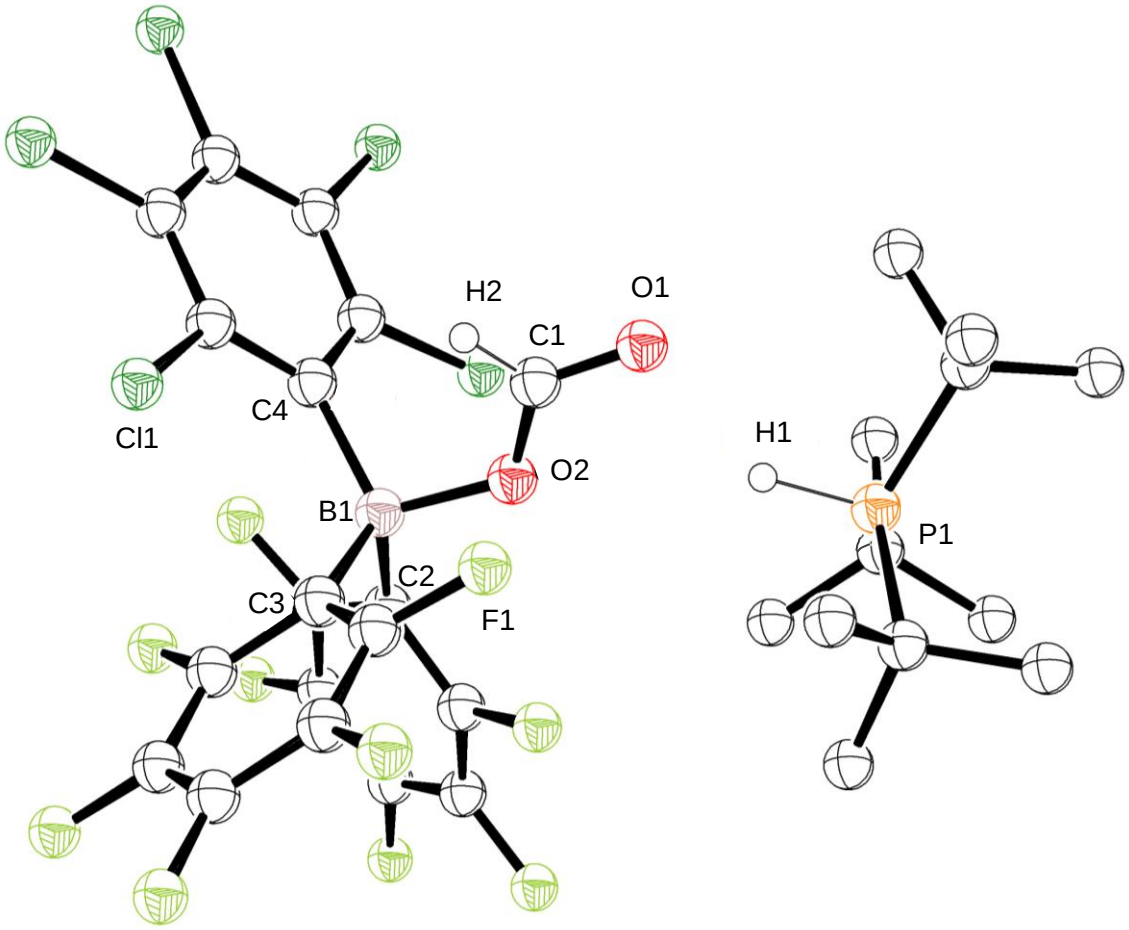

Figure 2.8 Solid-state structure of [**1**−OC(O)H][H−P^{t}Bu$_3$]. Thermal ellipsoids at 50% probability. *tert*-Butyl H-atoms are removed for clarity.

The B−O (1.524 Å) and C=O (1.215 Å) bond distances in [**1**−OC(O)H][H−P^{t}Bu$_3$] are slightly shorter compared to [(C$_6$F$_5$)$_3$B−OC(O)H][H−TMP], supporting the postulate that the boron centre in **1** is more electron deficient than B(C$_6$F$_5$)$_3$. Increased length of B−C bonds in [**1**−OC(O)H][H−P^{t}Bu$_3$] was observed when compared to those of [(C$_6$F$_5$)$_3$B−OC(O)H][H−TMP], which is reasonable since **1** is more sterically demanding than B(C$_6$F$_5$)$_3$. The C2−B1−C3 bond angle (102.87°) is comparatively smaller than the bond angles of C2−B1−C4 (112.74°) and C3−B1−C4 (118.97°), which is due to the bulky C$_6$Cl$_5$ ring pushing the two C$_6$F$_5$ rings away.

Table 2.3 Comparison of metrical parameters (bond lengths in Å, angles in °) in [**1**−OC(O)H][H−P^{t}Bu$_3$] and [(C$_6$F$_5$)$_3$B−OC(O)H][H−TMP]. (esds are given in parentheses).

	[1−OC(O)H][H−P^{t}Bu$_3$]	**[(C$_6$F$_5$)$_3$B−OC(O)H][H−TMP]**[53]
C1−O1	1.215(2)	1.236
C1−O2	1.307(2)	1.288
B1−O2	1.524(2)	1.546
B1−C2	1.649(3)	1.639
B1−C3	1.656(3)	1.648
B1−C4	1.660(2)	1.645
C2−B1−C3	102.87(13)	110.8
C2−B1−C4	112.74(14)	113.5
C3−B1−C4	118.97(14)	112.4
C4−B1−O2	106.09(13)	104.1
C3−B1−O2	109.13(13)	111.6
C2−B1−O2	106.43(13)	104.0

2.4.3 Synthesis of [1−OCH$_3$][H−P^{t}Bu$_3$] *via* Route A2

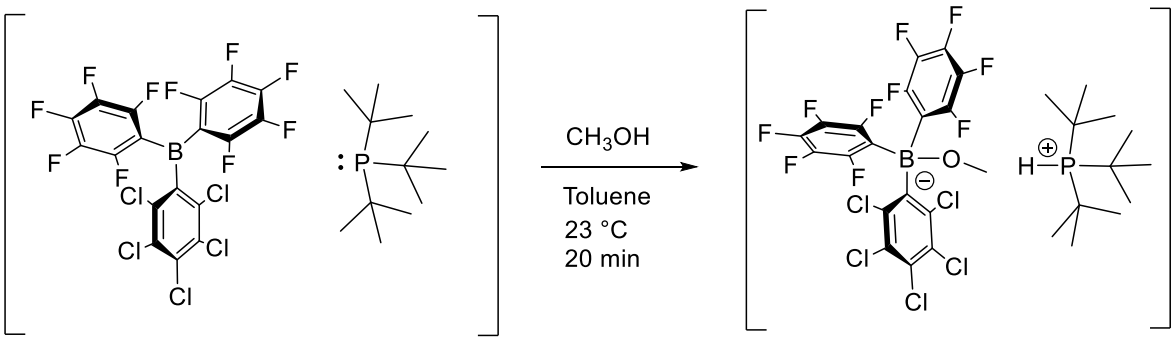

Equation 2.3 Synthesis of [**1**−OCH$_3$][H−P^{t}Bu$_3$] through reaction of [**1**/P^{t}Bu$_3$] with methanol.

[**1**−OCH$_3$][H−P^{t}Bu$_3$] was synthesised by reaction of [**1**/P^{t}Bu$_3$] with a stoichiometric amount of MeOH at 23 °C (Equation 2.3). The reaction completed in 20 minutes to yield analytically pure [**1**−OCH$_3$][H−P^{t}Bu$_3$] as a colourless oil, and was characterised by ^{1}H, ^{11}B, ^{13}C, ^{19}F and ^{31}P NMR spectroscopy.

The ^{1}H NMR spectrum (Figure 2.9a) displays a doublet resonance at 5.4 ppm ($^1J_{PH}$ = 445) and a doublet at 1.6 ppm ($^3J_{PH}$ = 15.6). These resonances are attributed to [H−P^{t}Bu$_3$]$^+$

species. A resonance at 2.95 ppm corresponding to 3H is assigned to B−OCH_3 species. The characteristic methoxy resonance can also be observed at 52.3 ppm in the $^{13}C\{H\}$ NMR spectrum (2.9b).

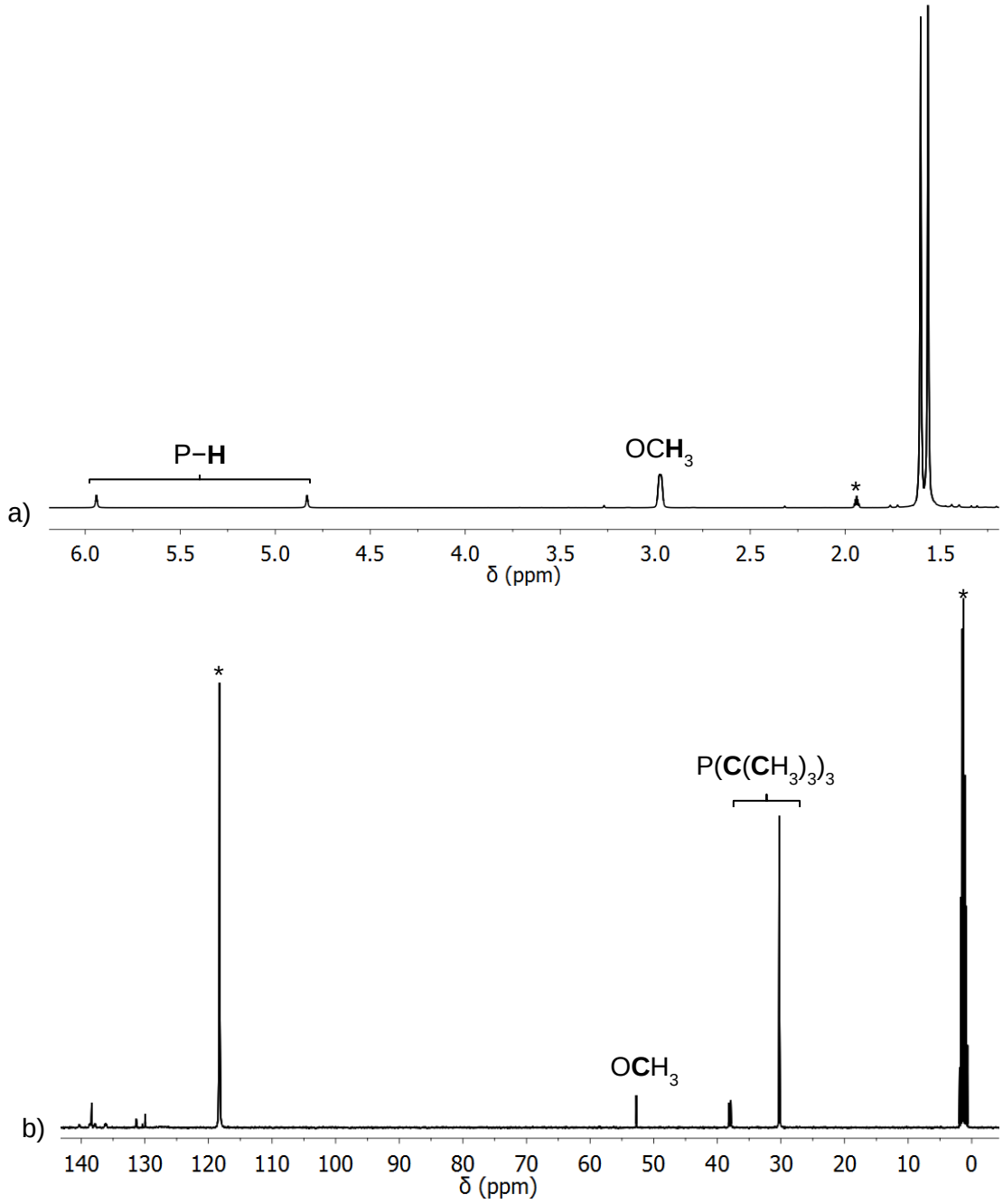

Figure 2.9 a) ^{1}H and b) ^{13}C NMR spectrum of [**1**−OCH_3][H−P^{t}Bu$_3$] in CD_3CN. *residual protio solvent signal.

The ^{31}P NMR spectrum is very similar to that of [**1**−H][H−P^{t}Bu$_3$], showing a doublet of multiplets at 55.8 ppm ($^1J_{PH}$ = 445 Hz and $^3J_{PH}$ = 16 Hz), consistent with the formation of a phosphonium cation. The appearance of a sharp resonance at −0.2 ppm in the ^{11}B NMR spectrum (Figure 2.10b) and a set of resonances at −133.3, −164.3 and −167.7 with $\Delta\delta_{m,p}$ value of 3.4 ppm in the ^{19}F NMR spectrum (Figure 2.10c) are consistent with the formation of a tetra-coordinate [**1**−OCH$_3$]$^-$ anion.

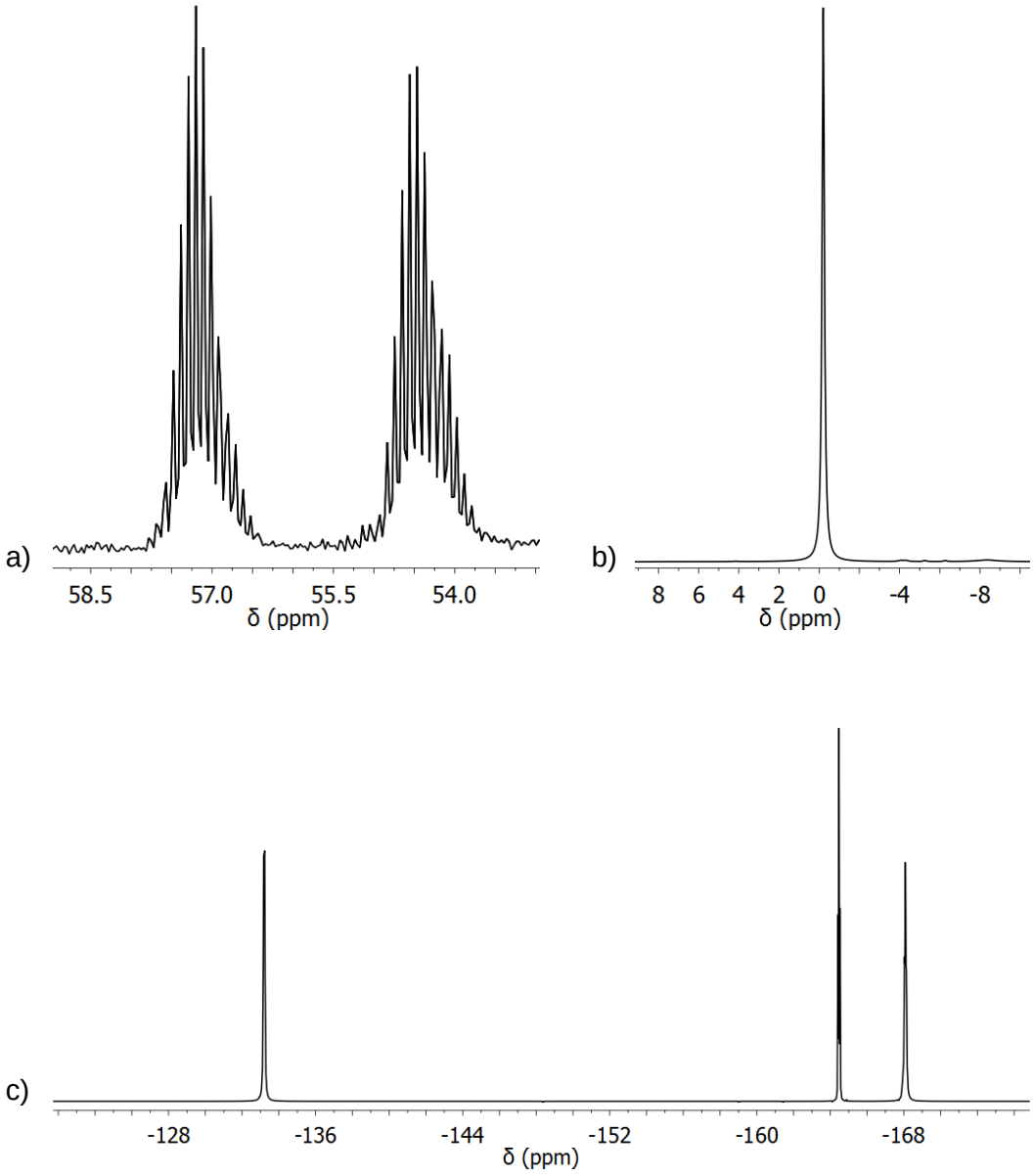

Figure 2.10 a) ^{31}P, b) ^{11}B, and c) ^{19}F NMR spectrum of [**1**−OC(O)H][H−P^{t}Bu$_3$] in CD$_3$CN.

2.4.4 CO_2 insertion reaction with [1−H][H−P^{t}Bu$_3$] *via* Route B1

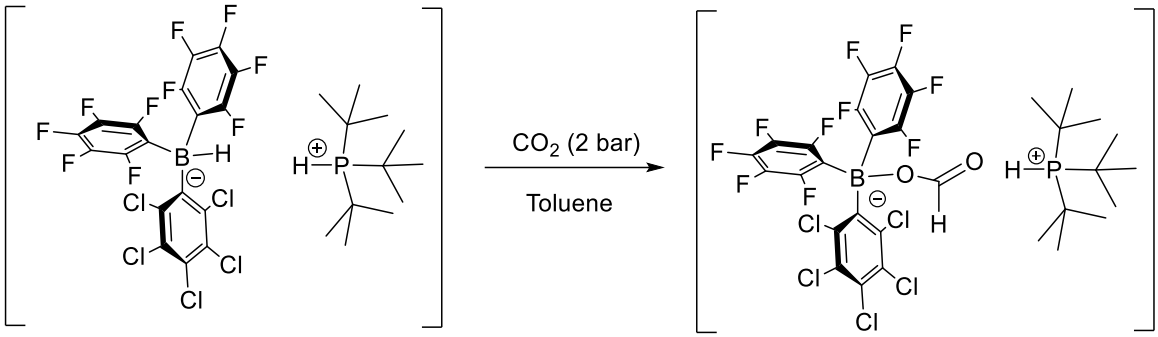

Equation 2.4 Reaction of [**1**−H][H−P^{t}Bu$_3$] with CO_2.

Synthesis of [**1**−OC(O)H][H−P^{t}Bu$_3$] *via* the reaction of [**1**−H][H−P^{t}Bu$_3$] with CO_2 was attempted and the reaction was monitored by NMR spectroscopy. No spectroscopic evidence for CO_2 insertion into the B−H bond was observed at room temperature, therefore the reaction mixture was heated. The characteristic resonances for the [**1**−H][H−P^{t}Bu$_3$] (see section 2.4.1) remained visible at temperature up to 65 °C, however, after 72 h at 90 °C, the hydride salt was consumed, as confirmed by the disappearance of the P−*H* doublet at 5.4 ppm and the B−*H* quadrupolar quartet at 3.94 ppm. However, there was no evidence of the formation of [**1**−OC(O)H][H−P^{t}Bu$_3$], and a mixture of side product was detected. C_6F_5H can be observed in the ^{1}H and ^{19}F NMR spectra, indicating that decomposition of the FLP had occurred. The mechanism for the decomposition can be explained by the appearance of a resonance corresponding to free P^{t}Bu$_3$ in the ^{31}P NMR spectrum, indicating that at high temperatures, [H−P^{t}Bu$_3$]$^+$ protonates the *ipso*-C of the C_6F_5 ring (Scheme 2.1). The ^{11}B NMR spectrum, several narrow resonances are visible at around 1.3 ppm, in the region expected for borate species, however these signals do not correspond to those of the independently synthesised [**1**−OC(O)H][H−P^{t}Bu$_3$] or [**1**−OCH$_3$][H−P^{t}Bu$_3$]. However, since [**1**−OC(O)H][H−P^{t}Bu$_3$] can be synthesised via Route

A1, partial deoxygenation of [**1**−OC(O)H][H−P^{t}Bu$_3$] to [**1**−OCH$_3$][H−P^{t}Bu$_3$] was investigated.

2.4.5 Partial Hydrodeoxygenation of [1−OC(O)H][H−P^{t}Bu$_3$] by [1/P^{t}Bu$_3$] FLP

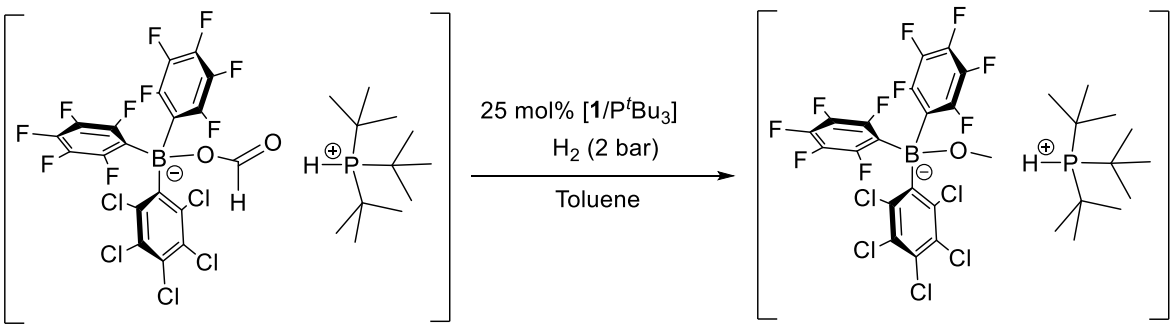

Equation 2.4 Partial deoxygenation of [**1**−OC(O)H][H−P^{t}Bu$_3$] by [**1**/P^{t}Bu$_3$].

Addition of H_2 to a NMR tube containing a toluene mixture of [**1**−OC(O)H][H−P^{t}Bu$_3$] (synthesised via route A1) with 25 mol % of [**1**/P^{t}Bu$_3$]. The progress of the reaction was monitored by ^{1}H, ^{11}B, ^{31}P and ^{19}F NMR spectroscopy. Upon addition of H_2 to the reaction mixture, the H_2 activation product [**1**−H][H−P^{t}Bu$_3$] was generated. This was evidenced by the appearance of characteristic [B−H]$^-$ signals in ^{1}H, ^{11}B and ^{19}F NMR spectrum. Room temperature overnight and subsequent heating up 90 °C showed no signs of hydrodeoxygenation of [**1**−OC(O)H][H−P^{t}Bu$_3$]. However, after heating the mixture at 110 °C for 72 hours, a small amount of [**1**−OCH$_3$][H−P^{t}Bu$_3$] was observed, as confirmed by the observation of a resonance at 2.95 ppm corresponding to −OCH$_3$ group in the ^{1}H NMR spectrum (Figure 2.11b), as well as a borate resonance at −0.2 ppm in the ^{11}B NMR spectrum (Figure 2.12b).

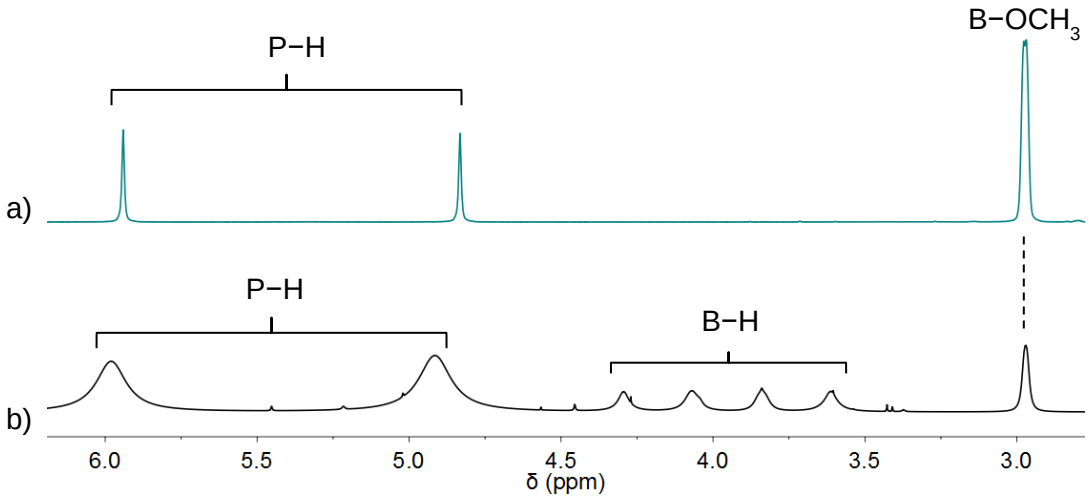

Figure 2.11 ^{1}H NMR spectra of: a) [**1**−OCH_3][H−P^{t}Bu$_3$] synthesised *via* route A1 and b) partial hydrodeoxygenation of [1−OC(O)H][H−P^{t}Bu$_3$] after heating at 110 °C for 72 hours in CD_3CN.

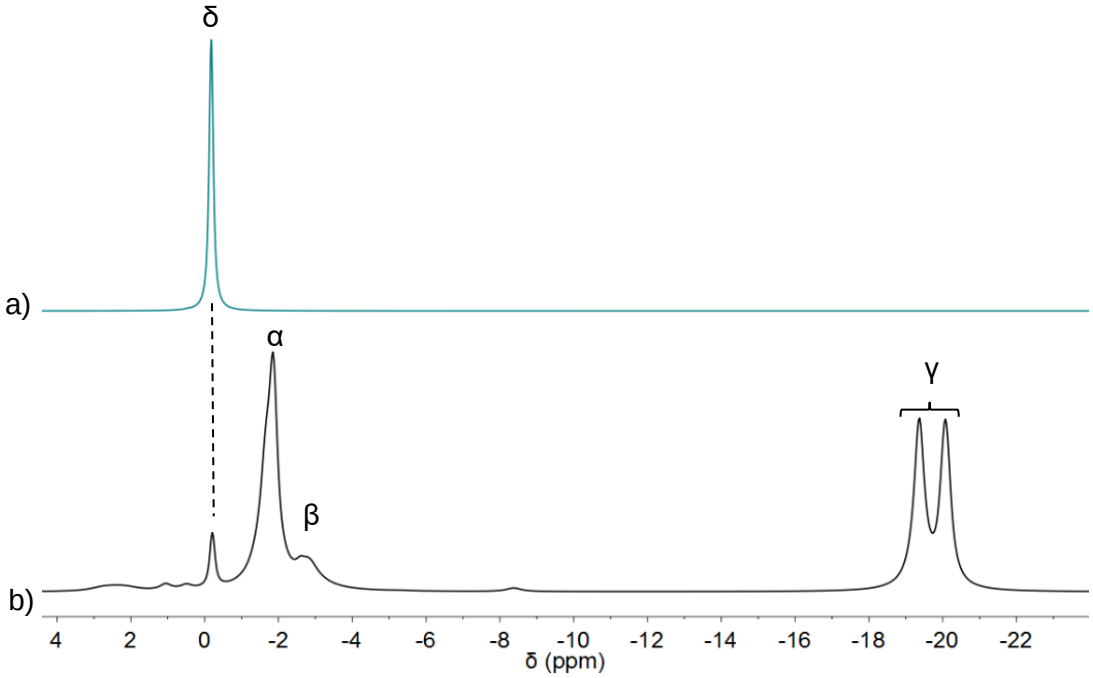

Figure 2.12 ^{11}B NMR spectra of: a) [**1**−OCH_3][H−P^{t}Bu$_3$] synthesised *via* route A1 and b) partial hydrodeoxygenation of [1−OC(O)H][H−P^{t}Bu$_3$] after heating at 110 °C for 72 hours showing (α) [**1**−OC(O)H], (β) [**1**−OH], (γ) [**1**−H] and (δ) [**1**−OCH_3]; in CD_3CN.

The ^{19}F NMR spectrum shows the appearance of a set of resonances in relative low intensity with a $\Delta\delta_{m,p}$ value of 3.7, consistent with the formation of [**1**−OCH_3]$^-$. The decrease in the intensity of resonance associated with [**1**−OC(O)H][H−P^{t}Bu$_3$] is also consistent with the conversion of formatoborate species to the methoxyborate species (Figure 2.13b).

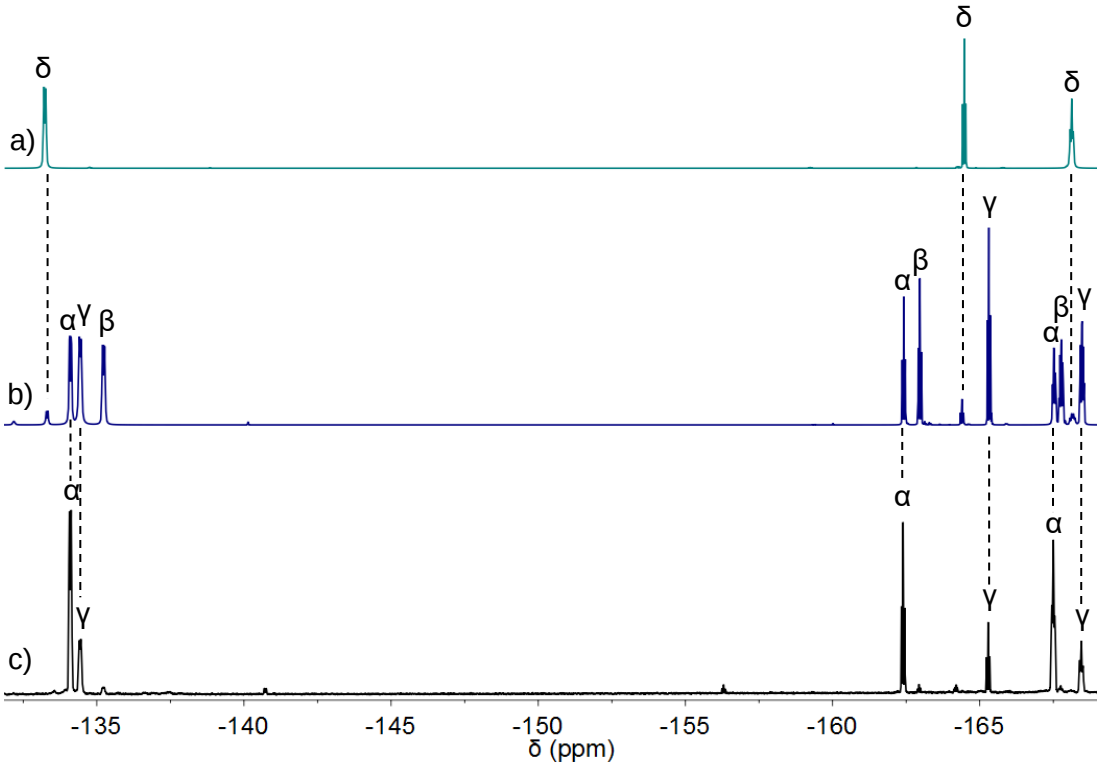

Figure 2.13 ^{19}F NMR spectra of: a) [**1**−OCH_3][H−P^{t}Bu$_3$] synthesised *via* route A1; Partial hydrodeoxygenation of [1−OC(O)H][H−P^{t}Bu$_3$] b) after and c) before heating at 110 °C for 72 hours showing (α) [**1**−OC(O)H], (β) [**1**−OH], (γ) [**1**−H] and (δ) [**1**−OCH_3].

In addition to [**1**−H][H−P^{t}Bu$_3$], [**1**−OC(O)H][H−P^{t}Bu$_3$] and [**1**−OC(O)H][H−P^{t}Bu$_3$] species, an additional species was identified in the ^{11}B and ^{19}F NMR spectra (Figure 2.12 and 2.13). The broad resonance at −2.75 ppm in the ^{11}B NMR spectrum and the three resonances at −135.2, −164 and −168 ppm in the ^{19}F NMR spectrum are attributed to the formation of [**1**−OH]$^-$ during the hydrodeoxygenation reaction.[11,53] Moreover, small amount of C_6F_5H can be detected in the ^1H NMR spectrum indicating decomposition of the

Lewis acid through protonolysis of [**1**−OH]⁻, although this decomposition occurs much faster at higher temperatures. As decomposition had already been observed at this early stage, it was concluded that the system could not operate catalytically.

Large amount of unreacted [**1**−OCH_3][H−P^tBu_3] and [**1**−H][H−P^tBu_3] were still present in the reaction mixture, and formation of free methanol was not detected by NMR spectroscopy. This could be due to the reaction being performed in a closed system, and that the formation of methanol may have been inhibited, which instead encourages the decomposition pathway.

Further heating of the reaction to 130 °C for 1 week led to further decomposition and no significant increase in concentration of the species of interest, therefore the reaction was terminated. Other works have shown that increasing the pressure of CO_2 and H_2 could force the reaction equilibrium towards the formation of the methoxyborate species, while retaining a mild reaction temperature can prevent decomposition (protonation of the C_6F_5 occurs at higher temperatures).[54,69] However, carrying out reactions under high pressure conditions were beyond the scope of our current studies.

Comparing to Ashley's [$B(C_6F_5)_3$/TMP] system which was able to reduce CO_2 to methoxyborate at 160 °C, [**1**/P^tBu_3] is more reactive and operates under milder conditions. The increased reactivity of [**1**/P^tBu_3] could be explained by the stronger electrophilicity of **1** compared to $B(C_6F_5)_3$. Moreover, this increased Lewis acidity also strengthens the B−O bond, as seen in the shortened B−O bond distance in the solid-state structure of [**1**−OC(O)H][H−P^tBu_3], which in turn had prevented the liberation of methanol.

2.4.6 One-pot Hydrogenation of CO_2 by [1/P^tBu_3]

As previously discussed [**1**/P^tBu_3] demonstrates effective H_2 activation at mild conditions, and partial hydrodeoxygenation of [**1**−OC(O)H][H−P^tBu_3] species to

[**1**−OCH_3][H−P^tBu_3] species. However, each reaction was carried out independently, whereas under catalytic conditions, all reagents will be mixed in one vessel. Therefore, the behaviour of [**1**/P^tBu_3] in a CO_2/H_2 mixed gas environment was investigated. Due to the difference in solubility between the unreacted FLP [**1**/P^tBu_3] and the ionic products ([**1**−H][H−P^tBu_3], [**1**−OC(O)H][H−P^tBu_3], and [**1**−OCH_3][H−P^tBu_3]), bromobenzene was chosen as since it offers good solubility for all species.

H_2 (2 bar) and CO_2 (2 bar) was admitted to a J-Young's NMR tube containing [**1**/P^tBu_3] in C_6D_5Br. The reaction was left at room temperature for 16 hours, and characteristic resonances for [**1**−H][H−P^tBu_3] appeared in the ^{31}P, ^{11}B, ^{19}F and ^1H NMR spectra. The mixture was heated at 65 °C for 16 hours then increased to 95 °C, but the only species remained visible was [**1**−H][H−P^tBu_3]. However, after 72 hours at 110 °C, a new resonance at −0.32 ppm in the ^{11}B NMR spectrum and a low intensity resonance at 3.1 ppm in the ^1H NMR spectrum appeared (Figure 2.14). These resonances are consistent with a [$BOCH_3$] species, and hence it was postulated that methoxyborate [**1**−OCH_3][H−P^tBu_3] has been formed.

Stephan *et al*. reported that [B(C_6F_5)$_3$/P^tBu_3] is capable of reversibly binding CO_2 by addition across the C=O bond in similar fashion to the ethylene addition, to form (C_6F_5)$_3$BO−C(O)P^tBu_3.[70] Similarly, Ashley *et al*. and Tran *el al.* reported the observation of formatoborate species during the reduction of CO_2 using [B(C_6F_5)$_3$/TMP] and [B(C_6F_5)$_3$/Lut] systems.[53,54] However, these products were not observed with the [**1**/P^tBu_3] system. It is possible that since the **1** is a bulkier and more electrophilic borane than B(C_6F_5)$_3$, H_2 activation occursed at a much higher rate than the competing CO_2 addition to [**1**/P^tBu_3] in the CO_2/H_2 mixed gas environment, and any [**1**−OC(O)H][H−P^tBu_3] intermediate produced was rapidly converted to [**1**−OCH_3][H−P^tBu_3].

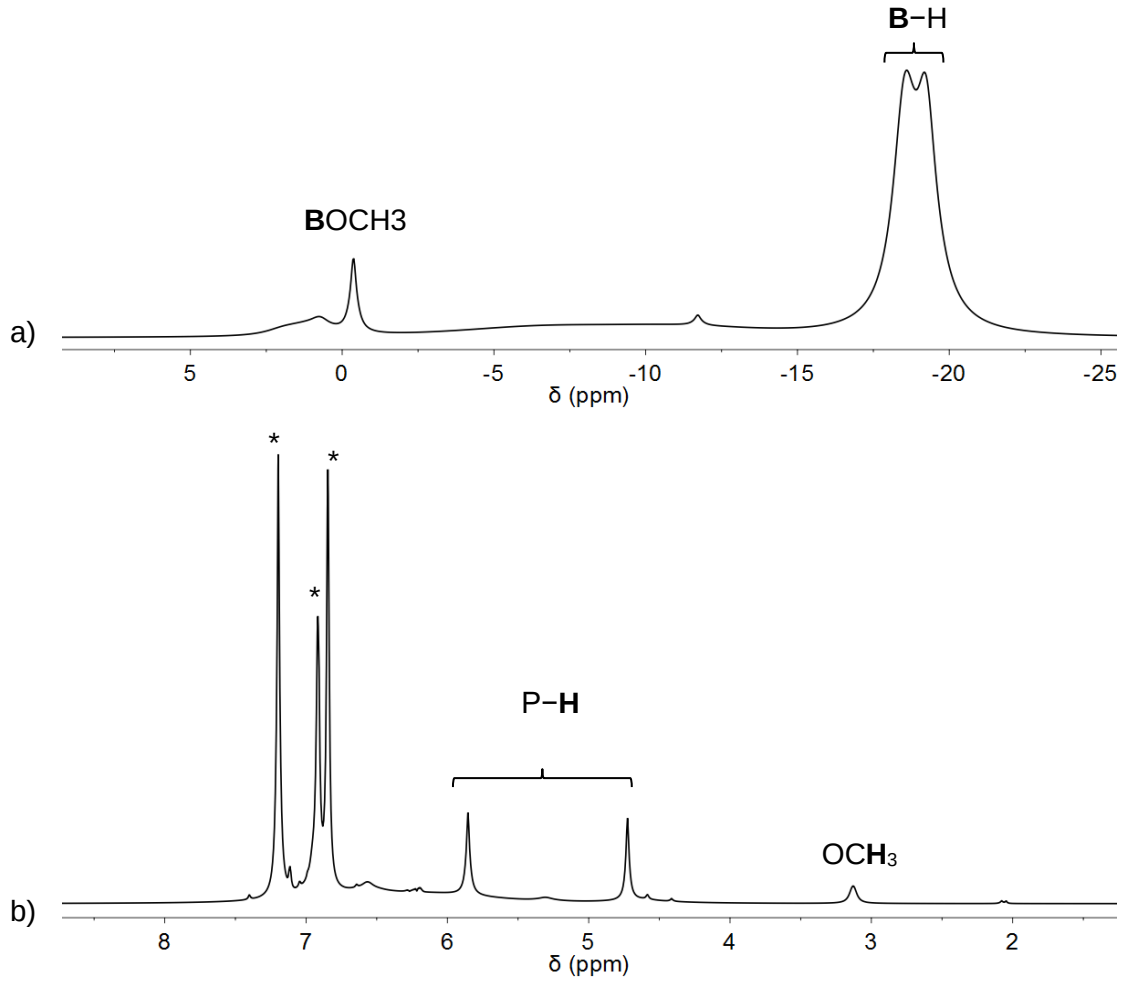

Figure 2.14 a) ^{11}B and b) ^{1}H NMR spectrum of the reduction of CO_2 using [**1**/P^{t}Bu$_3$] and H_2 after 72 hour at 130 °C showing the formation of [**1**−OCH_3]$^-$ species

Since large amount of [**1**−H][H−P^{t}Bu$_3$] was still present in the reaction mixture, the reaction was continued for another 5 days at 140 °C. Growth of the resonance at −0.32 ppm was observed with the development of additional peaks in the ^{1}H NMR spectrum associated with C_6F_5H and other unknown species, indicating decomposition of the products, and therefore the reaction was terminated. Distillation of the reaction mixture to determine the presence of free methanol has been attempted. However, the NMR analysis of the distillate only showed the presence of C_6H_5Br, C_6F_5H and trace amount of P^{t}Bu$_3$. Free methanol was not isolated.

2.5 Conclusions

The ability of the modified Lewis acid $B(C_6Cl_5)(C_6F_5)_2$ (**1**) to form FLPs with P^tBu_3, $P(o\text{-tolyl})_3$, and $P(p\text{-tolyl})_3$ bases was investigated. Between the two isomers of tritolylphophines, $P(p\text{-tolyl})_3$ was unable to form a FLP with **1**, whereas for $P(o\text{-tolyl})_3$, despite being successful in forming a FLP with **1**, did not show any reactivity towards heteroytic cleavage of H_2. In contrast, the [**1**/P^tBu_3] system showed H_2 cleavage at 23 °C without formation of side products.

Reaction of the borohydride salt [**1**−H][H−P^tBu_3] with CO_2 was investigated. Synthesis of [**1**−OC(O)H][H−P^tBu_3] and [**1**−OCH_3][H−P(*t*Bu)$_3$] by direct reaction with formic acid and methanol proceeded cleanly without the formation of any side product. Efforts to prepare [**1**−OC(O)H][H−P^tBu_3] *via* CO_2 insertion with [**1**−H][H−P^tBu_3] were not successful. However, using the preformed formatoborate, in the presence of 25 mol % H_2 activated FLP, [**1**−H][H−P^tBu_3] was generated *in situ*, which successfully reduced [**1**−OC(O)H][H−P^tBu_3] to [**1**−OCH_3][H−P(*t*Bu)$_3$] in >12% yield by NMR. Heating of the reaction to 160 °C in the attempt to isolate methanol, only resulted in decomposition of the methoxyborate to afford a mixture of products that could not be unambiguously identified.

Finally, based on the success in the reduction of [**1**−OC(O)H]$^-$ to [**1**−OCH_3]$^-$ direct hydrogenation of CO_2 using [**1**/P^tBu_3] was performed. Unlike the literature reported [BCF][TMP] and [BCF][Lut] systems, only [**1**−OCH_3][H−P^tBu_3] was observed by NMR spectroscopy. Rapid conversion of the formatoborate intermediate to the methoxyborate product, suggests that [**1**−H][H−P^tBu_3] is a more active reducing agent. Despite [**1**/P^tBu_3] having demonstrated CO_2 reduction to the methoxyborate under milder conditions compared to the [BCF][TMP] system reported by Ashley *et al*., the [**1**/P^tBu_3] system was unable to produce methanol with the same efficiency as those found by Ashley *et al.*[53] and

Sgro *et al.*[71] The degradation of the methoxyborate *via* protonolysis leaves [**1**/P^{t}Bu$_3$] system unable to catalytically reduce CO_2 to methanol.

2.6 References

1 J. Hansen, *Science*, 2005, **308**, 1431–1435.

2 A. R. Brandt, A. Millard-Ball, M. Ganser and S. M. Gorelick, *Environ. Sci. Technol.*, 2013, **47**, 8031–8041.

3 K. Huang, C.-L. Sun and Z.-J. Shi, *Chem. Soc. Rev.*, 2011, **40**, 2435–2452.

4 W. Wang, S. Wang, X. Ma and J. Gong, *Chem. Soc. Rev.*, 2011, **40**, 3703–3727.

5 M. Aresta, A. Dibenedetto and A. Angelini, *Chem. Rev.*, 2014, **114**, 1709–1742.

6 C. Rosorius, J. Möricke, B. Wibbeling, A. C. McQuilken, T. H. Warren, C. G. Daniliuc, G. Kehr and G. Erker, *Chem. - Eur. J.*, 2016, **22**, 1103–1113.

7 M.-A. Courtemanche, É. Rochette, M.-A. Légaré, W. Bi and F.-G. Fontaine, *Dalton Trans.*, 2016, **45**, 6129–6135.

8 R. J. Blagg and G. G. Wildgoose, *RSC Adv.*, 2016, **6**, 42421–42427.

9 E. J. Lawrence, V. S. Oganesyan, D. L. Hughes, A. E. Ashley and G. G. Wildgoose, *J. Am. Chem. Soc.*, 2014, **136**, 6031–6036.

10 L. L. Zeonjuk, N. Vankova, A. Mavrandonakis, T. Heine, G.-V. Röschenthaler and J. Eicher, *Chem. - Eur. J.*, 2013, **19**, 17413–17424.

11 A. L. Travis, S. C. Binding, H. Zaher, T. a Q. Arnold, J.-C. Buffet and D. O'Hare, *Dalton Trans.*, 2013, **42**, 2431–2437.

12 H. Li, A. J. A. Aquino, D. B. Cordes, F. Hung-Low, W. L. Hase and C. Krempner, *J. Am. Chem. Soc.*, 2013, **135**, 16066–16069.

13 C. B. Caputo, K. Zhu, V. N. Vukotic, S. J. Loeb and D. W. Stephan, *Angew. Chem., Int. Ed.*, 2013, **52**, 960–963.

14 A. Karkamkar, K. Parab, D. M. Camaioni, D. Neiner, H. Cho, T. K. Nielsen and T. Autrey, *Dalton Trans.*, 2013, **42**, 615–619.

15 T. A. Rokob and I. Pápai, in *Frustrated Lewis Pairs I*, ed. D. W. Erker, Gerhard, Stephan, Springer, Berlin, 1st edn., 2013, vol. 332, pp. 157–211.

16 S. C. Binding, H. Zaher, F. Mark Chadwick and D. O'Hare, *Dalton Trans.*, 2012, **41**, 9061–9066.

17 T. J. Herrington, A. J. W. Thom, A. J. P. White and A. E. Ashley, *Dalton Trans.*, 2012, **41**, 9019–9022.

18 K. Takeuchi and D. W. Stephan, *Chem. Commun.*, 2012, **48**, 11304–11306.

19 K. Chernichenko, M. Nieger, M. Leskelä and T. Repo, *Dalton Trans.*, 2012, **41**, 9029–9032.

20 L. Greb, P. Oña-Burgos, B. Schirmer, S. Grimme, D. W. Stephan and J. Paradies, *Angew. Chem., Int. Ed.*, 2012, **51**, 10164–10168.

21 C. Jiang, O. Blacque, T. Fox and H. Berke, *Organometallics*, 2011, **30**, 2117–2124.

22 F. Schulz, V. Sumerin, S. Heikkinen, B. Pedersen, C. Wang, M. Atsumi, M. Leskelä, T. Repo, P. Pyykkö, W. Petry and B. Rieger, *J. Am. Chem. Soc.*, 2011, **133**, 20245–20257.
23 D. W. Stephan and G. Erker, *Angew. Chem., Int. Ed.*, 2010, **49**, 46–76.
24 R. C. Neu, E. Y. Ouyang, S. J. Geier, X. Zhao, A. Ramos and D. W. Stephan, *Dalton Trans.*, 2010, **39**, 4285–4294.
25 E. Theuergarten, D. Schlüns, J. Grunenberg, C. G. Daniliuc, P. G. Jones and M. Tamm, *Chem. Commun.*, 2010, **46**, 8561–8563.
26 C. Jiang, O. Blacque and H. Berke, *Organometallics*, 2009, **28**, 5233–5239.
27 T. A. Rokob, A. Hamza and I. Pápai, *J. Am. Chem. Soc.*, 2009, **131**, 10701–10710.
28 S. J. Geier and D. W. Stephan, *J. Am. Chem. Soc.*, 2009, **131**, 3476–3477.
29 P. A. Chase and D. W. Stephan, *Angew. Chem., Int. Ed.*, 2008, **47**, 7433–7437.
30 V. Sumerin, F. Schulz, M. Nieger, M. Leskelä, T. Repo and B. Rieger, *Angew. Chem., Int. Ed.*, 2008, **47**, 6001–6003.
31 D. Holschumacher, T. Bannenberg, C. G. Hrib, P. G. Jones and M. Tamm, *Angew. Chem., Int. Ed.*, 2008, **47**, 7428–7432.
32 H. Wang, R. Fröhlich, G. Kehr and G. Erker, *Chem. Commun.*, 2008, **92**, 5966–5968.
33 T. A. Rokob, A. Hamza, A. Stirling, T. Soós and I. Pápai, *Angew. Chem., Int. Ed.*, 2008, **47**, 2435–2438.
34 G. C. Welch and D. W. Stephan, *J. Am. Chem. Soc.*, 2007, **129**, 1880–1881.
35 P. A. Chase, G. C. Welch, T. Jurca and D. W. Stephan, *Angew. Chem., Int. Ed.*, 2007, **46**, 8050–8053.
36 G. C. Welch, R. R. S. Juan, J. D. Masuda and D. W. Stephan, *Science*, 2006, **314**, 1124–1126.
37 Á. Gyömöre, M. Bakos, T. Földes, I. Pápai, A. Domján and T. Soós, *ACS Catal.*, 2015, **5**, 5366–5372.
38 T. Mahdi and D. W. Stephan, *J. Am. Chem. Soc.*, 2014, **136**, 15809–15812.
39 D. J. Scott, M. J. Fuchter and A. E. Ashley, *J. Am. Chem. Soc.*, 2014, **136**, 15813–15816.
40 D. J. Scott, T. R. Simmons, E. J. Lawrence, G. G. Wildgoose, M. J. Fuchter and A. E. Ashley, *ACS Catal.*, 2015, **5**, 5540–5544.
41 K. Chernichenko, Á. Madarász, I. Pápai, M. Nieger, M. Leskelä and T. Repo, *Nat. Chem.*, 2013, **5**, 718–723.
42 G. Erős, K. Nagy, H. Mehdi, I. Pápai, P. Nagy, P. Király, G. Tárkányi and T. Soós, *Chem. - Eur. J.*, 2012, **18**, 574–585.
43 Y. Segawa and D. W. Stephan, *Chem. Commun.*, 2012, **48**, 11963–11965.
44 J. S. Reddy, B.-H. Xu, T. Mahdi, R. Fröhlich, G. Kehr, D. W. Stephan and G. Erker, *Organometallics*, 2012, **31**, 5638–5649.
45 B. Inés, D. Palomas, S. Holle, S. Steinberg, J. A. Nicasio and M. Alcarazo, *Angew. Chem., Int. Ed.*, 2012, **51**, 12367–12369.
46 L. Greb, P. Oña-Burgos, A. Kubas, F. C. Falk, F. Breher, K. Fink and J. Paradies,

Dalton Trans., 2012, **41**, 9056–9060.
47 G. Erős, H. Mehdi, I. Pápai, T. A. Rokob, P. Király, G. Tárkányi and T. Soós, *Angew. Chem., Int. Ed.*, 2010, **49**, 6559–6563.
48 X. Feng and H. Du, *Tetrahedron Lett.*, 2014, **55**, 6959–6964.
49 S. Wei and H. Du, *J. Am. Chem. Soc.*, 2014, **136**, 12261–12264.
50 P. Spies, S. Schwendemann, S. Lange, G. Kehr, R. Fröhlich and G. Erker, *Angew. Chem., Int. Ed.*, 2008, **47**, 7543–7546.
51 S. A. Weicker and D. W. Stephan, *Chem. - Eur. J.*, 2015, **21**, 13027–13034.
52 G. Ghattas, D. Chen, F. Pan and J. Klankermayer, *Dalton Trans.*, 2012, **41**, 9026–9028.
53 A. E. Ashley, A. L. Thompson and D. O'Hare, *Angew. Chem., Int. Ed.*, 2009, **48**, 9839–9843.
54 S. D. Tran, T. A. Tronic, W. Kaminsky, D. Michael Heinekey and J. M. Mayer, *Inorg. Chim. Acta*, 2011, **369**, 126–132.
55 A. E. Ashley, T. J. Herrington, G. G. Wildgoose, H. Zaher, A. L. Thompson, N. H. Rees, T. Krämer and D. O'Hare, *J. Am. Chem. Soc.*, 2011, **133**, 14727–14740.
56 D. W. Stephan and G. Erker, *Angew. Chem., Int. Ed.*, 2015, **54**, 6400–6441.
57 D. W. Stephan, *Org. Biomol. Chem.*, 2008, **6**, 1535–1539.
58 D. W. Stephan, *Acc. Chem. Res.*, 2015, **48**, 306–316.
59 D. W. Stephan, *Org. Biomol. Chem.*, 2012, **10**, 5740–5746.
60 D. W. Stephan, *J. Am. Chem. Soc.*, 2015, **137**, 10018–10032.
61 D. W. Stephan, S. Greenberg, T. W. Graham, P. Chase, J. J. Hastie, S. J. Geier, J. M. Farrell, C. C. Brown, Z. M. Heiden, G. C. Welch and M. Ullrich, *Inorg. Chem.*, 2011, **50**, 12338–12348.
62 T. Allman and R. G. Goel, *Can. J. Chem.*, 1982, **60**, 716–722.
63 A. Streitwieser, A. E. McKeown, F. Hasanayn and N. R. Davis, *Org. Lett.*, 2005, **7**, 1259–1262.
64 P. Feldhaus, B. Schirmer, B. Wibbeling, C. G. Daniliuc, R. Fröhlich, S. Grimme, G. Kehr and G. Erker, *Dalton Trans.*, 2012, **41**, 9135–9142.
65 G. Erker, *C. R. Chim.*, 2011, **14**, 831–841.
66 C. A. Tolman, *Chem. Rev.*, 1977, **77**, 313–348.
67 H. Jacobsen, H. Berke, S. Döring, G. Kehr, G. Erker, R. Fröhlich and O. Meyer, *Organometallics*, 1999, **18**, 1724–1735.
68 T. Beringhelli, D. Donghi, D. Maggioni and G. D'Alfonso, *Coord. Chem. Rev.*, 2008, **252**, 2292–2313.
69 T. Wang and D. W. Stephan, *Chem. Commun.*, 2014, **50**, 7007–7010.
70 C. M. Mömming, E. Otten, G. Kehr, R. Fröhlich, S. Grimme, D. W. Stephan and G. Erker, *Angew. Chem., Int. Ed.*, 2009, **48**, 6643–6646.
71 M. J. Sgro, J. Dömer and D. W. Stephan, *Chem. Commun.*, 2012, **48**, 7253–7255.

CHAPTER THREE

Siloxane and Silsesquioxane bound FLPs

3.1 Introduction

Despite the impressive number of analytical tools currently available for probing the surface/solid-state chemistry (IR spectroscopy, EXAFS, XANES and solid-state NMR spectroscopy),[1] the level of understanding of heterogeneous catalysts is still limited, especially when compared to their homogeneous analogues.[2–4] In addition, the small number of active sites in heterogeneous catalysts often makes it difficult to determine a clear structure-activity correlation, and in most cases, impossible to obtain a precise description of the mechanism for the chemistry occurring at the active sites. Besides these solid-state methods, various ligand systems have been used as molecular models for mimicking the surface of catalyst supports. This is because the availability of high quality solution-phase characterisation techniques makes the study of homogeneous analogues a valuable source of chemical insight that can be applied to surface supported systems. Although other inorganic supports such as $MgCl_2$ have been modelled,[5–8] silica has been by far the most extensively studied support using such approach.[9–12]

Metal compounds derived from silanols[13] and polyhedral oligomeric silsesquioxanes (POSS) are the most commonly used soluble molecular models for silica-supported catalysts,[12,14–19] especially metallasilsesquioxane systems are generally regarded as "realistic" model systems as POSS exhibit rich coordination modes,[20] most advanced structural similarity with silica and have p*K*a values of the Si-OH units close to those of silica.[14] The pioneering work by Feher *et al*., showed that partially condensed

silsesquioxanes can function as "realistic" model systems,[9] to give well-defined homogeneous metal complexes that maintain comparable reactivity to their silica-supported congeners.[21] Furthermore, chemical shifts obtained for those soluble model systems can be used as important references for solid-state NMR data obtained for surface supported complexes.[12,14,15,17,19,22] For instance, Duchateau and co-workers reported the synthesis of group-4 half-sandwich silsesquioxane complexes, Cp"[(*c*-C_5H_9)$_7$$Si_8O_{13}$]$TiR_2$ and Cp"[(*c*-C_5H_9)$_7$$Si_8O_{13}$]$ZrR_2$, and showed that they can serve as soluble model systems for silica-supported olefin polymerisation catalysts.[14,17] Subsequently, they demonstrated that this strategy can also be applied to main group compounds, by using the synthesised borato-silsesquioxane complexes {[(*c*-C_5H_9)$_7$$Si_8O_{13}$]$B(C_6F_5)_3$}$^-X^+$ and {[(*c*-C_5H_9)$_7$$Si_8(OH)_2O_{10}$]$B(C_6F_5)_3$}$^-X^+$ as solution model systems for silica-grafted borate olefin polymerisation co-catalysts.[19]

The reactive components of silica are the surface silanol groups and siloxane bridges, it is therefore necessary to have a wide range of molecular models that represent these various functional sites. As introduced in Chapter One that surface silanol groups can be classified into three types: isolated silanol groups, geminal silanol groups and vicinal silanol groups. These different surface functional sites can be modelled by their corresponding trialkyl-silanol and silsesquioxane analogues (Table 3.1).[9,10,12,23,24]

This chapter aims to explore the use of trialkylsilanol and silsesquioxane in frustrated Lewis pair chemistry as soluble model systems to mimic silica-supported FLPs. The synthesis and characterisation of a series of silanol and silsesquioxane bound Lewis acid models will be described. Their potential to form FLPs with phosphine bases, and subsequent H_2 activation properties will be studied using solution-state NMR spectroscopy.

Table 3.1 Summary of various types of surface silanol groups, and selected molecular models that mimic the corresponding silanol groups of a silica surface.

Surface Silanol Groups	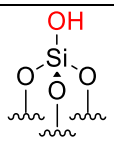 Isolated Silanol	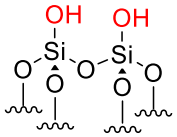 Vicinal silanol groups	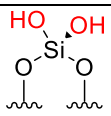 Geminal silanol groups
Model for surface silanol groups	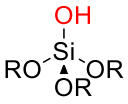 Isolated silanol mimic	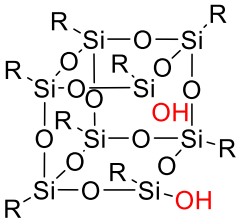 Vicinal silanol mimic	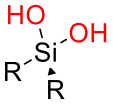 Isolated silanol mimic

3.2 Choice of Lewis Acids

The choice of the Lewis acids was based on the existing ≡SiOB(C_6F_5)$_2$ (***s*-BCF**). Although it has been reported as a co-catalyst for heterogeneous polymerisation reactions, its use in heterogeneous FLP chemistry has never been explored. One of the limitations with using (***s*-BCF**) is that it is susceptible to nucleophilic attack at the *para*-C of one the C_6F_5 ring by phosphines leading to the formation of phosphonium borate zwitterion (as described in Chapter Two).[25,26] Such decomposition can be avoided by removal of *para*-F atoms as reported by Ullrich *et al*.[27,28] An appropriate alternative substituent would be to use 3,5-bis-trifluoromethylphenyl (fluoro-*meta*-xylyl, Fxyl) ring due to the absent *para*-F atoms. Recently, Samigullin *et al*. reported the synthesis of (Fxyl)$_2$BX (X = H, F, Cl, Br, OH and OMe), which provided convenient routes for implementing (Fxyl)$_2$B building block into more sophisticated frameworks.[29] Herrington *et al*. reported that B(Fxyl)$_3$ possess a slightly higher Lewis acidity than B(C_6F_5)$_3$ according to Gutmann-Beckett analysis.[30] Moreover, absence of *ortho*-F atoms reduces steric crowding around the boron centre which led to increased FLP reactivities.[30,31]

3.3 Synthesis of Borato-Siloxane and Borato-Silsesquioxane Models

3.3.1 Synthesis of (^{t}BuO)$_3$SiOB(C$_6$F$_5$)$_2$

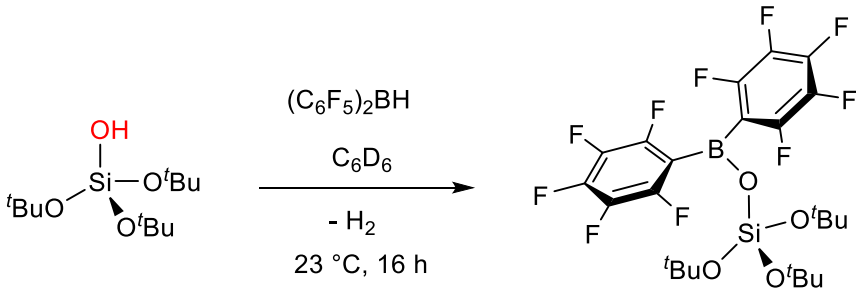

Equation 3.1 Synthesis of (^{t}BuO)$_3$SiOB(C$_6$F$_5$)$_2$.

Facile preparation of (^{t}BuO)$_3$SiOB(C$_6$F$_5$)$_2$ can be achieved by the reaction of (^{t}BuO)$_3$SiOH with (C$_6$F$_5$)$_2$BH in benzene. Upon dissolution of the reagents, evolution of a gas was observed, which was later identified as H$_2$ (singlet at 4.49 ppm in the ^{1}H NMR spectrum). The reaction completed after 16 hours at room temperature, as confirmed by NMR spectroscopy, with a yield >95%. (^{t}BuO)$_3$SiOB(C$_6$F$_5$)$_2$ appears as an off-white sticky gel, with very high solubility in both aromatic and aliphatic solvents.

Upon completion of the reaction, the initial Si−O*H* resonance at 2.30 ppm in the ^{1}H NMR spectrum had disappeared, accompanied by the appearance of H$_2$ resonance at 4.49 ppm. The initial ^{t}Bu resonance at 1.35 ppm has shifted to 1.28 ppm (Figure 3.1). The ^{11}B NMR spectrum contains a broad resonance at 41 ppm (Figure 3.2a), and the ^{19}F NMR spectrum exhibits resonances at −131.6, −150.5 and −161.9 ppm (*ortho*-, *para*- and *meta*-F respectively) corresponding to $\Delta\delta_{m,p}$ = 12 ppm (Figure 3.2b). These results are consistent with the formation of a tri-coordinate borane containing an electron donating OR group.[32] In the ^{29}Si NMR spectra, the initial resonance at −89 ppm corresponding to the *Si*OH had shifted to −100 ppm upon the formation of SiOB(C$_6$F$_5$)$_2$ (Figure 3.3).

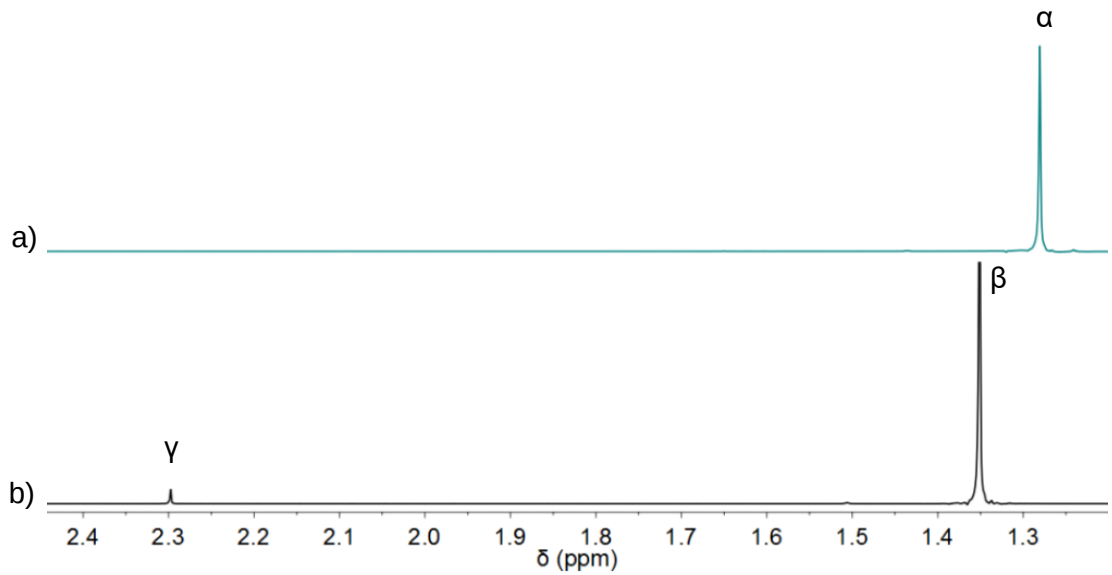

Figure 3.1 ^{1}H NMR spectra in C_6D_6 of : a) (^{t}BuO)$_3$SiOB(C_6F_5)$_2$ (α) ^{t}Bu resonance, and b) (^{t}BuO)$_3$SiOH, (β) ^{t}Bu and (γ) O*H* and resonances.

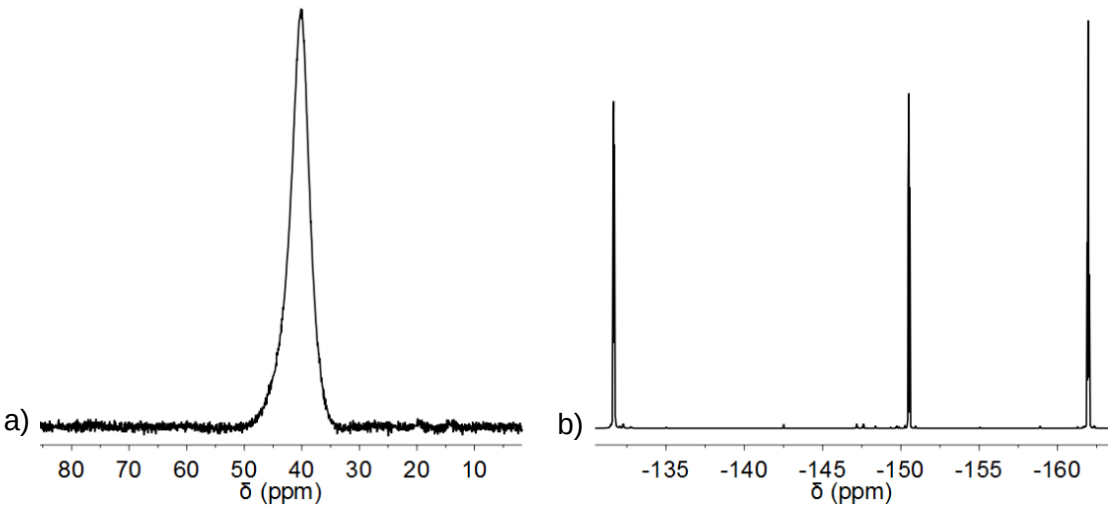

Figure 3.2 NMR spectra of (^{t}BuO)$_3$SiOB(C_6F_5)$_2$ in C_6D_6: a) ^{11}B and b) ^{19}F.

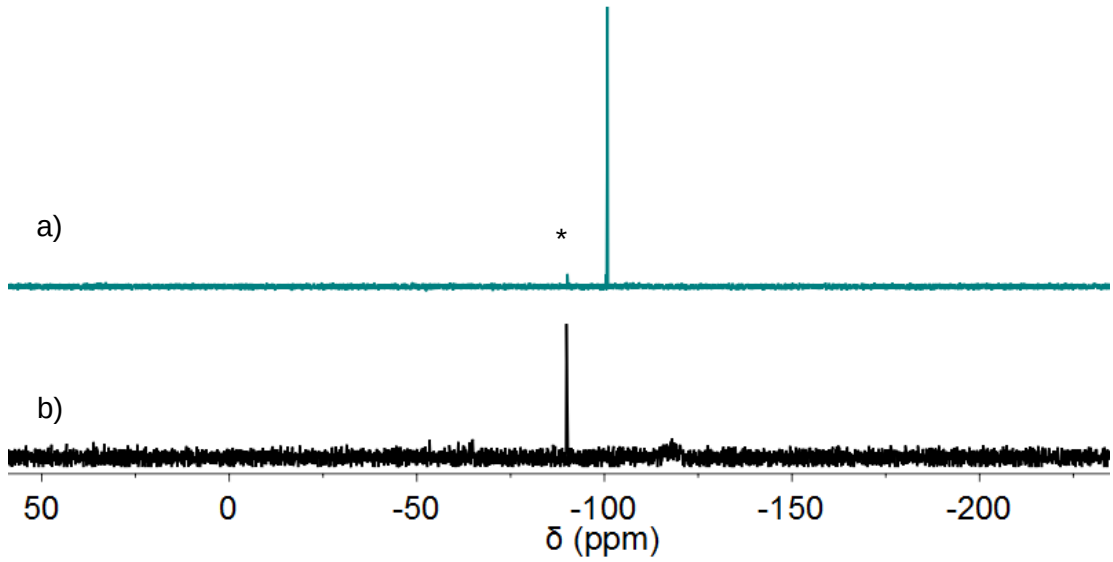

Figure 3.3 ^{29}Si NMR spectra of a) (^{t}BuO)$_3$SiOB(C$_6$F$_5$)$_2$ and b) (^{t}BuO)$_3$SiOH in C$_6$D$_6$; * unreacted (^{t}BuO)$_3$SiOH.

3.3.2 Synthesis of (^{t}BuO)$_3$SiOB(Fxyl)$_2$

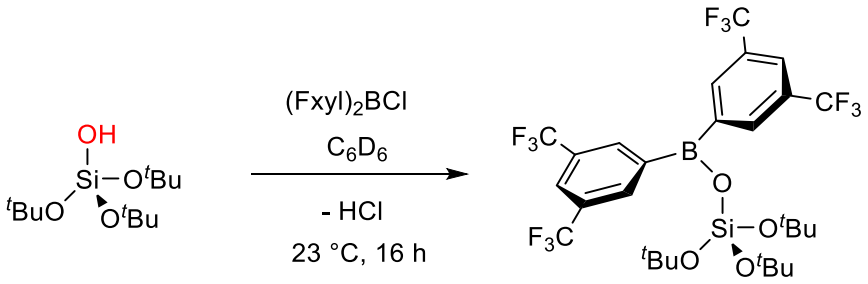

Equation 3.2 Synthesis of (^{t}BuO)$_3$SiOB(Fxyl)$_2$.

Reaction of (^{t}BuO)$_3$SiOH with (Fxyl)$_2$BCl in benzene completed after 16 hours under room temperature. The solvent and HCl were removed under reduced pressure to afford (^{t}BuO)$_3$SiOB(Fxyl)$_2$ as a colourless sticky oil in high purity (92% yield).

The ^{1}H NMR spectrum shows a doublet at 1.26 ppm corresponding to ^{t}Bu H-atoms. Resonances at 8.19 and 7.81 ppm (in the ratio of 2:1) are consistent with the (Fxyl)$_2$BCl starting material (Figure 3.4a). Both ^{29}Si and ^{11}B NMR spectra of (^{t}BuO)$_3$SiOB(Fxyl)$_2$ are very similar to those of (^{t}BuO)$_3$SiOB(C$_6$F$_5$)$_2$. The ^{29}Si NMR spectrum of

(^{t}BuO)$_3$SiOB(Fxyl)$_2$ displays a resonance at −102 ppm, and the ^{11}B NMR spectrum exhibits a broad resonance at 42 ppm, both are consistent with the formation of a B−OR species.[19,32] A resonance at 62.7 ppm can be observed in the ^{19}F NMR spectrum which corresponds to the *meta*-CF_3 groups on the aromatic ring (Figure 3.4b)

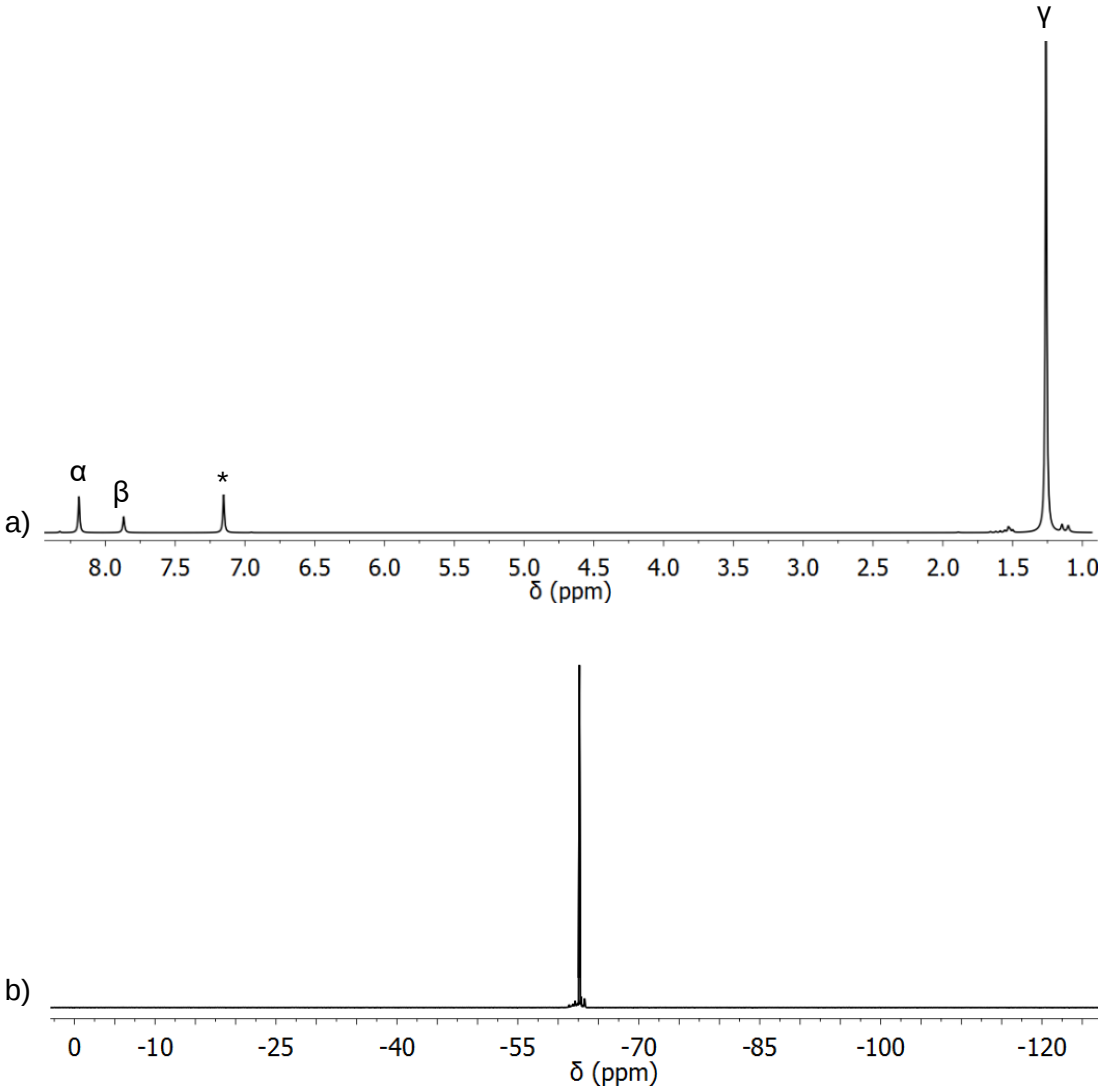

Figure 3.4 a) ^{1}H b) ^{19}F NMR spectrum of (^{t}BuO)$_3$SiOB(Fxyl)$_2$ in C_6D_6 showing aromatic H resonances at (α) 8.19 ppm, (β) 7.81 ppm, and (γ) ^{t}Bu resonance at 1.35 ppm; *Residual protio solvent signal.

3.3.3 Synthesis of $[T_8(OB(C_6F_5)_2)_2]$

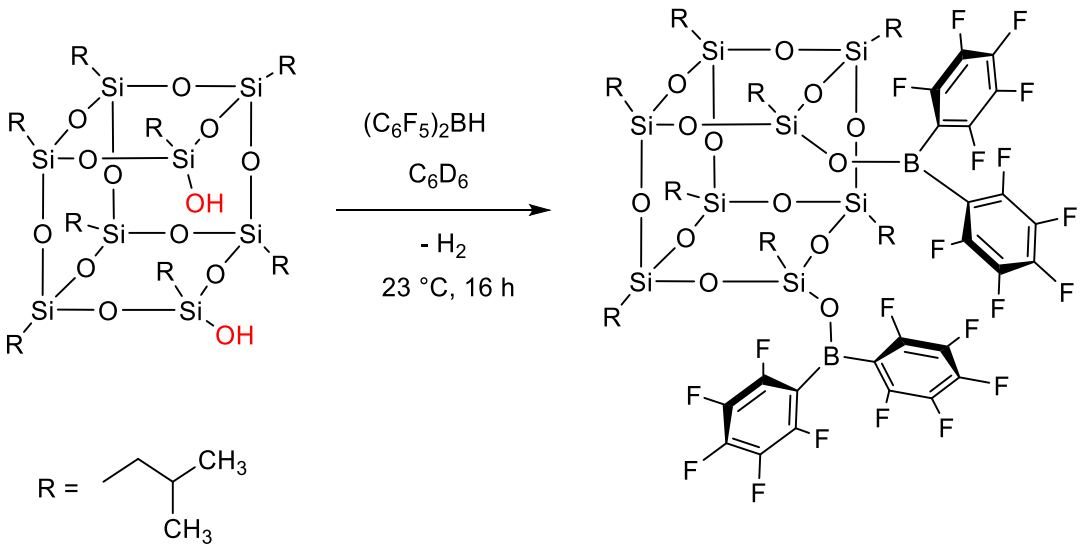

Equation 3.3 Synthesis of $T_8(OB(C_6F_5)_2)_2$.

A stoichiometric amount of $(C_6F_5)_2BH$ was stirred with $(i\text{-}C_4H_9)_8Si_8O_{12}(OH)_2$ at 23 °C. After 16 hours the solvent was removed under reduced pressure to afford $[T_8(OB(C_6F_5)_2)_2]$ as a colourless sticky solid in high purity (>97%) at 92% yield (Equation 3.3).

The ^{1}H NMR spectrum of $T_8(OB(C_6F_5)_2)_2$ shows the absence of the Si−OH resonance at 4.60 ppm suggesting complete conversion of the OH group to $OB(C_6F_5)_2$ (Figure 3.5). The ^{11}B NMR spectrum displays a broad resonance at 40 ppm (Figure 3.6a), and the ^{19}F NMR spectrum (Figure 3.6b) contains a set of resonance at −131.9, −148.8 and 161.6 ppm (*ortho*-F, *para*-F and *meta*-F respectively) ($\Delta\delta_{m,p}$ = 12.8 ppm) suggesting the formation of three-coordinate borate.[19,32] The results showed that only one boron species was observed in the NMR spectra suggesting that the two Lewis acid centres in the silsesquioxane framework are equivalent. Moreover, despite the close proximity of the two

OH groups, the reaction proceeded selectively to afford the corresponding $[T_8(OB(C_6F_5)_2)_2]$, without the formation of side-product $[T_8(O_2B(C_6F_5)]$.

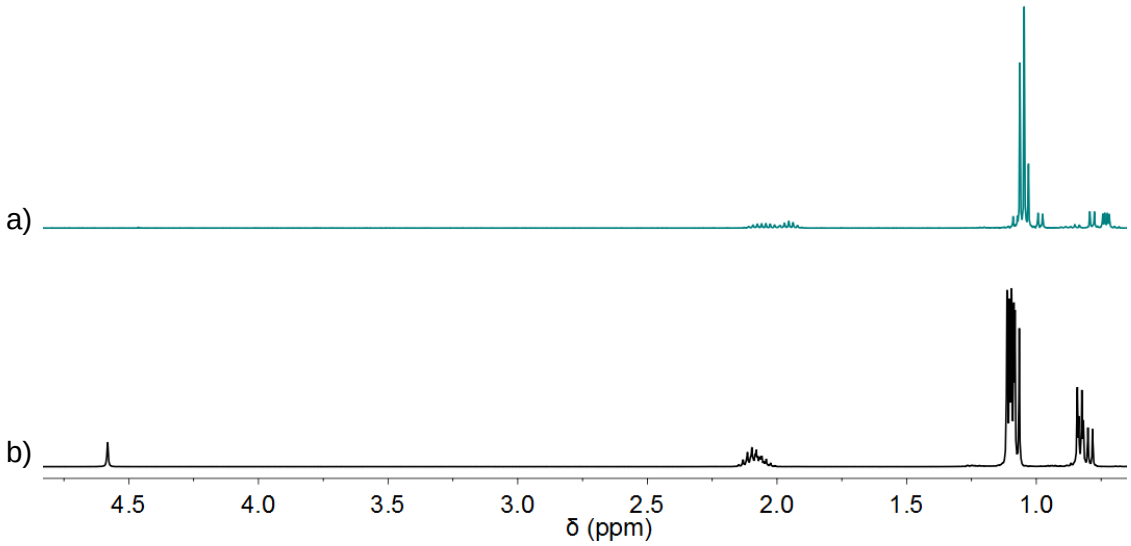

Figure 3.5 ^{1}H NMR spectra in C_6D_6 of: a) $[T_8(OB(C_6F_5)_2)_2]$ b) $(i\text{-}C_4H_9)_8Si_8O_{12}(OH)_2$.

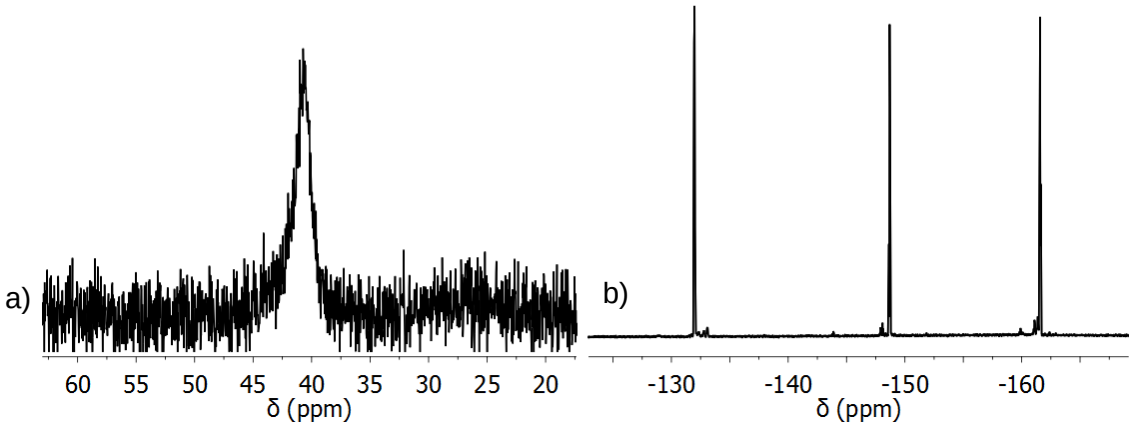

Figure 3.6 a) ^{11}B and b) ^{19}F NMR spectrum of $[T_8(OB(C_6F_5)_2)_2]$ in C_6D_6 indicating the formation of a tri-coordinate boron.

3.3.4 Synthesis of $[T_8(OB(Fxyl)_2)_2]$

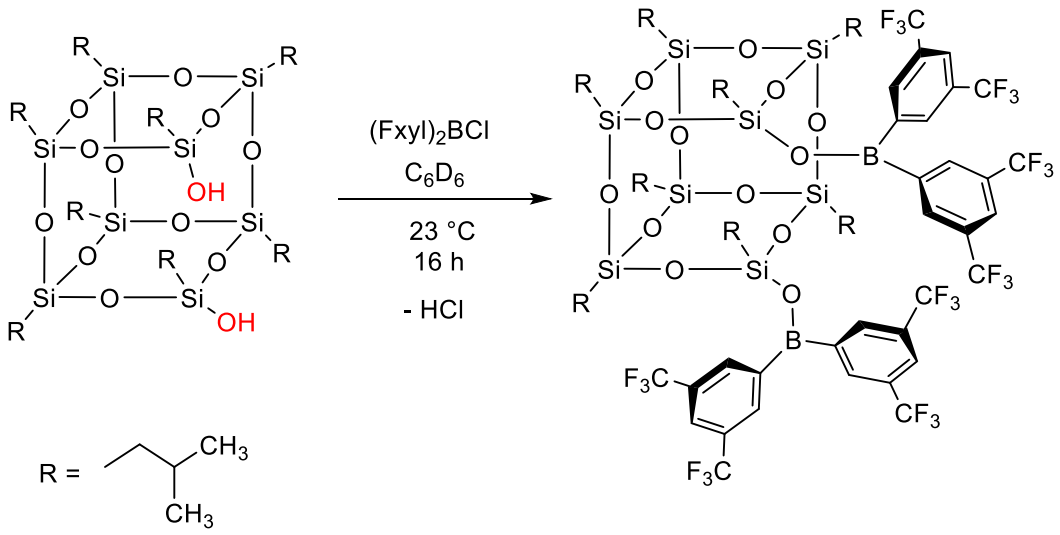

Equation 3.4 Synthesis of $T_8(OB(Fxyl)_2)_2$.

Similar to the $[T_8(OB(C_6F_5)_2)_2]$ complex, the reaction of $(i\text{-}C_4H_9)_8Si_8O_{12}(OH)_2$ with two equivalents of $(Fxyl)_2BCl$ was carried out at 23 °C in benzene to afford $[T_8(OB(Fxyl)_2)_2]$ give HCl as by-product. Removal of the solvent under reduced pressure afforded $[T_8(OB(Fxyl)_2)_2]$ as a pale yellow solid in high purity (> 92%).

^{1}H NMR spectrum of the mixture confirmed the absence of the Si−OH resonance after 16 hours of reaction indicating that all $(i\text{-}C_4H_9)_8Si_8O_{12}(OH)_2$ has been consumed. There are two new resonances at 8.23 and 8.02 ppm in the ratio of 2:1 corresponding to *ortho*-H and *para*-H on the Fxyl ring (Figure 3.7a). The ^{11}B NMR spectrum (Figure 3.7b) showed a broad resonance at 44 ppm, and the ^{19}F NMR spectrum (Figure 3.7c) displayed a resonance at −62.5 ppm, both of which are similar to the observed resonances of $(^t\text{BuO})_3\text{SiOB(Fxyl)}_2$.

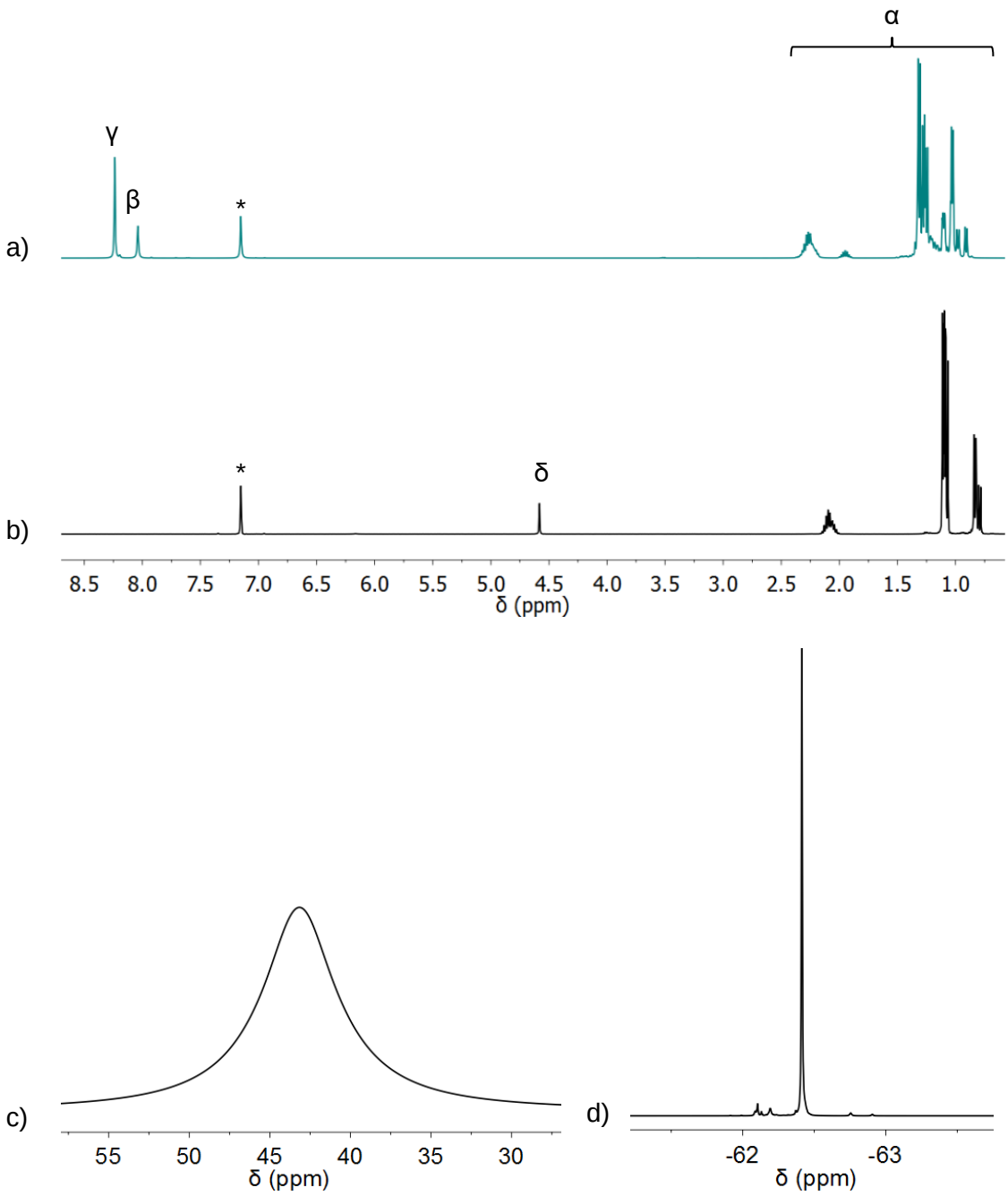

Figure 3.7 ^{1}H NMR spectra of a) $[T_8(OB(Fxyl)_2)_2]$ showing (α) *i*-Bu resonances, (β) *ortho*-H and (γ) *para*-H; b) $(i\text{-}C_4H_9)_8Si_8O_{12}(OH)_2$ showing (δ) O*H* resonance; c) ^{11}B and d) ^{19}F NMR spectra of $[T_8(OB(Fxyl)_2)_2]$. *Residual protio solvent signal.

3.4 Preparation of Siloxane and Silsesquioxane bound FLPs

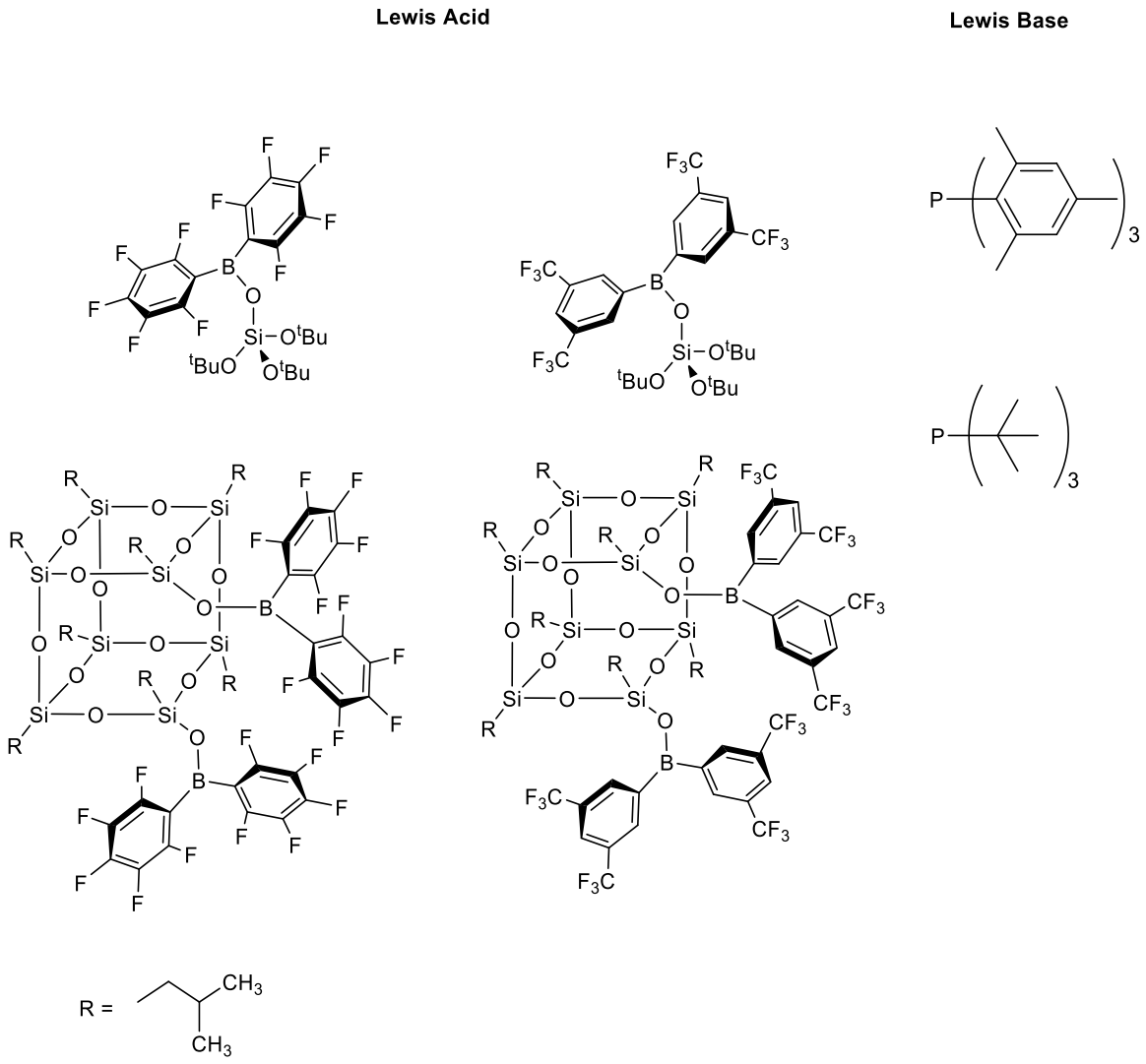

Figure 3.8 Scope of the Lewis pairs investigated for FLP formation.

The ability of Lewis acid functionalised siloxane and silsesquioxanes described in Section 3.2 and 3.3 to form FLPs with phosphine bases was investigated. Stoichiometric combination of the siloxane and silsesquioxane Lewis acids and phosphine bases afforded seven FLP systems ([(^{t}BuO)$_3$SiOB(Fxyl)$_2$/PMes$_3$] was not included in this study). All FLP preparations were carried out in J-Young's tap NMR tubes according to literature procedures[33–35] and monitored using ^{11}B, ^{31}P and ^{19}F NMR spectroscopy. Chemical shifts

of the pair of core hetero-nuclei (^{11}B and ^{31}P) remain unchanged for all seven systems, indicating unquenched Lewis acidic and basic centres, and successful formation of FLPs (Table 3.2).

Table 3.2 Summary of ^{11}B, ^{19}F and ^{31}P NMR spectroscopic data for the preparation of siloxane and silsesquioxane bound FLPs.

Frustrated Lewis Pairs	**δ^{11}B Free borane**	**δ^{31}P Free phosphine**	**δ^{11}B FLP**	**δ^{31}P FLP**	**δ^{19}F**				
					o-F	*p*-F	*m*-F	$\Delta\delta_{m,p}$	CF_3
$(^t$BuO$)_3$SiOB$(C_6F_5)_2$ P^{t}Bu$_3$	40	62	40	62	−132	−150	−162	12	
$(^t$BuO$)_3$SiOB(Fxyl)$_2$ P^{t}Bu$_3$	44	62	44	62	-	-	-	-	62
$(^t$BuO$)_3$SiOB$(C_6F_5)_2$ PMes$_3$	40	−36	40	−36	−132	−150	−162	12	
T_8(OB(Fxyl)$_2)_2$ (P^{t}Bu$_3)_2$	45	62	45	62	-	-	-	-	62
T_8(OB$(C_6F_5)_2)_2$ (P^{t}Bu$_3)_2$	40	62	40	62	−132	−149	−162	13	
T_8(OB$(C_6F_5)_2)_2$ (PMes$_3)_2$	40	−36	40	−36	−132	−149	−162	13	
T_8(OB(Fxyl)$_2)_2$ (PMes$_3)_2$	45	−36	45	−36	-	-	-	-	62

*Chemical shifts are quoted in ppm.

3.5 Reactions of Siloxane and Silsesquioxane bound FLPs with H_2

Following the successful preparation of seven siloxane and silsesquioxane bound FLP systems as described in Section 3.4, the H_2 activation properties of these FLPs were investigated. All reactions were performed in J-Young's quartz NMR tubes filled with either C_6D_6 or C_6D_5Br solutions containing the FLPs, and pressurised with 2 bar H_2.

3.5.1 Reaction of [(^{t}BuO)$_3$SiOB(C$_6$F$_5$)$_2$/P^{t}Bu$_3$] with H$_2$

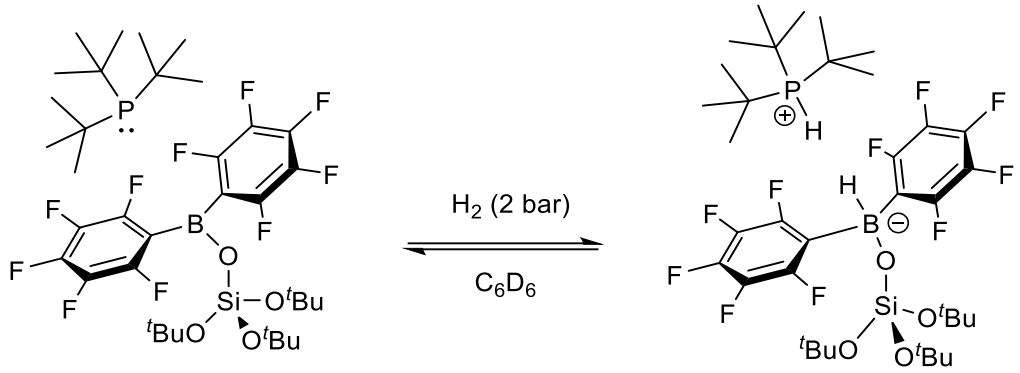

Equation 3.5 Reaction of [(^{t}BuO)$_3$SiOB(C$_6$F$_5$)$_2$/P^{t}Bu$_3$] with H$_2$.

A solution of [(^{t}BuO)$_3$SiOB(C$_6$F$_5$)$_2$/P^{t}Bu$_3$] reacts with H$_2$ (2 bar) slowly at room temperature. A low intensity doublet of multiplet in the ^{31}P NMR spectrum (Figure 3.9a) at 57.5 ppm ($^1J_{PH}$ = 435 Hz, $^3J_{PH}$ = 15 Hz), and a low intensity doublet at 3.77 ppm ($^1J_{HP}$ = 435 Hz) in the ^{1}H NMR spectrum (Figure 3.9b) were detected, which are characteristics of [H−P^{t}Bu$_3$]$^+$ cation[36] as a result of H$_2$ heterolysis (5% conversion by ^{31}P NMR). A weak sharp signal at 1.79 ppm in the ^{11}B NMR spectrum (Figure 3.9c) was also observed, consistent with the formation of a four-coordinate [(^{t}BuO)$_3$SiOB(H)(C$_6$F$_5$)$_2$]$^-$ anion.

After 72 hours at room temperature, NMR resonances corresponding to the hydridoborate and phosphonium species in the ^{31}P and ^{11}B NMR spectra increased in intensity (45% conversion by ^{31}P NMR spectroscopy). The appearance of an additional weak sextet at 5.8 ppm in the ^{1}H NMR spectrum and a set of minor resonances at −138.2, −153.4, and −161.9 ppm in the ^{19}F NMR spectrum are characteristics of C$_6$F$_5$H as a result of minor decomposition.[37] Moreoever, the ^{11}B NMR spectrum exhibits an additional broad resonance 23 ppm, which was later identified as a decomposition product as a result of ligand redistribution, similar to the observation by Neu *et al*.[36]

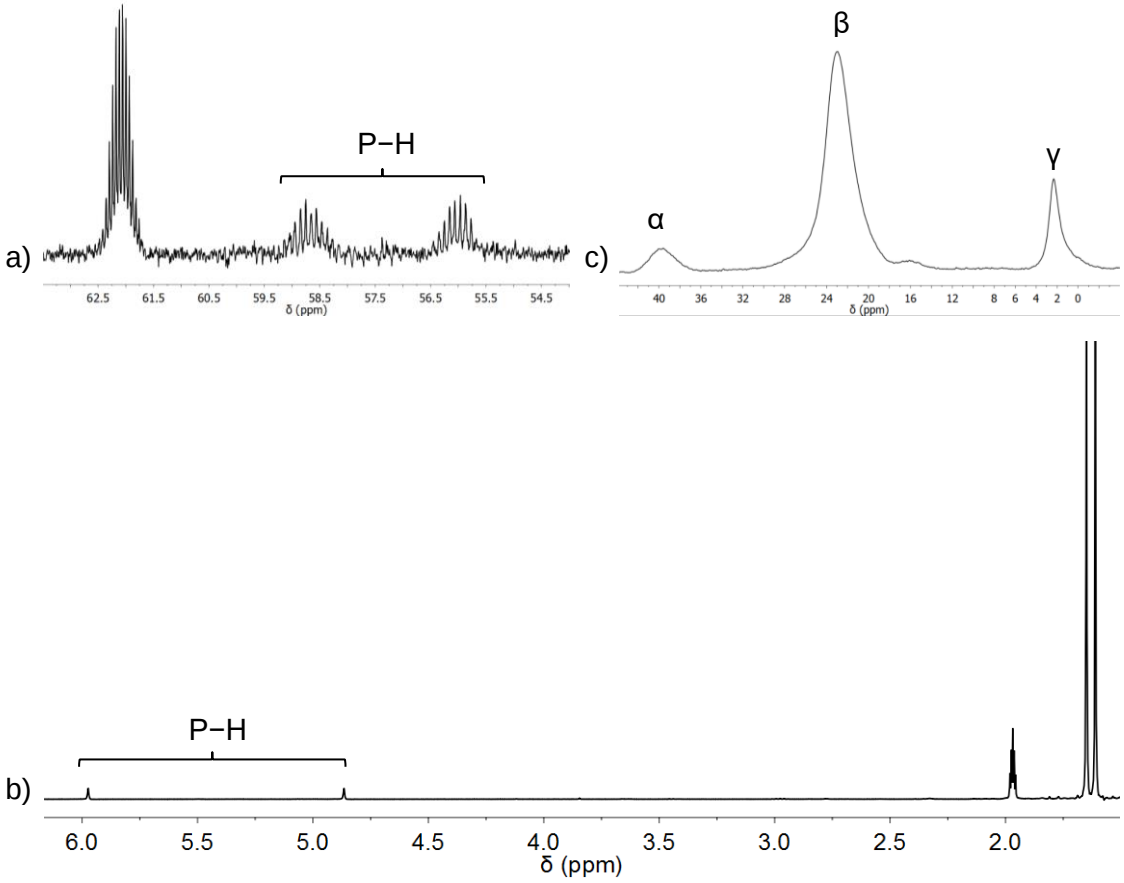

Figure 3.9 a) ^{31}P, b) ^{11}B ((α) unreacted (^{t}BuO)$_3$SiOB(C$_6$F$_5$)$_2$, (β) ((^{t}BuO)$_3$SiO)$_2$BC$_6$F$_5$ and (γ) [(^{t}BuO)$_3$SiOB(H)(C$_6$F$_5$)$_2$]$^-$) and c) ^{1}H NMR spectrum of H_2 cleavage reaction by [(^{t}BuO)$_3$SiOB(C$_6$F$_5$)$_2$/P^{t}Bu$_3$] in C$_6$D$_6$ after 2 hours at 60 °C.

Heating the reaction at 60 °C led to further decomposition and release of H_2, suggesting that the reaction could involve an equilibrium with unreacted FLP and decomposition products. The side product in large quantities appearing at 23 ppm in the ^{11}B NMR spectrum was isolated from the reaction mixture by recrystallisation from hot acetonitrile (Figure 3.10a). ^{1}H NMR spectrum of the side product exhibits a large singlet at 1.34 ppm (Figure 3.10b), consistent with a ^{t}Bu group, however, no signal was detected in ^{31}P NMR spectroscopy. The ^{19}F NMR spectrum displays a set of resonances at −131.2, −156.1 and −164.6 ppm, indicating that the species contains at least one C$_6$F$_5$ group, and the $\Delta\delta_{m,p}$ value (9 ppm) is consistent with a three-coordinate borane (Figure 3.10c). The

side product was later revealed to be $((^{t}BuO)_3SiO)_2BC_6F_5$ using single crystal X-ray crystallography as (Figure 3.12).

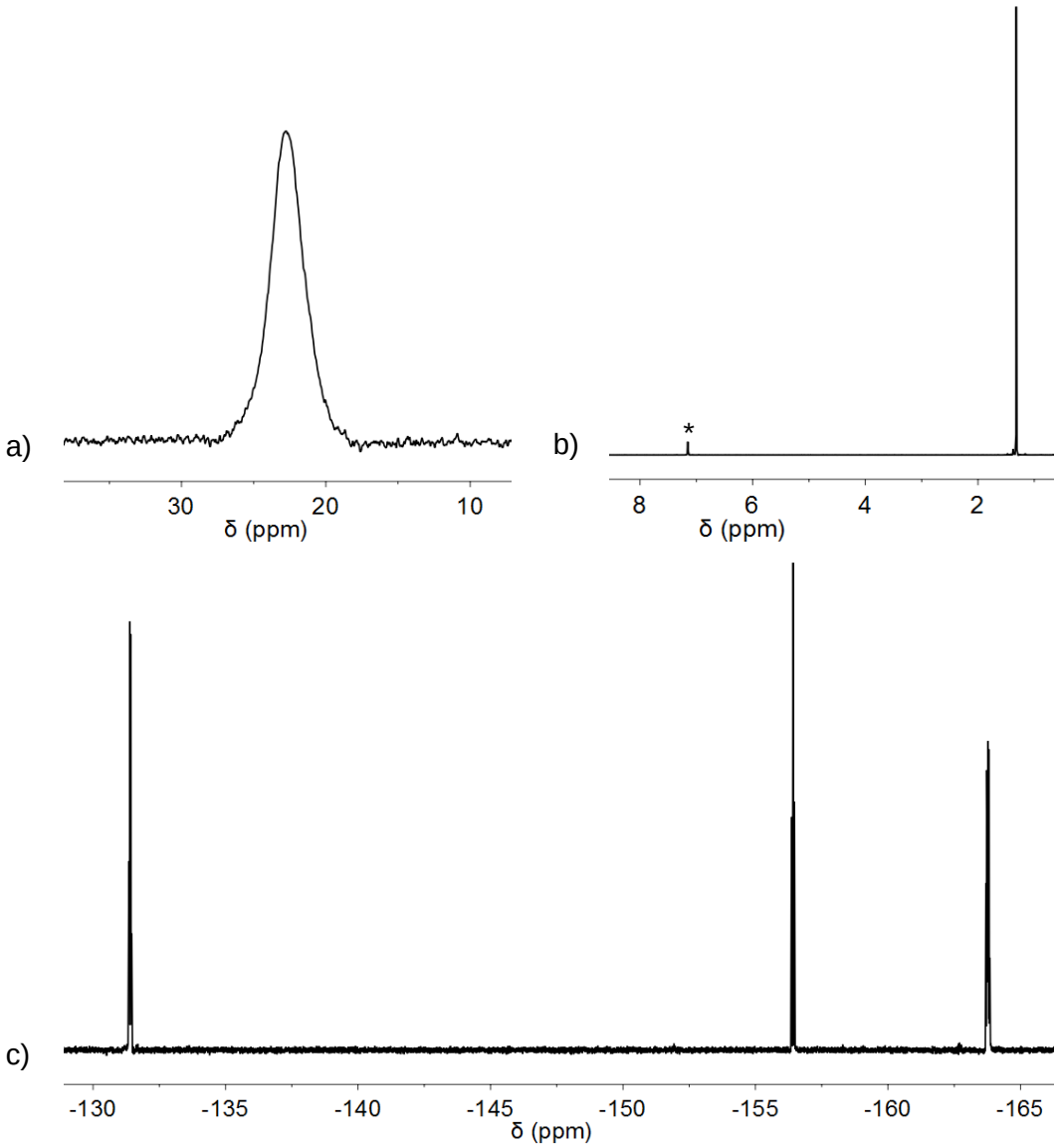

Figure 3.10 a) ^{11}B, b) ^{1}H and c) ^{19}F NMR spectrum of $((^{t}BuO)_3SiO)_2BC_6F_5$ in C_6D_6. *residual protio solvent signal.

3.5.2 Solid-State Structure of $(({}^{t}BuO)_3SiO)_2BC_6F_5$

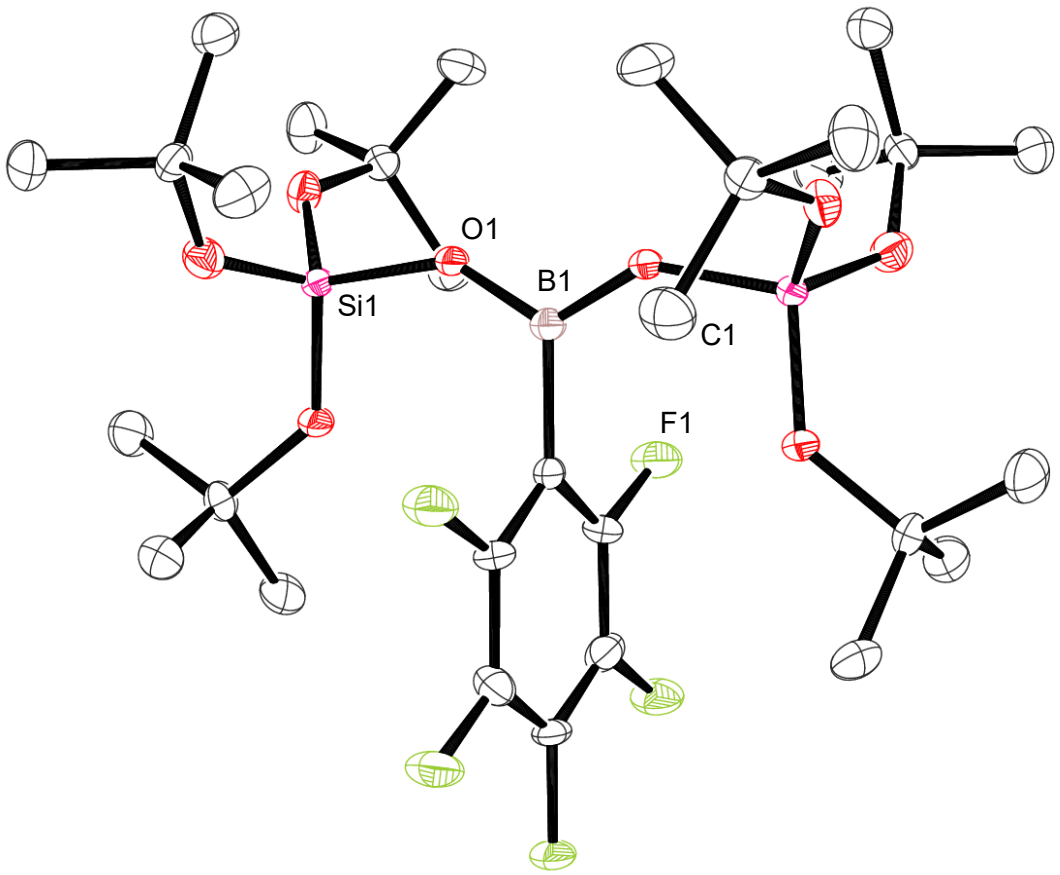

Figure 3.11 Solid-state structure of $(({}^{t}BuO)_3SiO)_2B(C_6F_5)$. Thermal ellipsoids at 50% probability (C atoms black, F atoms light green, B atom pink, O atoms red, Si atom bright pink). H atoms have been removed for clarity.

X-ray quality single crystals of the decomposition product $(({}^{t}BuO)_3SiO)_2BC_6F_5$ were grown from slow cooling of a hot acetonitrile solution, the solid-state structure of $(({}^{t}BuO)_3SiO)_2BC_6F_5$ (Figure 3.11) is consistent with the NMR data. The exact mechanism for the formation of this side product is unclear. However, Neu *et al.* reported similar findings in 2010 during the investigation of H_2 cleavage by $[B(OC_6F_5)_3/P^tBu_3]$ system.[36] While the reaction was believed to proceed *via* the initial generation of $[(C_6F_5O)_3B{-}H][H{-}P^tBu_3]$, it appears that this species is unstable and subject to ligand redistribution, prompting the formation of $[B(OC_6F_5)_4][H{-}P^tBu_3]$. The decomposition of

$[B(OC_6F_5)_4][H{-}P^tBu_3]$ and $[(^tBuO)_3SiOB(H)(C_6F_5)_2][H{-}P^tBu_3]$ could be a result of protonolysis of the C_6F_5 group by protonated phosphonium cation, following similar type of mechanism for the decomposition of $[(C_6F_5)_3BOMe][TMPH]$ proposed by Ashley *et al.*,[35] hence explaining the observation of C_6F_5H in the ^1H and ^{19}F NMR spectrum.

3.5.3 Reaction of $[(^tBuO)_3SiOB(C_6F_5)_2/PMes_3]$ with H_2

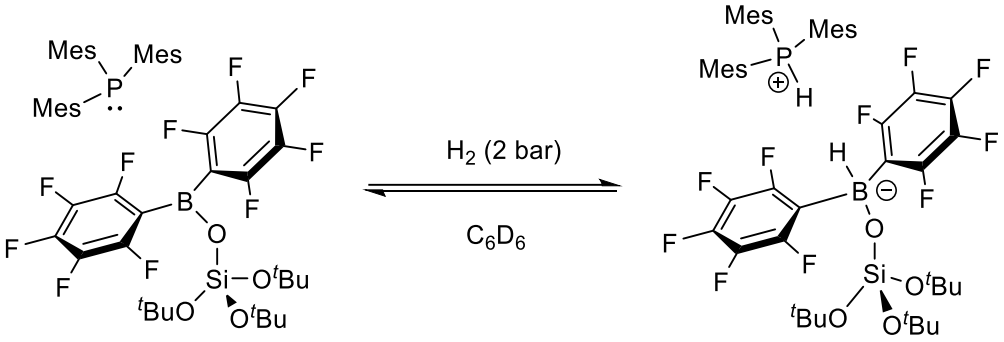

Equation 3.6 Reaction of $[(^tBuO)_3SiOB(C_6F_5)_2/PMes_3]$ with H_2.

Unlike in the case of $[(^tBuO)_3SiOB(C_6F_5)_2/P^tBu_3]$, an intense pink colour was observed when a solution of $[(^tBuO)_3SiOB(C_6F_5)_2/PMes_3]$ was cooled in liquid N_2, during the freeze-pump-thaw degass cycles prior to H_2 addition. However, the solution returns to colourless on warming back to room temperature. Perhaps this is due to the enhanced π-π interaction between the mesityl group and the C_6F_5 group in the solid-state. This finding is consistent with the observations by Welch *et al.*[33]

For a solution of $[(^tBuO)_3SiOB(C_6F_5)_2/PMes_3]$ after 16 hours at 23 °C under 2 bar H_2, a low intensity doublet at −27 ppm ($^1J_{PH}$ = 490 Hz) developed in the ^{31}P NMR spectrum, consistent with the formation of the $[H{-}PMes_3]^+$ cation.[38] A doublet at 8.8 ppm ($^1J_{PH}$ = 490 Hz) was also observed in the ^1H NMR spectrum, which further supports the formation of $[H{-}PMes_3]^+$ cation (Figure 3.12a). In the ^{11}B NMR spectrum, in addition to the $(^tBuO)_3SiOB(C_6F_5)_2$ signal at 40 ppm, a weak resonance close to 2 ppm can be observed,

suggesting the formation of $[(^{t}BuO)_3SiOB(H)(C_6F_5)_2]^-$ anion. However, almost 90% of $[(^{t}BuO)_3SiOB(C_6F_5)_2/PMes_3]$ still remain unreacted. The slower reactivity of $[(^{t}BuO)_3SiOB(C_6F_5)_2/PMes_3]$ compared to the $[(^{t}BuO)_3SiOB(C_6F_5)_2/P^{t}Bu_3]$ system could due to $PMes_3$ being more sterically hindered than $P^{t}Bu_3$.

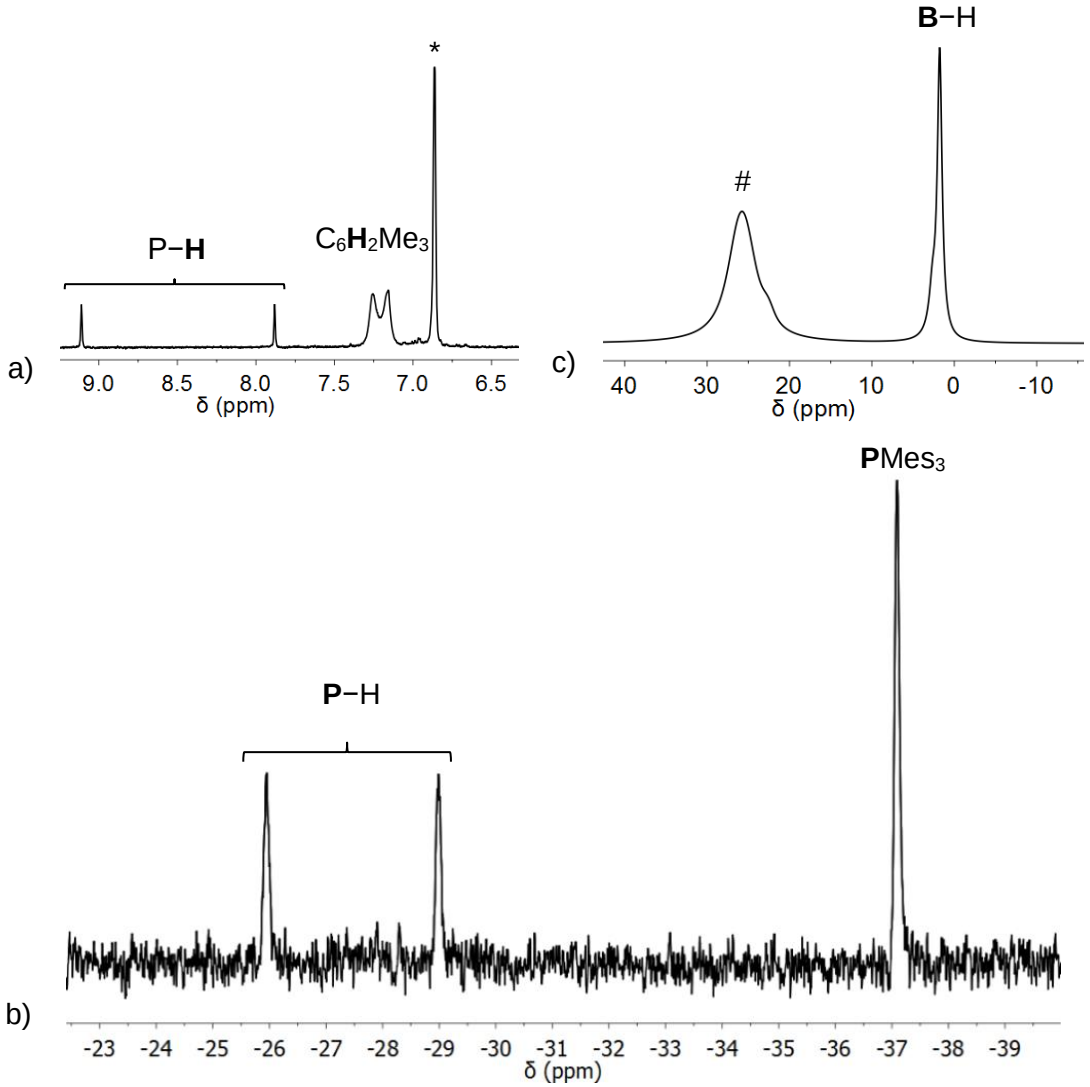

Figure 3.12 a) ^{1}H, b) ^{11}B and ^{31}P NMR spectra of H_2 cleavage reaction by $[(^{t}BuO)_3SiOB(C_6F_5)_2/PMes_3]$ in C_6D_6 after 16 hours at 60 °C. #$((^{t}BuO)_3SiO)_2BC_6F_5$. *residual protio solvent signal.

When the reaction mixture was heated to 60 °C for 16 hours, the doublet corresponding to $[H{-}PMes_3]^+$ cation in the ^{31}P NMR spectrum grew in intensity,

integration of the product resonance and unreacted $PMes_3$ resonance reveals a 1:1 in ratio (Figure 3.12b). The ^{11}B NMR spectrum shows disappearance of the resonance corresponding to unreacted $(^tBuO)_3SiOB(C_6F_5)_2$, and the growth in intensity of the resonance at 1.8 ppm corresponding to the $[(^tBuO)_3SiOB(H)(C_6F_5)_2]^-$ anion (Figure 3.12c). However, a broad resonance that at around 23 ppm was also observed, and this could be assigned to $((^tBuO)_3SiO)_2BC_6F_5$ species as a result of ligand redistribution reaction, similar to the observation for $[(^tBuO)_3SiOB(H)(C_6F_5)_2][H{-}P^tBu_3]$ system.

3.5.4 Reaction of $[(^tBuO)_3SiOB(Fxyl)_2/P^tBu_3]$ with H_2

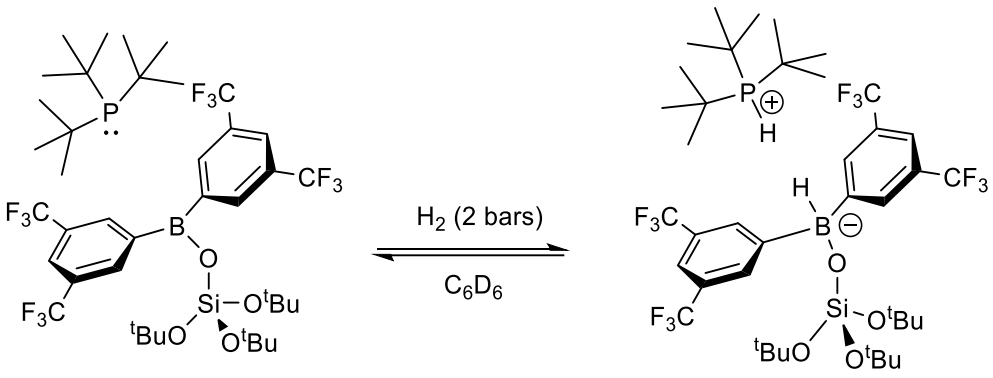

Equation 3.7 Reaction of $[(^tBuO)_3SiOB(Fxyl)_2/P^tBu_3]$ with H_2.

A deuterated benzene solution containing $[(^tBuO)_3SiOB(Fxyl)_2/P^tBu_3]$ was charged with H_2 (2 bar) at room temperature. After 16 hours a small singlet at 59 ppm ($^1J_{PH}$ = 430 Hz) was observed in the ^{31}P $\{^1H\}$ NMR spectrum (Figure 3.13a) and a doublet at 4.45 ppm was observed in the ^1H NMR spectrum (Figure 3.13c), (formation of protonated phosphonium cation $[H{-}P^tBu_3]^+$). The ratio of the phosphonium signal to the unreacted free phosphine indicates that almost 20% of the $[(^tBuO)_3SiOB(Fxyl)_2/P^tBu_3]$ has reacted with H_2 at room temperature after 16 hours. The ^{11}B NMR spectrum contains a broad signal at 45 ppm corresponding to unreacted $(^tBuO)_3SiOB(Fxyl)_2$, and a narrower signal

appearing at 0.2 ppm consistent with the formation of a four-coordinate $[(^{t}BuO)_3SiOB(H)(Fxyl)_2]^-$ anion (Figure 3.13b). The *m*-CF_3 resonance of the $[(^{t}BuO)_3SiOB(H)(Fxyl)_2]^-$ anion appears as a singlet at 61.85 ppm in the ^{19}F NMR spectrum (Figure 3.13d).

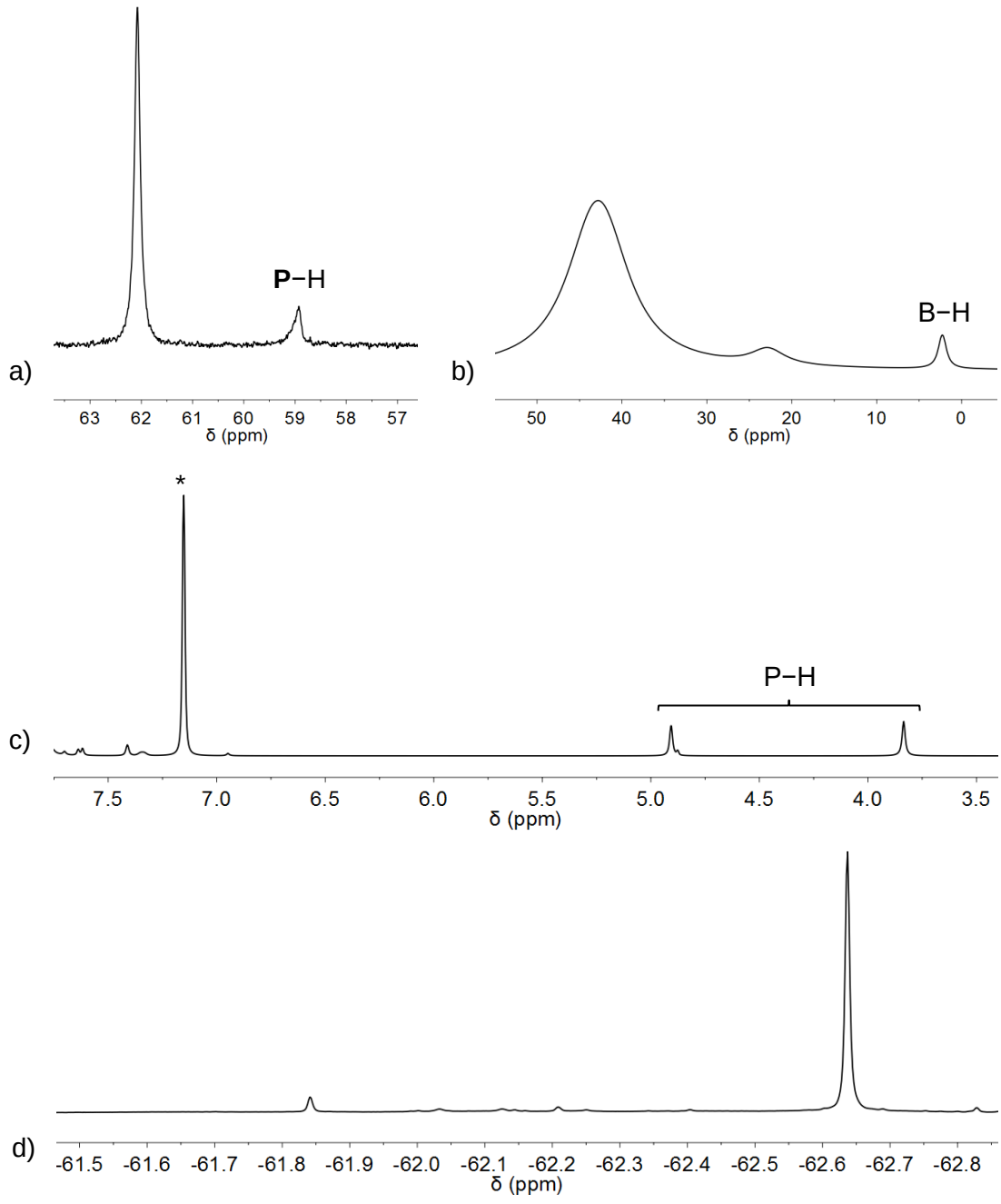

Figure 3.13 a) ^{31}P, b) ^{11}B, c) ^{1}H and d) ^{19}F NMR spectra of H_2 cleavage reaction by $[(^{t}BuO)_3SiOB(Fxyl)_2/P^{t}Bu_3]$ in C_6D_6 after 16 hours at 23 °C. *residual protio solvent signal.

The H_2 cleavage product of [(^{t}BuO)$_3$SiOB(Fxyl)$_2$/P^{t}Bu$_3$] was found to decompose at elevated temperatures similar to the [(^{t}BuO)$_3$SiOB(C_6F_5)$_2$/PMes$_3$] and [(^{t}BuO)$_3$SiOB(C_6F_5)$_2$/P^{t}Bu$_3$] systems, leading to the formation of a broad resonance at 24 ppm in the ^{11}B NMR spectrum. This additional signal could be assigned to ((^{t}BuO)$_3$SiO)$_2$B(Fxyl) formed *via* ligand redistribution as discussed earlier. Heating to 80 °C led to complete decomposition of the [(^{t}BuO)$_3$SiOB(Fxyl)$_2$/P^{t}Bu$_3$] system.

3.5.5 Reaction of [T$_8$ (OB(C_6F_5)$_2$)$_2$/(P^{t}Bu$_3$)$_2$] with H_2

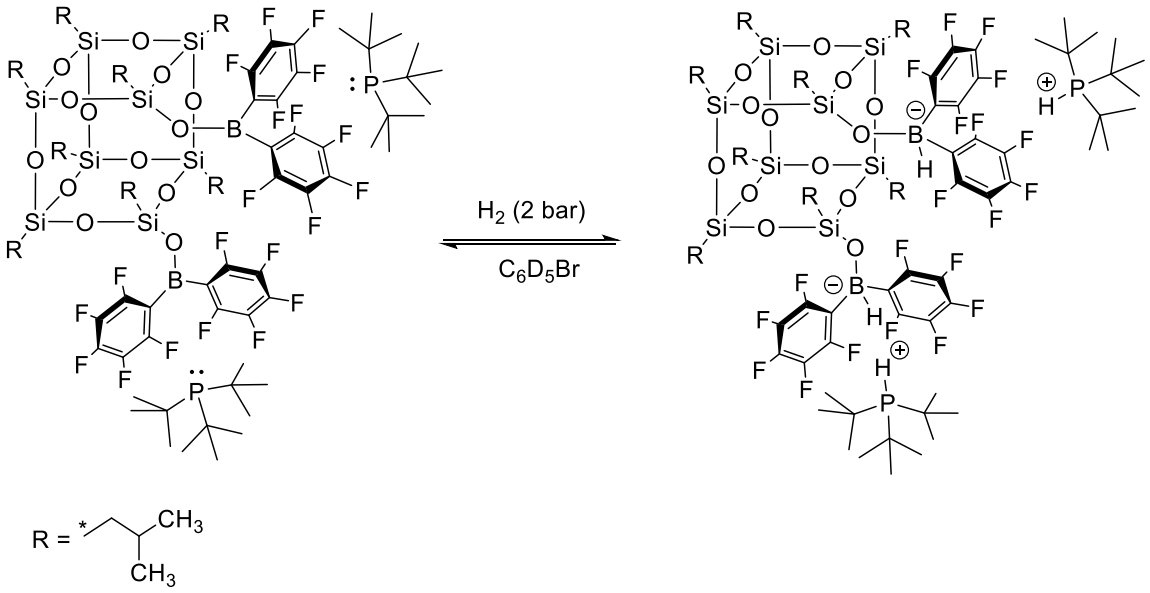

Equation 3.8 Reaction of [T$_8$ (OB(C_6F_5)$_2$)$_2$/(P^{t}Bu$_3$)$_2$] with H_2

A benzene solution containing [T$_8$(OB(C_6F_5)$_2$)$_2$/(P^{t}Bu$_3$)$_2$] was exposed to H_2 (2 bar). [T$_8$(OB(H)(C_6F_5)$_2$)$_2$][H−P^{t}Bu$_3$]$_2$ was observed after 2 hours at 25 °C. Evidence for the formation of the hydride salt was supported by the observation of [H−P^{t}Bu$_3$]$^+$ cation in the ^{31}P and ^{1}H NMR spectra. The characteristic doublet of multiplets observed at 59.2 ppm ($^1J_{PH}$ = 435 Hz) in the ^{31}P NMR spectrum and the doublet displayed at 4.48 ppm ($^1J_{PH}$ = 435 Hz) in the ^{1}H NMR spectrum are in good agreement with the literature and other

siloxane bound FLP systems describe previously in this chapter. The initial broad signal at 40 ppm in the ^{11}B NMR spectrum, which corresponds to the tri-coordinate $T_8(OB(C_6F_5)_2)_2$ has shifted to 2.8 ppm. This is consistent with formation of a four-coordinate hydridoborate $[T_8(OB(H)(C_6F_5)_2)_2]^{2-}$ dianion.

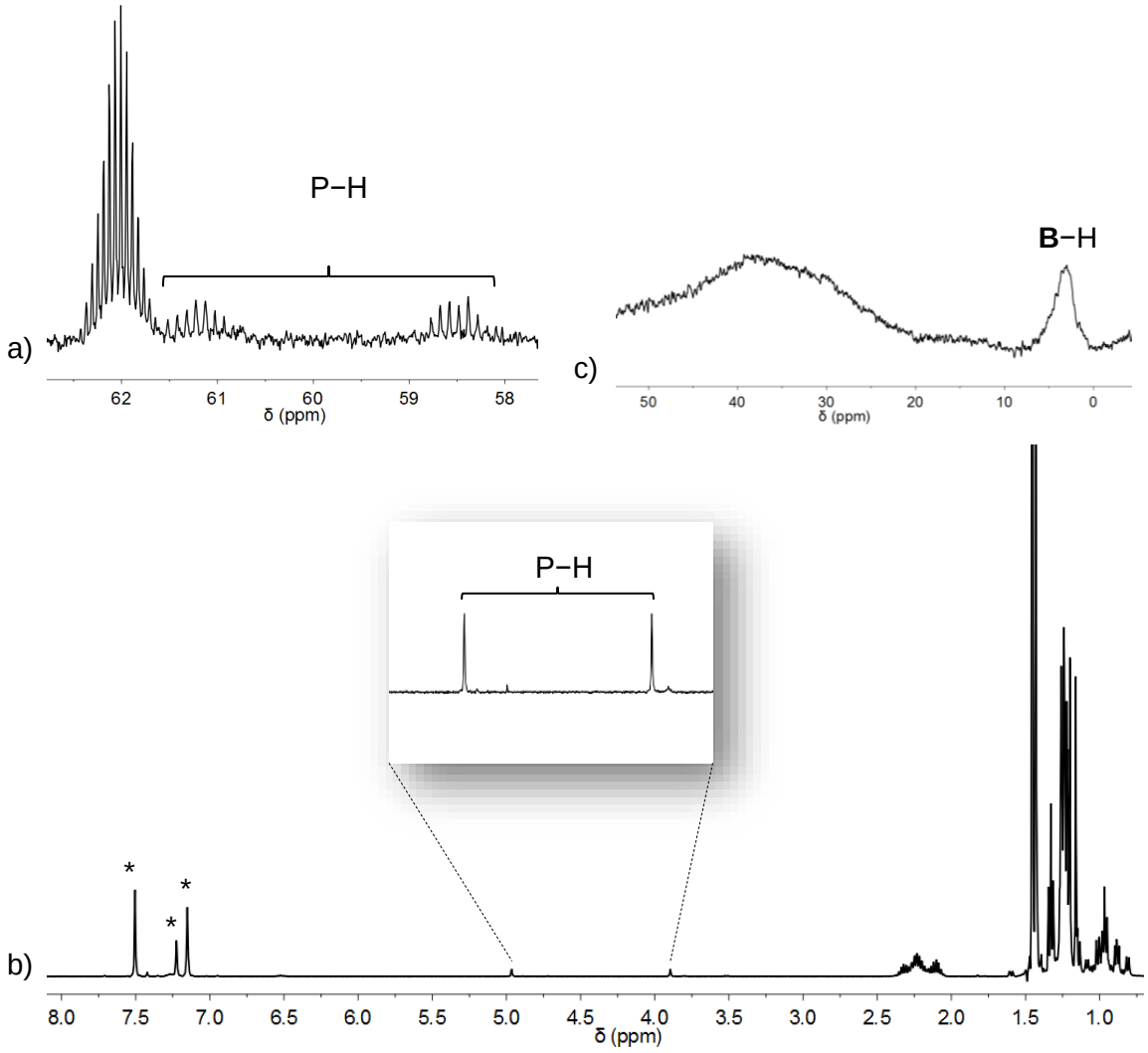

Figure 3.14 a) ^{31}P, b) ^{11}B and c) ^{1}H NMR spectrum of H_2 cleavage reaction by $[T_8(OB(C_6F_5)_2)_2/(P^tBu_3)_2]$ in C_6D_5Br after 16 hours at 60 °C showing the formation of $[H{-}P^tBu_3]^+$ cation. *residual protio solvent signals

$[T_8(OB(C_6F_5)_2)_2/(P^tBu_3)_2]$ is more thermally robust than its siloxane analogue. Heating the reaction mixture at 60 °C for 16 hours resulted in an increase of the yield of

$[T_8(OB(H)(C_6F_5)_2)_2][H{-}P^tBu_3]_2$ without the observation of significant decomposition (28% by ^{31}P NMR spectroscopy). Both the ^{31}P and ^{1}H NMR spectra show an increase in the intensity of the $[H{-}P^tBu_3]^+$ signals (Figure 3.14a and 3.14b). The broad signal in the ^{11}B NMR spectrum corresponding to the tri-coordinate $T_8(OB(Fxyl)_2)_2$ starting material had disappeared and only the narrower signal at 2.8 ppm corresponding to the $[T_8(OB(H)(C_6F_5)_2)_2]^{2-}$ dianion was visible (Figure 3.14c). Ligand redistribution product formation similar to the borato-siloxane systems was not observed for the $[T_8(OB(H)(C_6F_5)_2)_2][H{-}P^tBu_3]_2$ system, possibly due to the steric hinderance of the large bulky POSS framework reducing the rate of the ligand redistribution process.

3.5.6 Reaction of $[T_8(OB(C_6F_5)_2)_2/(PMes_3)_2]$ with H_2

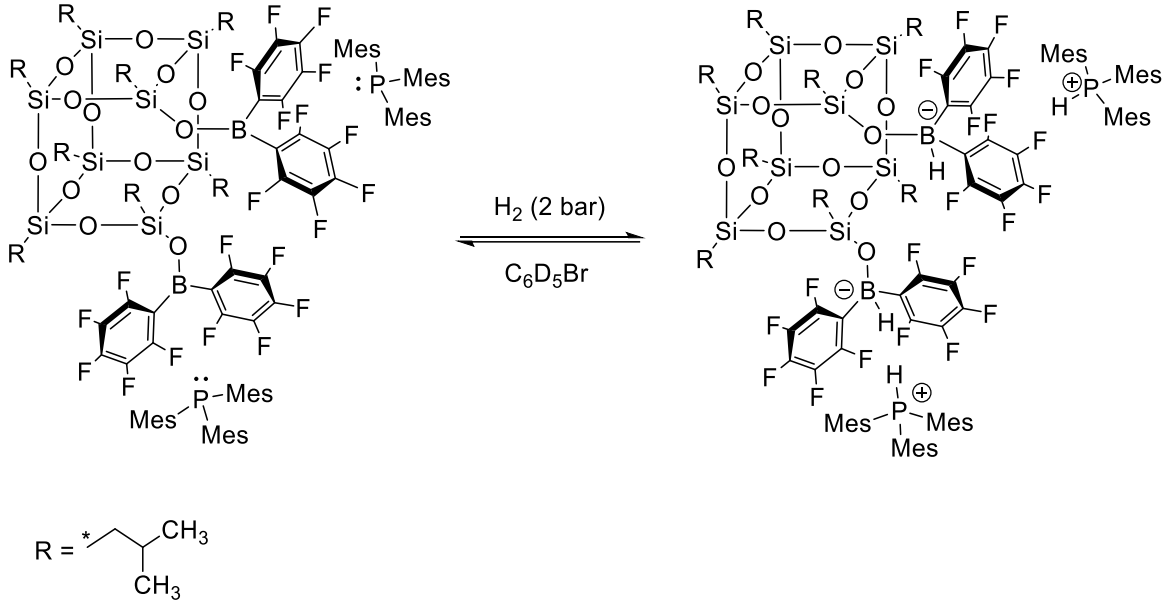

Equation 3.9 Reaction of $[T_8(OB(C_6F_5)_2)_2/(PMes_3)_2]$ with H_2.

Upon addition of H_2 gas to a C_6D_5Br solution containing $[T_8(OB(C_6F_5)_2)_2/(PMes_3)_2]$, immediate room temperature H_2 activation to yield the $[T_8(OB(H)(C_6F_5)_2)_2][H{-}P(Mes)_3]_2$ hydride salt was observed. The formation of $[H{-}P(Mes)_3]^+$ cation was confirmed by the

observation of a doublet at −28 ppm ($^1J_{PH}$ = 479 Hz) in the ^{31}P NMR spectrum (Figure 3.15a), and a doublet at 8.25 ppm ($^1J_{HP}$ = 479 Hz) in the ^{1}H NMR spectrum (Figure 3.15b). These results are consistent with the literature[33] as well as with the [(^{t}BuO)$_3$SiOB(C$_6$F$_5$)$_2$/PMes$_3$] system previously described. Evidence for the formation of [T$_8$(OB(H)(C$_6$F$_5$)$_2$)$_2$]$^{2-}$ dianion was supported by the appearance of a new resonance at −1.3 ppm in the ^{11}B NMR spectrum (Figure 3.15c). After 16 hours at 23 °C the conversion has reached 27% by ^{31}P NMR spectroscopy.

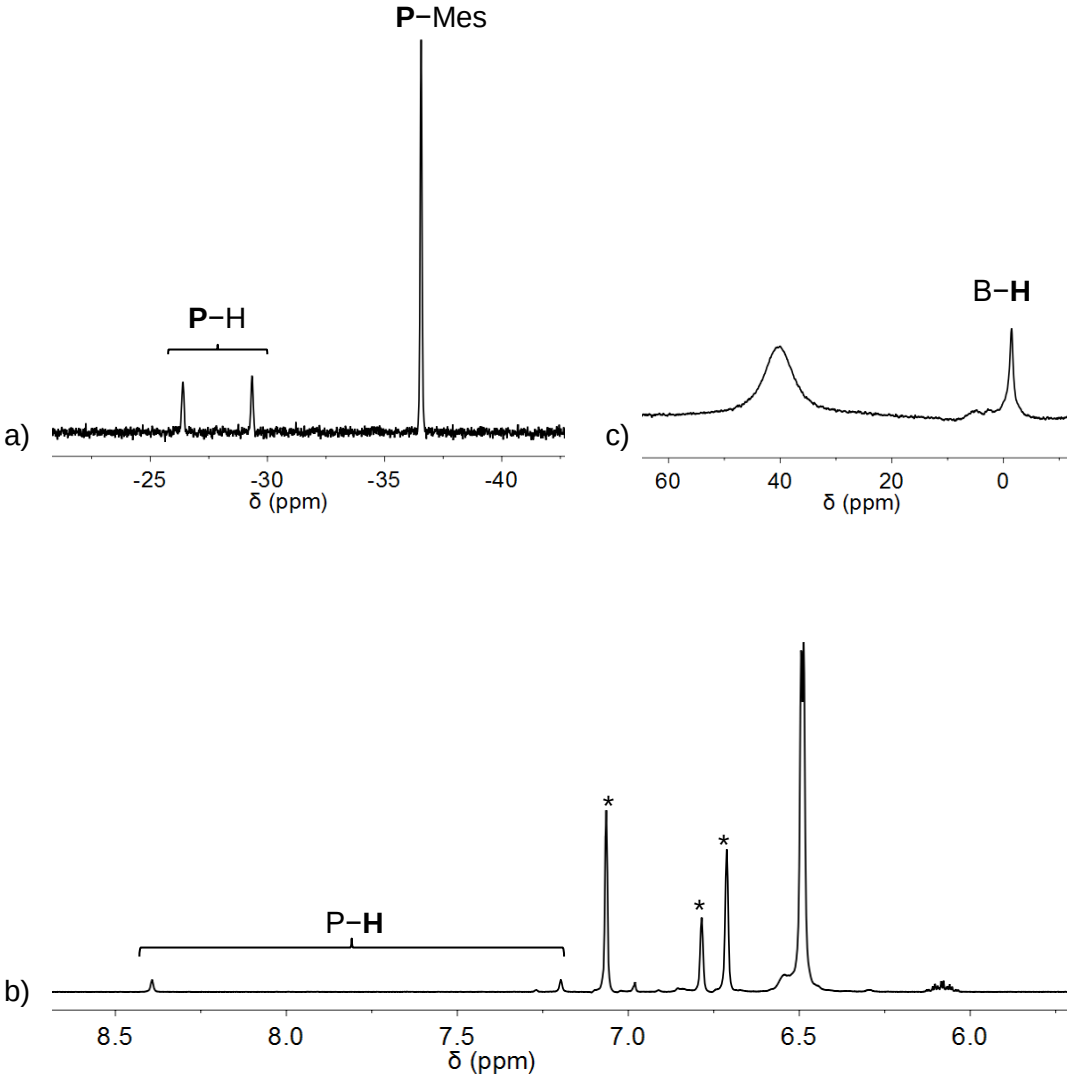

Figure 3.15 a) ^{31}P, b) ^{11}B and c) ^{1}H NMR spectrum of H_2 cleavage reaction [T$_8$(OB(H)(C$_6$F$_5$)$_2$)$_2$/(PMes$_3$)$_2$] in C$_6$D$_6$ after 16 hours at 23 °C showing (α) [H−PMes$_3$]$^+$ cation and free PMes$_3$.

Further heating the reaction mixture to 60 °C did not result in significant increase in the yield of H_2 cleavage product, instead, decomposition of $[T_8(OB(H)(C_6F_5)_2)_2]^{2-}$ was observed as confirmed by the appearance of C_6F_5H in the ^1H and ^{19}F NMR spectra, alongside unidentifiable decomposition products, presumably formed *via* a combination of protonolysis and ligand redistribution process. The large amount of decomposition observed at such an early stage indicates that this system is unsuitable for further investigations.

3.5.7 Reaction of $[T_8(OB(Fxyl)_2)_2/(P^tBu_3)_2]$ with H_2

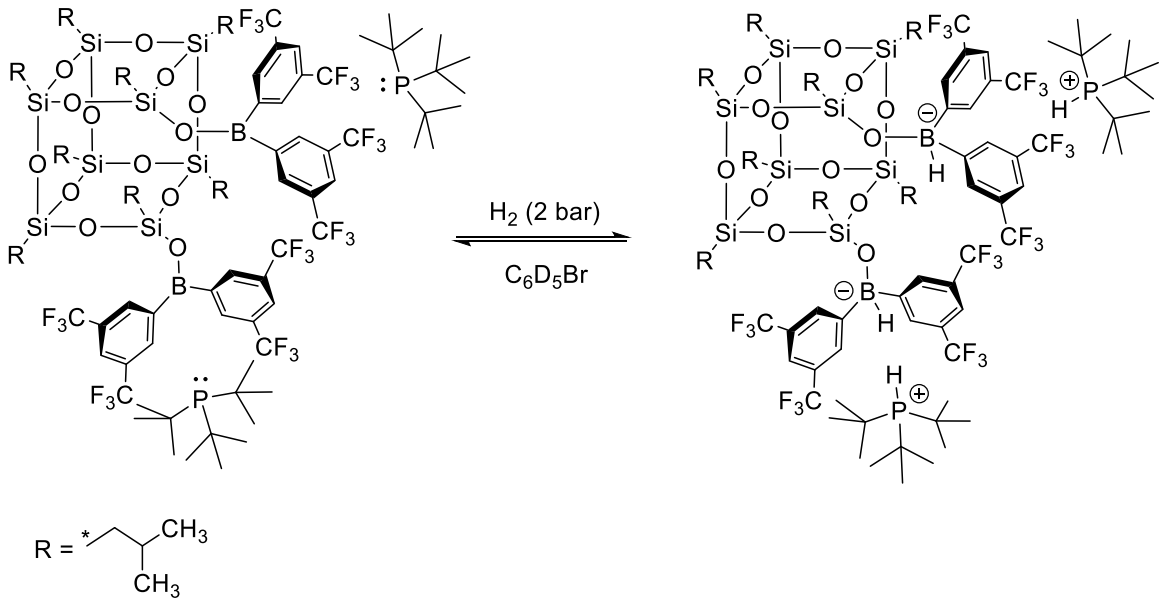

Equation 3.10 Reaction of $[T_8(OB(Fxyl)_2)_2(P^tBu_3)_2]$ with H_2.

$[T_8(OB(Fxyl)_2)_2/(P^tBu_3)_2]$ showed higher reactivity towards H_2 cleavage than $[T_8(OB(C_6F_5)_2)_2/(P^tBu_3)_2]$. This has been initially confirmed by the immediate observation of a doublet at 56.2 ppm ($^1J_{PH}$ = 441 Hz) in the ^{31}P NMR spectrum (Figure 3.16a), and a doublet at 4.62 ppm ($^1J_{HP}$ = 441 Hz) in the ^1H NMR spectrum (Figure 3.16b), up addition of H_2 consistent with the formation $[H{-}P^tBu_3]^+$ cation. According to integration of the

resonances in the ^{31}P NMR spectrum, the yield of the $[H{-}P^tBu_3]^+$ cation reached 41% after 16 hours at room temperature. This is surprising given the maximum yield of $[H{-}P^tBu_3]^+$ obtained with $[(^tBuO)_3SiOB(Fxyl)_2/P^tBu_3]$ was only 19%. The formation of $[T_8(OB(H)(Fxyl)_2)_2]^{2-}$ dianion can be observed by the development of a sharp signal at 1 ppm in the ^{11}B NMR spectrum (Figure 3.16c). In addition, a very broad resonance at 30 ppm in the ^{11}B NMR spectrum was observed, suggesting the formation of a similar decomposition product as seen previously for other borato-siloxane and silsesquioxane systems.

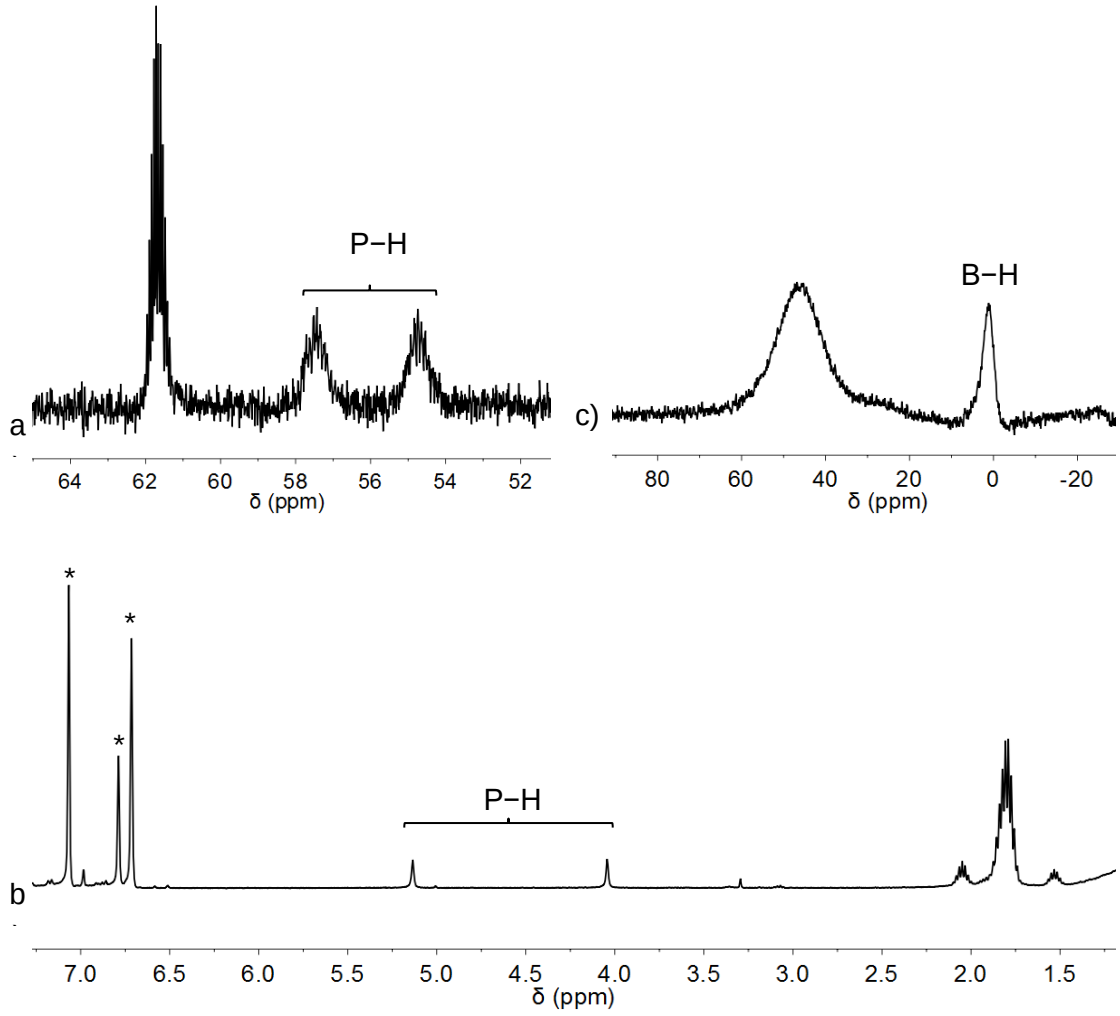

Figure 3.16 a) ^{31}P, b) ^{1}H and c) ^{11}B NMR spectrum of H_2 cleavage reaction by $[T_8(OB(Fxyl)_2)_2/(P^tBu_3)_2]$ in C_6D_5Br after 16 hours at room temperature. *residual protio solvent signals.

Heating the reaction to 60 °C only resulted in decomposition of the H_2 activation product and formation of a mixture of unidentifiable by-products, indicating that this system is not thermally stable, and readily undergoes ligand redistribution.

3.5.8 Reaction of $[T_8(OB(Fxyl)_2)_2/(PMes_3)_2]$ with H_2

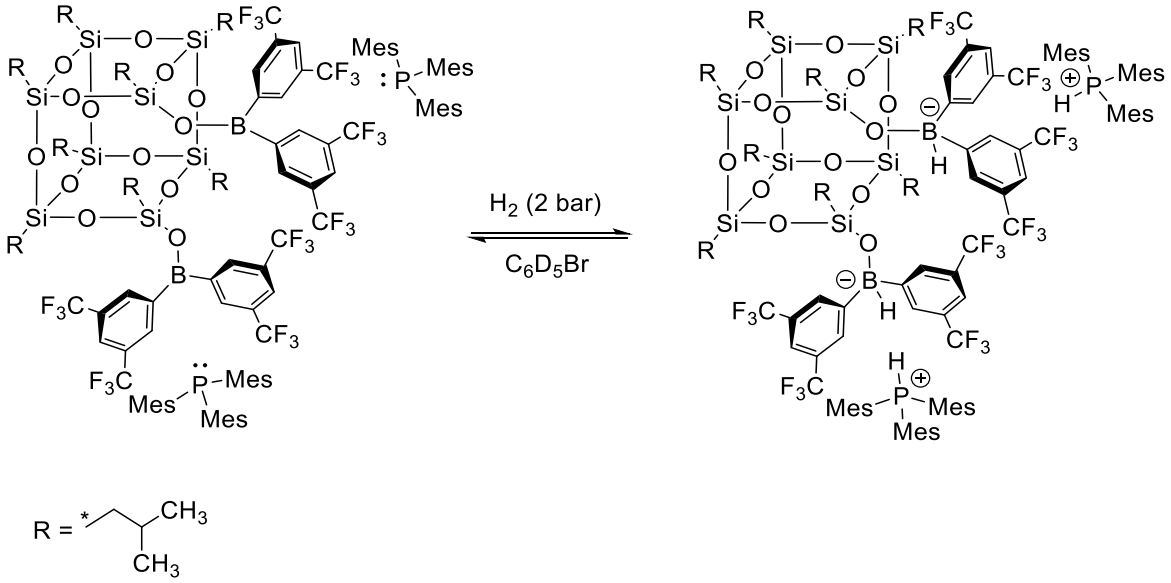

Equation 3.11 Reaction of $[T_8(OB(Fxyl)_2)_2/(PMes_3)_2]$ with H_2.

Similar to the $[T_8(OB(Fxyl)_2)_2/(P^tBu_3)_2]$ system, the $[T_8(OB(Fxyl)_2)_2/(PMes_3)_2]$ demonstrated room temperature H_2 activation. The development of a set of doublet signal at −27.4 ppm ($^1J_{PH}$ = 480 Hz) in the ^{31}P NMR spectrum (Figure 3.17a), coupled with the observation of a small doublet at 8.28 ppm ($^1J_{PH}$ = 480 Hz) in the ^1H NMR spectrum after 16 hours at 23 °C are consistent with the formation of a $[H{-}PMes_3]^+$ cation (38% by ^{31}P NMR spectroscopy). The ^{11}B NMR spectrum displayed a narrow resonance at 1.3 ppm which also indicates the formation of four-coordinate $[T_8(OB(H)(C_6F_5)_2)_2]^{2-}$ dianion, consistent with the observation of H_2 cleavage by $[T_8(OB(Fxyl)_2)_2/(P^tBu_3)_2]$ aforementioned (Figure 3.17b). Unfortunately, this system is also highly unstable at 60 °C, and underwent similar decomposition process as with the $[T_8(OB(Fxyl)_2)_2/(P^tBu_3)_2]$

analogue, forming large amount of unidentifiable side products, rendering it unsuitable for further studies.

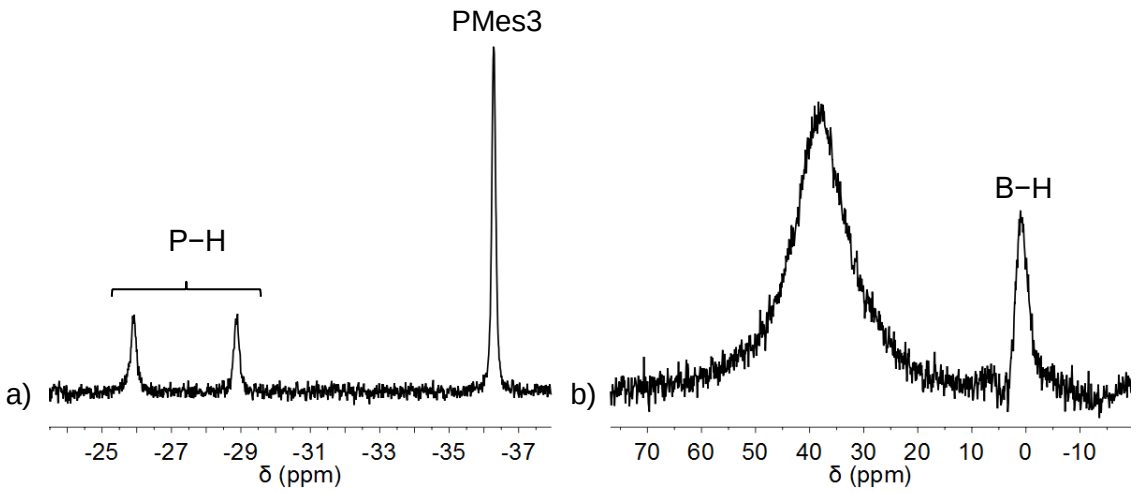

Figure 3.17 a) ^{31}P and b) ^{11}B NMR spectrum of H_2 cleavage reaction by $[T_8(OB(Fxyl)_2)_2/(PMes_3)_2]$ in C_6D_5Br after 16 hours at 23 °C.

3.6 Conclusions

In total, four analytically pure Lewis acids functionalised siloxane/POSS complexes; $(({}^tBuO)_3SiOB(C_6F_5)_2$, $({}^tBuO)_3SiOB(Fxyl)_2$, $[T_8(OB(C_6F_5)_2)_2]$ and $[T_8(OB(Fxyl)_2)_2]$) have been successfully synthesised *via* the reaction of either $({}^tBuO)_3SiOH$ or $(i\text{-}C_4H_9)_8Si_8O_{12}(OH)_2$ with either $(C_6F_5)_2BH$ or $(Fxyl)_2BCl$. These interesting Lewis acids have been studied as soluble molecular mimicks for the Lewis acid-modified surface sites on silica supported Lewis acids. All the products were fully characterised using ^1H, ^{19}F, ^{11}B, and ^{29}Si NMR spectroscopy.

The ability for these Lewis acids to form FLPs with bulky phosphine bases has been investigated. Using P^tBu_3 and $PMes_3$, a total of seven new FLP systems have been synthesised. The solution-state NMR characterisation of these FLP systems serve as the

basis for interpretation of the solid-state NMR data of silica supported FLPs in the next chapter, as well as for studying their subsequent reactivity with H_2.

Solutions of these seven new FLP systems show unprecedented H_2 activation properties under mild conditions. The H_2 cleavage was initially confirmed by the observation of protonated phophonium cations, as the result of heterolytic cleavage of H_2. However, due to the hydridoborate anions being highly unsymmetrical, the expected doublet signal for $[B{-}H]^-$ anions was not observed. Based on the integrations of the ^{31}P NMR resonances, none of these systems produce more than a 50% yield of the H_2 activation products under 2 bar H_2. FLP systems containing Fxyl groups were found to activate H_2 at room temperature, whereas the FLPs containing C_6F_5 groups requires thermal activation. However, the hydride salts of these FLP systems are unstable, at room temperature *via* a combination of ligand redistribution and protonolysis. In particular, FLPs containing Fxyl substituents not only showed increased reactivity towards hydrogen activation, but also accelerated decomposition. In these cases, removing *ortho*-F atoms removes the steric protection of the boron core, leading to increased reactivity particularlty when applied to sterically demanding POSS cages, however, their propensity for decomposition is much greater than C_6F_5 analogues.

The thermal decomposition product of $[(^t\text{BuO})_3\text{SiOB}(C_6F_5)_2(H)][H{-}P^t\text{Bu}_3]$ was isolated and characterised using a combination of X-ray crystallography and NMR spectroscopy, and identified as $((^t\text{BuO})_3\text{SiO})_2\text{B}(C_6F_5)$. All other systems have also shown similar type of ligand redistribution process, rendering these systems unlikely to serve as hydrogenation catalyst. Nonetheless, the NMR studies of these hydrocarbon soluble models provides valuable insights for understanding the reactivity of solid-state silica supported FLPs.

3.7 References

1 G. Ertl, H. Knözinger and J. Weitkamp, in *Climate Change 2013 - The Physical Science Basis*, ed. Intergovernmental Panel on Climate Change, Cambridge University Press, Cambridge, 2014, pp. 1–30.

2 C. Copéret, M. Chabanas, R. Petroff Saint-Arroman and J.-M. Basset, *Angew. Chem., Int. Ed.*, 2003, **42**, 156–181.

3 M. J. Sprague, *Chem. Ing. Tech.*, 1985, **57**, 430–430.

4 K. Tamaru, *Proc. Jpn. Acad., Ser. B*, 2004, **80**, 119–127.

5 P. Sobota and S. Szafert, *J. Chem. Soc., Dalton Trans.*, 2001, **73**, 1379–1386.

6 P. Sobota, Z. Józef Utko, K. Sztajnowska and L. B. Jerzykiewicz, *New J. Chem.*, 1998, **22**, 851–855.

7 Z. Janas, L. B. Jerzykiewicz, P. Sobota and J. Utko, *New J. Chem.*, 1999, **23**, 185–188.

8 R. W. J. M. Hanssen, A. Meetsma, R. A. van Santen and H. C. L. Abbenhuis, *Inorg. Chem.*, 2001, **40**, 4049–4052.

9 F. J. Feher, D. A. Newman and J. F. Walzer, *J. Am. Chem. Soc.*, 1989, **111**, 1741–1748.

10 R. H. Baney, M. Itoh, A. Sakakibara and T. Suzuki, *Chem. Rev.*, 1995, **95**, 1409–1430.

11 F. J. Feher and D. A. Newman, *J. Am. Chem. Soc.*, 1990, **112**, 1931–1936.

12 T. W. Dijkstra, R. Duchateau, R. A. van Santen, A. Meetsma and G. P. A. Yap, *J. Am. Chem. Soc.*, 2002, **124**, 9856–9864.

13 R. Murugavel, A. Voigt, M. G. Walawalkar and H. W. Roesky, *Chem. Rev.*, 1996, **96**, 2205–2236.

14 R. Duchateau, U. Cremer, R. J. Harmsen, S. I. Mohamud, H. C. L. Abbenhuis, R. A. van Santen, A. Meetsma, S. K.-H. Thiele, M. F. H. van Tol and M. Kranenburg, *Organometallics*, 1999, **18**, 5447–5459.

15 F. J. Feher, D. Soulivong and G. T. Lewis, *J. Am. Chem. Soc.*, 1997, **119**, 11323–11324.

16 J. Annand, H. C. Aspinall and A. Steiner, *Inorg. Chem.*, 1999, **38**, 3941–3943.

17 R. Duchateau, H. C. L. Abbenhuis, R. A. van Santen, S. K.-H. Thiele and M. F. H. van Tol, *Organometallics*, 1998, **17**, 5222–5224.

18 F. J. Feher, T. A. Budzichowski, K. Rahimian and J. W. Ziller, *J. Am. Chem. Soc.*, 1992, **114**, 3859–3866.

19 R. Duchateau, R. A. van Santen and G. P. A. Yap, *Organometallics*, 2000, **19**, 809–816.

20 V. Lorenz, A. Fischer, S. Gießmann, J. W. Gilje, Y. Gun'ko, K. Jacob and F. T. Edelmann, *Coord. Chem. Rev.*, 2000, **206**–**207**, 321–368.

21 F. J. Feher and T. A. Budzichowski, *Polyhedron*, 1995, **14**, 3239–3253.

22 P. D. Lickiss, in *Advances in Inorganic Chemistry*, ed. A. G. Sykes, Elsevier, 1995, vol. 42, pp. 147–262.

23 F. Schindler and H. Schmidbaur, *Angew. Chem., Int. Ed. Engl.*, 1967, **6**, 683–694.

24 H. Schmidbaur, *Angew. Chem., Int. Ed.*, 1965, **4**, 201–211.

25 G. C. Welch, L. Cabrera, P. A. Chase, E. Hollink, J. D. Masuda, P. Wei and D. W. Stephan, *Dalton Trans.*, 2007, **75**, 3407–3414.

26 G. C. Welch, R. R. S. Juan, J. D. Masuda and D. W. Stephan, *Science*, 2006, **314**, 1124–1126.

27 M. Ullrich, A. J. Lough and D. W. Stephan, *Organometallics*, 2010, **29**, 3647–3654.

28 M. Ullrich, A. J. Lough and D. W. Stephan, *J. Am. Chem. Soc.*, 2009, **131**, 52–53.

29 K. Samigullin, M. Bolte, H.-W. Lerner and M. Wagner, *Organometallics*, 2014, **33**, 3564–3569.

30 T. J. Herrington, A. J. W. Thom, A. J. P. White and A. E. Ashley, *Dalton Trans.*, 2012, **41**, 9019–9022.

31 K. Samigullin, I. Georg, M. Bolte, H.-W. Lerner and M. Wagner, *Chem. - Eur. J.*, 2016, **22**, 3478–3484.

32 G. J. P. Britovsek, J. Ugolotti and A. J. P. White, *Organometallics*, 2005, **24**, 1685–1691.

33 G. C. Welch and D. W. Stephan, *J. Am. Chem. Soc.*, 2007, **129**, 1880–1881.

34 V. Sumerin, F. Schulz, M. Nieger, M. Leskelä, T. Repo and B. Rieger, *Angew. Chem., Int. Ed.*, 2008, **47**, 6001–6003.

35 A. E. Ashley, A. L. Thompson and D. O'Hare, *Angew. Chem., Int. Ed.*, 2009, **48**, 9839–9843.

36 R. C. Neu, E. Y. Ouyang, S. J. Geier, X. Zhao, A. Ramos and D. W. Stephan, *Dalton Trans.*, 2010, **39**, 4285–4294.

37 W. L. Respess and C. Tamborski, *J. Organomet. Chem.*, 1969, **18**, 263–274.

38 G. Ménard, L. Tran, J. S. J. McCahill, A. J. Lough and D. W. Stephan, *Organometallics*, 2013, **32**, 6759–6763.

CHAPTER FOUR

Silica-Supported Frustrated Lewis Pairs

4.1 Introduction

As discussed in Chapter One, FLPs have demonstrated extensive solution phase catalytic hydrogenation activity,[1–10] however, for the successful implementation of this technology in large-scale processes, heterogeneous catalysts are preferred due to their many well-documented industrial requirements (easy catalyst separation, uses in continuous gas or liquid feed fixed bed reactors, or in slurry-phase reactors).[11,12]

Silica and modified silica have been overwhelmingly used as supports for heterogeneous catalyst, for example as a support for single-site polymerisation catalysts,[13] this is usually due to its inert properties and facile control of surface hydroxyl content by simple thermo-treatments.[14–16] The preparation of single-site catalysts usually includes the combination of a precatalyst (transition metal complex) with an activator such as methylaluminoxane (MAO) leading to a cationic active catalyst. Although active silica supported metallocene catalyst without co-catalyst do exist,[17] the presence of a co-catalyst improves the catalyst activity and performance drastically. Different methods have been used to prepare solid catalysts by grafting the metal complex then reaction with a co-catalyst, or *vice versa*.[11,12] The former method which involves pre-contacting an inorganic oxide with a precatalyst prior to the addition of MAO is not a common procedure for catalyst immobilisation. This is because the resulting catalysts have been reported to contain more than one metal species due to the presence of different silica surface sites.[15,18,19] The second method which is based on the preparation of supported activators in

particular SiO_2/MAO has been one of the earliest and most frequently used method for the immobilisation of single site polymerisation catalyst. However, MAO suffers some significant drawbacks, including the cost and poorly defined structure. The discovery of fluoaryl-based activators such as $[B(C_6F_5)_4][HNR_3]$,[20] $[B(C_6F_5)_4][Ph_3C]$[21] and $B(C_6F_5)_3$ (BCF)[22] led to the isolation and characterisation of single-site catalyst that exhibit commercially significant activities.

A decade ago, silica-supported BCF co-catalysts were developed by Tian *et al*. through the reaction of ≡SiOH with either BCF ($[\equiv SiOB(C_6F_5)_3][H]$) or $(C_6F_5)_3BX$ ($\equiv SiOB(C_6F_5)_2$). These heterogeneous BCF analogues showed activation of Cp_2ZrMe_2 for olefin polymerisation.[23,24] However, leaching of supported BCF was observed, and formation of $Me_2B(C_6F_5)$ and $Cp_2ZrMe(C_6F_5)$ by-products (*via* the decomposition of $[Cp_2ZrMe_2][Me_2B(C_6F_5)_2]$ ion pair) were detected in solution, suggesting reversible binding of BCF with surface ≡SiOH groups. Wanglee *et al*. provided a detailed alternative synthesis of well-characterised irreversibly grafted $\equiv SiO{-}B(C_6F_5)_2$ (***s*-BCF**) *via* the reaction of $B(C_6F_5)_3$ with thermally pre-treated (500 °C, 4 h, 0.001 mbar) dehydrated silica ($SiO_{2\text{-}500}$) in the presence of a catalytic amount of H_2O.[25] Remarkably, when ***s*-BCF** was combined with [*N*-(2,6-dimethylphenyl)-2-(2,6-dimethylphenylimino)propanamidato -κ^2-*N,N*](η^1-benzyl)(trimethylphosphino)nickel(II) (inactive in the absence of a co-catalyst) polyethylene was obtained even at 40 °C.

Very recently, Taoufik *et al.*[26] reported the immobilisation of a (4-hydroxyphenyl)diphenylphosphine on a tri-isobutyl aluminium modified silica support and the subsequent treatment with $B(C_6F_5)_3$ or $(C_6F_5)_2BH$ to produce surface bound FLPs (*s*-FLPs) (Scheme 4.1). Both systems have shown high Z-selective reduction of 3-hexyne under 40 bar, H_2 at 80 °C. This promising result is the first example demonstrating the concept of heterogeneous FLP catalytic hydrogenation, and certainly encourages further

development of solid-supported FLPs for potential industrial applications.[26] However, direct utilisation of ***s*-BCF** as the Lewis acid for *s*-FLP formation has never been explored.

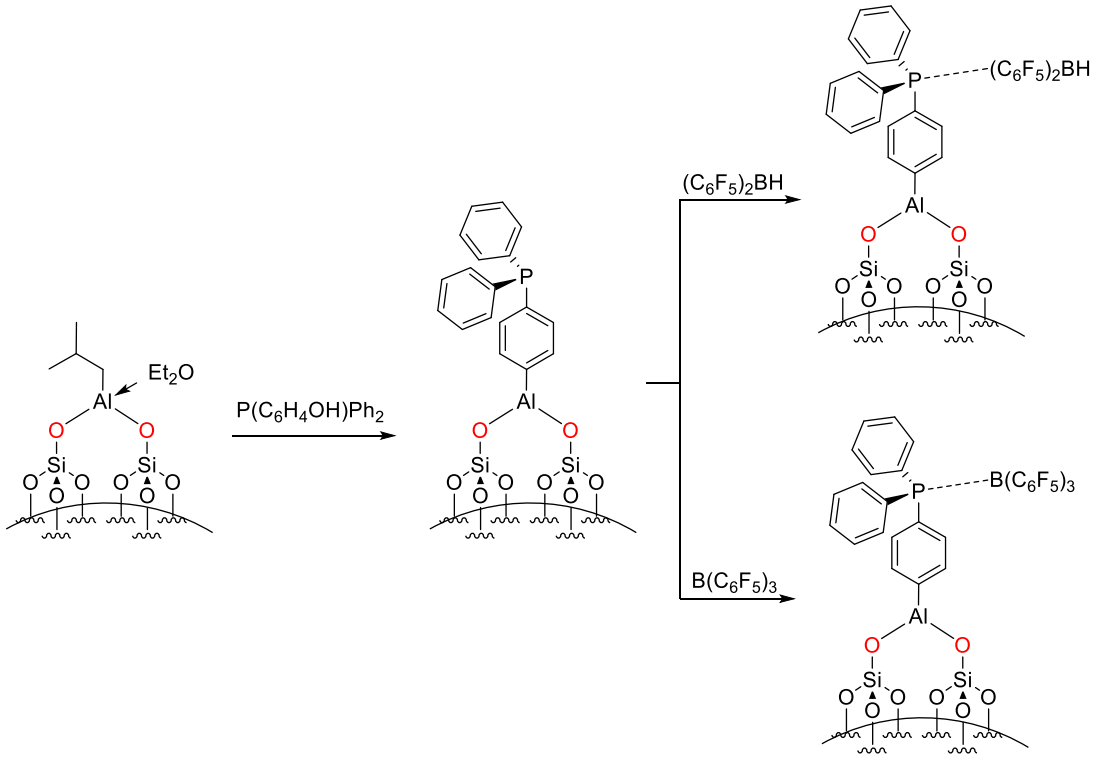

Scheme 4.1 Synthesis of *s*-FLPs by Taoufik and co-workers. [26]

This chapter describes the synthesis of a series of silica supported FLPs *via* a simple two-step approach utilising borane-modified silica Lewis acids, and the study of their H_2 activation behaviour using a combination of Fourier Transform IR (FTIR) and solid-state NMR spectroscopic techniques.

4.2 Synthesis of Silica-immobilised Lewis Acids

Reaction of thermally pre-treated $SiO_{2\text{-}500}$with either $(C_6F_5)_2BH$ or $(Fxyl)_2BCl$ (where X = Cl, Fyxl = $(3,5\text{-}CF_3)_2C_6H_3$) affords ***s*-BCF** and ***s*-BFxyl**. These supported Lewis acids have been characterised using IR, solid-state NMR spectroscopy, and elemental analysis.

4.2.1 Synthesis of ≡SiOB(C_6F_5)$_2$ (*s*-BCF)

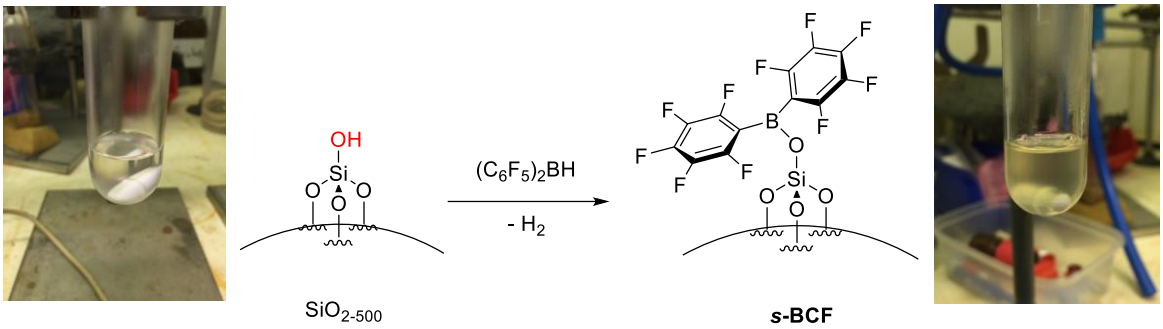

Equation 4.1 Synthesis of ***s*-BCF**.

Reaction of $SiO_{2\text{-}500}$ (pre-treated at 500 °C, under 0.001 mbar pressure for 4 hours, specific surface area: 310 $m^2\,g^{-1}$ (BET), containing 0.57 mmol g^{-1} of accessible ≡SiOH) with stoichiometric amount of $(C_6F_5)_2BH$ led to the formation of ***s*-BCF** (loading of 16.6 wt. %, confirmed by EA) (Equation 4.1). The reaction proceeded cleanly at room temperature in a toluene slurry, and was indirectly monitored by solution-state ^{19}F NMR spectroscopy of the supernatant. After 16 h, almost all of the $(C_6F_5)_2BH$ has been consumed. Trace amounts of $(C_6F_5)_2BOH$ can be observed as the only side product generated as the result of condensation of surface silanol groups (also seen by Wanglee *et al.*).[25] The reaction mixture was further heated to 100 °C for 1 hour in order to ensure that any $(C_6F_5)_2BOH$ present has also reacted with the support, before the solid was filtered and dried to afford a slightly yellow powder in 90% isolated yield. The solution ^{19}F NMR spectrum of the toluene washing showed no fluorine containing compounds, indicating completion of the grafting process.

FTIR Spectrum of pristine $SiO_{2\text{-}500}$ contains a sharp absorption at 3746 cm^{-1} and a broad shoulder at 3680 cm^{-1} (Figure 4.1). The sharp absorption is consistent with isolated surface hydroxyl groups, and the broad shoulder corresponds to internal inaccessible

silanol groups.[16,27] The IR spectrum of ***s*-BCF** (a) does not contain a sharp absorption band at 3746 cm^{-1}, indicating that all surface hydroxyl groups have been successfully converted to $-OB(C_6F_5)_2$. Several vibration modes are present in the range from 1455 to 1660 cm^{-1} in spectrum (a), which are associated with B−O stretching, C−B−C wagging and C_6F_5 ring breathing modes, and are consistent with the spectrum of $HB(C_6F_5)_2$ (b) as well as with the literature reported values for ***s*-BCF**.[24] Furthermore, comparison of the FTIR spectra for ***s*-BCF** (a) and $(C_6F_5)_2BH$ (b) suggests preservation of a well-defined complex on the silica surface (Figure 4.1).

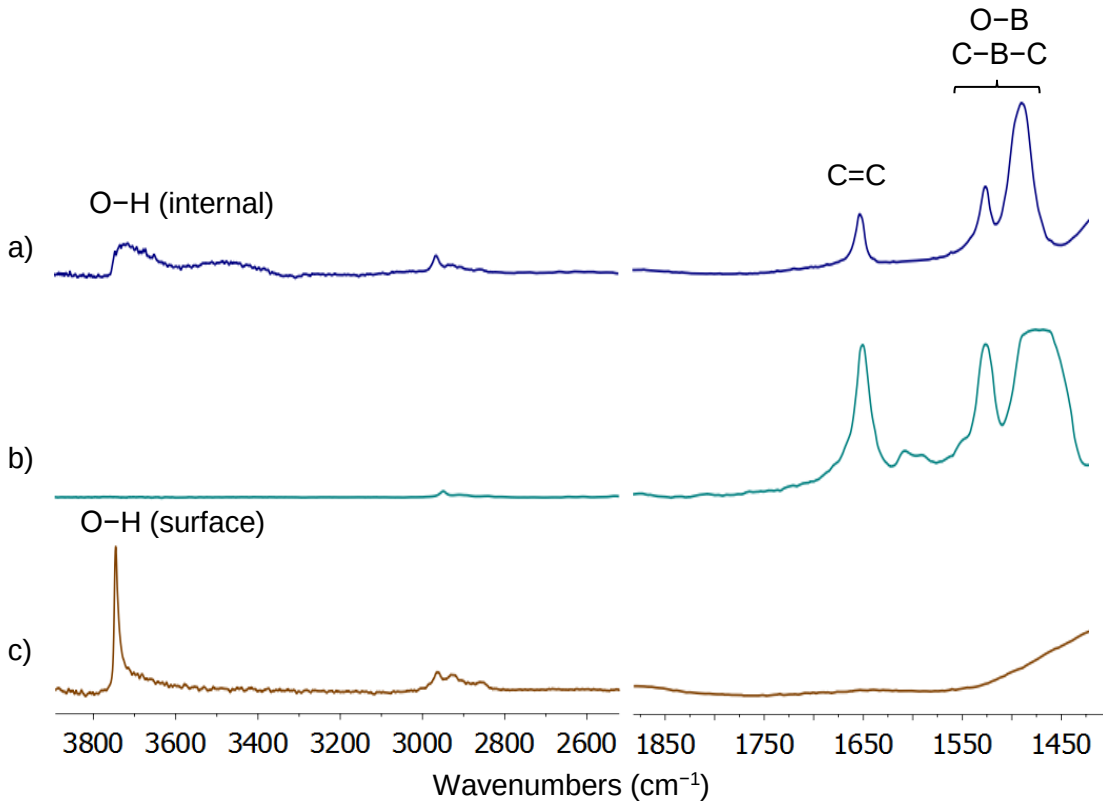

Figure 4.1 FTIR spectra of: a) ***s*-BCF**, b) $(C_6F_5)_2BH$ and c) $SiO_{2\text{-}500}$.

The solid-state ^{11}B NMR spectrum of ***s*-BCF** was influenced by second-order nuclear electric quadrupolar coupling perturbations. The corresponding line fit parameters,

namely quadrupolar coupling constant (C_Q), and asymmetry parameter (η_Q) are highly sensitive to boron coordination number, which affects the breadth of the NMR signal. The $^{11}B\{^1H\}\{^{19}F\}$ DEPTH NMR spectrum of ***s*-BCF** contains a broad resonance at 20 ppm with a shoulder at 10 ppm (Figure 4.2). The broad signal is consistent with the formation of the expected tri-coordinate ***s*-BCF**, whereas the shoulder at 10 ppm corresponds to unwanted $(\equiv SiO)_2B(C_6F_5)$ sites caused by further side reaction of $\equiv SiOB(C_6F_5)_2$ with neighbouring ≡SiOH groups similar to the observation by Wanglee *et al*.[25]

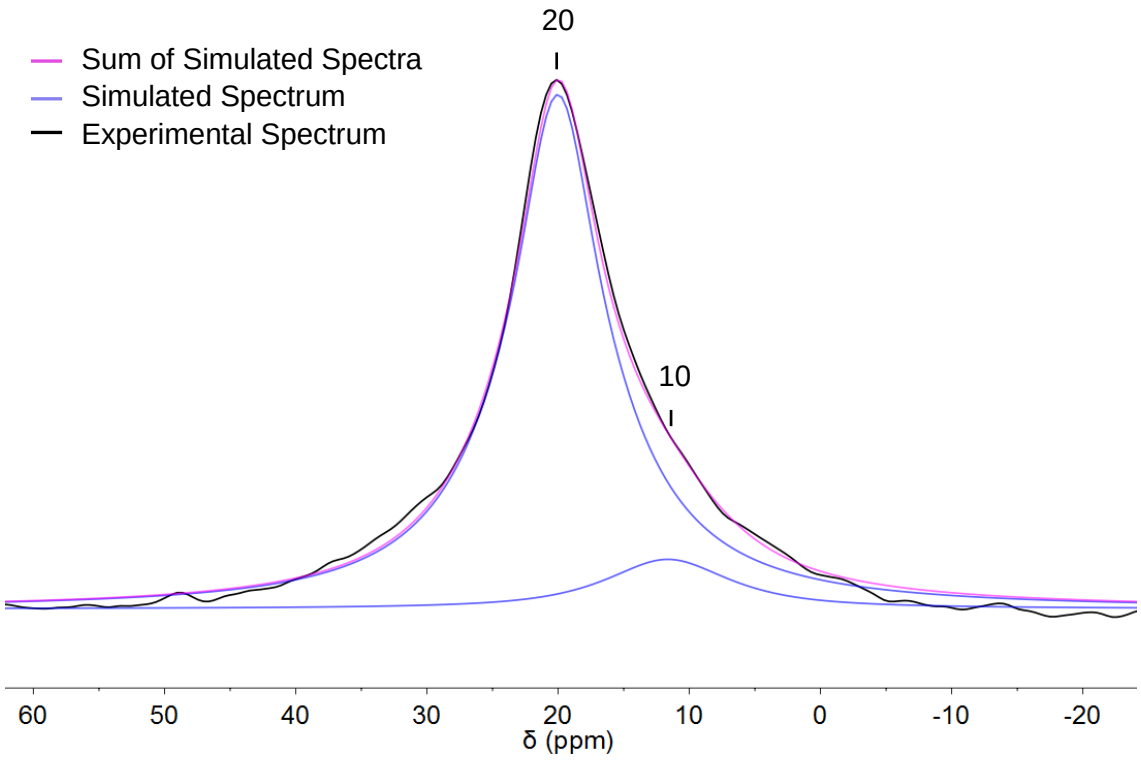

Figure 4.2 Solid-state $^{11}B\ \{^1H\}\{^{19}F\}$ DEPTH MAS NMR spectrum of $\equiv SiOB(C_6F_5)_2$ (***s*-BCF**) at 24 kHz spinning rate.

The ^{19}F direct polarisation (DP) MAS NMR spectrum exhibits a set of broad resonances at −130, −150 and −163 ppm ($\Delta\delta_{m,p}$ = 13 ppm) corresponding to *ortho*-, *para*- and *meta*-F in ***s*-BCF** (Figure 4.3a), in good agreement with $[T_8(OB(C_6F_5)_2)_2]$

silsesquioxane molecular model described in Chapter Three (Figure 4.3b). As mentioned in previous chapters, large $\Delta\delta_{m,p}$ values indicates lower boron coordination number, and in this case it is consistent with a tri-coordinate borane.

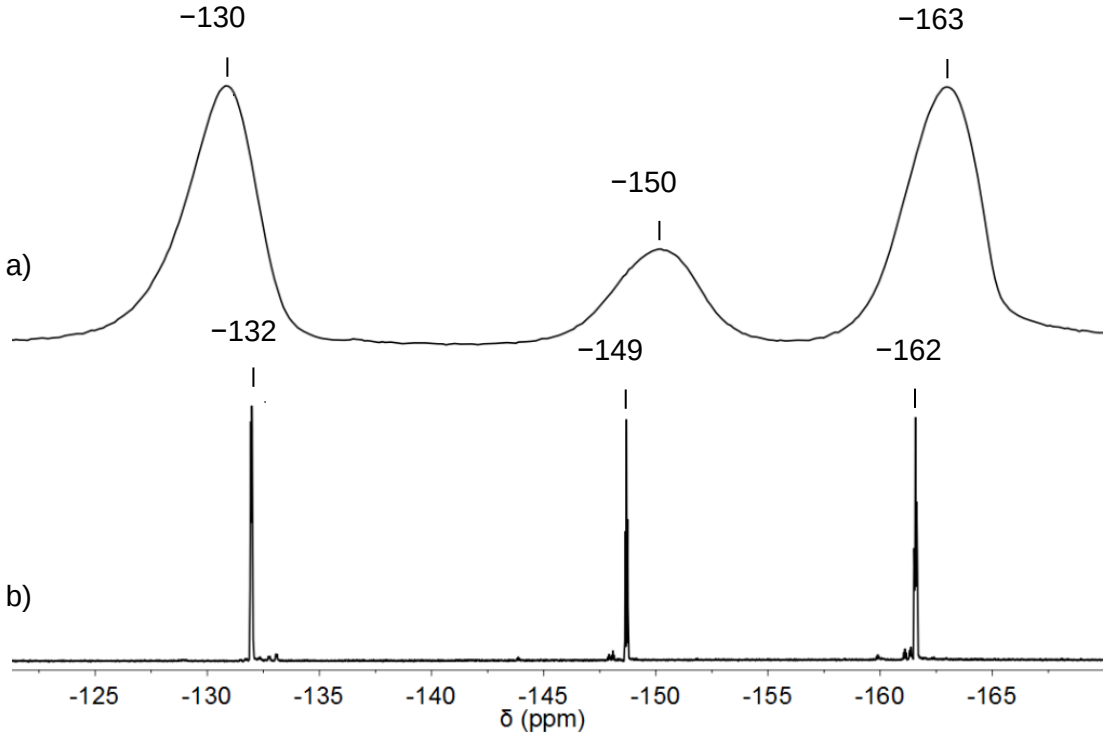

Figure 4.3 a) Solid-state ^{19}F DPMAS NMR spectrum of ≡SiOB(C_6F_5)$_2$ (***s*-BCF**) at 24 kHz spinning rate and b) solution-state ^{19}F NMR spectrum of [T_8(OB(C_6F_5)$_2$)$_2$].

The ^{29}Si Cross Polarisation (CP) MAS NMR spectrum of the ***s*-BCF** exhibits a resonance at −100 ppm, corresponding to the $\boldsymbol{Q^3}$ Si atoms containing internal inaccessible OH groups (Figure 4.4). The shoulder at −109 ppm is consistent with $\boldsymbol{Q^4}$ siloxane atoms (**Si**(OSi)$_4$).[28,29] The broad resonance at −17 ppm with a complex line shape is consistent with electron deficient Si environment,[14,28] and this could be assigned to the surface $\boldsymbol{Q^3}$ silicon atoms containing bound Lewis acid (≡**Si**OB(C_6F_5)).

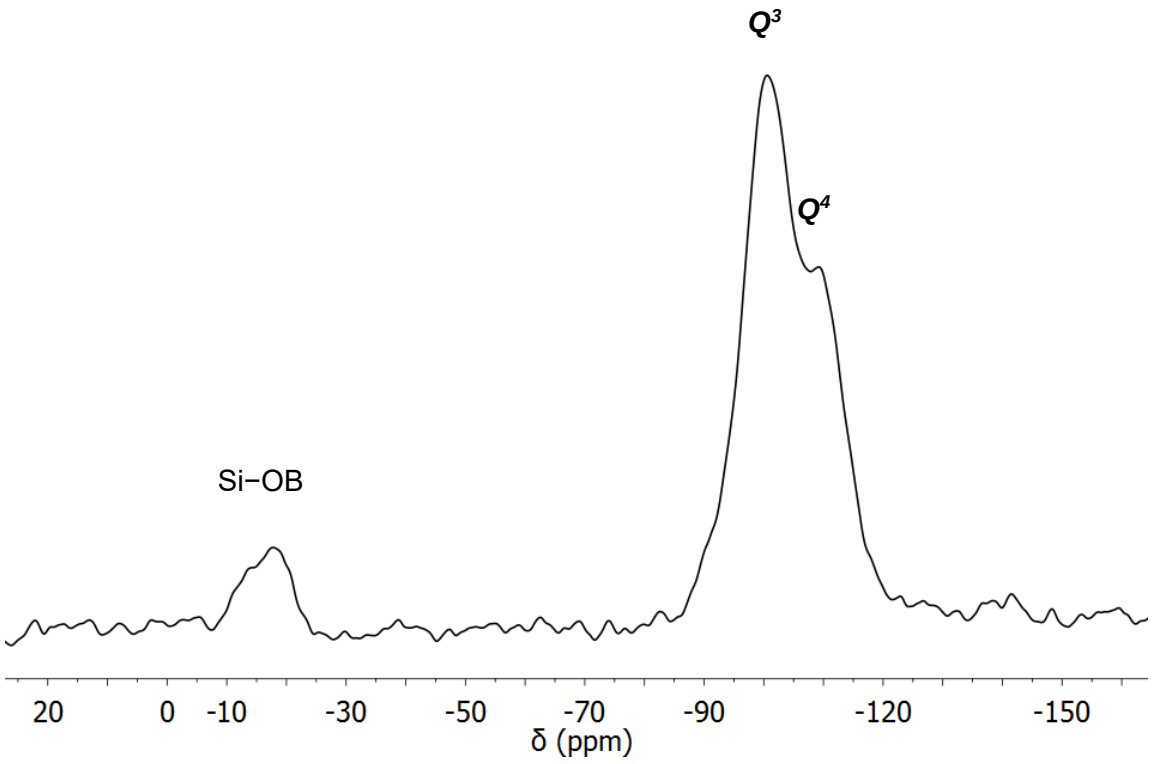

Figure 4.4 Solid-state ^{29}Si CPMAS NMR spectrum of ≡SiOB(C_6F_5)$_2$ (***s*-BCF**) at 10 kHz spinning rate.

4.2.2 Synthesis of ≡SiOB(Fxyl)$_2$ (*s*-BFxyl)

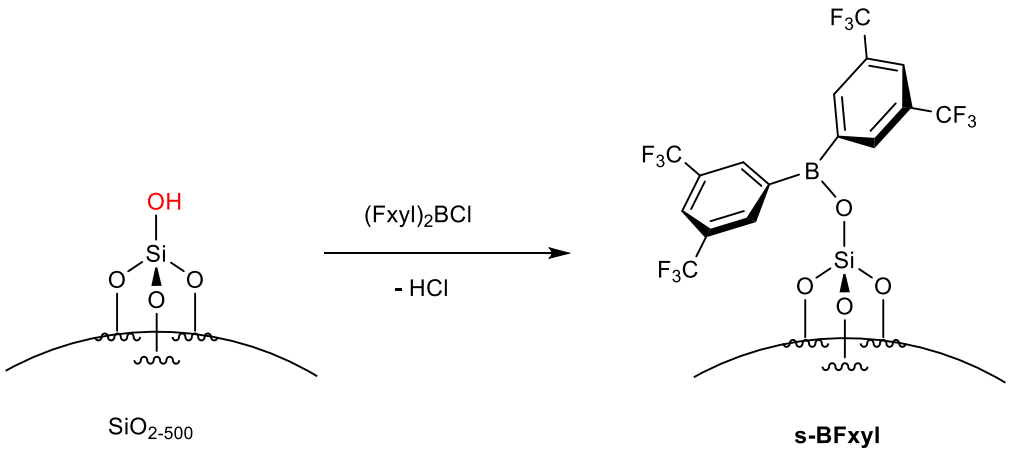

Equation 4.2 Synthesis of ***s*-BFxyl**.

$SiO_{2\text{-}500}$ was treated with stoichiometric amount of $(Fxyl)_2BCl$ in a toluene suspension (Equation 4.2). The reaction proceeded more vigorously than with $(C_6F_5)_2BH$, due to the formation of HCl as a side product, therefore the reaction mixture was initially cooled in an ice bath, followed by gradual warming to room temperature with further stirring for additional 16 hours before being filtered, washed with toluene and dried under vacuum to afford analytically pure ***s*-BFxyl** as a colourless powder in 86% yield with BFxyl loading of 14.8 wt. %. The loading of the Lewis acid is slightly lower than that of ***s*-BCF** possibly due to the Fxyl group being more spatially demanding compared to the C_6F_5 group. This is also consistent with the observation of unreacted $(Fxyl)_2BCl$ in solution-phase ^{19}F NMR spectrum of the washing.

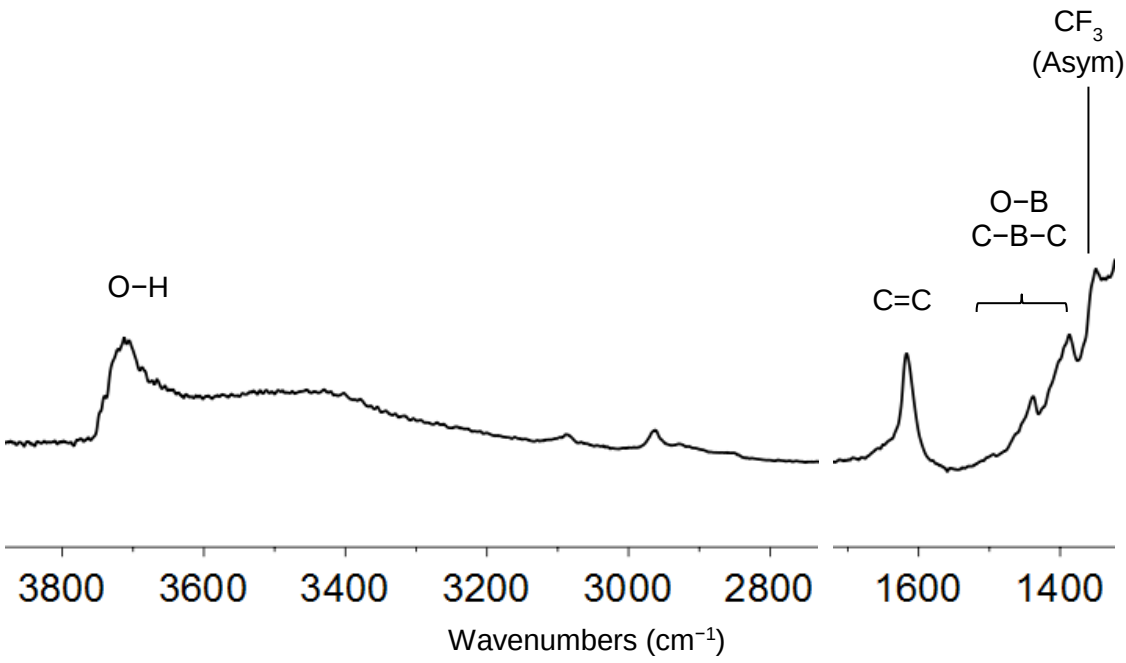

Figure 4.5 IR spectrum of ***s*-BFxyl**.

The IR spectrum of ***s*-BFxyl** does not contain a sharp O–H absorption at 3745 cm^{-1}, indicating that any unreacted surface OH silanol groups could only be present in trace amount. Additionally, CF_3 antisymmetric stretch is observable at 1363 cm^{-1} as well as the

aforementioned aromatic ring breathing, B−O bond stretch and C−B−C wagging motions in the range of 1400-1625 cm^{-1} (Figure 4.5).

Solid-state $^{11}B\{^{19}F\}\{^{1}H\}$ DEPTH NMR spectrum exhibits a broad resonance with a complex line shape at 12 ppm, which is consistent with the formation of the three coordinate $OB(Fxyl)_2$ (Figure 4.6a). The $^{19}F\{^{1}H\}$ DEPTH NMR spectrum displays a single sharp resonance at −70 ppm, which corresponds to the CF_3 groups (Figure 4.6b). The $^{13}C\{^{1}H\}$-$\{^{19}F\}$ CPMAS NMR spectrum exhibits a sharp signal at 116 ppm, which is diagnostic of the CF_3 group. The $^{13}C\{^{19}F\}$-$\{^{1}H\}$ CPMAS decoupled NMR spectrum displays two signals, the signal at 125 ppm corresponds to the *ortho*-C, whereas the weaker signal at 117 ppm corresponds to *para*-C (*ipso*- and *meta*-C were not observable). These results are consistent with the solution-state NMR spectra of the molecular model $[T_8(OB(Fxyl)_2)_2]$ described in Chapter Three.

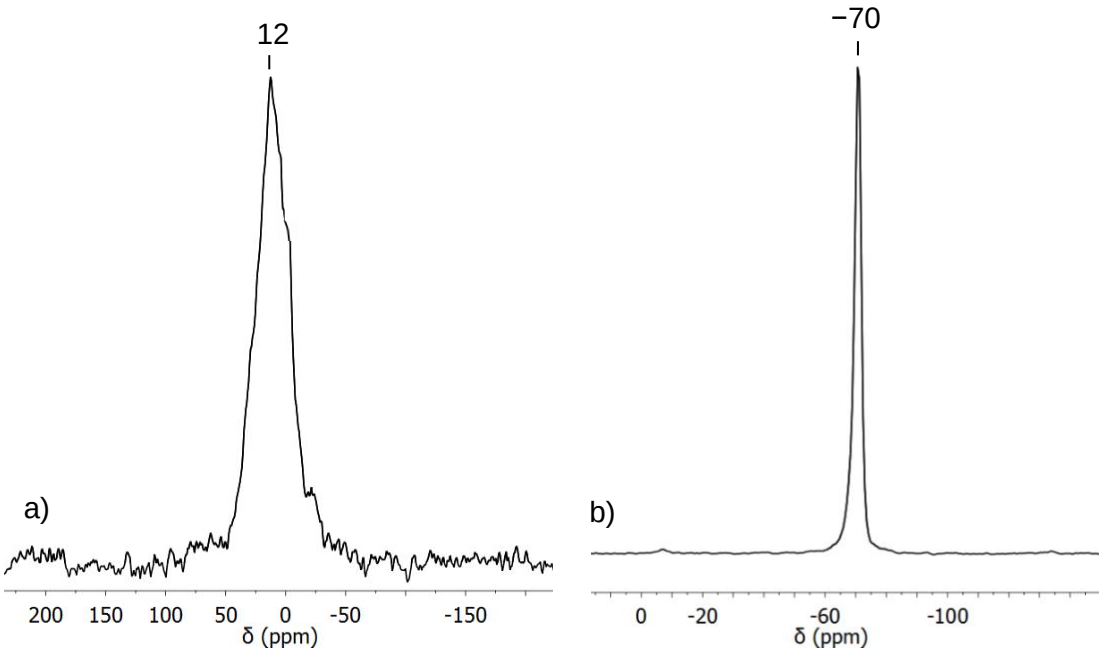

Figure 4.6 Solid state NMR spectra of ≡SiOB(Fxyl)$_2$ (***s*-BFxyl**) at 24 kHz spinning rate: a) $^{11}B\{^{19}F\}\{^{1}H\}$ DEPTH and b) $^{19}F\{^{1}H\}$ DEPTH.

4.3 Preparation of Solid-Phase FLPs (*s*-FLPs)

^{31}P NMR spectroscopy provides a convenient method for monitoring FLP formation, the sterically demanding P^{t}Bu$_3$ was chosen as the Lewis base for the investigation of solid-phase FLP formation with previously synthesised solid-supported ***s*-BCF** or ***s*-BFxyl** Lewis acids.

4.3.1 Preparation of [≡SiOB(C$_6$F$_5$)$_2$/P^{t}Bu$_3$]

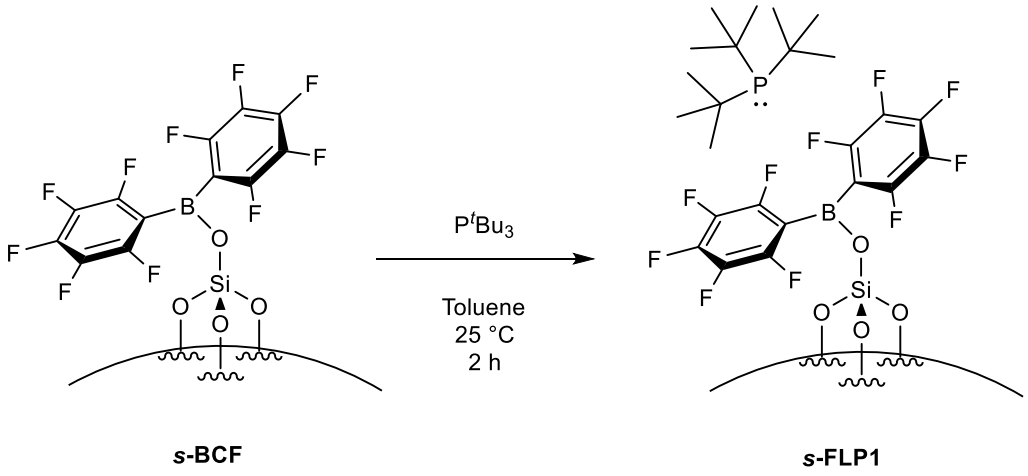

Equation 4.3 Formation of [≡SiOB(C$_6$F$_5$)$_2$/P^{t}Bu$_3$] ***s*-FLP1**.

Stoichiometric ratio of ***s*-BCF** was reacted with P^{t}Bu$_3$ in toluene and stirred for 2 hours at room temperature. The mixture was filtered, washed with dry toluene and dried under reduced pressure (1 x 10^{-3} mbar) for 2 hours to afford the corresponding ***s*-FLP1** as a colourless solid in 72% yields. ***s*-FLP1** was characterised by FTIR and solid-state NMR spectroscopy.

The IR spectrum of ***s*-FLP1** exhibits, in addition to the aforementioned absorptions in the range between 1325 and 1660 cm^{-1} associated with the BCF unit, new absorptions at 2946 and 1466 cm^{-1} corresponding to C−H absorptions associated with the ^{t}Bu groups on

the Lewis base (Figure 4.7). The C=C stretching band due to C_6F_5 ring breathing motion which appears at 1650 cm^{-1} has broadened and red-shifted to 1639 cm^{-1} in the presence of P^tBu_3. This perhaps can be explained by reduced C_6F_5 ring breathing motion caused by strong steric repulsion between the Lewis acid and Lewis base as well as possible B-P coordination, which caused a change in the local geometry of ***s*-BCF**.

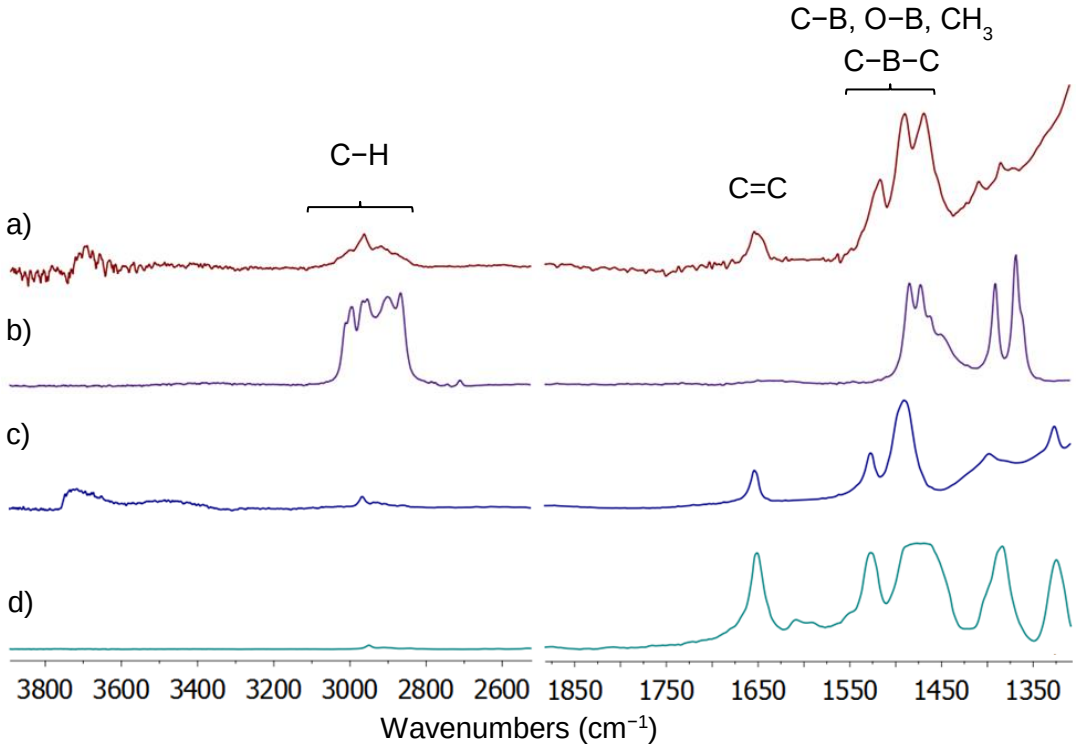

Figure 4.7 FTIR spectra of: a) [≡SiOB$(C_6F_5)_2$/P^tBu_3] (***s*-FLP1**); b) neat P^tBu_3; c) ***s*-BCF**); d) $(C_6F_5)_2BH$.

Solid-state NMR spectroscopic characterisation of ***s*-FLP1** revealed that a weak B−P interaction was indeed present, as evidenced by the change in the isotropic chemical shifts (δ_{iso}) of the pair of core heteronuclei (^{11}B and ^{31}P).

The ^{11}B DEPTH $\{^1H\}$-$\{^{19}F\}$ decoupled spectrum of ***s*-FLP1** features a narrow resonance at 1 ppm and a broad shoulder with a complex line shape at 10 ppm, (Figure 4.8). The resonance at 1 ppm is consistent with Lewis base coordinated ***s*-BCF**.[25] The change

from tri- to tetra-coordination has resulted in reduction of the NMR line fit parameters (C_Q and η_Q value) hence narrowing of the NMR resonance.[30] The broad shoulder at 10 ppm is consistent with tri-coordinate ≡$(SiO)_2B(C_6F_5)$ However, due to the amorphous nature of ***s*-FLP1**, the exact C_Q and η_Q values were difficult to extract. The ^{31}P High Power Decoupling (HPDEC) MAS NMR spectrum of ***s*-FLP1** features a sharp resonance with an extremely broad base at 48 ppm (free phosphine appears at 67 ppm) (Figure 4.9). The sharp signal corresponds to the phosphine coordinated to the Lewis acid, whereas, the underlying broad component is perhaps due to the fluxional character of ***s*-FLP1**.[31–34]

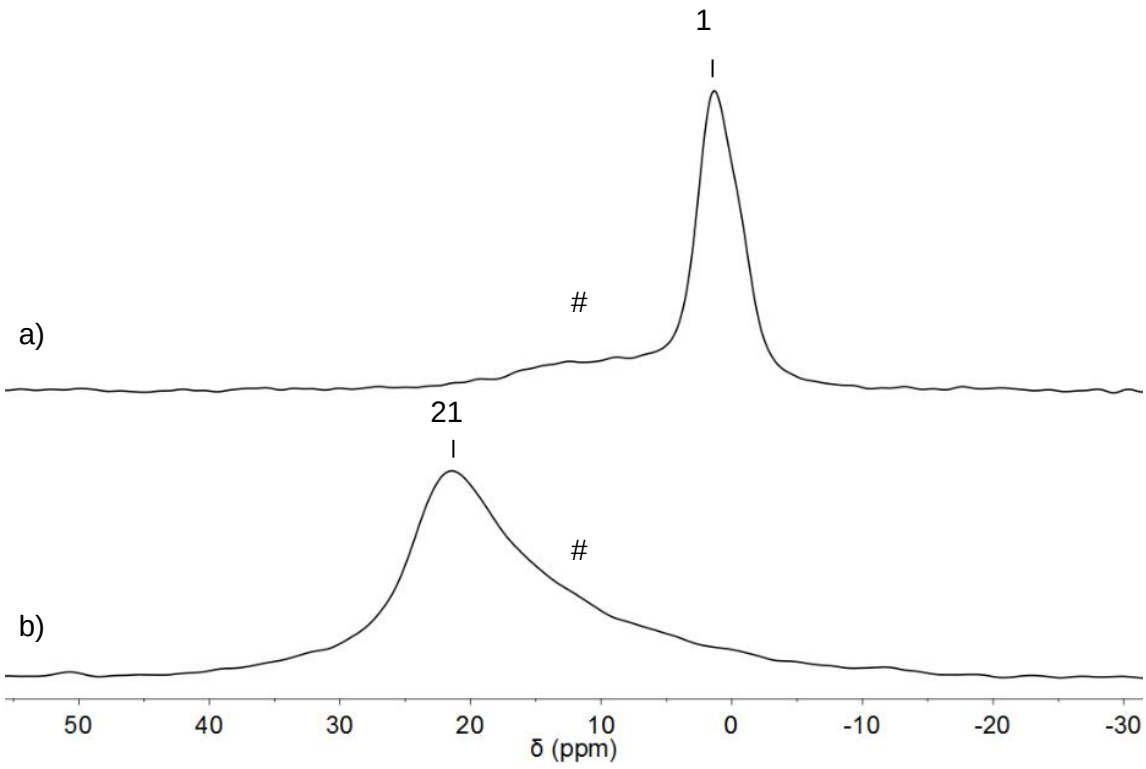

Figure 4.8 $^{11}B\{^1H\}\{^{19}F\}$ DEPTH NMR spectra at 24 kHz spinning rate of: a) ***s*-FLP1** and b) ***s*-BCF**; # $(\equiv SiO)_2B(C_6F_5)$.

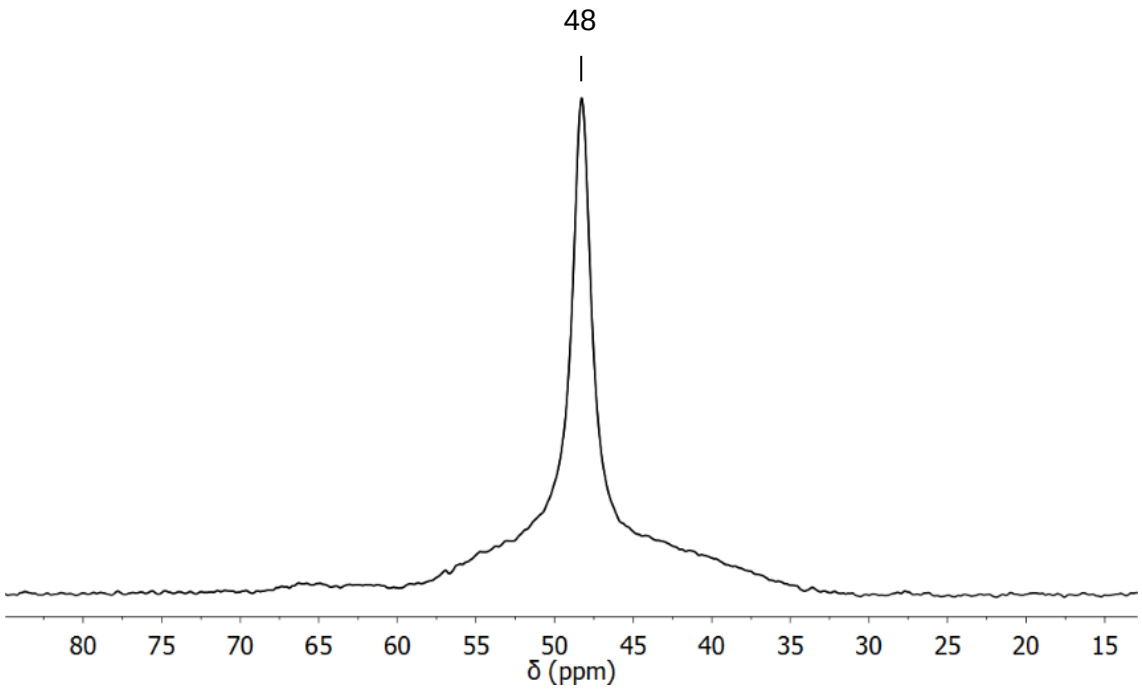

Figure 4.9 Solid-state ^{31}P HPDEC MAS NMR spectrum of ***s*-FLP1** at 24 kHz spinning rate.

{^{11}B-^{31}P} HETCOR (Heteronuclei Correlation) MAS NMR spectroscopy of ***s*-FLP1** was acquired, which correlates ^{11}B and ^{31}P nuclei through their through-space dipolar coupling and can provide direct evidence of covalent interactions giving insights into the "*degree of frustration*" in the solid-state (Figure 4.10).[26] The spectrum shows that the signal at 1 ppm in ^{11}B-dimension correlates with the signal at 48 ppm in ^{31}P-dimension. Interestingly, Wiegand *et al*. reported the solid-state {^{11}B-^{31}P} heteronuclear 2D *J*-resolved NMR spectrum of $(C_6F_5)_3B{-}PPh_3$ adduct, which shows splitting of the signal due to isotropic spin-spin coupling.[34] However, the solid-state HETCOR NMR spectrum of ***s*-FLP1** does not show splitting of the signal, this is consistent with the observations made by Szeto *et al*.[26] Perhaps this indicates that the B-P internuclear distance is larger than that of classical Lewis adducts, hence further demonstrates a weak B-P interaction in ***s*-FLP1**. The asymmetrical shape of the signal probably arises from the additional residual dipolar interaction with the ^{11}B nucleus.[26,34]

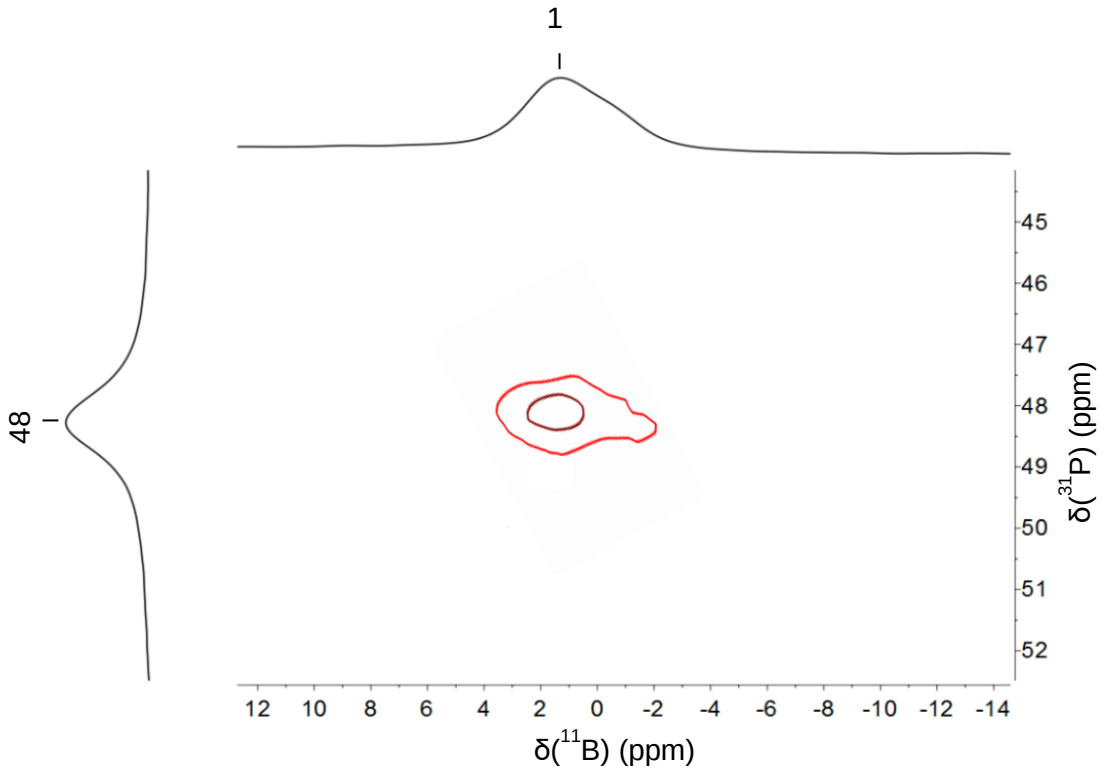

Figure 4.10 {^{11}B-^{31}P} HETCOR MAS spectrum ***s*-FLP1** at 10 kHz spinning rate.

Although weak Lewis adduct formation was observed in ***s*-FLP1**, this does not necessarily mean that ***s*-FLP1** is unreactive, since some of the highly reactive intramolecular FLP systems developed by Erker *et al*. feature weak interactions between the Lewis acid and Lewis base, especially the geminal vinylene-bridged phosphine-borane adducts.[31–35] The adduct of ***s*-FLP1** was found to readily dissociate when dispersed in toluene. This conclusion was supported by the observation of free unbound P^{t}Bu$_3$ in the solution-state ^{31}P and ^{1}H NMR spectra of a suspension of ***s*-FLP1**. This indicates that the strength of the interaction between the Lewis acid and the Lewis base must be relatively weak, and that the steric repulsion may be sufficient to establish a dissociative equilibrium between the bound and unbound phosphine in a solvent suspension. However, when the suspension of ***s*-FLP1** was filtered and washed with toluene, inspection of the solution-state NMR spectra of the combined filtrate/washing (concentrated and redissolved

in fresh toluene-d^8) only showed trace amount of free P^{t}Bu$_3$, indicating that the majority of the Lewis base remain adsorbed on the silica surface. The aforementioned FTIR and solid-state NMR spectroscopic data of ***s*-FLP1** suggest that P^{t}Bu$_3$ is chemically adsorbed to the Lewis acidic sites, and not adsorbing to other siloxane bridge or residual SiOH sites on the silica surface.

To further validate this point, a control experiment was performed by the attempt to react P^{t}Bu$_3$ with unmodified SiO$_{2\text{-}500}$. However, overnight stirring at room temperature, and heating up to 75 °C led to no reaction. Inspection of the solution-state ^{31}P and ^{1}H NMR spectra of the filtrate after the mixture was filtered and washed with toluene shows the presence of free unreacted P^{t}Bu$_3$. Examination of the solid using FTIR spectroscopy revealed a sharp absorption at 3750 cm^{-1} corresponding to the preserved isolated surface hydroxyl groups.

4.3.2 Preparation of [≡SiOB(Fxyl)$_2$/P^{t}Bu$_3$]

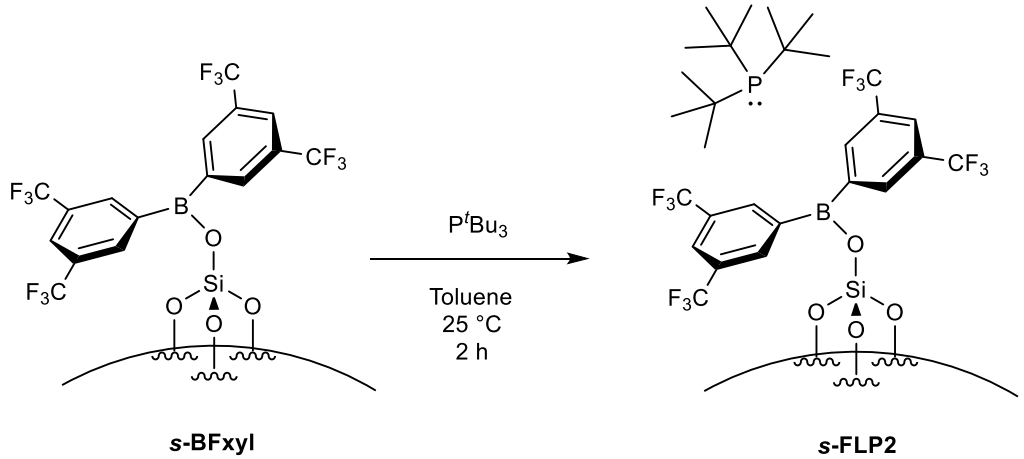

Equation 4.4 Formation of [≡SiOB(Fxyl)$_2$/P^{t}Bu$_3$] ***s*-FLP2**.

***s*-FLP2** was prepared *via* a stoichiometric reaction of ***s*-BFxyl** with P^{t}Bu$_3$ in a toluene slurry (Equation 4.4). The mixture was stirred for 2 hours at room temperature, filtered,

washed and dried under reduced pressure (1 x 10^{-3} mbar) to afforded a colourless powder in 86% yield. Examination of the filtrate using solution-state ^{31}P NMR spectroscopy revealed the presence of free P^{t}Bu$_3$, indicating that small amount of P^{t}Bu$_3$ was washed away by toluene.

The FTIR spectrum of ***s*-FLP2** contains absorptions for C−H bond stretching and CH_3 deformation motion at 3030-2880 cm^{-1} and 1460 cm^{-1}, which evidently supports the adsorption of P^{t}Bu$_3$ to ***s*-BFxyl** (Figure 4.11). Slightly broadened absorption corresponding to aromatic ring breathing motion at 1619 cm^{-1} is consistent with increased diversity in the local environment, perhaps caused by the steric repulsion between the Lewis acid and the Lewis base. This result is also consistent with the observations for ***s*-FLP1**.

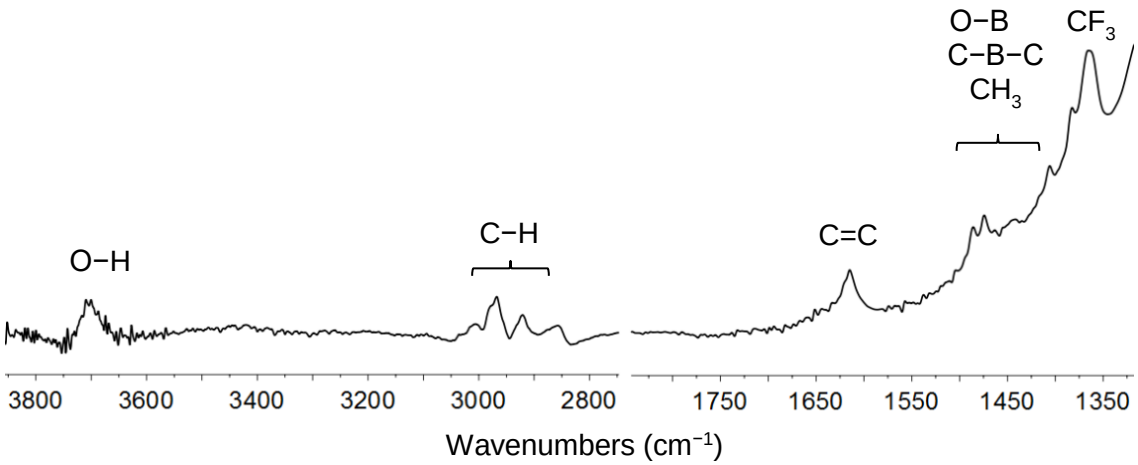

Figure 4.11 FTIR spectrum of ***s*-FLP2**.

Solid-state ^{11}B{^{19}F}{^{1}H} DEPTH NMR spectrum of ***s*-FLP2** displays an intense sharp resonance at −1 ppm, and a weak broad resonance at 12 ppm. The sharp component corresponds to a phosphine coordinated four-coordinate boron environment similar to the result obtained for ***s*-FLP1**, and the broad resonance at 12 ppm is consistent with uncoordinated ***s*-BFxyl** sites where the coordinated phosphine was washed away by the

solvent (Figure 4.12a). This result coupled with the observation of free P^{t}Bu$_3$ in the filtrate indicate that the strength of B-P interaction of ***s*-FLP2** is weaker than that of ***s*-FLP1**, therefore allowing P^{t}Bu$_3$ to be washed away by solvents. This was again further highlighted by the presence of free P^{t}Bu$_3$ in the solution-state ^{1}H and ^{31}P NMR spectra of a suspension of ***s*-FLP2**.

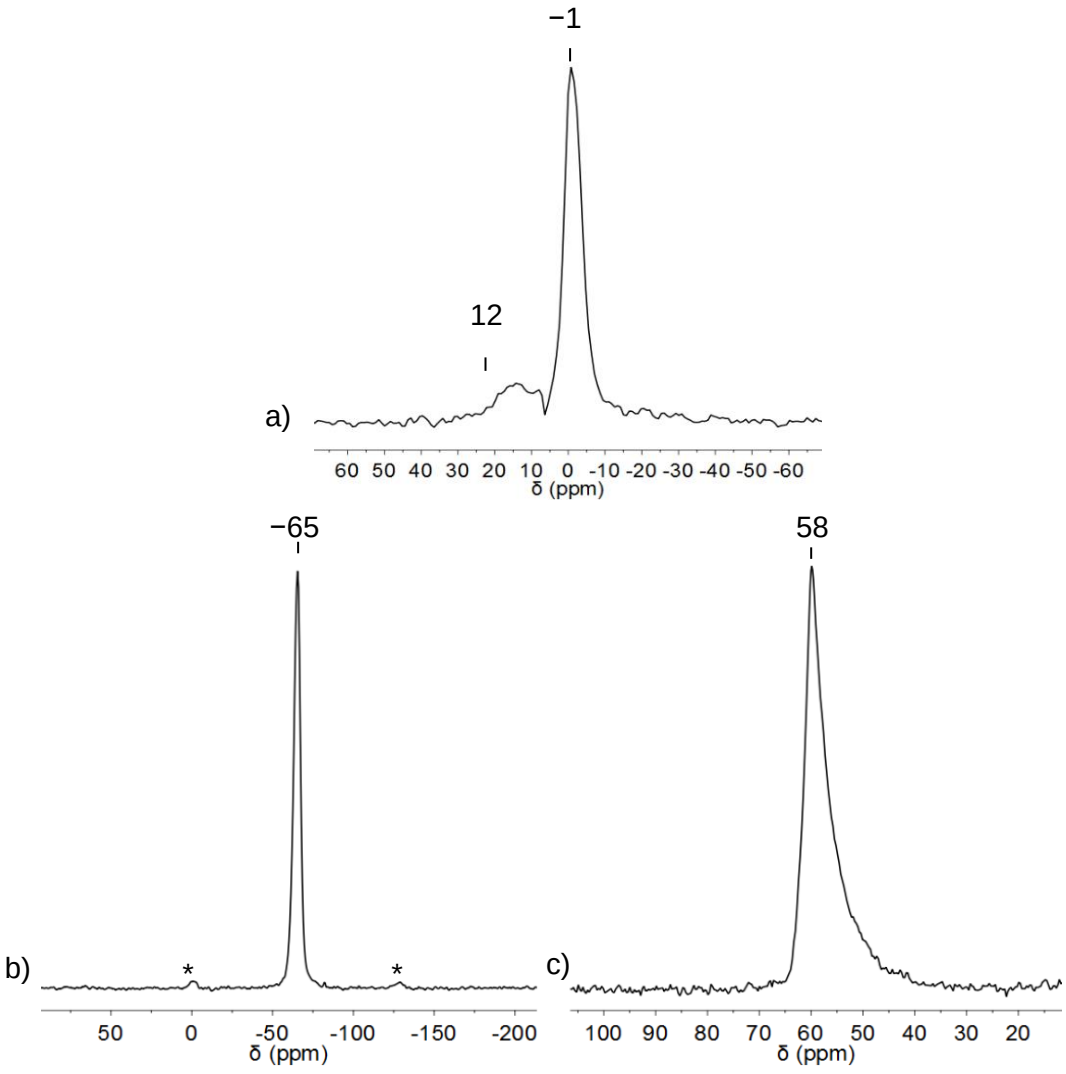

Figure 4.12 Solid-state NMR spectra of ***s*-FLP2** at 24 kHz spinning rate: a) ^{11}B DEPTH {^{1}H}-{^{19}F} decoupled, b) ^{19}F DEPTH {^{1}H} decoupled and c) ^{31}P HPDEC. # uncoordinated ***s*-BFxyl**. *non-isotropic spinning side bands.

The ^{19}F environment is also slightly affected by the change in the local boron geometry upon phosphine coordination, which has reflected in the change of the chemical shift of the CF_3 group from −70 to −65 ppm in the $^{19}F\{^1H\}$ DEPTH NMR spectrum (Figure 4.12b). The ^{31}P HPDEC NMR spectrum of ***s*-FLP2** exhibits a resonance at 59 ppm, which is only slightly deviates from the value of free P^tBu_3 which appears at 62 ppm (Figure 4.12c). This result provides further evidence to support the relative weak B-P interaction in ***s*-FLP2**.

4.4 Small Molecule Activation by *s*-FLPs

As seen in Chapter Three, the soluble siloxane and silsesquioxane mimic FLP systems have all exhibited unprecedented H_2 activation properties, which has led us to believe that such FLP reactivity could preserved when the they are supported on silica. Therefore, the reaction of ***s*-FLP1** and ***s*-FLP2** towards polar (CD_3OD) and non-polar (H_2/D_2) substrates have been studied using solid-state NMR, FTIR, and indirectly, by solution-state NMR spectroscopic techniques.

4.4.1 H_2 and D_2 Cleavage by *s*-FLP1

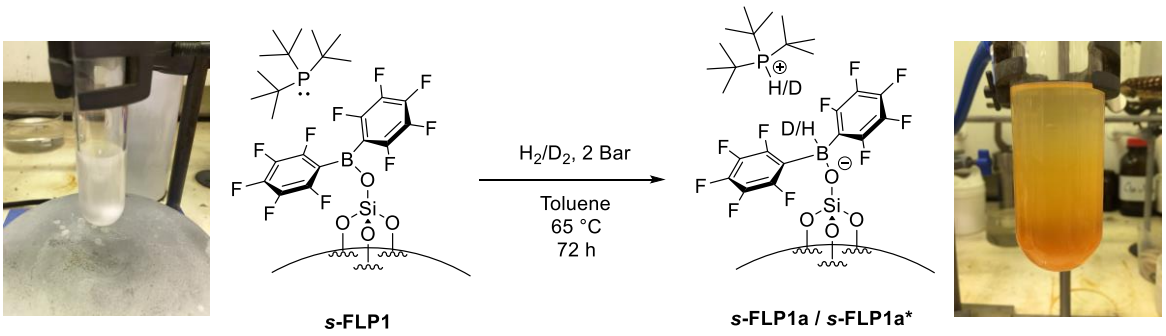

Equation 4.5 Reactions of ***s*-FLP1** with H_2 or D_2.

A suspension of ***s*-FLP1** in toluene (freeze-pump-thaw degassed) was pressurised with 2 bar of H_2, and stirred at 65 °C (Equation 4.5). An aliquot of the reaction mixture was examined daily using solution-state ^{1}H and ^{31}P NMR spectroscopy for the appearance of $[H{-}P^{t}Bu_3]^{+}$ cation. After 72 hours of heating and stirring the reaction mixture became intense orange. A small doublet at 4.7 ppm ($^{1}J_{HP}$ = 450 Hz) in the ^{1}H NMR spectrum and a weak doublet of multiplet at 54 ppm ($^{1}J_{HP}$ = 450 Hz) in the ^{31}P NMR spectrum were observed. These results are consistent with the formation of $[H{-}P^{t}Bu_3]^{+}$ cation,[36] suggesting successful H_2 cleavage by ***s*-FLP1**. The mixture was therefore filtered, and washed with toluene and dried under reduced pressure to afford a pale yellow powder in 72% yield. Examination of the isolated solid by FTIR spectroscopy revealed a weak absorption at 2350 cm^{-1}, which appears in the B−H stretching region (Figure 4.13a), suggesting the formation of $[{\equiv}SiOB(H)(C_6F_5)_2]$ species. Moreover, the FTIR spectrum of the yellow solid closely resembles the spectrum of $[(C_6F_5)_3B{-}H][H{-}P^{t}Bu_3]$ (Figure 4.13b), supporting the formation of $[{\equiv}SiOB(H)(C_6F_5)_2][H{-}P^{t}Bu_3]$ (***s*-FLP1a**).

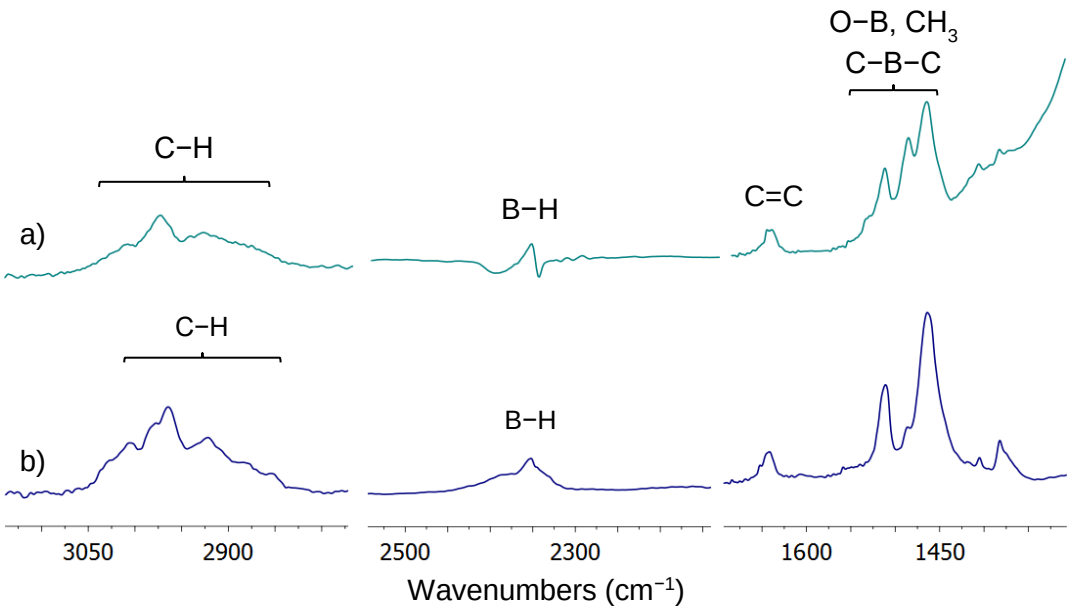

Figure 4.13 FTIR spectra of: a) $[{\equiv}SiOB(H)(C_6F_5)_2][H{-}P^{t}Bu_3]$ and b) $[(C_6F_5)_3B{-}H][H{-}P^{t}Bu_3]$.

Further evidence for the formation of ***s*-FLP1a** can be demonstrated by ^{11}B and ^{31}P solid-state NMR spectroscopy. ^{11}B-{^{1}H} CPMAS NMR spectrum of ***s*-FLP1a** contains a sharp resonance at −2.3 ppm. This result strongly supports the formation of a B−H bond, since this signal is only visible when the inter-nuclear distance of B-atom and H-atom is small (e.g. bonded) (Figure 4.14a). The ^{31}P-{^{1}H} CP MAS spectrum of ***s*-FLP1a** exhibits a signal at 57 ppm (Figure 4.14b) suggesting the formation of [H−P^{t}Bu$_3$]$^+$ species, and the chemical shift of this signal is also in close agreement with that for [H−P^{t}Bu$_3$]$^+$ species (55 ppm in toluene) in solution-state ^{31}P NMR spectroscopy.[36]

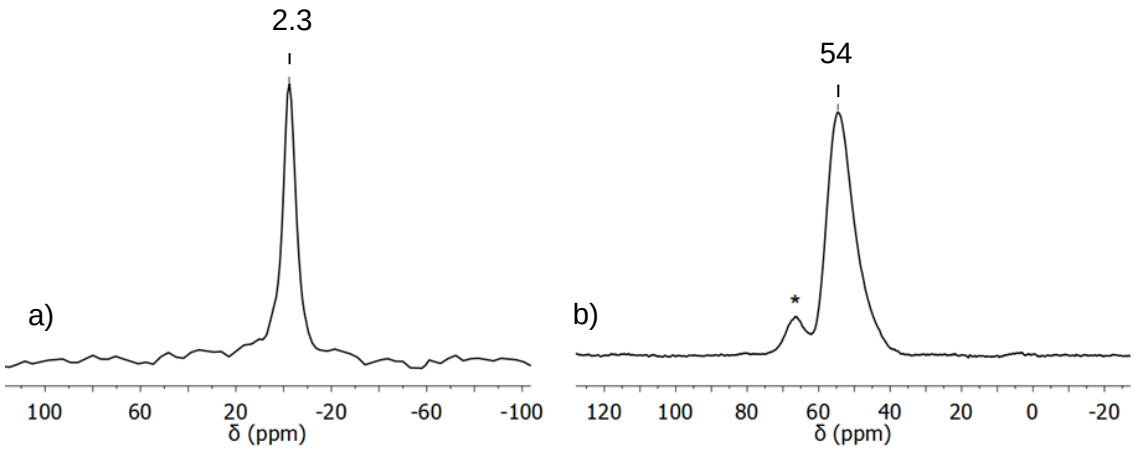

Figure 4.14 Solid-state NMR spectra of ***s*-FLP1a**: a) ^{11}B-{^{1}H} CP MAS at spinning rate of 10 kHz; b) ^{31}P-{^{1}H} CP MAS at spinning rate of 10 kHz; * free P^{t}Bu$_3$.

Due to the presence of large amount of inaccessible internal OH groups in silica, direct observation of the H_2 cleavage product using solid-state ^{1}H NMR spectroscopy is difficult. Therefore, D_2 was reacted with ***s*-FLP1** to afford [≡SiOB(D)(C$_6$F$_5$)$_2$][D−P^{t}Bu$_3$] (***s*-FLP1a***) as a pale yellow powder in 81% yield. The ^{2}H DPMAS NMR spectrum of [≡SiOB(D)(C$_6$F$_5$)$_2$][D−P^{t}Bu$_3$] displayed a broad signal with complex line shape in the range between 1 to 10 ppm showing that D_2 cleavage by ***s*-FLP1** had occurred (Figure 4.15). It is difficult to separate the B−D and P−D signals due to the small difference in

chemical shifts and the broadness of the signals observed. Moreover, the line shape of the spinning side band in the ^{2}H DPMAS NMR spectrum is highly sensitive to dynamics in the solid sample. For instance, if the solid sample is completely static, dipolar coupling of the pair of nuclei would give rise to splitting of the spectrum to produce a Pake doublet.[37] However, if motion is present in the sample and the rate is sufficiently fast it will cause merging of the Pake doublet. In the case for ***s*-FLP1a***, two superimposed Pake doublets are shown in the ^{2}H DPMAS NMR spectrum, indicating that two different ^{2}H-environments are present in the sample, consistent with the formation of P−**D** and B−**D** bonds.

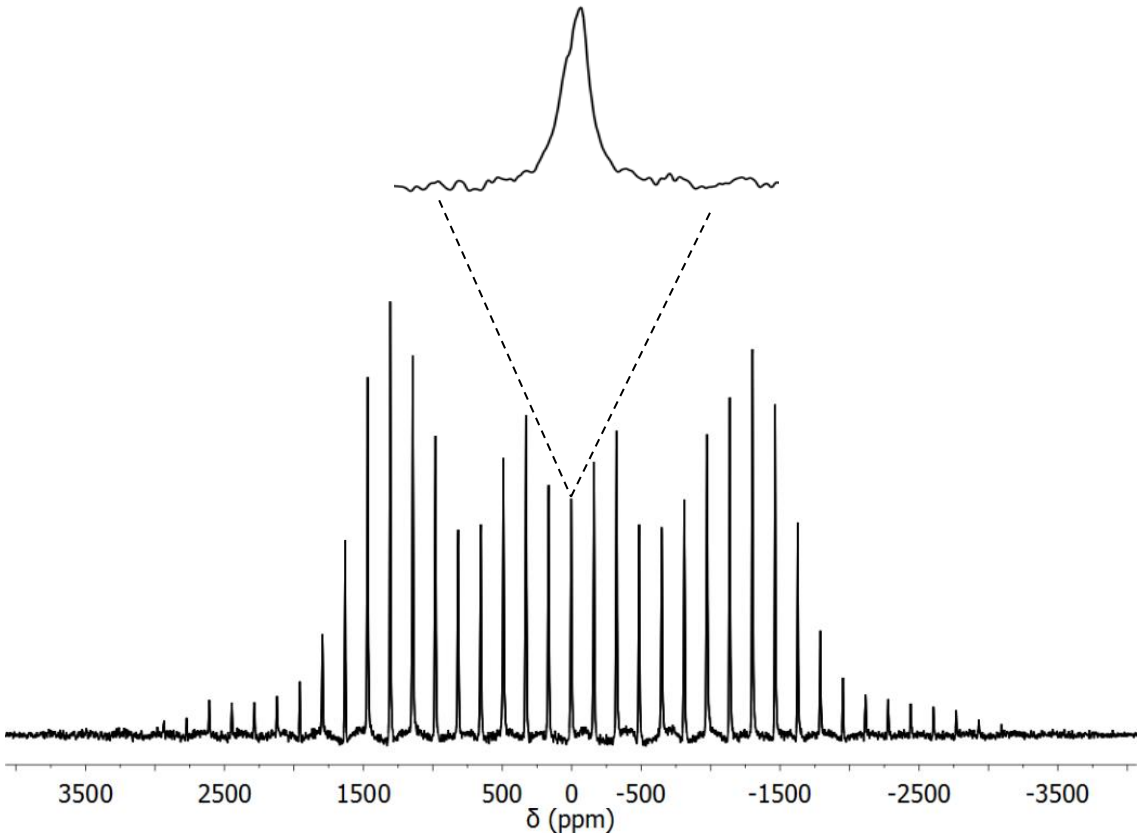

Figure 4.15 ^{2}H DPMAS NMR spectrum of ***s*-FLP1a*** at spinning rate of 10 kHz.

As discussed in Chapter Two, the $\Delta\delta_{m,p}$ value provides useful indication of the boron coordination number.[29] The ^{19}F DEPTH NMR spectrum of ***s*-FLP1a** displays a set of resonances at −141, −171 and −175 ppm with $\Delta\delta_{m,p}$ value of 4 ppm, and this is consistent with the $\Delta\delta_{m,p}$ value of the analogous silsesquioxane model [T_8 $(OB(C_6F_5)_2)_2/(P^tBu_3)_2$] described in Chapter Three.

4.4.2 Reaction of *s*-FLP2 with H_2

A toluene slurry of ***s*-FLP2** was pressurised with H_2 and was heated at 65 °C. An aliquot of the reaction mixture was examined using ^{1}H and ^{31}P NMR spectrum daily for signs of the formation of $[H{-}P^tBu_3]^+$. However, even after 72 hours of heating and stirring, formation of phosphonium species was not observed. This result is surprising since the molecular model of ***s*-FLP2** ($[T_8(OB(Fxyl)_2)_2/(P^tBu_3)_2]$) displayed rapid H_2 cleavage as described in Chapter Three. This perhaps could be explained by several factors. Firstly, ***s*-FLP2** has demonstrated weaker Lewis acid/base interaction than ***s*-FLP1** (as observed by facile removal of the coordinated Lewis base by solvent), which could be caused by strong steric repulsion between the ^{t}Bu groups of the Lewis base and the *meta*-CF_3 groups of the Lewis acid, resulting in a larger internuclear distance between the B and P centres, hence weaker FLP reactivity. Secondly, Herrington *et al*. reported that although BCF and $B(Fxyl)_3$ possess similar Lewis acidity, their FLP reactivity with H_2 is very different. For instance, H_2 cleavage by solution-phase [$B(Fxyl)_3$/TMP] system results in the formation of a unique 'B−H−B' bridging hydride species.[38] It is possible that formation of similar type of bridging hydride species also occurred with the solution-phase models, $[T_8(OB(Fxyl)_2)_2/(P^tBu_3)_2]$ and $[T_8(OB(Fxyl)_2)_2/(PMes_3)_2]$ systems. However, formation of such bridging hydride species may not be possible on the silica surface for ***s*-FLP2** due to

larger inter molecular distance between the bound $BFxyl_2$ units, resulting in the deactivation of ***s*-FLP2**.

4.4.3 Reaction of *s*-FLP1 with CD_3OD

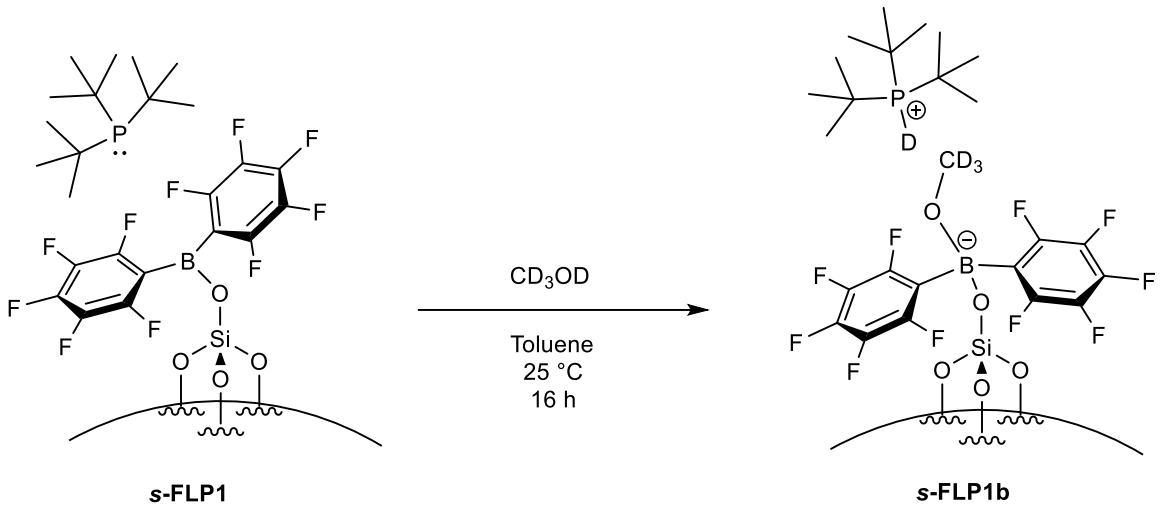

Equation 4.6 Reactions of ***s*-FLP1** with CD_3OD.

The reactivity of ***s*-FLP1** with a polar substrate was tested using deuterated methanol (CD_3OD) (Equation 4.6). After 16 hours at room temperature, facile cleavage of the polar OD bond was achieved to afford $[\equiv SiOB(OCD_3)(C_6F_5)_2][D{-}P^tBu_3]$ (***s*-FLP1b**) as an off-white powder in 91% yield The IR spectrum of **2** shows a characteristic absorption at 2083 cm^{-1} corresponding to the OCD_3 moiety, indicating successful cleavage of O−D bond (Figure 4.15).[39] Formation of ***s*-FLP1b** can be further evidenced by the appearance of a signal with a central band at 3.21 ppm in the ^2H DPMAS NMR spectrum (Figure 4.16), which is characteristic for the OCD_3 group, and is consistent with that of $[(C_6F_5)_3B(OCH_3)][TMPH]$ reported by Ashley *et al.* (OCH_3 at 3.12 ppm in CD_2Cl_2).[40] Furthermore, the rapid C_3 rotation of the CD_3 group about the O–C bond gave rise to a

motional averaged Lorentzian line shape displayed by the ^{2}H DPMAS NMR spectrum (Figure 4.16a).[41]

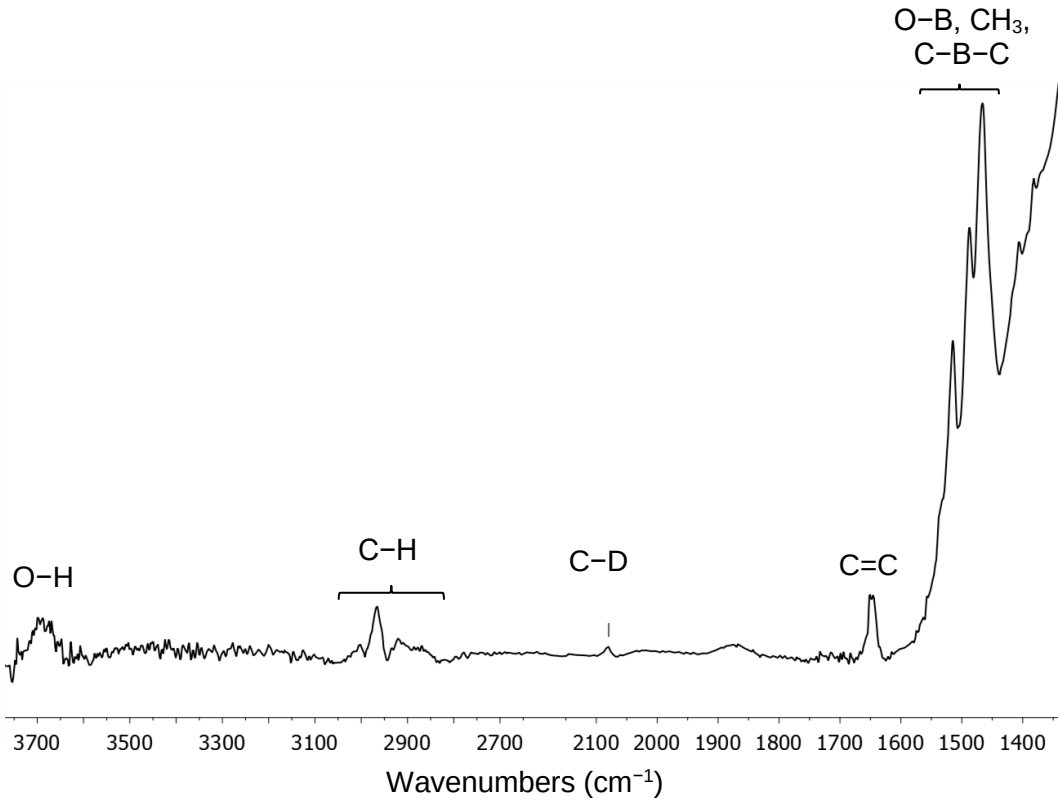

Figure 4.15 FTIR spectrum of [≡SiOB(OCD$_3$)(C$_6$F$_5$)$_2$][D−P^{t}Bu$_3$] (***s*-FLP1b**).

^{11}B DEPTH NMR spectrum of ***s*-FLP1b** exhibits a narrow resonance at 0 ppm, which consistent with the formation of a four-coordinate boron containing more than one O-atom (Figure 4.16b).[40,42–44] Formation of the [D−P^{t}Bu$_3$]$^+$ cation can also be confirmed by the appearance of a sharp resonance at 54 ppm in the ^{31}P CPMAS NMR spectrum (Figure 4.16c), which is consistent with the ^{31}P CPMAS NMR spectrum of ***s*-FLP1a**, as well as with the literature reported solution-state ^{31}P NMR spectrum of [H−P^{t}Bu$_3$]$^+$.[36]

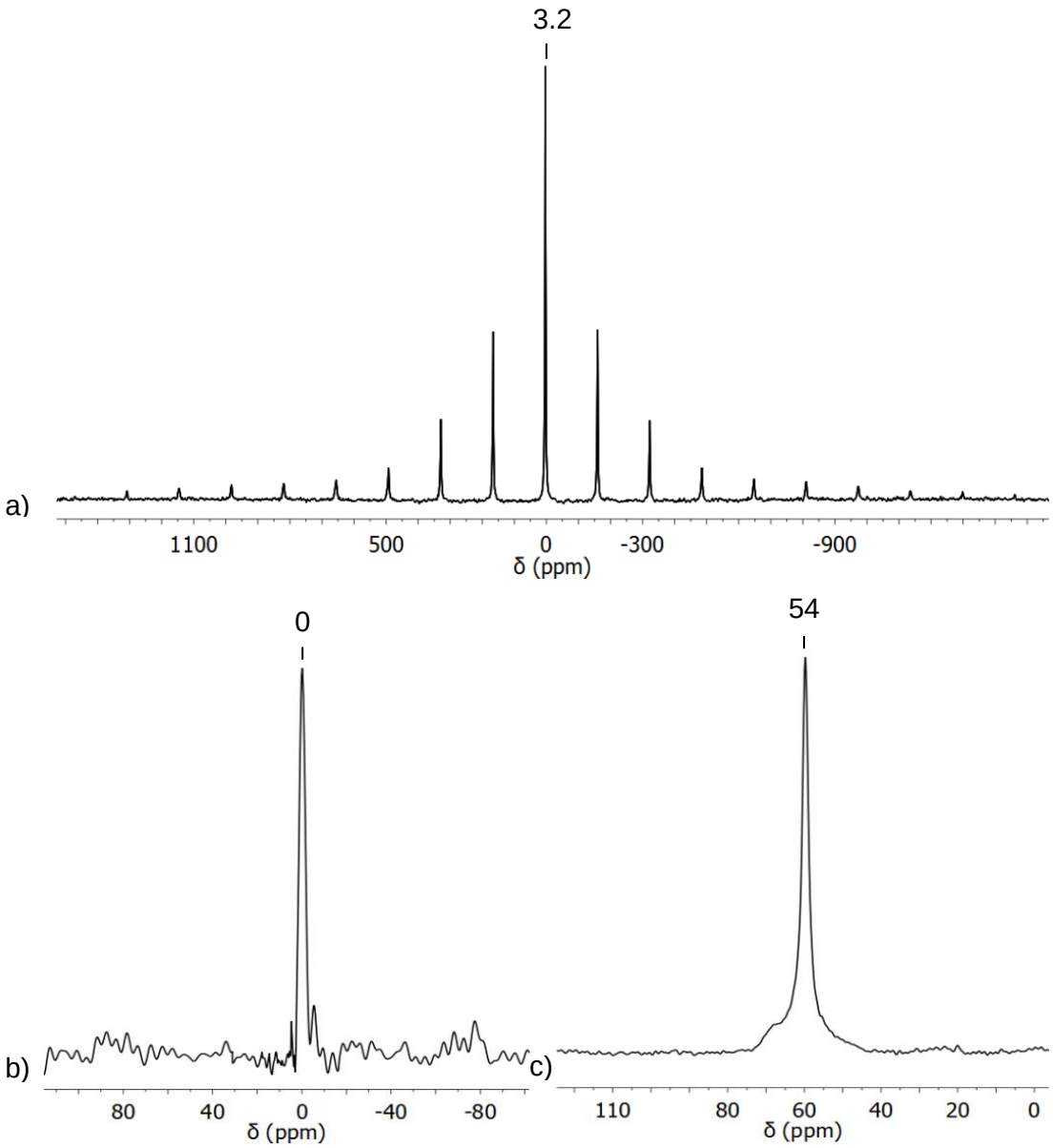

Figure 4.16 Solid-state a) ^{2}H DPMAS b) ^{11}B DEPTH and c) ^{31}P-{^{1}H} CP NMR spectra of ***s*-FLP1b** at spinning rate of 10 kHz.

4.4.4 Stoichiometric Reduction of 1,1-diphenylethylene by s-FLP1

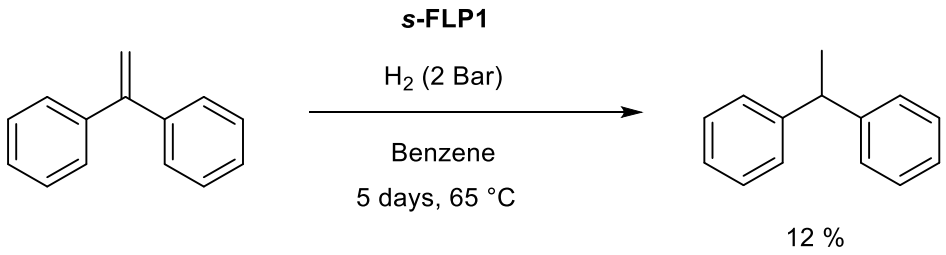

Equation 4.7 Schematic representation of the hydrogenation of 1,1-diphenylethylene by ***s*-FLP1**.

Preliminary results show that ***s*-FLP1** demonstrated stoichiometric reduction of 1,1-diphenylethylene (Equation 4.7) even under mild conditions (2 bar H_2, 65 °C). The solution phase ^{1}H NMR spectrum after 5 days of reaction shows the appearance of $[H{-}P^tBu_3]^+$ and resonances for the corresponding alkane. Integration of the NMR resonances indicates that approximately 12% conversion has been achieved. However, further analysis of the reaction using gas chromatography is required to further confirm this observation. Currently, this initial result is much lower than the system described by Taoufik *et al*., which showed 25% conversion of 1,2-diphenylethylene (10 bar H_2, 16 hour, 80 °C 2mol% catalyst loading). Nonetheless, we anticipate that under similar conditions with ***s*-FLP1**, improved turnover could be achieved.

4.5 Conclusions

A cleaner and more efficient method to produce ***s*-BCF** and its analogue ***s*-BFxyl** has been developed. The resulting solid-state NMR data of the materials produced are in close agreement with the solution-state NMR spectroscopic data of the molecular models described in Chapter Three, as well as with the literature.

Combination of either ***s*-BCF** or ***s*-BFxyl** with P^{t}Bu$_3$ allowed the formation of two silica supported FLP systems, ***s*-FLP1** and ***s*-FLP2**. Solid-state NMR spectroscopy of the two ***s*-FLPs** revealed weak Lewis pair interaction, as confirmed by the changes in the chemical shifts of the ^{11}B and ^{31}P nuclei. However, free unbound P^{t}Bu$_3$ was observed in solution-state NMR spectra of the supernatant, indicating that the strength of the interaction must be relatively weak.

***s*-FLP1** has demonstrated unprecedented reactivity towards H_2/D_2 and CD_3OD to form ***s*-FLP1a** and ***s*-FLP1b**, whereas ***s*-FLP2** did not react with H_2. Formation of ***s*-FLP1a** was confirmed by the observation of B−H absorption band in the FTIR spectrum. Moreover, D_2 cleavage was directly observed by ^{2}H DPMAS NMR spectroscopy. Formation of ***s*-FLP1b** was supported by the observation of a characteristic C−D absorption band in the FTIR spectrum. ^{2}H DPMAS experiment of ***s*-FLP1b** revealed rapid motion in the solid-state, due to rapid rotation of the CD_3 group. Furthermore, preliminary results have shown that ***s*-FLP1a** can mediate the hydrogenation of 1,1-diphenylethylene under mild reaction conditions, however further analysis using GC is required to confirm this observation. Although the current homogeneous FLP systems exhibit much higher hydrogenation activity, ***s*-FLP1** has shown promising results which provides an important step towards the development of *s*-FLPs as an effective heterogeneous hydrogenation catalyst.

4.6 Reference

1 K. Chernichenko, Á. Madarász, I. Pápai, M. Nieger, M. Leskelä and T. Repo, *Nat. Chem.*, 2013, **5**, 718–723.

2 M. Lindqvist, K. Borre, K. Axenov, B. Kótai, M. Nieger, M. Leskelä, I. Pápai and T. Repo, *J. Am. Chem. Soc.*, 2015, **137**, 4038–4041.

3 L. Shi and Y.-G. Zhou, *ChemCatChem*, 2015, **7**, 54–56.

4 Á. Gyömöre, M. Bakos, T. Földes, I. Pápai, A. Domján and T. Soós, *ACS Catal.*,

2015, **5**, 5366–5372.
5 G. Erős, K. Nagy, H. Mehdi, I. Pápai, P. Nagy, P. Király, G. Tárkányi and T. Soós, *Chem. - Eur. J.*, 2012, **18**, 574–585.
6 P. A. Chase, G. C. Welch, T. Jurca and D. W. Stephan, *Angew. Chem., Int. Ed.*, 2007, **46**, 8050–8053.
7 P. Spies, S. Schwendemann, S. Lange, G. Kehr, R. Fröhlich and G. Erker, *Angew. Chem., Int. Ed.*, 2008, **47**, 7543–7546.
8 D. W. Stephan and G. Erker, *Angew. Chem., Int. Ed.*, 2015, **54**, 6400–6441.
9 D. W. Stephan, *Acc. Chem. Res.*, 2015, **48**, 306–316.
10 K. V. Axenov, G. Kehr, R. Fröhlich and G. Erker, *J. Am. Chem. Soc.*, 2009, **131**, 3454–3455.
11 J. R. Severn, J. C. Chadwick, R. Duchateau and N. Friederichs, *Chem. Rev.*, 2005, **105**, 4073–4147.
12 G. G. Hlatky, *Chem. Rev.*, 2000, **100**, 1347–1376.
13 C. Copéret, M. Chabanas, R. Petroff Saint-Arroman and J.-M. Basset, *Angew. Chem., Int. Ed.*, 2003, **42**, 156–181.
14 S. Leonardelli, L. Facchini, C. Fretigny, P. Tougne and A. P. Legrand, *J. Am. Chem. Soc.*, 1992, **114**, 6412–6418.
15 L. T. Zhuravlev, *Colloids Surf., A*, 2000, **173**, 1–38.
16 B. A. Morrow and A. J. McFarlan, *J. Phys. Chem.*, 1992, **96**, 1395–1400.
17 US5863853, 1996.
18 K. Soga, J. R. Park and T. Shiono, *Polym. Commun.*, 1991, **32**, 310–313.
19 J. Xu, J. Zhao, Z. Fan and L. Feng, *Macromol. Rapid Commun.*, 1997, **18**, 875–882.
20 US5198401, 1991.
21 US5387568, 1992.
22 X. Yang, C. L. Stern and T. J. Marks, *J. Am. Chem. Soc.*, 1991, **113**, 3623–3625.
23 J. Tian, S. Wang, Y. Feng, J. Li and S. Collins, *J. Mol. Catal. A: Chem.*, 1999, **144**, 137–150.
24 S. Charoenchaidet, S. Chavadej and E. Gulari, *J. Mol. Catal. A: Chem.*, 2002, **185**, 167–177.
25 Y.-J. Wanglee, J. Hu, R. E. White, M.-Y. Lee, S. M. Stewart, P. Perrotin and S. L. Scott, *J. Am. Chem. Soc.*, 2012, **134**, 355–366.
26 K. C. Szeto, W. Sahyoun, N. Merle, J. L. Castelbou, N. Popoff, F. Lefebvre, J. Raynaud, C. Godard, C. Claver, L. Delevoye, R. M. Gauvin and M. Taoufik, *Catal. Sci. Technol.*, 2016, **6**, 882–889.
27 G. L. Rice and S. L. Scott, *Langmuir*, 1997, **13**, 1545–1551.
28 C. C. Liu and G. E. Maciel, *J. Am. Chem. Soc.*, 1996, **118**, 5103–5119.
29 T. Beringhelli, D. Donghi, D. Maggioni and G. D'Alfonso, *Coord. Chem. Rev.*, 2008, **252**, 2292–2313.
30 G. Engelhardt and D. Michel, *High-Resolution Solid-State NMR of Silicates and Zeolites.*, John Wiley & Sons, Chinchester, 1987.
31 C. Rosorius, C. G. Daniliuc, R. Fröhlich, G. Kehr and G. Erker, *J. Organomet. Chem.*, 2013, **744**, 149–155.

32 M. Sajid, A. Klose, B. Birkmann, L. Liang, B. Schirmer, T. Wiegand, H. Eckert, A. J. Lough, R. Fröhlich, C. G. Daniliuc, S. Grimme, D. W. Stephan, G. Kehr and G. Erker, *Chem. Sci.*, 2013, **4**, 213–219.

33 T. Wiegand, H. Eckert, O. Ekkert, R. Fröhlich, G. Kehr, G. Erker and S. Grimme, *J. Am. Chem. Soc.*, 2012, **134**, 4236–4249.

34 T. Wiegand, M. Siedow, H. Eckert, G. Kehr and G. Erker, *Isr. J. Chem.*, 2015, **55**, 150–178.

35 D. W. Stephan and G. Erker, *Angew. Chem., Int. Ed.*, 2010, **49**, 46–76.

36 G. C. Welch and D. W. Stephan, *J. Am. Chem. Soc.*, 2007, **129**, 1880–1881.

37 G. E. Pake, *J. Chem. Phys.*, 1948, **16**, 327–336.

38 T. J. Herrington, A. J. W. Thom, A. J. P. White and A. E. Ashley, *Dalton Trans.*, 2012, **41**, 9019–9022.

39 H. Chang, J. Lin, J. Wu and K. Chen, *J. Phys. Chem.*, 1995, **99**, 11081–11088.

40 A. E. Ashley, A. L. Thompson and D. O'Hare, *Angew. Chem., Int. Ed.*, 2009, **48**, 9839–9843.

41 E. Meirovitch, Z. Liang and J. H. Freed, *J. Phys. Chem. B*, 2015, **119**, 14022–14032.

42 I. Peuser, R. C. Neu, X. Zhao, M. Ulrich, B. Schirmer, J. a. Tannert, G. Kehr, R. Fröhlich, S. Grimme, G. Erker and D. W. Stephan, *Chem. - Eur. J.*, 2011, **17**, 9640–9650.

43 T. Wang and D. W. Stephan, *Chem. Commun.*, 2014, **50**, 7007–7010.

44 T. Voss, T. Mahdi, E. Otten, R. Fröhlich, G. Kehr, D. W. Stephan and G. Erker, *Organometallics*, 2012, **31**, 2367–2378.

CHAPTER FIVE

Layered Double Hydroxide-Supported FLPs

5.1 Introduction

As introduced in Chapter One, LDHs have attracted considerable amount of attention especially in the field of heterogeneous catalysis. The two main attractive features of LDHs are the abundant basic hydroxide sites, and uniformly distributed metal cations in which could both be catalytically active, allowing these materials to be used both as solid-state Lewis basic catalysts, as well as catalyst supports for the immobilisation of other catalytically active species.[1] An additional attractive feature of LDHs is that calcination of LDHs at intermediate temperatures (450−600 °C) can lead to the formation of Lewis basic mixed metal oxides (MMOs), which are potential catalysts for a range of organic transformations.[2–4] Through controlled rehydration in the absence of CO_2, MMOs can return to layered structures with OH^- sites in the interlayer region, producing activated LDHs with Brønsted basic sites. These activated LDHs and MMOs have been reported to catalyse the formation of C−C and C=C bonds.[5–8]

In addition to their uses as heterogeneous catalysts and as catalysts precursors, MMOs and LDHs have also received significant attention as catalyst supports for noble metal nanoparticles (NPs). LDH and MMO-supported Au-NPs exhibited enhanced catalytic performance in the aerobic homocoupling of phenylboronic acid, and various oxidation and deoxygenation reactions.[9–15] LDH supported nanopalladium has also demonstrated higher selectivity and superior activity in Heck coupling reactions than homogeneous $PdCl_2$ system as well as some of the supported catalysts, including Pd/C,[16]

Pd/SiO_2,[16] Pd/Al_2O_3[17] and resin-$PdCl_4^{2-}$.[17] The use of LDH-Pd-NP has also been extended to Suzuki-, Sonogashira- and Stille-type coupling reactions, exhibiting excellent yields in coupling products with superior TONs over the best homogeneous and supported ligand-free Pd systems.[18] Platinum NPs have also been supported on LDHs. Recently, Xiang and co-workers demonstrated that LDH supported Pt-NPs catalysed the selective hydrogenation of cinnamaldehyde to cinnamyl alcohol (85%) in water with high activity (TOF 1757 h^{-1}).[19]

Buffet and colleagues explored the use of AMO-LDHs[20] (aqueous miscible organic-LDH) as a support for metallocene catalysed ethylene polymerisation.[21] These unique organophilic LDHs can be dispersed in aromatic hydrocarbons, which enabled facile surface modification using organometallic reagents through reactions with the surface OH groups. A series of zirconocene complexes were immobilised on methylaluminoxane (MAO) treated AMO-LDHs. These AMO-LDH/MAO supported catalysts exhibited high activity for slurry ethylene polymerisation, with MgAl-SO_4-LDH supported *rac*-ethylenebis(1-indenyl) zirconium dichloride ((EBI)$ZrCl_2$) demonstrating the highest activity. In a related study, Buffet *et al*. exploited AMO-Mg_3Al-CO_3 LDH as a catalyst support for ethylene polymerisation, and showed that MAO treated Mg_3Al-CO_3 supported (^{Mes}PDI)$FeCl_2$ catalyst exhibited the highest catalytic activity compare to other AMO-LDH-supported metallocene catalysts.[22] The AMO-LDH used in this study was thermally treated at 150 °C under reduced pressure. The thermal gravimetric analysis (TGA) of Mg_3Al-CO_3 confirmed the loss of intercalated solvent molecules (acetone and water) between 80-150 °C while maintaining the layered structure of the LDH. However, decomposition of CO_3^{2-} anions was observed at temperatures above 260 °C.[22]

To expand on the scope of heterogeneous frustrated Lewis pairs, $Mg_3Al\text{-}CO_3$-LDH was explored as an alternative supporting material for heterogeneous *s*-FLPs, these preliminary results will be reported in this chapter.

5.2 Synthesis of $Mg_3Al\text{-}CO_3/B(C_6F_5)_2$

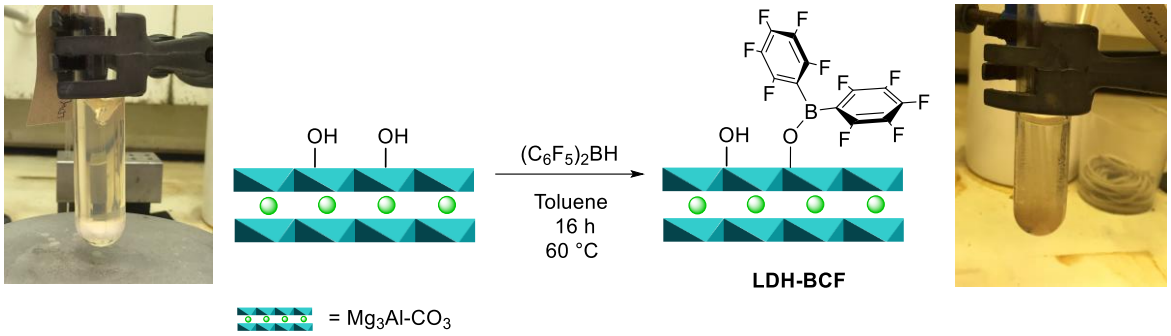

Equation 5.1 Reaction of $Mg_3Al\text{-}CO_3$ with Piers' borane.

Thermally pre-treated $[Mg_6Al_2(OH)_{16}]CO_3{\cdot}4H_2O$ (abbreviated as $Mg_3Al\text{-}CO_3$) (150 °C under reduced pressure, according to the published procedures[22]) was reacted with $(C_6F_5)_2BH$ in the ratio of 3:1 (by mass) respectively (Equation 5.1) in toluene at 60 °C. The initial cream coloured finely dispersed solid turned muddy brown and became more aggregated as the reaction proceeded. After 16 hours, the solid was allowed to settle, and the supernatant solution was examined by ^{1}H, ^{19}F and ^{11}B NMR spectroscopy. The NMR spectra revealed the absence of unreacted Piers' borane[23] indicating that the reaction had gone to completion. The solid was washed with fresh toluene, before filtration and drying (100 °C under reduced pressure, 2 hours) to afford $Mg_3Al\text{-}CO_3/B(C_6F_5)_2$ (**LDH-BCF**) with a predicted borane loading of 25 wt. % (estimated by assuming all hydroborane was grafted onto the LDH). The solid was characterised by IR spectroscopy, ^{11}B, ^{19}F, ^{27}Al solid-state NMR (ssNMR) spectroscopy and Transmission Electron Microscopy (TEM).

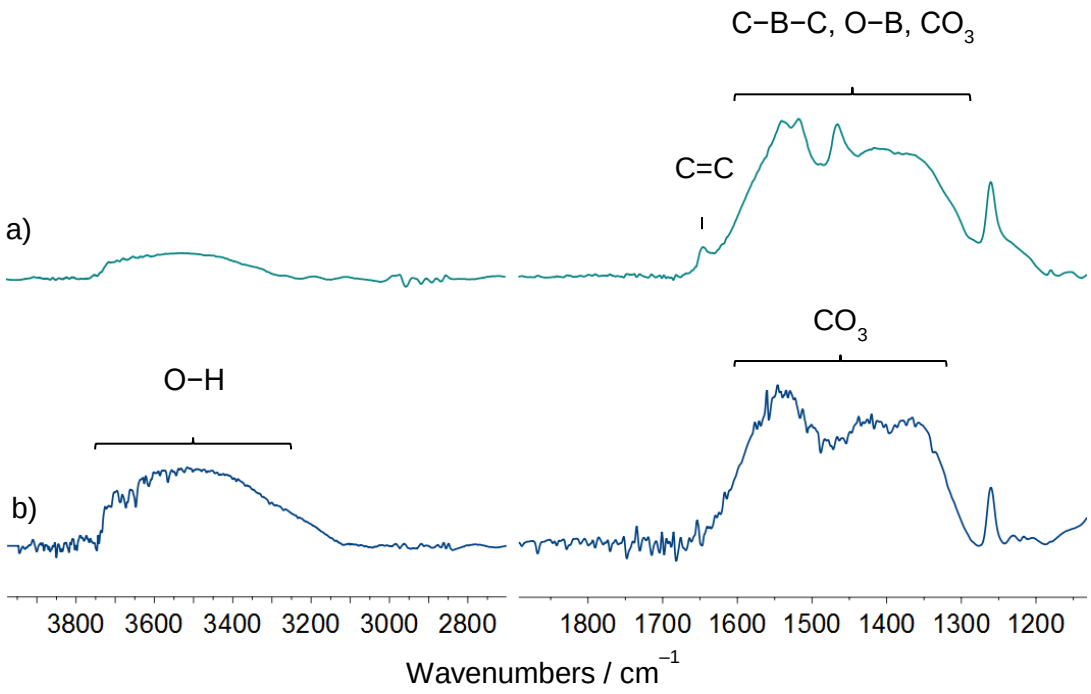

Figure 5.1 FTIR spectrum of a) Mg_3Al-CO_3/$B(C_6F_5)_2$ and b) unmodified Mg_3Al-CO_3-LDH.

The IR spectrum of Mg_3Al-CO_3 (Figure 5.1b) displays a very broad absorption at 3750−3100 cm^{-1} and a strong split absorption band at 1750−1300 cm^{-1}. These absorptions are associated with OH groups and interlayer CO_3^{2-} anions of Mg_3Al-CO_3 LDH.[24] Additional absorption bands can be observed at 1645, 1544 and 1465 cm^{-1} in the IR spectrum of **LDH-BCF**. These absorption modes are associated with aromatic ring breathing, C−B−C wagging and O−B stretching motions, consistent with the immobilisation of $B(C_6F_5)_2$ on LDH, and are also consistent with the IR spectrum of ***s*-BCF** (Chapter Four, section 4.2.1). Reduction in the relative intensity for the OH absorption band in **LDH-BCF** is also consistent with the conversion of OH groups to $OB(C_6F_5)_2$.

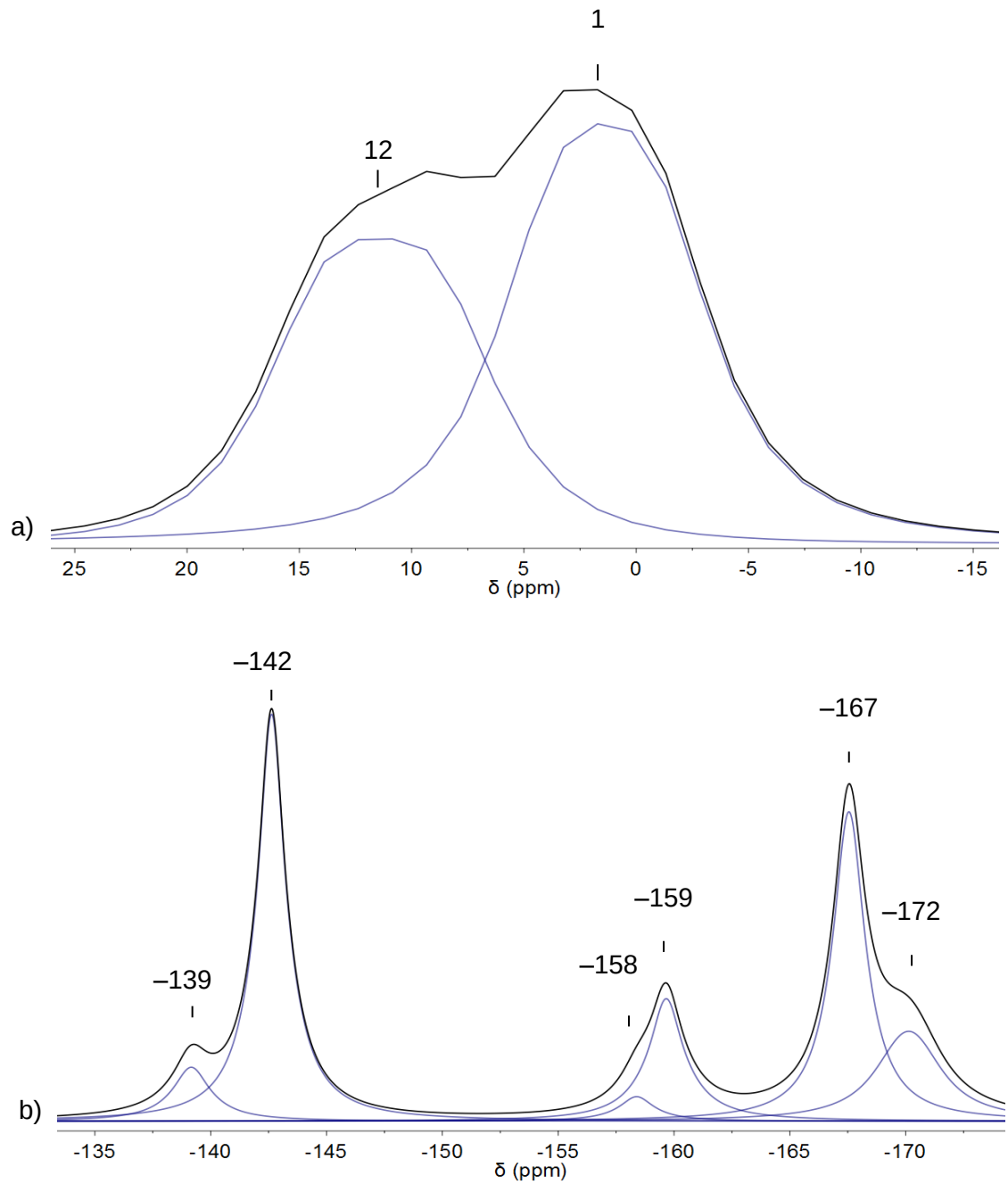

Figure 5.2 Solid-state NMR spectra of LDH-B(C_6F_5)$_2$: a) ^{11}B-{^{19}F} Hahn echo and b) ^{19}F DPMAS at spinning rate of 15 kHz (black line: experimental spectrum; blue line: simulated spectrum).

The solid-state ^{11}B-{^{19}F} Hahn echo spectrum displays two very broad overlapped resonances in the range between −10 and 20 ppm. Using MestReNova line simulation tool, the two overlapped resonances was separated, showing two maxima at 1 and 12 ppm, indicating two boron species could be present (Figure 5.2a). This is also consistent with the two sets of overlapping broad resonances (−139, −158, −170 and −142, −159 −167 ppm) observed in the ^{19}F DPMAS spectrum (Figure 5.2b). These resonances correspond to *ortho*-, *para*- and *meta*-F atoms on the C_6F_5 ring. The $\Delta\delta_{m,p}$ values (difference between the chemical shift of *para*- and *meta*-F) of 12 and 8 ppm suggest that the bound boranes are tri-coordinate $-OB(C_6F_5)_2$ species and are also similar to that of $\equiv SiOB(C_6F_5)_2$ (***s*-BCF**) species discussed in Chapter Four. In contrast to ***s*-BCF**, two different environments were observed for LDH bound $B(C_6F_5)_2$ species in both ^{11}B and ^{19}F ssNMR spectra. This observation could be due to that the $B(C_6F_5)_2$ species bound by surface hydroxyl groups are different to those on the edge of the LDH layers (possible interactions with neighbouring OH groups/anions).

The solid state ^{27}Al NMR spectrum exhibits a sharp resonance at 8 ppm and two overlapping broad resonances with maxima at 57 and 73 ppm (Figure 5.3). These resonances indicate octahedral and tetrahedral Al species respectively.[25] The change from octahedral to tetrahedral coordination may be due to migration of Al to the surface and complexation to form $Al–\{OB(C_6F_5)_2\}_x$ species. Tetrahedral ^{27}Al environments are also consistent with the observation of two different $OB(C_6F_5)_2$ species in ^{11}B and ^{19}F ssNMR spectra.

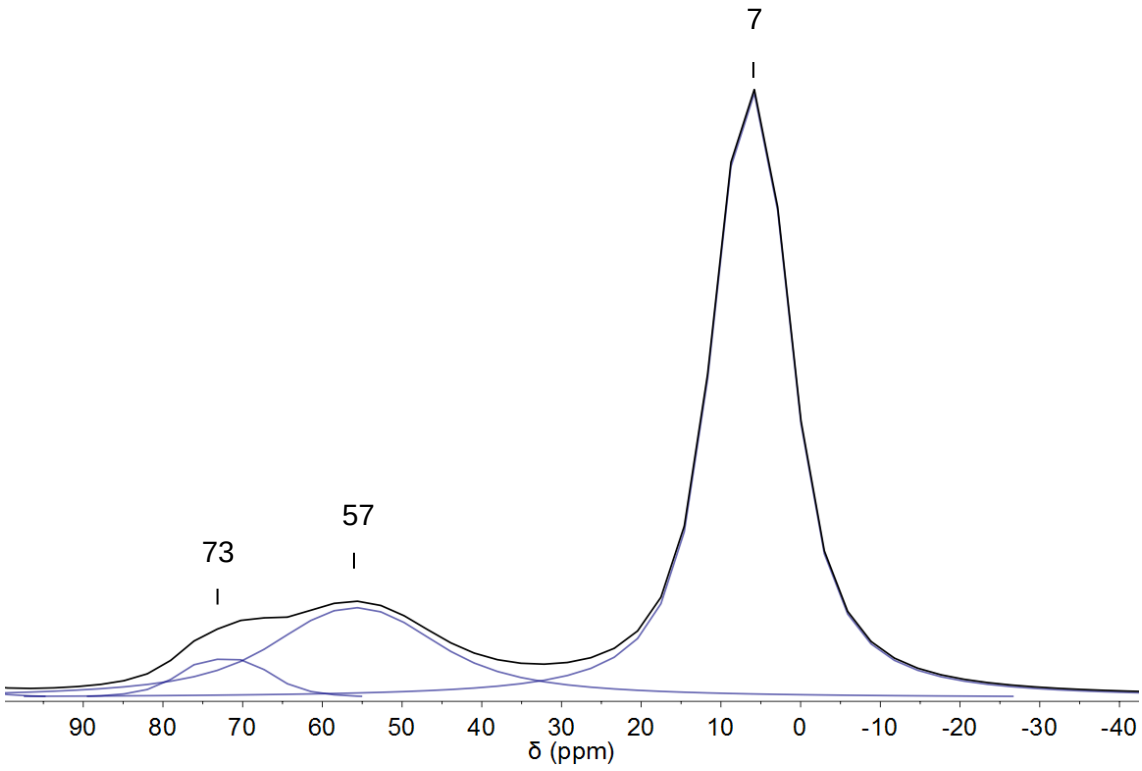

Figure 5.3 ^{27}Al DPMAS NMR spectrum of Mg_3Al-CO_3/$B(C_6F_5)_2$ at 10 kHz spinning rate (black line: experimental spectrum; blue line: simulated spectrum).

The morphology of **LDH-BCF** was examined by TEM (Figure 5.4a). The TEM images of the **LDH-BCF** shows that the modified LDH particles maintained the floral/crystalline platelet morphology similar to that of unmodified AMO-Mg_3Al-CO_3 (Figure 5.4b).[20] However, the particles are highly aggregated. This increased aggregation is possibly due to the increased hydrogen bonding between C_6F_5 groups and surface OH groups [−F···OH].

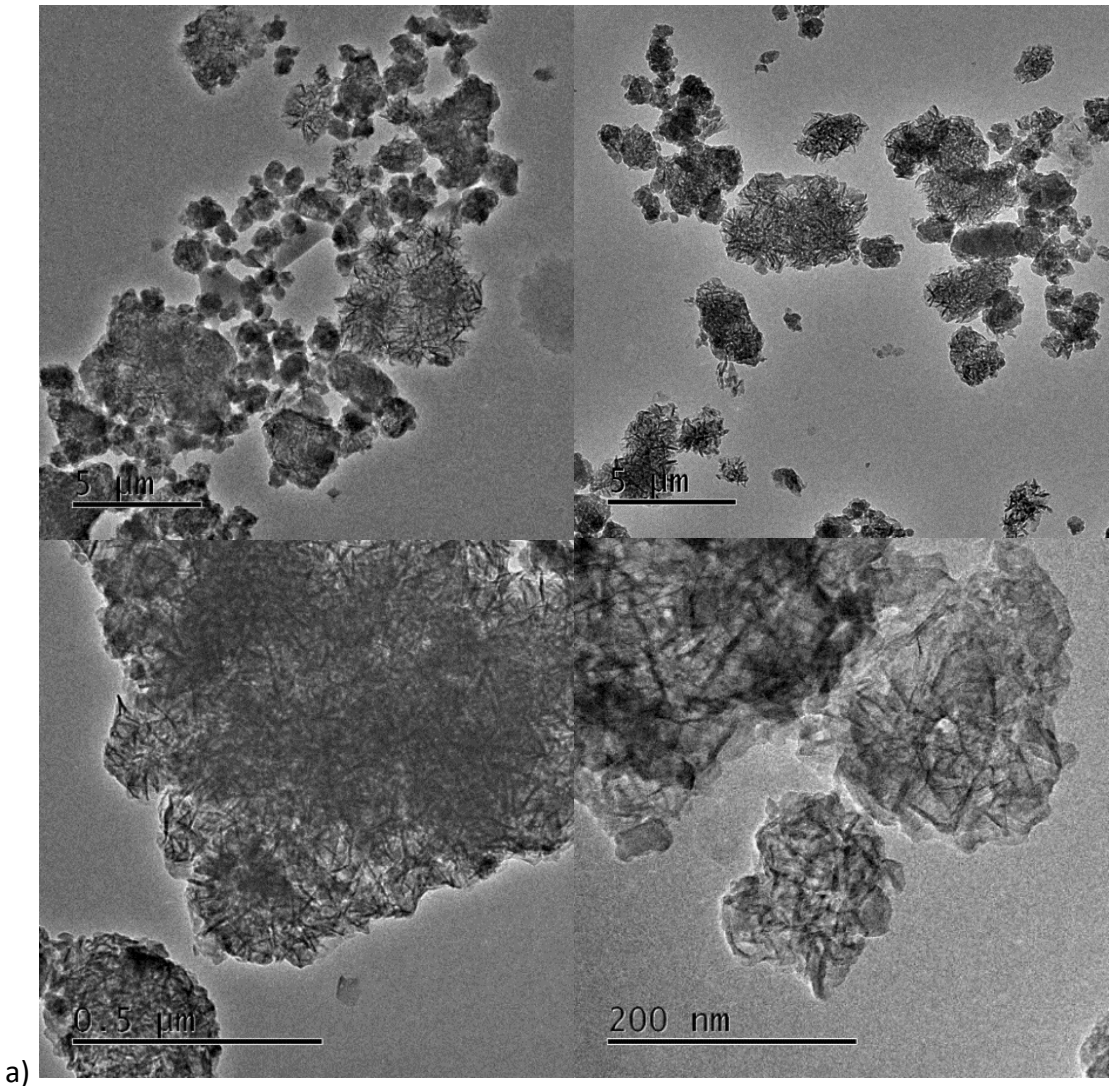

a)

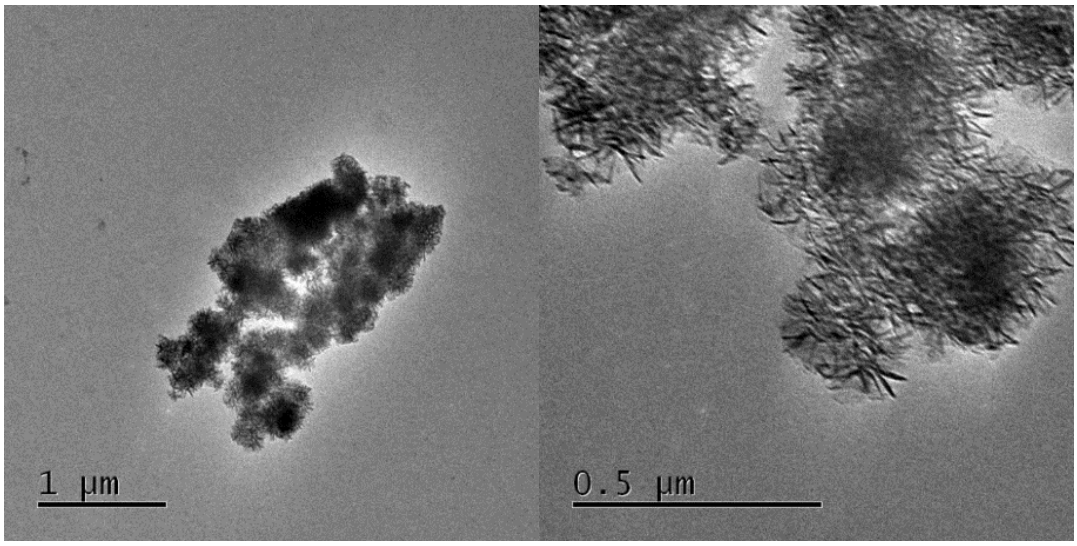

b)

Figure 5.4 TEM images of a) $Mg_3Al\text{-}CO_3/B(C_6F_5)_2$ and b) pure unmodified AMO-$Mg_3Al\text{-}CO_3$

5.3 Formation of $Mg_3Al\text{-}CO_3/[B(C_6F_5)_2/P^tBu_3]$

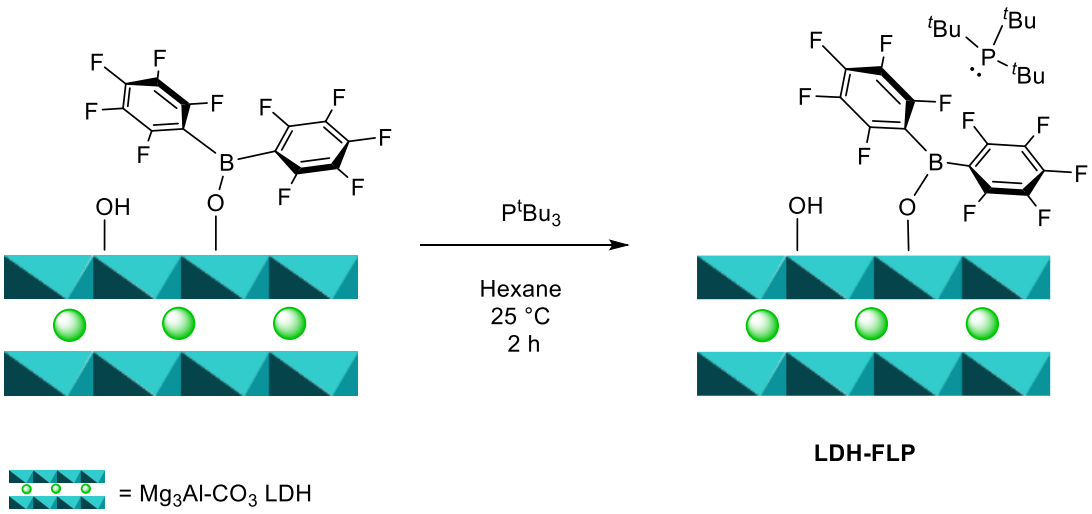

Equation 5.2 Formation of LDH-FLP.

A stoichiometric amount of P^tBu_3 was added to $Mg_3Al\text{-}CO_3/B(C_6F_5)_2$ (25 wt.% borane) suspended in toluene at room temperature (Equation 5.2). The slurry was stirred for 2 hours before the solvent was removed under reduced pressure, and dried under vacuum for further 2 hours, to afford $Mg_3Al\text{-}CO_3/[B(C_6F_5)_2/P^tBu_3]$ (**LDH-FLP**) as an off white solid. Small amount of the solid was re-suspended in toluene-d^8 and examined using solution ^1H and ^{31}P NMR spectroscopy. The NMR spectra revealed the presence of free P^tBu_3 in the solution, suggesting that the Lewis base component of the **LDH-FLP** is neither strongly bound to the LDH *via* chemical reaction with the hydroxyl groups or forming adduct with the Lewis acid, similar to what was observed for the ***s*-FLP** systems described in Chapter Four.

The IR spectrum of the **LDH-FLP** contains some new absorption bands in addition to those bands associated with **LDH-BCF**, including C−H bond stretch at 2800−3000 cm^{-1} and −C−H bending motions at 1350−1480 cm^{-1} (Figure 5.5a). These absorptions in

addition to some of the other new features correspond well with the spectrum of pure P^{t}Bu$_3$ (Figure 5.5b), indicating the formation of **LDH-FLP**.

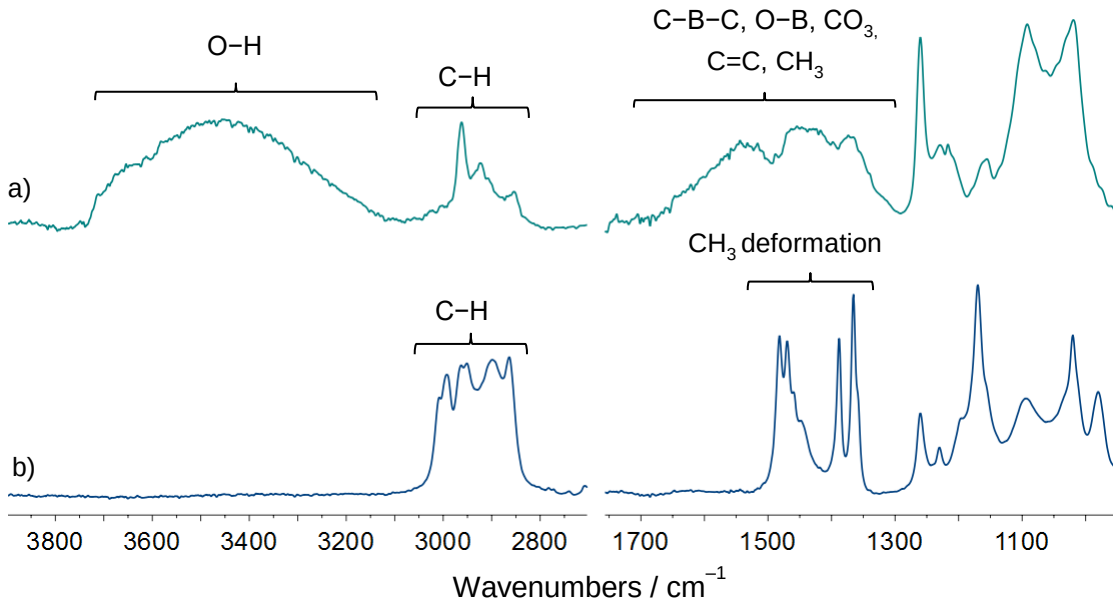

Figure 5.5 IR spectra of a) Mg_3Al-CO_3/$B(C_6F_5)_2$/P^{t}Bu$_3$ and b) neat P^{t}Bu$_3$

5.4 Reaction of LDH-FLP with H_2 or D_2

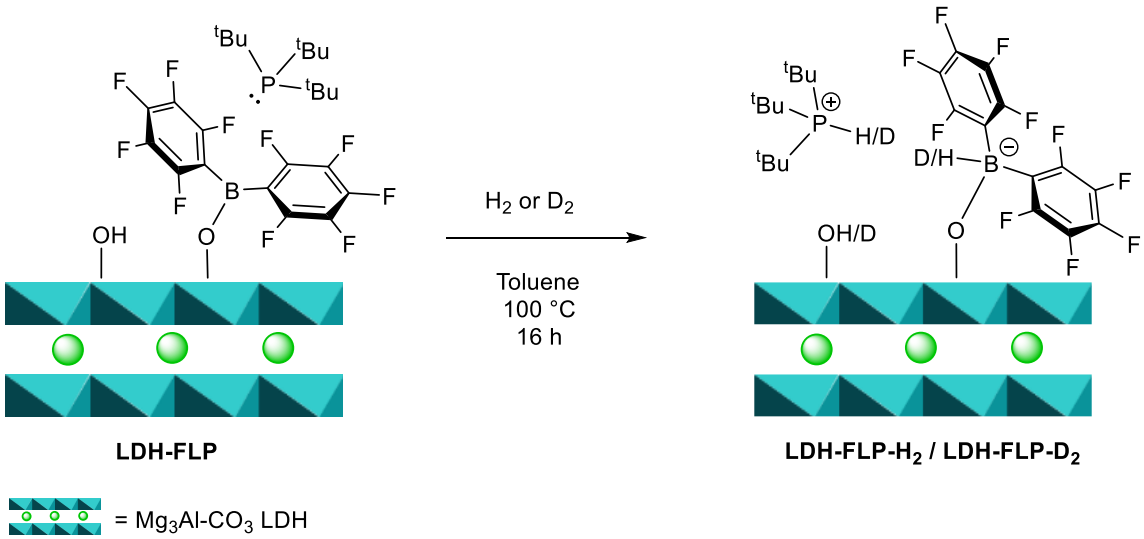

Equation 5.3 Reaction of **LDH-FLP** with H_2 and D_2.

Preliminary studies of the reactivity of **LDH-FLP** with either H_2 or D_2 were performed. A suspension of **LDH-FLP** in toluene (freeze-pump-thaw degassed) was pressurised with either H_2 or D_2 (2 bar), and stirred at 100 °C for 16 hours (Equation 5.3), before removal of the solvent and under reduced pressure for 2 hours. The solids were then characterised by ssNMR, and FTIR spectroscopy.

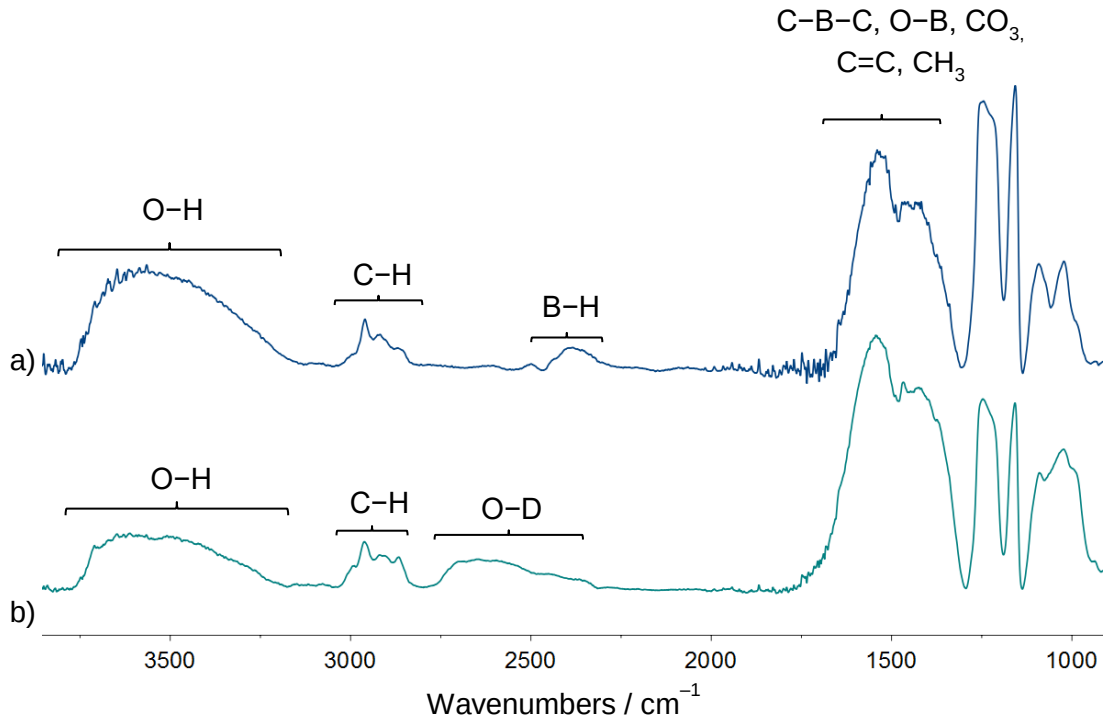

Figure 5.6 IR spectra of a) **LDH-FLP-H₂** and b) **LDH-FLP-D₂**.

The IR spectrum of **LDH-FLP-H₂** exhibits a characteristic B−H absorption at 2400 cm^{-1} in addition to those absorptions associated with **LDH-FLP** (Figure 5.6a). This observation indicates successful H_2 cleavage. However, for **LDH-FLP-D₂**, a broad absorption at 2761−2329 cm^{-1} was observed (Figure 5.6b). This is a characteristic O−D absorption, and it is consistent with the calculated value according to the reduced mass formula (around 2750 cm^{-1}). The exact mechanism for the formation of OD is currently unknown, however, several plausible mechanisms could be proposed: i) D_2 cleavage by

LDH-FLP followed by H/D scrambling *via* reaction between $[D{-}P^tBu_3]^+$ and surface hydroxyl groups; ii) formation of a frustrated Lewis pair between $-OB(C_6F_5)_2$ and nearby basic −OH (in a similar fashion to the nanostructured solid-state [InOH···In] FLP system developed by Ozin *et al*.[26,27]) thereby achieving direct D_2 cleavage. A control reaction was performed by heating a suspension of pure LDH in toluene under D_2 (2 bar). O−D absorption was not observed in IR spectrum (the FTIR spectrum is identical to that of unmodified LDH, indicating that LDH alone could not catalyse the D_2 cleavage reaction.

The ^{2}H DPMAS NMR spectrum of **LDH-FLP-D$_2$** (Figure 5.7) shows a complex ^{2}H environment. The shape of the spinning side bands (Figure 5.7b) represents superimposition of a large Pake doublet (a static ^{2}H environment) and a motion averaged Lorentzian distribution, giving rise to three large peaks in the spectrum (an overall partially static spectrum).[28,29] The mobile ^{2}H environment could be assigned to O−**D** *via* rapid H/D exchange with $[D{-}P^tBu_3]^+$ on the NMR timescale, whereas the static environment could be assigned to B−**D**. The broad central isotropic band contains two overlapping resonances (Figure 5.7a). The broader resonance at 5 ppm is assigned to O−**D**, and the narrower resonance at 1 ppm was assigned B−**D**.

The ^{31}P CPMAS NMR spectra of **LDH-FLP-H$_2$** and **LDH-FLP-D$_2$** are shown in Figure 5.8. The ^{31}P CPMAS spectrum of **LDH-FLP-H$_2$** displays a sharp resonance at 54 ppm, and a weak shoulder at 62 ppm (Figure 5.8a). The sharp resonance is assigned to the protonated phosphonium species $[H{-}\mathbf{P}^tBu_3]^+$ as the result of H_2 cleavage, whereas the weak shoulder could be assigned to free P^tBu_3 species. These results are consistent with the existing literature values for $[H{-}\mathbf{P}^tBu_3]^+$ and P^tBu_3.[30] In contrast, the spectrum for **LDH-FLP-D$_2$** contains a very broad resonance, which also appears at 54 ppm, and is assigned to $[D{-}\mathbf{P}^tBu_3]^+$ species. The broadness of the resonance could be affected by a combination of dipolar interactions between the quadrupolar ^{2}H nucleus and ^{31}P nucleus,

and rapid H/D exchange between $[D{-}\mathbf{P}^t Bu_3]^+$ species and neighbouring OH groups, consistent with the aforementioned FTIR spectrum as well as the ^2H DPMAS spectrum.

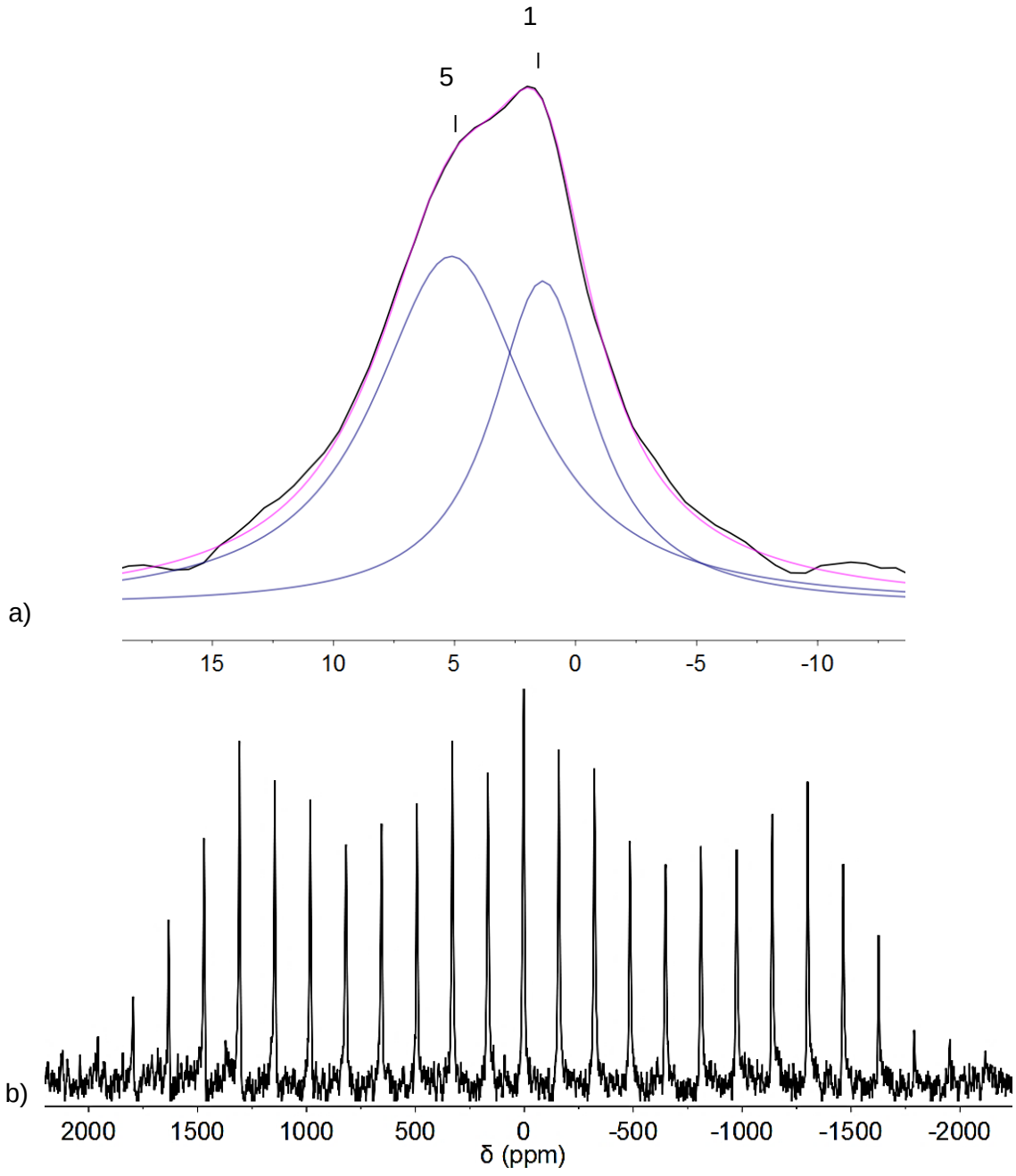

Figure 5.7 ^2H DPMAS NMR spectrum of **LDH-FLP-D$_2$** at 10 kHz spinning rate, showing a) enlarged central isotropic band and b) entire spectrum. (black: experimental spectrum; magenta: sum of peaks; blue: simulated spectrum).

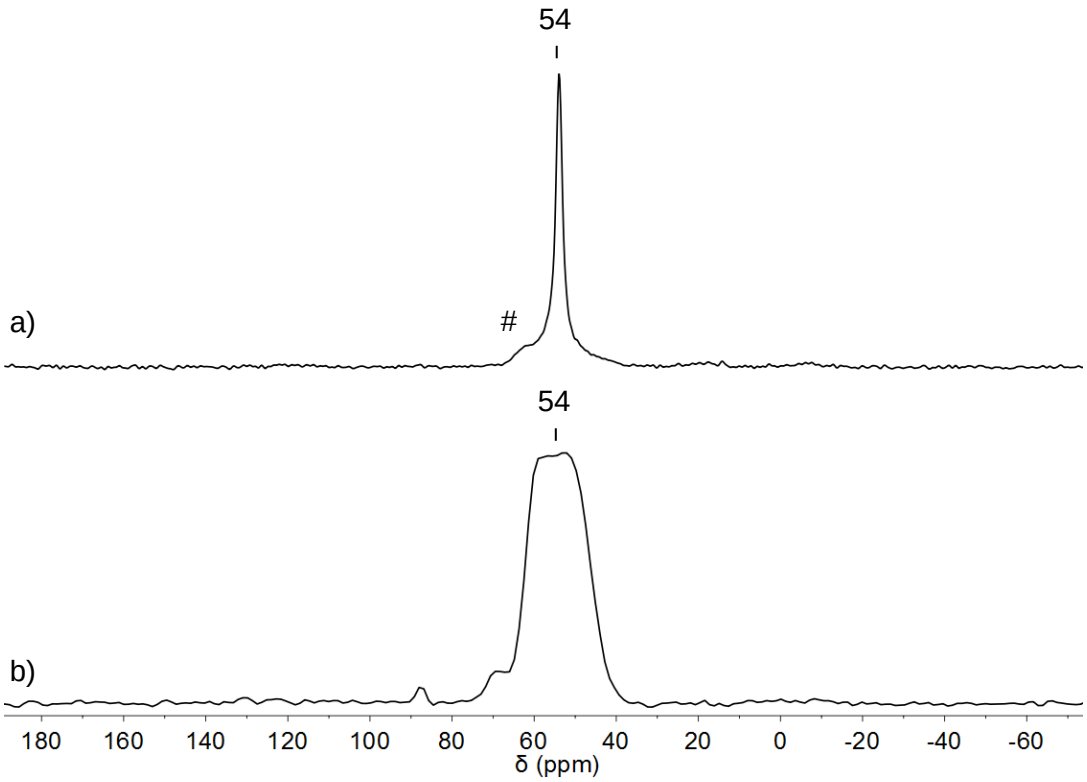

Figure 5.8 ^{31}P CPMAS NMR spectra a) **LDH-FLP-H$_2$** b) **LDH-FLP-D$_2$**.

5.5 Conclusions

Reaction of Piers' borane with Mg_3Al-CO_3-LDH afforded a Lewis acid modified **LDH-BCF**. Solid-state NMR spectroscopy studies revealed the presence of more than one boron species in the sample. Treatment of **LDH-BCF** with P^{t}Bu$_3$ yields what we tentatively believe to be the first LDH supported FLP system. FTIR spectroscopy was used to monitor the formation of **LDH-FLP**, and solution-phase ^{1}H and ^{31}P NMR confirmed that P^{t}Bu$_3$ does not form a conventional adduct with **LDH-BCF** or react with the surface hydroxy groups.

LDH-FLP reactions with both D_2 and H_2 to give bond cleavage products. H_2 bond cleavage was initially confirmed by the appearance of a B−H absorption band in the FTIR spectrum of **LDH-FLP-H$_2$**. This result was further supported by ^{2}H DPMAS NMR

spectrum of **LDH-FLP-D$_2$**. We believe **LDH-FLP-D$_2$** rapidly undergoes H/D scrambling between the [D−**P**^{t}Bu$_3$]$^+$ species and the basic OH groups to generate OD species as confirmed by the observation of a characteristic O−D stretch in the IR spectrum.

These preliminary findings have demonstrated that LDH could be an alternative support for heterogeneous FLPs with great potential. Much more extensive studies will be required in order to fully understand the nature of LDH supported FLP systems. The interplay between different calcination temperatures, charge balancing anions and metal cations may also greatly affect the performance of the supported FLPs.

5.6 Reference

1 G. Fan, F. Li, D. G. Evans and X. Duan, *Chem. Soc. Rev.*, 2014, **43**, 7040–7066.
2 C. Qi, J. C. Amphlett and B. A. Peppley, *Appl. Catal., A*, 2006, **302**, 237–243.
3 H. Morioka, Y. Shimizu, M. Sukenobu, K. Ito, E. Tanabe, T. Shishido and K. Takehira, *Appl. Catal., A*, 2001, **215**, 11–19.
4 F. Li, J. Liu, D. G. Evans and X. Duan, *Chem. Mater.*, 2004, **16**, 1597–1602.
5 B. M. Choudary, M. Lakshmi Kantam, V. Neeraja, K. Koteswara Rao, F. Figueras and L. Delmotte, *Green Chem.*, 2001, **3**, 257–260.
6 B. M. Choudary, M. Lakshmi Kantam, C. R. Venkat Reddy, K. Koteswara Rao and F. Figueras, *J. Mol. Catal. A: Chem.*, 1999, **146**, 279–284.
7 S. K. Sharma, P. A. Parikh and R. V. Jasra, *J. Mol. Catal. A: Chem.*, 2007, **278**, 135–144.
8 S. Abelló, S. Dhir, G. Colet and J. Pérez-Ramírez, *Appl. Catal., A*, 2007, **325**, 121–129.
9 L. Wang, H. Wang, W. Zhang, J. Zhang, J. P. Lewis, X. Meng and F.-S. Xiao, *J. Catal.*, 2013, **298**, 186–197.
10 T. Mitsudome, A. Noujima, T. Mizugaki, K. Jitsukawa and K. Kaneda, *Green Chem.*, 2009, **11**, 793–797.
11 T. Mitsudome, A. Noujima, T. Mizugaki, K. Jitsukawa and K. Kaneda, *Adv. Synth. Catal.*, 2009, **351**, 1890–1896.
12 S. Nishimura, A. Takagaki and K. Ebitani, *Green Chem.*, 2013, **15**, 2026–2042.
13 T. Mitsudome, A. Noujima, Y. Mikami, T. Mizugaki, K. Jitsukawa and K. Kaneda, *Angew. Chem., Int. Ed.*, 2010, **49**, 5545–5548.
14 A. Noujima, T. Mitsudome, T. Mizugaki, K. Jitsukawa and K. Kaneda, *Angew. Chem., Int. Ed.*, 2011, **50**, 2986–2989.
15 W. Fang, Q. Zhang, J. Chen, W. Deng and Y. Wang, *Chem. Commun.*, 2010, **46**, 1547–1549.

16 F. Zhao, B. M. Bhanage, M. Shirai and M. Arai, *Chem. - Eur. J.*, 2000, **6**, 843–848.
17 A. Biffis, M. Zecca and M. Basato, *Eur. J. Inorg. Chem.*, 2001, **2001**, 1131–1133.
18 B. M. Choudary, S. Madhi, N. S. Chowdari, M. L. Kantam and B. Sreedhar, *J. Am. Chem. Soc.*, 2002, **124**, 14127–14136.
19 X. Xiang, W. He, L. Xie and F. Li, *Catal. Sci. Technol.*, 2013, **3**, 2819–2827.
20 C. Chen, M. Yang, Q. Wang, J.-C. Buffet and D. O'Hare, *J. Mater. Chem. A*, 2014, **2**, 15102–15110.
21 J.-C. Buffet, N. Wanna, T. A. Q. Arnold, E. K. Gibson, P. P. Wells, Q. Wang, J. Tantirungrotechai and D. O'Hare, *Chem. Mater.*, 2015, **27**, 1495–1501.
22 J.-C. Buffet, Z. R. Turner, R. T. Cooper and D. O'Hare, *Polym. Chem.*, 2015, **6**, 2493–2503.
23 D. J. Parks, R. E. von H. Spence and W. E. Piers, *Angew. Chem., Int. Ed.*, 1995, **34**, 809–811.
24 J. T. Kloprogge, D. Wharton, L. Hickey and R. L. Frost, *Am. Mineral.*, 2002, **87**, 623–629.
25 A. Vyalikh, F. R. Costa, U. Wagenknecht, G. Heinrich, D. Massiot and U. Scheler, *J. Phys. Chem. C*, 2009, **113**, 21308–21313.
26 K. K. Ghuman, L. B. Hoch, P. Szymanski, J. Y. Y. Loh, N. P. Kherani, M. A. El-Sayed, G. A. Ozin and C. V. Singh, *J. Am. Chem. Soc.*, 2016, **138**, 1206–1214.
27 K. K. Ghuman, L. B. Hoch, T. E. Wood, C. Mims, C. V. Singh and G. A. Ozin, *ACS Catal.*, 2016, **6**, 5764–5770.
28 G. E. Pake, *J. Chem. Phys.*, 1948, **16**, 327–336.
29 A. E. Ashley, A. L. Thompson and D. O'Hare, *Angew. Chem., Int. Ed.*, 2009, **48**, 9839–9843.
30 G. C. Welch and D. W. Stephan, *J. Am. Chem. Soc.*, 2007, **129**, 1880–1881.

CHAPTER SIX

Experimental Details and Characterisation Data

6.1 General Procedures and Physical Measurements

6.1.1 General Procedures

All reactions and compounds were manipulated under N_2 using either standard Schlenk line techniques on a double-manifold gas-inlet (N_2)/vacuum line or in an MBraun 130-BG glovebox under a nitrogen atmosphere, unless indicated otherwise. All glassware used for air-sensitive reactions was heated to 180 °C before use. Solvents and solutions were transferred using steel cannulae under a positive flow of N_2, or via plastic syringes fitted with steel needles for volumes less than 20 mL. Filtrations were performed using either glassware fitted with a fritted glass disc, or through modified steel cannulae fitted with glass microfiber filters. Hexane, pentane, benzene, toluene, dichloromethane and acetonitrile were dried using MBraun SPS-800 solvent-purification system, whereas Et_2O was distilled from potassium; all except CH_2Cl_2 and acetonitrile were stored over K-mirrored ampoules. Anhydrous methanol and formic acid was purchased from Sigma Aldrich, dried and stored over activated 4 Å molecular sieves under N_2. Deuterated solvents for NMR spectroscopy of air-sensitive materials were dried over Na/K (C_7D_8, C_6D_6), calcium hydride (THF-d_8, CD_3CN, CD_3OD, CD_2Cl_2, $CDCl_3$, C_6D_5Br) respectively, purified by trap-to-trap distillation and freeze-pump-thaw degassed three times prior to use.

6.1.2 NMR Spectroscopy

Solution-state ^{1}H, ^{11}B, ^{13}C, ^{31}P and ^{19}F NMR spectra were recorded at room temperature on Bruker 400 Avance III HD NanoBay spectrometer operating at 400 MHz or a Bruker AVII perating at 500 MHz using quartz NMR tubes with standard J. Young valve. ^{1}H NMR spectra were referenced internally to the residual protio solvent signals, and chemical shifts are reported in ppm. Solid-state ^{2}H, ^{13}C, ^{11}B, ^{19}F and ^{31}P MAS NMR spectra were collected by Dr. Nick Rees (University of Oxford) on a Bruker Avance III HD 400 MHz Solid State NMR Spectrometer. Samples were packed in 3.2mm ZrO_2 rotors and spun at the magic angle (54.71°). ^{2}H, ^{19}F, ^{31}P and ^{11}B NMR spectra were collected at spin rates of 10, 24 kHz. Chemical shifts for all solid-state MAS NMR spectra were reported in ppm.

6.1.3 Elemental Analysis

Elemental Analysis for all samples were carried out by Mr. Stephen Boyer of the Elemental Analysis Service, London Metropolitan University, London.

6.1.4 Fourier Transform Infrared Spectroscopy

All FTIR spectra were recorded under N_2 at room temperature in a transmission mode on a Bio-Rad FTS 7000 FTIR spectrometer in the range of 500−4000 cm^{-1}; 100 scans at 4 cm^{-1} resolution. Self-supporting pellets were made by pressing a finely grinded powder containing 1-2 mg of samples and 5 mg of KBr with a hand press. The sample pellets were loaded into air-tight cells with KBr windows inside the glovebox prior to measurements to ensure the samples are moisture free.

6.1.5 Mass Spectrometry

Samples were analysed by Mr. Colin Sparrow of the Mass Spectrometry Service, Chemistry Research Laboratory, University of Oxford.

6.1.6 Crystal Structure Determinations

Data collection, structure determination and refinements, were carried out by Dr. Zoë Turner and Dr. Samantha Binding of the Chemistry Research Laboratory, University of Oxford. Crystals were mounted on MiTeGen MicroMounts using perfluoropolyether oil, then transferred to a goniometer head on the diffractometer and cooled rapidly to 150 K in a stream of cold N_2 using an Oxford Cryosystems CRYOSTREAM unit.[1] Data collection was performed using either: an Enraf-Nonius FR590 KappaCCD diffractometer using graphite-monochromated Mo Kα X-ray radiation (λ = 0.71073 Å), or an Oxford Diffraction Supernova dual-source diffractometer equipped with a 135 mm Atlas CCD area detector using mirror monochromated Cu Kα radiation (λ = 1.5418 Å). Intensity data were processed using the DENZO-SMN package. Structures were solved using the direct-methods program SIR92. Subsequent full-matrix least-squares refinements were carried out using the CRYSTALS program suite.

6.1.7 Brunauer–Emmett–Teller (BET) Surface Area Analysis

Brunauer–Emmett–Teller (BET) specific surface area analyses were measured by Dr. Alexander Kilpatrich (Chemistry Research Laboratory, University of Oxford) from the N_2 adsorption and desorption isotherms at 77 K collected from a Micromeritic TriStar.

6.1.8 Transmission Electron Microscopy

Transmission Electron Microscopy (TEM) analysis was performed on a JEOL 2100 microscope with an accelerating voltage of 200 kV. LDH nanoparticles were dispersed in toluene with sonication and then casted onto copper grids coated with Formvar film.

6.2 Source of Starting Materials

6.2.1 Commercially Available Starting Material

H_2 gas (>99.99%) was obtained from CK Special Gases Ltd., D_2 gas (>99.8%) was purchased from Sigma Aldrich and CO_2 gas (99.99%) was obtained from ARGO International Ltd.. All gases were connected directly onto a dual manifold Schlenk line through a three-way valve fitted with a Young's tap and used directly. BCl_3 (1.0 M in heptane), BBr_3 (99.9%), $BH_3{\cdot}SMe_2$, formic acid, Oleum (20%), 1,3,5,7,9,11-Octaisobutyltetracyclo[7.3.3.$1^{5,11}$]octasiloxane-*endo*-3,7-diol, tris(tertbutoxy)silanol, tri-*tert*-butyl phosphine, and trimesitylphosphine were purchased from Sigma Aldrich; all were used as received. Anhydrous methanol (99.8%) was purchased from Sigma Aldrich; BrC_6F_5 and 1,3-bis(trifluoromethyl)-5-bromobenzene were obtained from Fluorochem; were all stored over activated 4 Å molecular sieves under N_2. Silica provided by SCG Chemicals, has a surface area of 310 m^2/g.

6.2.2 Literature Preparations

$(C_6F_5)_2BH$[2,3], $(3,5\text{-}(CF_3)_2C_6H_3)_2BCl$[4], $B(C_6Cl_5)(C_6F_5)_2$[5], and $\equiv SiOB(C_6F_5)_2$[6,7] were prepared according to literature procedures.

6.3 Experimental Details for Chapter Two

6.3.1 Preparation of [$(C_6Cl_5)(C_6F_5)_2B{-}P(p\text{-tolyl})_3$]

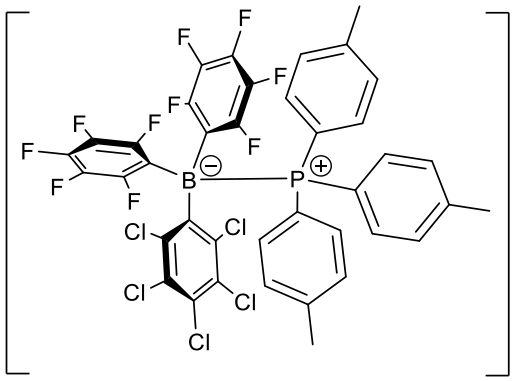

In a J-Young's NMR tube, a 1:1 mixture of $B(C_6Cl_5)(C_6F_5)_2$ and $P(p\text{-tolyl})_3$ were combined in C_6D_6 (0.5 mL). The mixture was monitored using ^{1}H, ^{11}B, ^{19}F and ^{31}P NMR spectroscopy. **^{1}H NMR (C_6D_6, 500 MHz):** δ 7.3-6.6 (m, 12H; Ar*H*); 2.27 (s, 9H; $P(C_6H_4(CH_3)_3)$. **^{11}B NMR (C_6D_6, 160 MHz):** δ −8.4 (br, s). **^{31}P NMR (C_6D_6, 202 MHz):** δ 17.9 (m, $P(C_6H_4(CH_3)_3)$). **^{19}F NMR (C_6D_6, 470 MHz):** δ −134.3 (br m, 4F, $^{3}J_{FF}$ = 20 Hz; *ortho*-C_6F_5); −158.5 (m, 2F, $^{3}J_{FF}$ = 20 Hz; *para*-C_6F_5); −165.8 (m, 4F, $^{3}J_{FF}$ = 20 Hz; *meta*-C_6F_5). Product was not isolated.

6.3.2 Preparation of [$B(C_6Cl_5)(C_6F_5)_2/P(o\text{-tolyl})_3$]

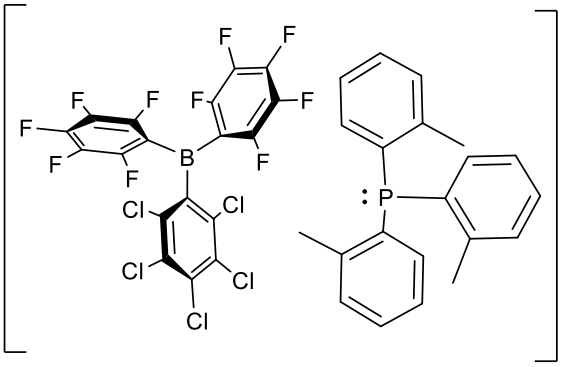

In a J-Young's NMR tube, a 1:1 mixture of $B(C_6Cl_5)(C_6F_5)_2$ and P(*o*-tolyl)$_3$ were combined in C_6D_6 (0.5 mL). Formation of the FLP was monitored using ^{1}H, ^{11}B, ^{19}F and ^{31}P NMR spectroscopy. **^{1}H NMR (C_6D_6, 500 MHz):** δ 7.2-6.8 (m, 12H; Ar*H*); 2.41 (s, 9H; P(C_6H_4(CH_3)$_3$). **^{11}B NMR (C_6D_6, 160 MHz):** δ 58.4 (br, s). **^{31}P NMR (C_6D_6, 202 MHz):** δ −29.7 (m, $^{3}J_{HP}$ = 16 Hz; *P*($C_6H_4(CH_3)_3$)). **^{19}F NMR (C_6D_6, 470 MHz):** δ −127.18 (br m, 4F, $^{3}J_{FF}$ =20 Hz;*ortho*-C_6F_5); −140.1 (m, 2F, $^{3}J_{FF}$ = 20 Hz; *para*-C_6F_5); −159.8 (m, 4F, $^{3}J_{FF}$ = 20 Hz; *meta*-C_6F_5).

6.3.3 Preparation of [B(C$_6$Cl$_5$)(C$_6$F$_5$)$_2$/P^{t}Bu$_3$]

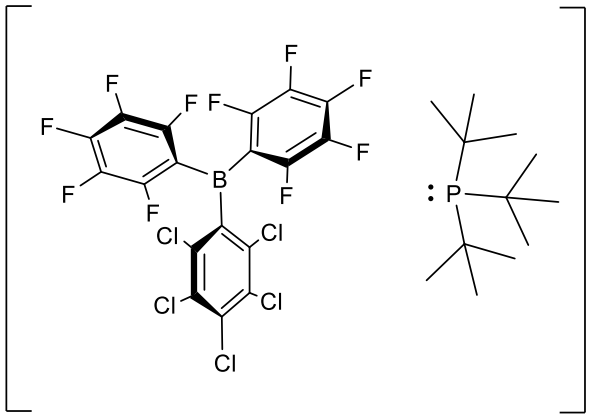

In a J-Young's NMR tube, a 1:1 mixture of $B(C_6Cl_5)(C_6F_5)_2$ and P^{t}Bu$_3$ were combined in C_6D_6 (0.5 mL). Formation of the FLP was monitored using ^{1}H, ^{11}B, ^{19}F and ^{31}P NMR spectroscopy. **^{1}H NMR (C_6D_6, 500 MHz):** δ 1.27 (d, 27H, $^{3}J_{HP}$ = 16 Hz; P{C(CH_3)$_3$}). **^{11}B NMR (C_6D_6, 160 MHz):** δ 60.1 (br, s). **^{31}P NMR (C_6D_6, 202 MHz):** δ 62.70 (m, $^{3}J_{HP}$ = 16 Hz; *P*{C(CH_3)$_3$}). **^{19}F NMR (C_6D_6, 470 MHz):** δ −127.18 (br m, 4F, $^{3}J_{FF}$ =20 Hz;*ortho*-C_6F_5); −140.1 (m, 2F, $^{3}J_{FF}$ = 20 Hz; *para*-C_6F_5); −159.8 (m, 4F, $^{3}J_{FF}$ = 20 Hz; *meta*-C_6F_5).

6.3.4 Synthesis of $[(C_6Cl_5)(C_6F_5)_2BH][HP^tBu_3]$

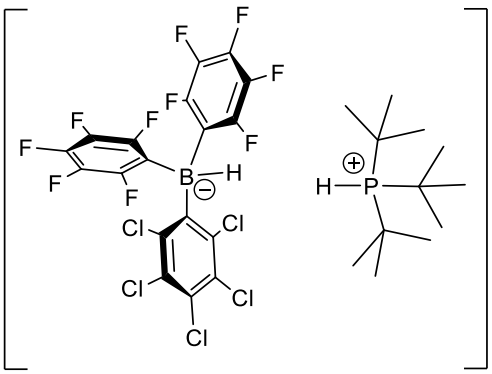

In a 25 mL ampoule, a magnetic stirrer bar, $B(C_6Cl_5)(C_6F_5)_2$ (300 mg, 0.5 mmol), P^tBu_3 (100 mg, 0.5 mmol) and benzene (10 mL) was added. The mixture was freeze-pump-thaw degassed three times, and pressurised with H_2 (2 bar). The mixture was allowed to stir for 16 hour at 23 °C. The solvent was removed under reduced pressure and the remaining oily residue was washed with pentane before further drying under vacuum (10^{-2} mbar) to yield an off-white solid (340 mg, 85%). **^{1}H NMR (CD_3CN, 500 MHz):** δ 5.40 (br d, 1H, $^1J_{PH}$ = 450Hz, P*H*); 3.90 (br q, 1H, $^1J_{BH}$ = 90Hz, B*H*); 1.59 (d, 27H, $^3J_{HP}$ = 16 Hz; P{C(CH_3)$_3$}). **^{11}B NMR (CD_3CN, 160 MHz):** δ −19.80 (d, $^1J_{HB}$ = 90 Hz). **^{31}P NMR (CD_3CN, 202 MHz):** δ 55.70 (dm, $^1J_{HP}$ = 450 Hz, $^3J_{HP}$ = 16 Hz; H*P*^{t}Bu$_3$. **^{19}F NMR (CD_3CN, 470 MHz):** δ −134.18 (br d, 4F, $^3J_{FF}$ =20 Hz; *ortho*-C$_6F_5$); −165.22 (t, 2F, $^3J_{FF}$ = 20 Hz; *para*-C$_6F_5$); −168.36 (m, 4F, $^3J_{FF}$ = 20 Hz; *meta*-C$_6F_5$). **^{13}C{^{1}H} NMR (CD_3CN, 125 MHz):** δ 148.58 (dm, $^1J_{FC}$ = 240 Hz; *ortho*-C$_6$F$_5$); 140.76 (s, *ortho*-C$_6$Cl$_5$); 139.36 (dm, $^1J_{FC}$ = 240 Hz; *para*-C$_6$F$_5$); 137.27 (dm, $^1J_{FC}$ = 240 Hz; *meta*-C$_6$F$_5$); 131.72 (s, *para*-C$_6$Cl$_5$); 130.52 (s, *meta*-C$_6$Cl$_5$); *ipso*-C not seen; 37.59 (d, $^1J_{PC}$ = 29 Hz; P*C*(CH$_3$)$_3$); 28.91 (s, C(*C*H$_3$)$_3$). **HRMS (ESI$^-$, *m/z*):** for $[C_{18}HBCl_5F_{10}]^-$ **Calcd**: 595.26. **Found:** 595.28. **IR (cm^{-1}):** 2956 (s), 2924 (s), 2854 (s), 2387 (B-H stretch, m), 1640 (m), 1460 (s), 1404 (s), 1379 (s), 1300 (m), 1271 (m), 1103 (s), 1078 (s) 966 (s), 806 (m), 607 (w). **Anal. Calcd.** for $C_{30}H_{29}BCl_5F_5P$: C 45.12; H 3.66 **Found:** C 45.15 H 3.52.

6.3.5 Synthesis of [(C_6Cl_5)(C_6F_5)$_2$BOCHO][HP^{t}Bu$_3$] via Route A1

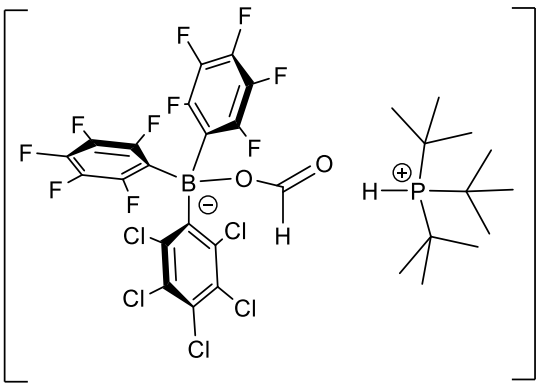

A 25 mL ampoule fitted with a magnetic stirring bar, was added B(C_6Cl_5)(C_6F_5)$_2$ (300 mg, 0.5 mmol), P^{t}Bu$_3$ (100 mg, 0.5 mmol), HCOOH (18.5 µL 0.5 mmol) and toluene (10 mL). After 30 minutes of stirring at 23 °C, the resulting colourless precipitate was collected by filtration and washed with cold pentane (3 x 5 mL) and dried under vacuum to afford a [(C_6Cl_5)(C_6F_5)$_2$BOCHO][HP^{t}Bu$_3$] (334 mg, 81% yield). Single crystals suitable for X-ray diffraction were grown by slow cooling of a saturated toluene solution. **^{1}H NMR (CD$_3$CN, 400 MHz):** δ 8.06 (s, 1H, -BOC*H*O); 5.48 (br d, 1H, $^1J_{PH}$ = 430Hz, P*H*); 1.58 (d, 27H, $^3J_{HP}$ = 16 Hz, P{C(C*H*$_3$)$_3$}). **^{11}B NMR (CD$_3$CN, 128 MHz):** δ −1.45 (s). **^{31}P NMR (CD$_3$CN, 161 MHz):** δ 55.78 (dm, $^1J_{HP}$ = 450 Hz, $^3J_{HP}$ = 16 Hz; H*P*^{t}Bu$_3$). **^{19}F NMR (CD$_3$CN, 376 MHz):** δ −134.13 (br d, 4F, $^3J_{FF}$ = 20 Hz; *ortho*-C_6F_5); −162.36 (t, 2F, $^3J_{FF}$ =20 Hz; *para*-C_6F_5); −167.56 (m, 4F, $^3J_{FF}$ =20 Hz; *meta*-C_6F_5). **^{13}C{^{1}H} NMR (CD$_3$CN, 100 MHz):** δ 165.05 (s, BO*C*HO); 148.68 (dm, $^1J_{FC}$ = 240 Hz; *ortho*-*C*$_6$F$_5$); 140.62 (s, *ortho*-C_6Cl_5); 139.33 (dm, $^1J_{FC}$ = 240 Hz; *para*-*C*$_6$F$_5$); 137.30 (dm, $^1J_{FC}$ = 240 Hz; *meta*-*C*$_6$F$_5$); 131.69 (s, *para*-*C*$_6$Cl$_5$); 129.98 (s, *meta*-*C*$_6$Cl$_5$); *ipso*-C not seen; 37.55 (d, $^1J_{PC}$ = 29 Hz; P*C*(CH$_3$)$_3$); 30.1 (s, C(*C*H$_3$)$_3$). **HRMS (ESI$^-$, *m/z*):** [$C_{19}HO_2BCl_5F_{10}$]$^-$ **Calcd:** 639.27 **Found:** 639.31. **IR (cm^{-1}):** 2956 (s), 2924 (s), 2854 (s), 1698 (s), 1464 (s), 1460 (s),

1378 (s), 1085 (w), 721 (m). **Anal. Calcd.** for $C_{31}H_{27}O_2BCl_5F_{10}P$: C 44.29; H 3.24 **Found:** C 44.32; H 3.26. **X-Ray data:** DX2_1.cif

6.3.6 Synthesis of $[(C_6Cl_5)(C_6F_5)_2BOCH_3][HP^tBu_3]$ via Route A2

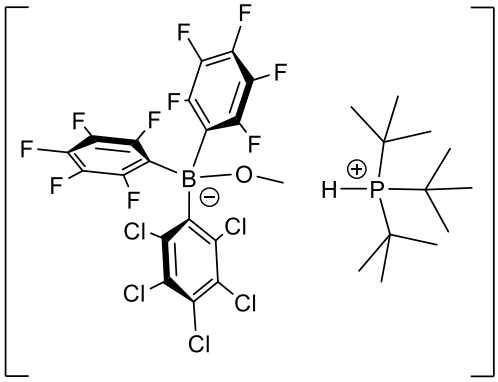

A 25 mL ampoule fitted with a magnetic stirring bar, was added $B(C_6Cl_5)(C_6F_5)_2$ (300 mg, 0.5 mmol), P^tBu_3 (100 mg, 0.5 mmol), CH_3OH (20 µL 0.5 mmol) and toluene (10 mL). The reaction was stirred at 23 °C for 16 h. The solvent was removed under vacuum to afford a sticky colourless solid, which was washed with cold dry pentane (3 x 5 mL) and dried under vacuum to give $[(C_6Cl_5)(C_6F_5)_2BOCH_3][HP^tBu_3]$ (356 mg, 90%). **^{1}H NMR (CD_3CN, 400 MHz):** δ 5.43 (br d, 1H, $^1J_{PH}$ = 430Hz, P*H*); 2.98 (s, 3H, -BOC*H*$_3$); 1.59 (d, 27H, $^3J_{HP}$ = 16 Hz P{C(C*H*$_3$)$_3$}). **^{11}B NMR (CD_3CN, 128 MHz):** δ −0.21 (s). **^{31}P NMR (CD_3CN, 161 MHz):** δ 55.75 (dm, $^1J_{HP}$ = 430 Hz, $^3J_{HP}$ = 16 Hz; H*P*^{t}Bu$_3$. **^{19}F NMR (CD_3CN, 376 MHz):** δ −133.23 (br d, 4F, $^3J_{FF}$ = 20 Hz; *ortho*-C$_6$*F*$_5$); −164.46 (t, 2F, $^3J_{FF}$ = 20 Hz; *para*-C$_6$*F*$_5$); −168.06 (m, 4F, $^3J_{FF}$ = 20 Hz; *meta*-C$_6$*F*$_5$). **^{13}C{^{1}H} NMR (CD_3CN, 100 MHz):** δ 148.54 (dm, $^1J_{FC}$ = 240 Hz, *ortho*-*C*$_6$F$_5$); 138.83 (dm, $^1J_{FC}$ = 240 Hz; *para*-*C*$_6$F$_5$); 137.98 (s, *ortho*-*C*$_6$Cl$_5$); 137.00 (dm, $^1J_{FC}$ = 240 Hz; *meta*-C$_6$F$_5$); 130.95 (s, *para*-*C*$_6$Cl$_5$); 129.53 (s, *meta*-*C*$_6$Cl$_5$); *ipso*-C not seen; 52.35 (s, O*C*H$_3$); 37.35 (d, $^1J_{PC}$ = 29 Hz; P*C*(CH$_3$)$_3$); 29.94 (s, C(*C*H$_3$)$_3$). **HRMS (ESI$^-$, *m/z*):** $[C_{19}H_3OBCl_5F_{10}]^-$ **Calcd:** 625.27 **Found:** 625.30 **IR (cm^{-1}):** 3007 - 2871 (br, s), 2352 (s), 1639 (s), 1514 (s), 1456 (s), 1450

(s), 1281 (s), 1082 (s), 972 (s), 932 (m), 888 (m), 762 (m), 674 (m) 560 (m). **Anal. Calcd.** for $C_{31}H_{27}O_2BCl_5F_{10}P$: C 44.99; H 3.65 **Found:** C 45.03; H 3.67.

6.3.7 Reduction of the Formatoborate to Methoxyborate using H_2

Reduction of $[(C_6Cl_5)(C_6F_5)_2BOCHO][HP^tBu_3]$ synthesised via route A1 to the methoxyborate using H_2 was attempted.

A quartz J-Young's NMR tube containing the formatoborate (20 mg, 0.023 mmol), and 15 mol% of the unreacted FLP $[B(C_6Cl_5)(C_6F_5)_2/P^tBu_3]$ in toluene-d^8 was freeze-pump-thaw degassed three times and pressurised with H_2 (2 bar). The reaction was heated to 110 °C for 72 h and monitored using ^1H, ^{11}B and ^{31}P NMR spectroscopy. Signals which corresponds to the methoxyborate species can be observed among other species such as the hydrogen activation product generated during the reaction under H_2 and unreduced formatoborate species. The conversion is about 5% by NMR integration.

6.3.8 Reduction of CO_2 by $[B(C_6Cl_5)(C_6F_5)_2/P^tBu_3]$ FLP using H_2

A Quartz J-Young's NMR tube containing $(C_6Cl_5)B(C_6F_5)_2$ (20 mg, 0.03 mmol) and P^tBu_3 (6 mg, 0.03 mmol) in bromobenzene-d^5 was freeze-pump-thaw degassed three times, and filled with CO_2 (2 bar) after allowed to warm to room temperature. The tube was then cooled in liquid N_2 again before filled with H_2 (2 bar). The reaction mixture was heated at 140 °C for 72 hours and monitored by ^1H, ^{11}B, ^{31}P, ^{19}F and ^{13}C NMR spectroscopy.

6.4 Experimental Details for Chapter Three

6.4.1 Synthesis of (^{t}BuO)$_3$SiOB(C$_6$F$_5$)$_2$

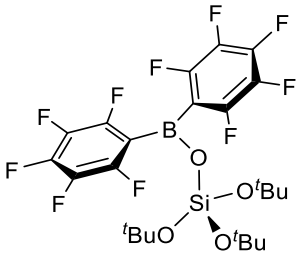

In a 25 mL ampoule containing a stirrer bar, was added (^{t}BuO)$_3$SiOH (135 mg, 0.51 mmol), (C$_6$F$_5$)$_2$BH (177, 0.51 mmol) and benzene 10 mL. After stirring for 16 h at 23 °C, solvent was stripped *in vacuo* to yield analytically pure (^{t}BuO)$_3$SiOB(C$_6$F$_5$)$_2$ (298 mg, 96%). **^{1}H NMR (C$_6$D$_6$, 400 MHz):** δ 1.21 (s, 27H, Si{OC(C*H*$_3$)$_3$}$_3$). **^{11}B NMR (C$_6$D$_6$, 128 MHz):** δ 40.21 (s). **^{19}F NMR (C$_6$D$_6$, 376 MHz):** δ −131.93 (dm, 4F, $^3J_{FF}$ = 20 Hz; *ortho*-C$_6$*F*$_5$); −150.26 (tt, 2F, $^3J_{FF}$ = 20 Hz, *para*-C$_6$*F*$_5$); −161.97 (td, 4F, $^3J_{FF}$ = 20 Hz; *meta*-C$_6$*F*$_5$). **^{13}C{^{1}H} NMR (C$_6$D$_6$, 100 MHz):** δ 147.84 (dm, $^1J_{FC}$ = 248 Hz; *ortho*-*C*$_6$F$_5$); 142.66 (dm, $^1J_{FC}$ = 248 Hz; *para*-*C*$_6$F$_5$); 137.18 (dm, $^1J_{FC}$ = 248 Hz; *meta*-*C*$_6$F$_5$); *ipso*-C not seen; 73.22 (s, 3C, Si{O*C*(CH$_3$)$_3$}$_3$); 30.72 (s, 9C, Si{OC(*C*H$_3$)$_3$}$_3$). **^{29}Si NMR (C$_6$D$_6$, 99 MHz):** δ −100.85 (s). **HRMS (ESI$^-$, *m/z*):** C$_{24}$H$_{27}$OBF$_{10}$ **Calcd:** 532.26 **Found:** 532.29 **IR (cm^{-1}):** 2966 (s), 2924 (s), 2990 (s), 2873 (s), 1652 (s), 1519 (s), 1488 (s), 1457(s), 1400 (s), 1371 (m), 1235 (m), 1114 (s), 969 (m), 749 (m), 482 (m). **Anal. Calcd.** for C$_{24}$H$_{27}$OBF$_{10}$: C 54.16; H 5.11 **Found**: C 54.03; H 5.17.

6.4.2 Synthesis of (^{t}BuO)$_3$SiOB(Fxyl)$_2$

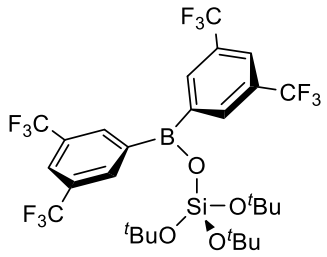

In a 25 mL ampoule containing a stirrer bar, was added (^{t}BuO)$_3$SiOH (135 mg, 0.51 mmol), (Fxyl)$_2$BCl (241, 0.51 mmol) and benzene 10 mL. After stirring for 16 h at 23 °C, solvent was stripped *in vacuo*, and yielded analytically pure (^{t}BuO)$_3$SiOB(Fxyl)$_2$ (315 mg, 84%). **^{1}H NMR (C$_6$D$_6$, 400 MHz):** δ 8.19 (s, 4H, *ortho*-Ar*H*); 7.87 (s, 2H, *para*-Ar*H*); 1.26 (s, 27H, Si{OC(C*H*$_3$)$_3$}$_3$); **^{11}B NMR (C$_6$D$_6$, 128 MHz):** δ 43.61 (s). **^{19}F NMR (C$_6$D$_6$, 376 MHz)**: δ −62.65 (s, 6F, C*F*$_3$). **^{29}Si NMR (C$_6$D$_6$, 99 MHz):** δ −101.84 (s). **^{13}C{^{1}H} NMR (C$_6$D$_6$, 100 MHz):** δ 138.2 (br, *ipso*-Ar*C*); 134.6 (*ortho*-Ar*C*); 132.06 (q, $^2J_{FC}$ = 31 Hz; *meta*-Ar*C*); 125.18 (m, *para*-Ar*C*); 123.73 (q, $^1J_{CF}$ = 270; *C*F$_3$); *ipso*-C not seen; 73.22 (s, 3C, Si{O*C*(CH$_3$)$_3$}$_3$); 30.72 (s, 9C, Si{OC(*C*H$_3$)$_3$}$_3$). **HRMS (ESI$^-$, *m/z*):** $C_{28}H_{33}BSiO_4F_{12}$ **Calcd:** 700.44 **Found:** 700.39 **IR (cm^{-1}):** 2966 (s), 2924 (s), 2872 (s), 1652 (s), 1521 (s), 1489 (s), 1456(s), 1402 (s), 1370 (m), 1235 (m), 1113 (s), 970 (m), 749 (m), 481 (m). **Anal. Calcd.** for $C_{28}H_{33}BSiO_4F_{12}$: C 48.01; H 4.75 **Found:** C 48.63; H 4.81.

6.4.3 Synthesis of $[T_8(OB(C_6F_5)_2)_2]$ (T_8= $(C_4H_9)_8Si_8O_{12}$)

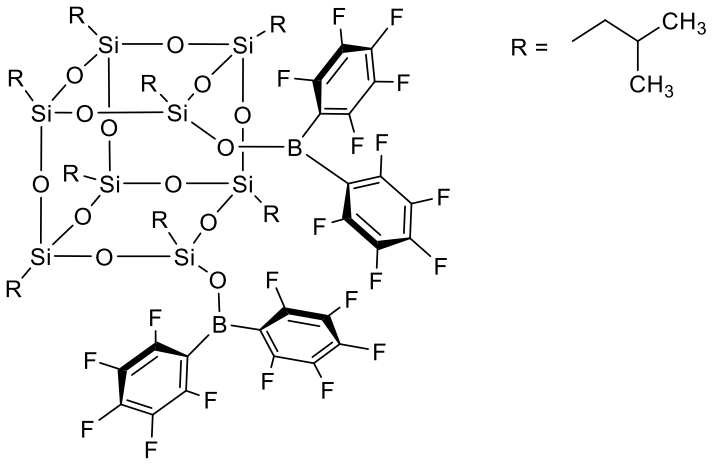

$(C_4H_9)_8Si_8O_{12}(OH)_2$ (446 mg, 0.50 mmol) and $(C_6F_5)_2BH$ (346 mg, 1.00 mmol) were combined in benzene (10 mL) in a 25 mL ampoule fitted with a magnetic stirrer bar. The reaction reached completion over night at 23 ºC. The solvent was stripped *in vacuo* and the solid collected was analytically pure $[(C_4H_9)_8Si_8O_{12}(OB(C_6F_5)_2)_2]$ (685 mg, 87%). **^{1}H NMR (C_6D_6, 400 MHz):** δ 2.16-0.7 ($SiCH_2C(CH_3)_2$); **^{19}F NMR (C_6D_6, 376.5 MHz):** δ −131.97 (dm, 2F, $^3J_{FF}$ = 20 Hz; *ortho*-C_6F_5), −148.69 (tt, 1F, $^3J_{FF}$ = 20 Hz; *para*-C_6F_5), −161.58 (td, 2F, $^3J_{FF}$ = 20 Hz; *meta*-C_6F_5). **^{13}C{^{1}H} NMR (C_6D_6, 100 MHz):** δ 148.58 (dm, $^1J_{FC}$ = 248 Hz; *ortho*-C_6F_5); 143.66 (dm, $^1J_{FC}$ = 248 Hz; *para*-C_6F_5); 137.43 (dm, $^1J_{FC}$ = 248 Hz; *meta*-C_6F_5); *ipso*-C not seen; 25.7-22.42 ($SiCH_2C(CH_3)_2$). **^{11}B NMR (C_6D_6, 128.4 MHz):** δ 40.62 (br). **^{29}Si NMR (C_6D_6, 99 MHz):** δ −65 (s, 2Si); −67 (s, 4Si); −69 (s, 2Si; *Si*-O-B). **IR (cm^{-1}):** 2966 (s), 2924 (s), 2990 (s), 2873 (s), 1652 (s), 1519 (s), 1488 (s), 1457(s), 1400 (s), 1371 (m), 1235 (m), 1114 (s), 969 (m), 749 (m), 482 (m). The NMR analysis showed the presence of a small impurity (<7%), therefore a satisfying elemental analysis could not be obtained.

6.4.4 Synthesis of $[T_8(OB(Fxyl)_2)_2]$ (T_8= $(C_4H_9)_8Si_8O_{12}$)

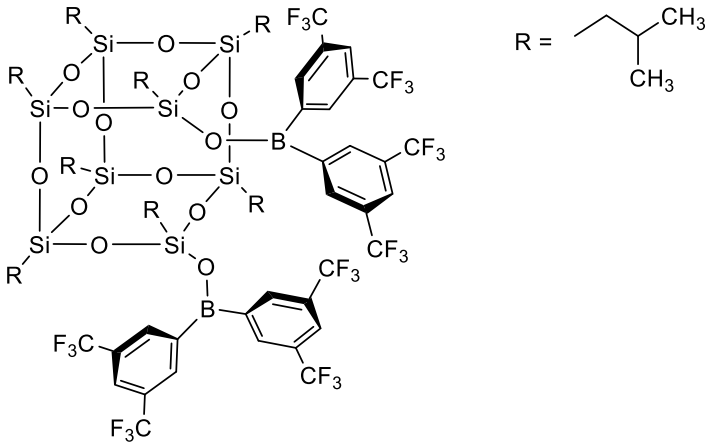

$(C_4H_9)_8Si_8O_{12}(OH)_2$ (445.85 mg, 0.5 mmol) and $(Fxyl)_2BCl$ (472.00 mg, 1.00 mmol) were combined in benzene (10 mL) in a 25 mL ampoule fitted with a magnetic stirrer bar. The reaction reached completion over night at 23 ºC. The solvent was stripped *in vacuo* and yielded $[(C_4H_9)_8Si_8O_{12}(OB(Fxyl)_2)_2]$ (685 mg, 86.5%). **^{1}H NMR (C_6D_5Br, 400 MHz):** δ 8.24 (s, 4H, *ortho*-Ar*H*); 8.04 (s, 2H, *para*-Ar*H*); 2.16-0.7 ($SiCH_2C(CH_3)_2$). **^{19}F NMR (C_6D_5Br, 376.5 MHz):** δ 62.48 (td, 2F, *meta*-CF_3). **^{11}B NMR (C_6D_5Br, 128.4 MHz):** δ 44 (br). **^{13}C{^{1}H} NMR (C_6D_6, 100 MHz):** δ 138.2 (br, *ipso*-Ar*C*); 135.13 (*ortho*-Ar*C*); 132.76 (q, $^2J_{FC}$ = 31 Hz; *meta*-Ar*C*); 125.18 (m, *para*-Ar*C*); 124.23 (q, $^1J_{CF}$ = 270; CF_3); *ipso*-C not seen; 26.13-22.12 ($SiCH_2C(CH_3)_2$). **^{29}Si NMR (C_6D_6, 128 MHz):** δ −64 (s, 2Si); −68 (s, 4Si); −72 (s, 2Si; *Si*-O-B). **IR (cm^{-1}):** 3085-2823 (s), 1649 (s), 1510 (s), 1486 (s), 1465 (s), 1405 (m), 1367 (m), 1333 (m), 1302 (m), 1266 (m), 1228 (s), 1107 (br, s), 974 (m), 835 (w), 796 (m), 744 (m), 482 (m). The NMR analysis showed the presence of impurities (<10%), therefore a satisfying elemental analysis could not be obtained.

6.4.5 Preparation of [(^{t}BuO)$_3$SiOB(C$_6$F$_5$)$_2$/P^{t}Bu$_3$]

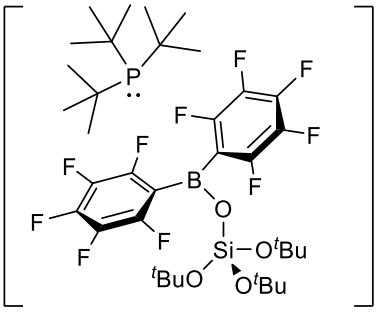

In a J-Young's NMR tube, a 1:1 mixture of (^{t}BuO)$_3$SiOB(C$_6$F$_5$)$_2$ and P^{t}Bu$_3$ were combined in C$_6$D$_6$ (0.5 mL). Formation of the FLP was monitored using ^{1}H, ^{11}B, ^{19}F and ^{31}P NMR spectroscopy. **^{1}H NMR (C$_6$D$_6$, 500 MHz):** δ 1.27 (d, 27H, $^3J_{HP}$ = 16 Hz; P{C(C*H*$_3$)$_3$}); 1.21 (s, 27H, Si{OC(C*H*$_3$)$_3$}$_3$). **^{11}B NMR (C$_6$D$_6$, 128 MHz):** δ 40.21 (s). **^{19}F NMR (C$_6$D$_6$, 376 MHz):** δ −131.93 (dm, 4F, $^3J_{FF}$ = 20 Hz; *ortho*-C$_6$*F*$_5$); −150.26 (tt, 2F, $^3J_{FF}$ = 20 Hz, *para*-C$_6$*F*$_5$); −161.97 (td, 4F, $^3J_{FF}$ = 20 Hz; *meta*-C$_6$*F*$_5$). **^{31}P NMR (C$_6$D$_6$, 202 MHz):** δ 62.1 (m, $^3J_{HP}$ = 16 Hz; *P*{C(CH$_3$)$_3$}).

6.4.6 Preparation of [(^{t}BuO)$_3$SiOB(C$_6$F$_5$)$_2$/PMes$_3$]

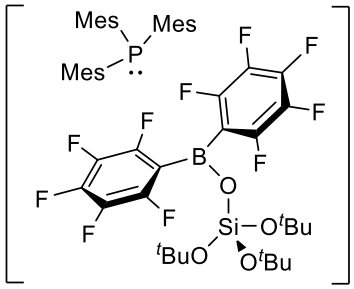

In a J-Young's NMR tube, a 1:1 mixture of (^{t}BuO)$_3$SiOB(C$_6$F$_5$)$_2$ and PMes$_3$ were combined in C$_6$D$_6$ (0.5 mL). Formation of the FLP was monitored using ^{1}H, ^{11}B, ^{19}F and ^{31}P NMR spectroscopy. **^{1}H NMR (C$_6$D$_6$, 500 MHz):** δ 6.7 (s, Ar*H*); 2.24 (s, Me); 1.21 (s, 27H, Si{OC(C*H*$_3$)$_3$}$_3$). **^{11}B NMR (C$_6$D$_6$, 128 MHz):** δ 40.76 (s). **^{19}F NMR (C$_6$D$_6$, 376 MHz):** δ −131.98 (dm, 4F, $^3J_{FF}$ = 20 Hz; *ortho*-C$_6$*F*$_5$); −149.9 (tt, 2F, $^3J_{FF}$ = 20 Hz,

para-C_6F_5); −161.89 (td, 4F, $^3J_{FF}$ = 20 Hz; *meta*-C_6F_5). **^{31}P NMR (C_6D_6, 202 MHz):** δ −36.4 (*P*Mes_3).

6.4.7 Preparation of [(^{t}BuO)$_3$SiOB(Fxyl)$_2$/P^{t}Bu$_3$]

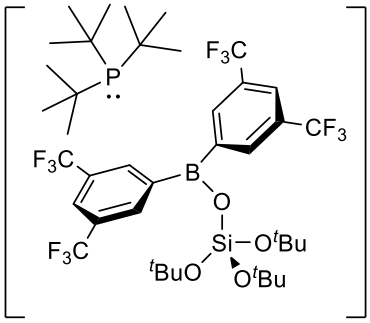

In a J-Young's NMR tube, a 1:1 mixture of (^{t}BuO)$_3$SiOB(Fxyl)$_2$ and ^{t}Bu$_3$ were combined in C_6D_6 (0.5 mL). Formation of the FLP was monitored using ^{1}H, ^{11}B, ^{19}F and ^{31}P NMR spectroscopy. **^{1}H NMR (C_6D_6, 500 MHz):** δ 8.19 (s, 4H, *o*-Ar*H*); 7.87 (s, 2H, *para*-Ar*H*); 1.27 (d, 27H, $^3J_{HP}$ = 16 Hz; P{C(C*H*$_3$)$_3$}); 1.26 (s, 27H, Si{OC(C*H*$_3$)$_3$}$_3$). **^{11}B NMR (C_6D_6, 128 MHz):** δ 45 (br, s). **^{19}F NMR (C_6D_6, 376 MHz):** δ 62.4 (s, 3F, C*F*$_3$). **^{31}P NMR (C_6D_6, 202 MHz):** δ 62.1 (m, $^3J_{HP}$ = 16 Hz; *P*{C(CH$_3$)$_3$}).

6.4.8 Preparation of [T$_8$ (OB(C$_6$F$_5$)$_2$)$_2$/(P^{t}Bu$_3$)$_2$]

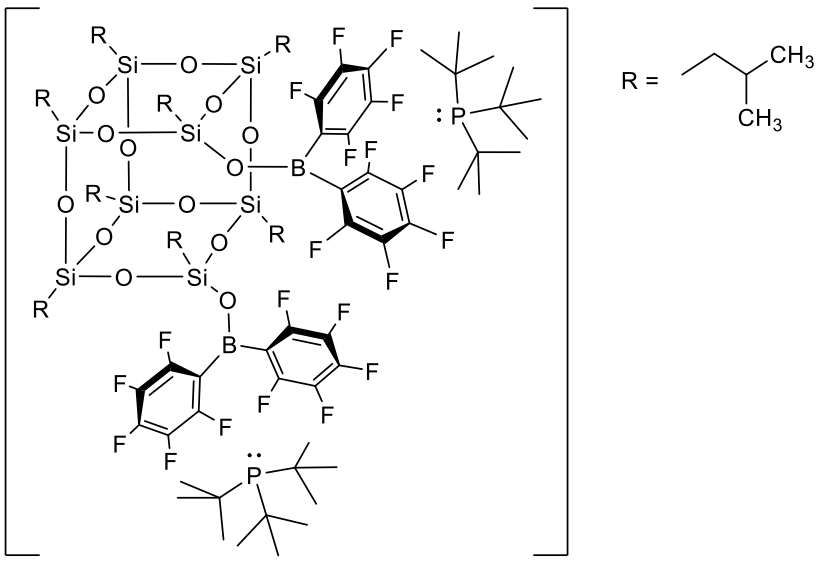

In a J-Young's NMR tube, a 1:2 mixture of $T_8(OB(C_6F_5)_2)_2$ and]were combined in C_6D_5Br (0.5 mL). Formation of the FLP was monitored using ^{1}H, ^{11}B, ^{19}F and ^{31}P NMR spectroscopy. **^{1}H NMR (C_6D_5Br, 400 MHz):** δ 2.16-0.7 (SiCH_2C(CH_3)$_2$); 1.45 (d, 27H, $^{3}J_{HP}$ = 16 Hz; P{C(CH_3)$_3$}). **^{19}F NMR (C_6D_5Br, 376.5 MHz):** δ −131.97 (dm, 2F, $^{3}J_{FF}$ = 20 Hz; *ortho*-C_6F_5), −148.69 (tt, 1F, $^{3}J_{FF}$ = 20 Hz; *para*-C_6F_5), −161.58 (td, 2F, $^{3}J_{FF}$ = 20 Hz; *meta*-C_6F_5). **^{11}B NMR (C_6D_5Br, 128.4 MHz):** δ 40.62 (br). **^{31}P NMR (C_6D_5Br, 202 MHz):** δ 62.1 (m, $^{3}J_{HP}$ = 16 Hz; *P*{C(CH$_3$)$_3$}).

6.4.9 Preparation of [T_8 ($OB(C_6F_5)_2)_2$/($PMes_3)_2$]

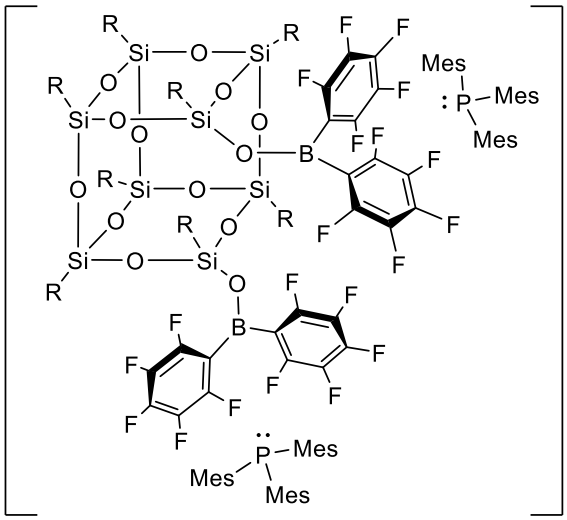

In a J-Young's NMR tube, a 1:2 mixture of $T_8(OB(C_6F_5)_2)_2$ and $PMes_3$ were combined in C_6D_5Br (0.5 mL). Formation of the FLP was monitored using ^{1}H, ^{11}B, ^{19}F and ^{31}P NMR spectroscopy. **^{1}H NMR (C_6D_5Br, 400 MHz):** δ 6.7 (s, Ar*H*); 2.24 (s, Me); 2.16-0.7 (SiCH_2C(CH_3)$_2$). **^{19}F NMR (C_6D_5Br, 376.5 MHz):** δ −131.1 (dm, 2F, $^{3}J_{FF}$ = 20 Hz; *ortho*-C_6F_5), −148.2 (tt, 1F, $^{3}J_{FF}$ = 20 Hz; *para*-C_6F_5), −160.7 (td, 2F, $^{3}J_{FF}$ = 20 Hz; *meta*-C_6F_5). **^{11}B NMR (C_6D_5Br, 128.4 MHz):** δ 40.1 (br). **^{31}P NMR (C_6D_5Br, 202 MHz):** δ −36.2 (*P*Mes$_3$).

6.4.10 Preparation of $[T_8(OB(Fxyl)_2)_2/(P^tBu_3)_2]$

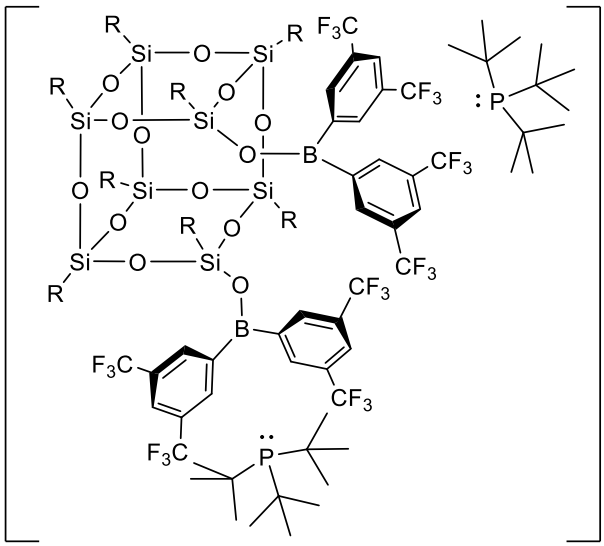

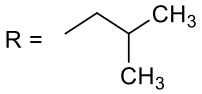

In a J-Young's NMR tube, a 1:2 mixture of $T_8(OB(Fxyl)_2)_2$ and P^tBu_3 were combined in C_6D_5Br (0.5 mL). Formation of the FLP was monitored using ^1H, ^{11}B, ^{19}F and ^{31}P NMR spectroscopy. **^{1}H NMR (C_6D_5Br, 500 MHz):** δ 8.24 (s, 4H, *ortho*-Ar*H*); 8.04 (s, 2H, *para*-Ar*H*); 2.16-0.7 (SiC*H*$_2$C(C*H*$_3$)$_2$). 1.01 (d, 27H, $^3J_{HP}$ = 16 Hz; P{C(C*H*$_3$)$_3$}). **^{11}B NMR (C_6D_5Br, 128 MHz):** δ 45 (br, s). **^{19}F NMR (C_6D_5Br, 376 MHz):** δ 62.2 (s, 3F, C*F*$_3$). **^{31}P NMR (C_6D_5Br, 202 MHz):** δ 61.7 (m, $^3J_{HP}$ = 16 Hz; *P*{C(CH$_3$)$_3$}).

6.4.11 Preparation of $[T_8(OB(Fxyl)_2)_2/(PMes_3)_2]$

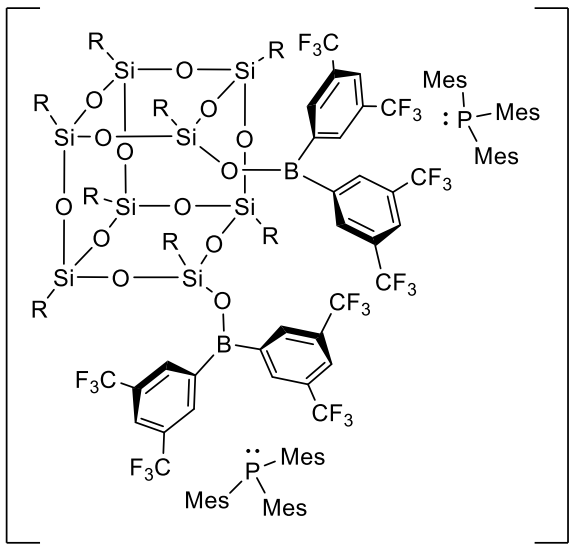

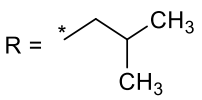

In a J-Young's NMR tube, a 1:2 mixture of $T_8(OB(Fxyl)_2)_2$ and P^tBu_3 were combined in C_6D_5Br (0.5 mL). Formation of the FLP was monitored using ^1H, ^{11}B, ^{19}F and ^{31}P NMR spectroscopy. **^{1}H NMR (C_6D_5Br, 500 MHz):** δ 8.24 (s, 8H, *ortho*-Fxyl-*H*); 8.04 (s, 4H, *para*-Fxyl-*H*); 6.86 (s 12H *ortho*-Mes-*H*); 2.24 (s, 54H Mes-CH_3) 2.16-0.7 (SiCH_2C(CH_3)$_2$). **^{11}B NMR (C_6D_5Br, 128 MHz):** δ 45 (br, s). **^{19}F NMR (C_6D_5Br, 376 MHz):** δ 62.2 (s, 3F, CF_3). **^{31}P NMR (C_6D_5Br, 202 MHz):** δ −36.2 (PMes$_3$).

6.4.12 Characterisation of $(({}^t\text{BuO})_3\text{SiO})_2\text{B}(C_6F_5)$

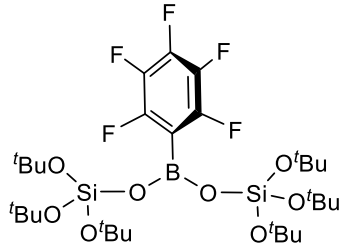

$(({}^t\text{BuO})_3\text{SiO})_2\text{B}(C_6F_5)$ formed via ligand redistribution of the $[({}^t\text{BuO})_3\text{SiOB}(H)(C_6F_5)_2][H{-}P({}^t\text{Bu})_3]$ hydride salt was found only sparingly soluble in acetonitrile at room temperature, which allowed facile isolation of the side product. Slow cooling of a saturated acetonitrile solution containing $(({}^t\text{BuO})_3\text{SiO})_2\text{B}(C_6F_5)$ yielded single crystals suitable for X-ray crystallographic analysis. **^{1}H NMR (C_6D_6, 400 MHz):** δ 1.33 (s, 27H, Si{OC(CH_3)$_3$}$_3$). **^{11}B NMR (C_6D_6, 128 MHz):** δ 23.1 (s). **^{19}F NMR (C_6D_6, 376 MHz):** δ −131.43 (dm, 4F, $^3J_{FF}$ = 20 Hz; *ortho*-C_6F_5); −156.26 (t, 2F, $^3J_{FF}$ = 20 Hz, *para*-C_6F_5); −163.77 (td, 4F, $^3J_{FF}$ = 20 Hz; *meta*-C_6F_5).

6.4.13 Reaction of Siloxane and Silsesquioxane bound FLPs with H_2

A J-Young's NMR tube containing a siloxane or silsquioxane bound Lewis acid with either P^tBu_3 or PMes$_3$ in either C_6D_6 or C_6D_5Br (0.5 mL) was freeze-pump-thaw degassed (x3) and pressurised with H_2 (2 bar). The reaction mixtures were left at 23 ºC overnight,

followed by heating to 60 ºC for 16 h, and monitored using ^{1}H, ^{11}B and ^{31}P NMR spectroscopy.

Frustrated Lewis Pair	Solvent	^{11}B B-H (ppm)	^{1}H P-H (ppm)	^{31}P P-H (ppm)	H_2 Cleavage*
$(^{t}BuO)_3SiOB(C_6F_5)_2$ $P^{t}Bu_3$	C_6D_6	2.47	3.99 d $^{1}J_{HP}$ = 439 Hz	57 dm $^{1}J_{HP}$ = 439 Hz	45 %
$(^{t}BuO)_3SiOB(C_6F_5)_2$ [$PMes_3$]	C_6D_6	1.74	8.78 d $^{1}J_{HP}$ = 492 Hz	−27 dm $^{1}J_{HP}$ = 492 Hz	49%
$(^{t}BuO)_3SiOB(Fxyl)_2$ $P^{t}Bu_3$	C_6D_5Br	0.30	4.32 d $^{1}J_{HP}$ = 429 Hz	59 $^{1}J_{HP}$ = 429 Hz	18 %
$T_8(OB(C_6F_5)_2)_2$ $(P^{t}Bu_3)_2$	C_6D_5Br	2.67	4.42 d $^{1}J_{HP}$ = 430 Hz	60 dm $^{1}J_{HP}$ = 430 Hz	28%
$T_8(OB(Fxyl)_2)_2$ $(P^{t}Bu_3)_2$	C_6D_5Br	1.43	4.6 d $^{1}J_{HP}$ = 433 Hz	56 dm $^{1}J_{HP}$ = 433 Hz	41%
$T_8(OB(C_6F_5)_2)_2$ $(PMes_3)_2$	C_6D_5Br	2.81	8.81 d $^{1}J_{HP}$ = 477 Hz	-28 d $^{1}J_{HP}$ = 477 Hz	25%
$T_8(OB(Fxyl)_2)_2$ $(PMes_3)_2$	C_6D_5Br	1.20	8.2 d $^{1}J_{HP}$ = 477 Hz	-27 d $^{1}J_{HP}$ = 480 Hz	38%

*calculations were based on the integration of protonated phosphonium cation signal in ^{31}P NMR spectrum.

6.5 Experimental Details for Chapter Four

6.5.1 Support Preparation

A fumed silica was provided by SCG chemicals, has a BET surface area of 310 m^2/g and no appreciable microporosity. It was thermally pretreated under vacuum (10^{-2} mBar) at 500 °C for 4 h. The resulting silica is denoted $silica_{500}$ contains 0.57 mmol/g of ≡SiOH, as predicted via the Zhuravlev model,[8] and later confirmed by elemental analysis after borane modification. The absence of physisorbed water on $silica_{500}$ was confirmed by the complete disappearance of the H−O−H bending mode at ca. 1635 cm^{-1} in the IR spectrum.

6.5.2 Synthesis of [≡SiOB(C_6F_5)$_2$] (s-BCF)

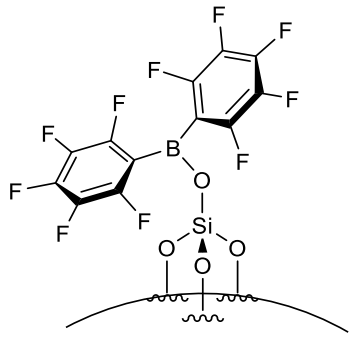

The synthesis of ≡SiOB(C_6F_5)$_2$ was adapted from literature procedures[4,5]. In a 100 mL glass ampoule charged with a magnetic stirrer bar, silica-$_{500}$ (1 g, pre-treated at 500 °C under vacuum for 4 h, BET surface area: 310 $m^2 g^{-1}$, containing 0.57 mmol g^{-1} of accessible ≡SiOH) was combined with (C_6F_5)$_2$BH (197 mg, 0.57 mmol) in toluene (30 mL). The mixture was stirred for 16 h at 23 °C followed by 1 h at 100 °C. The solid was filtered and washed with toluene (3 x 15 mL) on a fritted glass disc followed by drying at reduced pressure (1 x 10^{-3} mbar) for 3 h. Elemental analysis revealed that the solid contains 16.5 wt. % BCF. **^{11}B DEPTH NMR (24 kHz MAS)**: δ_{iso} 20. **^{19}F{^{1}H} HPDEC NMR (10 kHz MAS)**: δ_{iso} −130 (*ortho*-C_6F_5); −150 (*para*-C_6F_5); −163 (*meta*-C_6F_5). **^{13}C-{^{19}F} CPMAS {^{1}H} decoupled NMR (10 kHz MAS)**: δ_{iso} 144 (*ortho*-C_6F_5); 139 (*para*-C_6F_5); 132 (*meta*-C_6F_5); *ipso*-C_6F_5 not seen. **IR (cm^{-1})**: 3724 (br, w), 1650 (m), 1526 (m), 1494 (m), 1398 (m), 1327 (w), 1202 - 1101 (br, s), 821 (m). **Anal. Calcd.** for ≡SiOB(C_6F_5)$_2$: C 6.85 **Found:** C 6.87.

6.5.3 Synthesis of [≡SiOB(Fxyl)$_2$] (s-BFxyl)

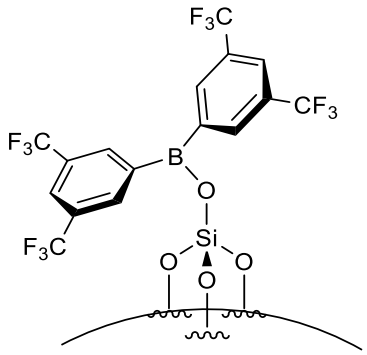

In a 100 mL glass ampoule charged with a magnetic stirrer bar, silica-$_{500}$ (1.0 g, pre-treated at 500 °C under vacuum for 4 h, BET surface area: 310 $m^2 g^{-1}$, containing 0.57 mmol g^{-1} of accessible ≡SiOH) was combined with $(Fxyl)_2BCl$ (249 mg, 0.57 mmol) in toluene (30 mL) at 0 °C. The mixture was kept cold for 30 min and further stirred at 23 °C for 16 h. The solid was filtered and washed with toluene (3 x 15 mL) on a fritted glass disc followed by drying at reduced pressure (1 x 10^{-3} mbar) for 3 h. Elemental analysis of the solid revealed that the solid contains 14.8 wt. % of $B(Fxyl)_2$. **^{11}B DEPTH NMR (24 kHz MAS)**: δ_{iso} 12. **^{19}F{^{1}H} DEPTH NMR (10 kHz MAS)**: δ_{iso} −70 (C*F*$_3$). **^{13}C-{^{19}F} CPMAS {^{1}H} decoupled NMR (10 kHz MAS)**: δ_{iso} 116 (br, *C*F$_3$). **^{13}C-{^{1}H} CPMAS {^{19}F} decoupled NMR (10 kHz)**: δ_{iso} 127 (*ortho*-Ar*C*); 117 (*para*-Ar*C*); *meta*-Ar*C* not seen. **IR (cm^{-1})**: 3721 (br, w), 3428 (br, w), 2959 (w), 2007 (br, m), 1854 (br, m), 1617 (m), 1445 (m), 1392 (m), 1354 (m), 1170 (br, s), 802 (m). **Anal. Calcd.** for ≡SiOB(C_6F_5)$_2$: C 8.77 **Found:** C 6.49.

6.5.4 Preparation of [≡SiOB(C$_6$F$_5$)$_2$/P^{t}Bu$_3$]

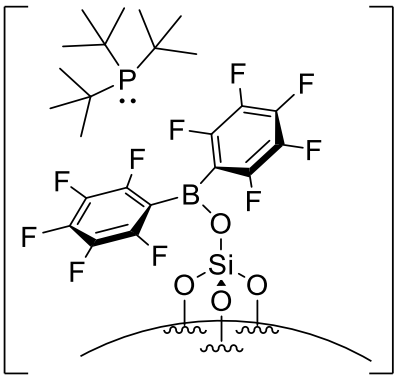

≡SiOB(C$_6$F$_5$)$_2$ (100 mg, 0.048 mmol borane) and P^{t}Bu$_3$ (9.7 mg, 0.048 mmol) were combined in toluene (10 mL) in an ampoule. After 2 hours of stirring at room temperature, the solid was filtered, washed with toluene (3 x 10 mL) and dried *in vacuo* for 2 h. **^{11}B DEPTH NMR (24 kHz)**: δ_{iso} 1.0. **^{31}P HPDEC NMR (24 kHz)**: δ_{iso} 48. **^{19}F{^{1}H} HPDEC NMR (10 kHz)**: δ_{iso} −144 (*ortho*-C$_6$F$_5$); −162 (*para*-C$_6$F$_5$); −169 (*meta*-C$_6$F$_5$). **^{13}C-{^{1}H} CPMAS {^{19}F} decoupled NMR (10 kHz)**: δ_{iso} 31 (P*C*(CH$_3$)$_3$); 24 (PC(*C*H$_3$)$_3$). **^{13}C-{^{19}F} CPMAS {^{1}H} decoupled NMR (10 kHz)**: δ_{iso} 149 (*ortho*-*C*$_6$F$_5$); 142 (*para*-*C*$_6$F$_5$); 137 (*meta*-*C*$_6$F$_5$); *ipso*-C$_6$F$_5$ not seen. **IR (cm^{-1})**: 3690 (br, wk), 2946 (m), 2919 (m), 1654 (w), 1518 (m), 1496 (m), 1466(m), 1227 (s), 1102 (s).

6.5.5 Preparation of [≡SiOB(Fxyl)$_2$/P^{t}Bu$_3$]

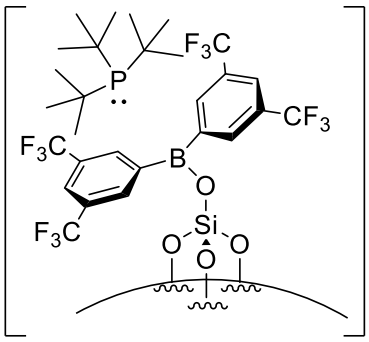

≡SiOB(Fxyl)$_2$ (100 mg, 0.034 mmol borane) and P^{t}Bu$_3$ (7 mg, 0.034 mmol) were combined in toluene (10 mL) in an ampoule. After 2 hours of stirring at room temperature, the solid was filtered, washed with toluene (3 x 10 mL) and dried *in vacuo* for 2 h. **^{11}B DEPTH {^{19}F} {^{1}H} NMR (24 kHz)**: δ_{iso} −1.0. **^{31}P CPMAS NMR (10 kHz)**: δ_{iso} 60. **^{19}F{^{1}H} DEPTH NMR (24 kHz)**: δ_{iso} −65 (C*F*$_3$). **^{13}C-{^{1}H} CPMAS {^{19}F} decoupled NMR (10 kHz)**: δ_{iso} 129 (*ortho*-Ar*C*); 124 (*meta*-Ar*C*); 118 (*para*-Ar*C*); 37 (P*C*(CH$_3$)$_3$); 29 (PC(*C*H$_3$)$_3$). **^{13}C-{^{19}F} CPMAS {^{1}H} decoupled NMR (10 kHz)**: δ_{iso} 129 (*ortho*-Ar*C*); 125 (*C*F$_3$); *meta*- and *ipso*-C$_6$F$_5$ not seen. **IR (cm^{-1})**: 3714 (br, w), 2957 (br. w), 1618 (w), 1488 (w), 1479 (w), 1412 (w), 1364 (m), 1279 (s), 1103 (br, s), 802 (m).

6.5.6 Synthesis of [≡SiOB(C$_6$F$_5$)$_2$(H/D)][(H/D)P^{t}Bu$_3$]

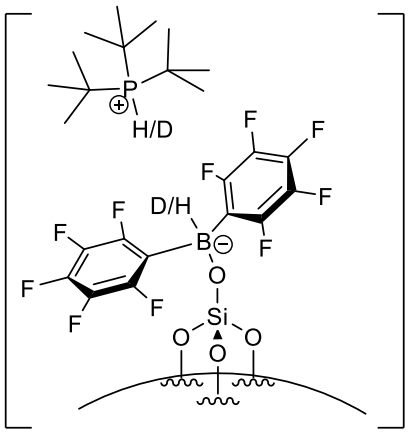

A toluene slurry containing [≡SiOB(C$_6$F$_5$)$_2$/P^{t}Bu$_3$] (110 mg, 0.048 mmol s-FLP) in a 5 mL glass ampoule was freeze-pump-thaw degassed three times, and filled with H$_2$ or D$_2$ (2 bar). The mixture was left stirring in an oil bath for 72 h at 65 ºC. The supernatant was removed and the solid was washed with dry toluene (3 x 15 mL) on a fritted glass disc, followed by drying *in vacuo* for 4 hours. **^{19}F DEPTH NMR (10 kHz MAS)**: δ_{iso} −138 (*ortho*−C$_6$F$_5$); −169 (*para*−C$_6$F$_5$); −172 (*meta*−C$_6$F$_5$). **^{11}B {^{1}H} CPMAS NMR (10 kHz MAS)**: δ_{iso} −2.14 (**B**−H). **^{31}P {^{1}H} CPMAS NMR (10 kHz MAS)**: δ_{iso} 54 (**P**-H). **^{13}C-{^{1}H}**

CPMAS {^{19}F} decoupled NMR (10 kHz): δ_{iso} 31 (P*C*(CH$_3$)$_3$); 23 (PC(*C*H$_3$)$_3$). **^{13}C-{^{19}F} CPMAS {^{1}H} decoupled NMR (10 kHz)**: δ_{iso} 142 (*ortho*-*C*$_6$F$_5$); 136 (*para*-*C*$_6$F$_5$); 131 (*meta*-*C*$_6$F$_5$); *ipso*-C$_6$F$_5$ not seen. **^{2}H DPMAS NMR (10 kHz MAS)**: δ_{iso} 8.5 (v. br). **IR (cm^{-1})**: 3690 (br, wk), 2967 (br, m), 2404 (v. w, B-H stretch), 1646 (w), 1532 (m), 1513 (m), 1488 (m), 1465(m), 1408 (w), 1383 (w), 1207 (br, s), 1102 (br, s), 812 (m).

6.5.7 Synthesis of [≡SiOB(Fxyl)$_2$(H)][HP^{t}Bu$_3$]

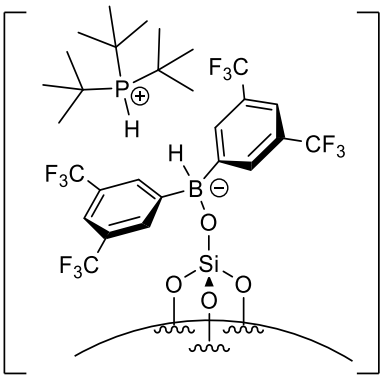

A toluene slurry containing [≡SiOB(Fxyl)$_2$/P^{t}Bu$_3$] (107 mg, 0.034 mmol s-FLP) in a 5 mL glass ampoule was freeze-pump-thaw degassed three times, and filled with H_2 (2 bar). The mixture was left stirring in an oil bath for 72 h at 65 ºC. The supernatant was removed and the solid was washed with dry toluene (3 x 15 mL) on a fritted glass disc, followed by drying *in vacuo* for 4 hours. **^{11}B DEPTH {^{19}F} {^{1}H} NMR (24 kHz)**: δ_{iso} −1.65. **^{31}P CPMAS NMR (10 kHz)**: δ_{iso} 59. **^{19}F{^{1}H} DEPTH NMR (24 kHz)**: δ_{iso} −65 (C*F*$_3$). **^{13}C-{^{1}H} CPMAS {^{19}F} decoupled NMR (10 kHz)**: δ_{iso} 129 (*ortho*-Ar*C*); 124 (*meta*-Ar*C*); 118 (*para*-Ar*C*); 37 (P*C*(CH$_3$)$_3$); 29 (PC(*C*H$_3$)$_3$). **^{13}C-{^{19}F} CPMAS {^{1}H} decoupled NMR (10 kHz)**: δ_{iso} 129 (*ortho*-Ar*C*); 125 (*C*F$_3$); *meta*- and *ipso*-C$_6$F$_5$ not seen. **IR (cm^{-1})**: 3714 (br, w), 2957 (br. w), 1618 (w), 1488 (w), 1479 (w), 1412 (w), 1364 (m), 1279 (s), 1103 (br,

s), 802 (m). The NMR and IR characterisation looks almost identical to the starting material, indicating that the reaction may not have succeeded.

6.5.8 Synthesis of [≡SiOB(OCD$_3$)(C$_6$F$_5$)$_2$][DP^{t}Bu$_3$]

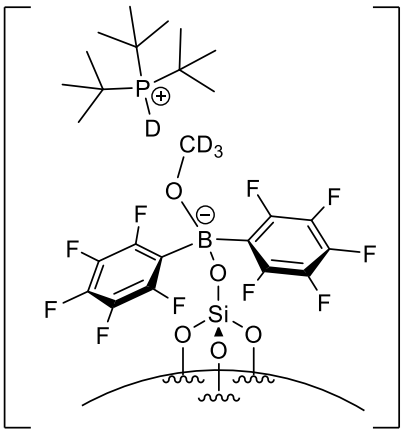

CD$_3$OD (2.2 µL, 0.048 mmol) was added to a toluene slurry containing [≡SiOB(C$_6$F$_5$)$_2$/P^{t}Bu$_3$] (110 mg, 0.048 mmol s-FLP) in an 5 mL ampoule. After stirring for 16 h at 25 ºC, the solid was filtered, washed with dry toluene (3 x 15 mL), followed by drying *in vacuo* for 4 hours. **^{2}H HAHNECHO NMR (10 kHz MAS)**: δ_{iso} 3.21 (B−OC*D*$_3$) (P−D is not observed). **^{11}B DEPTH NMR (10 kHz MAS)**: δ_{iso} 0 (*B*−OCD$_3$). **^{31}P CP NMR (10 kHz MAS)**: δ_{iso} 54 (*P*-H). **^{13}C-{^{1}H} CPMAS {^{19}F} decoupled NMR (10 kHz)**: δ_{iso} 57 (O*C*D$_3$); 31 (P*C*(CH$_3$)$_3$); 23 (PC(*C*H$_3$)$_3$). **^{13}C-{^{19}F} CPMAS {^{1}H} decoupled NMR (10 kHz)**: δ_{iso} 143 (*ortho*-*C*$_6$F$_5$); 137 (*para*-*C*$_6$F$_5$); 131 (*meta*-*C*$_6$F$_5$); *ipso*-*C*$_6$F$_5$ not seen. **IR (cm^{-1})**: 3703 (w, br), 2083 (v. w), 1648 (w), 1515 (m), 1487 (m), 1467 (m), 1212 (st), 1101 (st).

6.6 Experimental Details for Chapter Five

6.6.1 Support Preparation

$Mg_3Al\text{-}CO_3$ LDH (provided by SCG Chemicals) was heated at 150 ºC for 6 hours under reduced pressure, and stored under N_2 prior to use.

6.6.2 Reaction of $(C_6F_5)_2BH$ with $Mg_3Al\text{-}CO_3$ (LDH-BCF)

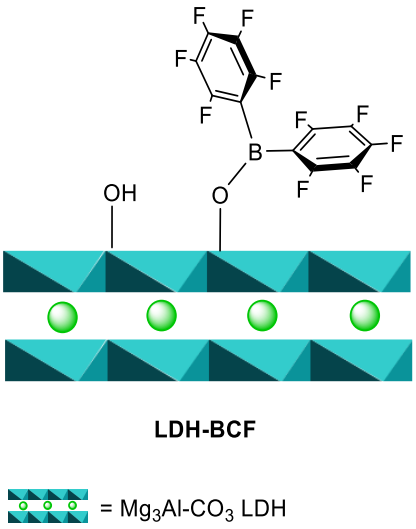

Under N_2, $Mg_3Al\text{-}CO_3$ (300 mg, 4.4 mmol) and $(C_6F_5)_2BH$ (100 mg, 0.289 mmol) were combined in toluene (10 mL) in an ampoule and stirred in an oil bath for 16 hours at 60 ºC. The supernatant was removed and the solid was washed with 2 x 10 mL dry toluene followed by drying *in vacuo* at 100 ºC for 2 hours affording **LDH-BCF** (25 wt.% loading of borane). **^{19}F DPMAS NMR (10 kHz MAS)**: δ_{iso} −139 (*ortho*−C_6F_5); −142 (*ortho*−C_6F_5); −158 (*para*−C_6F_5); −159 (*para*−C_6F_5); −167 (*meta*−C_6F_5); −172 (*meta*−C_6F_5). **^{13}C {^{19}F} CPMAS NMR:** δ 138 (*meta*-C_6F_5), 140 (*para*-C_6F_5), 148 (*ortho*-C_6F_5). **^{27}Al DPMAS NMR**: δ 73 (tetrahedral Al), 57 (tetrahedral Al), 7 (octahedral Al). **^{11}B MAS NMR:** δ 1.4 (interlayer −$OB(C_6F_5)_2$), 10 (surface −$OB(C_6F_5)_2$). **IR (cm^{-1}):**

3691 (m), 1645 (m), 1544 (m), 1465 (m), 1431 (m), 1257 (m), 1163 (m), 1090 (m), 1018 (m), 866 (w), 801 (m), 668 (w).

6.6.3 Preparation of $Mg_3Al\text{-}CO_3/[B(C_6F_5)_2/P^tBu_3]$ (LDH-FLP)

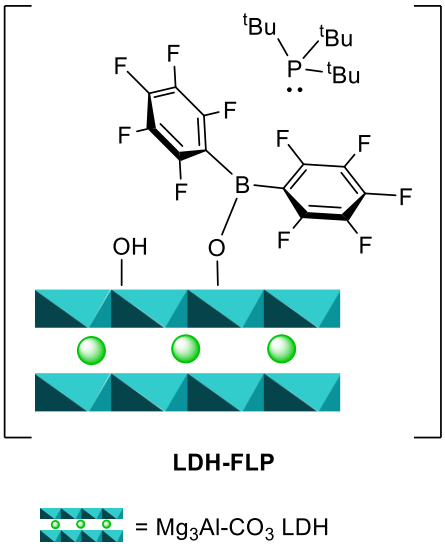

LDH-BCF (100 mg, 0.072 mmol borane) and P^tBu_3 (14.5 mg, 0.072 mmol) were combined in toluene (10 mL) in an ampoule. After 2 hours of stirring at room temperature, the solvent was removed and the remaining solid was dried in *in vacuo* to afford $Mg_3Al\text{-}CO_3/B(C_6F_5)_2/P^tBu_3$ **LDH-FLP**. **IR (cm^{-1}):** 3482 (br), 2878 (br), 1543 (br), 1447 (w), 1259 (m), 1218 (w), 1156 (m, ν C-F), 1092 (s), 1019 (s), 800 (m).

6.6.4 Reaction of $Mg_3Al\text{-}CO_3/[B(C_6F_5)_2/P^tBu_3]$ with H_2

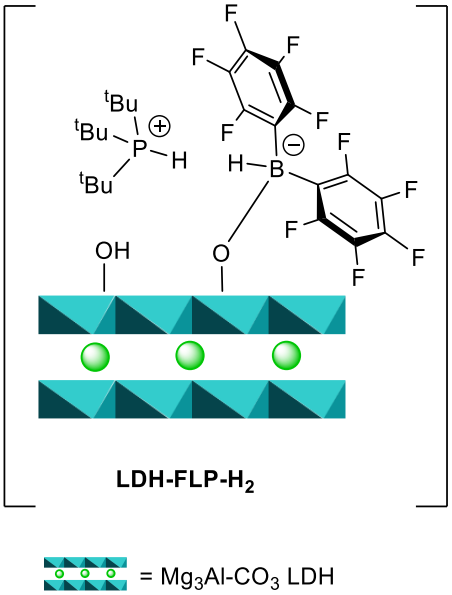

A toluene slurry containing [**LDH-BCF**/P ^{t}Bu$_3$] (100 mg) in a 5 mL glass ampoule was freeze-pump-thaw degassed three times, and filled with H_2 (2 bar). The mixture was left stirring in an oil bath for 16 h at 100 ºC. The supernatant was removed and the solid was washed with dry toluene (3 x 15 mL) and dried *in vacuo* for 2 hours. **IR (cm^{-1}):** 3563 (br), 2959 (m), 2918 (m), 2869 (m), 2400 (vw, ν B-H), 1532 (br), 1462 (m), 1424 (m), 1252 (m), 1218 (m), 1157 (m), 1090 (w), 1019 (m), 859 (w), 800 (m). **^{13}C {^{19}F} CPMAS NMR:** δ 137.7 (meta-C_6F_5), 140.8 (*para*-C_6F_5), 148.0 (*ortho*-C_6F_5). **^{13}C CPMAS NMR:** δ 165.7 (**C**O_3^{2-} LDH carbonate anion), 34.9 (H-P-**C**$(CH_3)_3$), 26.1 (H-P-C(**C**$H_3)_3$). **^{27}Al DPMAS NMR**: δ 66 (surface **Al**-O), 7 (bulk Al). **^{31}P CPMAS NMR:** δ 62 (-**P**-H). **^{11}B {^{19}F} hahnecho MAS NMR:** δ −12, 1.

6.6.5 Reaction of $Mg_3Al\text{-}CO_3/[B(C_6F_5)_2/P^tBu_3]$ with deuterium

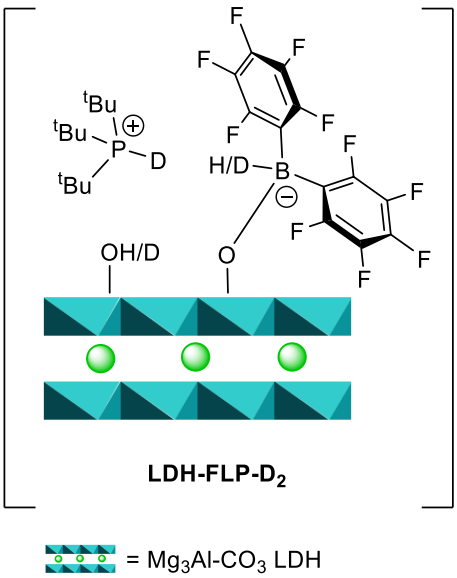

A toluene slurry containing **LDH-BCF**/P^{t}Bu$_3$ (100 mg) in a 5 mL glass ampoule was freeze-pump-thaw degassed three times, and filled with D_2 (2 bar). The mixture was left stirring in an oil bath for 16 h at 100 ºC. The supernatant was removed and the solid was washed with dry toluene (3 x 15 mL) and dried *in vacuo* for 2 hours. **IR (cm^{-1}):** 3553 (s, br), 2997, (w), 2962 (w), 2920 (w), 2870 (w), 2668 (m, br), 1540 (s), 1470 (s), 1422 (s), 1369 (s), 1247 (s), 1158 (s), 1090 (w), 1022, (w), 986 (m), 860 (w), 802 (m). **^{1}H DPMAS NMR:** 1.36 (HPC(C**H**$_3$)$_3$). **^{2}H hanecho MAS NMR:** δ 1 (B−**D**), 5 (O−**D**). **^{13}C {^{19}F} CPMAS NMR:** δ 137.3 (meta-C$_6$**F**$_5$), 140.9 (*para*-C$_6$**F**$_5$), 147.6 (*ortho*-C$_6$**F**$_5$). **^{13}C {^{19}F} hpdec MAS NMR:** 34.0 (H-P-**C**(CH$_3$)$_3$), 31.2 (H-P-C(**C**H$_3$)$_3$). **^{13}C CPMAS NMR:** δ 165.7 (**C**O$_3^{2-}$ LDH carbonate anion). **^{27}Al DPMAS NMR**: δ 66 (tetrahedral Al), 8 (octahedral Al). **^{31}P CPMAS NMR:** δ 54 (**P**-D). **^{11}B hahnecho MAS NMR:** δ −12, 1.

6.7 References

1 J. Cosier and A. M. Glazer, *J. Appl. Crystallogr.*, 1986, **19**, 105–107.

2 D. J. Parks, R. E. von H. Spence and W. E. Piers, *Angew. Chem., Int. Ed.*, 1995, **34**, 809–811.

3 D. J. Parks, W. E. Piers and G. P. a. Yap, *Organometallics*, 1998, **17**, 5492–5503.

4 K. Samigullin, M. Bolte, H.-W. Lerner and M. Wagner, *Organometallics*, 2014, **33**, 3564–3569.

5 A. E. Ashley, T. J. Herrington, G. G. Wildgoose, H. Zaher, A. L. Thompson, N. H. Rees, T. Krämer and D. O'Hare, *J. Am. Chem. Soc.*, 2011, **133**, 14727–14740.

6 J. Tian, S. Wang, Y. Feng, J. Li and S. Collins, *J. Mol. Catal. A: Chem.*, 1999, **144**, 137–150.

7 Y.-J. Wanglee, J. Hu, R. E. White, M.-Y. Lee, S. M. Stewart, P. Perrotin and S. L. Scott, *J. Am. Chem. Soc.*, 2012, **134**, 355–366.

8 L. T. Zhuravlev, *Colloids Surf., A*, 2000, **173**, 1–38.